Carbon-Coated Magnetic Nanobeads for the Synthesis and Recycling of High-Density Catalytic Systems

Dissertation

Zur Erlangung des Doktorgrades

Dr. rer. nat.

an der Fakultät für Chemie und Pharmazie

der Universität Regensburg

vorgelegt von

Roland Linhardt

aus Pyrbaum

Regensburg 2014

Die Arbeit wurde angeleitet von:		Prof. Dr. Oliver Reiser
Promotionsgesuch eingereicht am:		10. März 2014
Promotionskolloquium am:		04. April 2014
Prüfungsausschuss:	Vorsitz:	Prof. Dr. Antje J. Baeumner
	1. Gutachter:	Prof. Dr. Oliver Reiser
	2. Gutachter:	Priv. Doz. Dr. Sabine Amslinger
	3. Gutachter:	Prof. Dr. Arno Pfitzner

Der experimentelle Teil der vorliegenden Arbeit wurde in der Zeit von Oktober 2010 bis Dezember 2013 unter der Gesamtleitung von Prof. Dr. Oliver Reiser am Lehrstuhl für Organische Chemie der Universität Regensburg angefertigt. Zusätzliche Betreuer waren im Oktober 2012 Prof. Dr. Jean-Pierre Majoral, Prof. Dr. Anne-Marie Caminade und Dr. Armelle Ouali am Laboratoire de Chimie de Coordination in Toulouse (Frankreich).

Besonders bedanken möchte ich mich bei Herrn Prof. Dr. Oliver Reiser für die Aufnahme in seinen Arbeitskreis, die Überlassung des äußerst interessanten Themas, die anregenden Diskussionen sowie die stetige Unterstützung.

Meiner Familie

und

Meiner Freundin Julia

„Ich beschäftige mich nicht mit dem, was getan worden ist. Mich interessiert, was getan werden muß.“

Marie Curie

Table of contents

A. Introduction 1

1. Metal nanoparticles on carbon materials for liquid-phase catalysis 1

2. Synthesis of metal nanoparticles on carbon materials 2

3. Application of various carbon materials for MNP/carbon composites in liquid-phase catalysis 11

4. Conclusion and perspectives 30

5. References 31

B. Main Part 37

1. Carbon-coated, magnetic nanobeads for the synthesis of high-density catalytic systems 37

1.1 The requirement of efficient and economic catalytic systems 37

1.2 Outline 39

1.3 References 40

2. *N*-Alkylimidazole immobilized on high-loading, carbon-coated iron nanobeads as recyclable organocatalyst 41

2.1 Introduction 42

2.2 Results and discussion 43

2.3 Conclusion 51

2.4 Experimental section 52

2.5 References 57

3. Dendrimers or nanoparticles as supports for the design of efficient and recoverable organocatalysts? 59

3.1 Introduction 60

3.2 Results and discussion 61

3.3 Conclusion 69

3.4 Addendum 70

3.5 Experimental section 74

3.6 References 81

4. Palladium nanoparticles supported on ionic liquid modified, magnetic nanobeads – recyclable, high-capacity catalysts for alkene hydrogenation . 83
4.1 Introduction 84
4.2 Results and discussion 85
4.3 Conclusion 98
4.4 Addendum 100
4.5 Experimental section 102
4.6 References 115
5. Towards magnetically recyclable catalysts for C-H activation and olefin metathesis 117
5.1 Palladium nanoparticles supported on Co/C nanobeads for C-H activation 117
5.2 Ionic Liquid modified Co/C nanobeads as Grubbs catalyst precursor for olefin metathesis 120
5.3 Conclusion 123
5.4 Experimental section 124
5.5 References 126
C. Summary 127
D. Zusammenfassung 131
E. List of Abbreviations 135
F. Appendix 139
1. NMR spectra 139
2. HPLC data 147
3. GC data 155
4. List of publications 166
5. Congresses and scientific meetings 167
6. Curriculum vitae 169
G. Acknowledgement 173

A. Introduction

1. Metal nanoparticles on carbon materials for liquid-phase catalysis

Metal nanoparticles (MNPs) received particular interest for their use as catalysts during the last ten to fifteen years. Compared to the bulk metal they offer unique properties such as small size (<100 nm), high-surface-to-volume ratio, and quantum size effects.[1] Many synthetic methods are known for the control of MNPs regarding size, shape, and surface chemistry. The control of these parameters is essential for their efficient application in catalysis. However, making intense efforts for the synthesis of MNPs is not very convenient if the catalysts could not be reused. Hence, much attention is being paid on the immobilization of MNPs on solid supports, generating recoverable and recyclable catalytic systems.

Carbon materials offer several advantages as catalyst supports such as a high surface area, mechanical and chemical stability, tailorable shape and surface properties, low costs, and easy availability.[2] Furthermore, various methods are known to functionalize carbon materials, thus being able to vary the surface properties. These particular benefits predestine carbon materials as supports for metal nanoparticles and their application in catalysis.

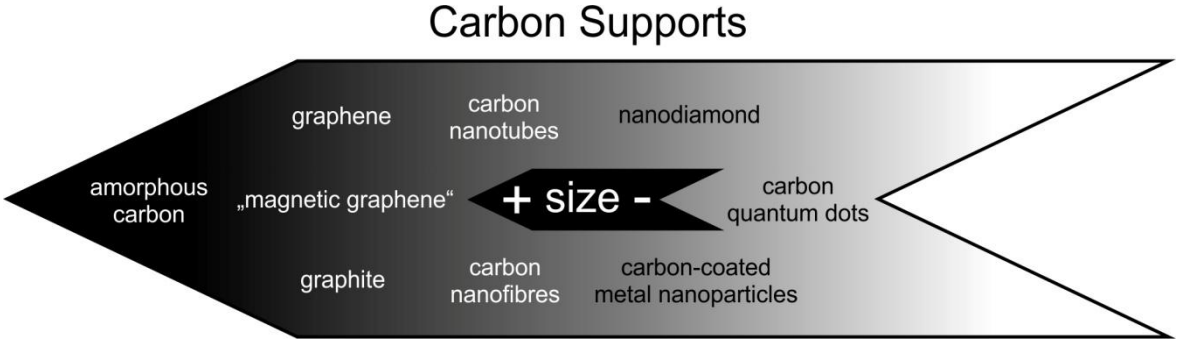

Fig. 1 Outline of carbon supports used for MNP/carbon composites as a function of size.

A lot of different carbon allotropes and modifications are described in the literature generating MNP/carbon composites for their use in fuel cells,[3] chemical sensors,[4] biosensors,[5,6,7] electrodes,[7] or catalysis. However, in this review we will especially focus on MNP/carbon composites for liquid-phase catalytic applica-

tions including e.g. hydrogenation, cross-coupling, oxidation, and photocatalytic reactions. The particular carbon materials used for these purposes are amorphous carbon, carbon nanotubes, graphene and graphene-like materials, mesoporous carbons, nanodiamonds, and “magnetic carbon” materials (Fig. 1).

In the first part we will discuss the preparation methods of MNP/composites and possibilities to tune the synthesis with regard to size, size distribution, and dispersion of MNPs as well as the MNP-support interaction. In the second part we will show the use of MNP/carbon hybrid materials in liquid-phase catalysis with focus on activity, stability, and recyclability.

2. Synthesis of metal nanoparticles on carbon materials

The catalytic activity of metal nanoparticles on a solid support is mainly affected by the preparation method of the material and the interaction between MNP and the support.[8] Applying various supports and different methods in the synthesis one can tune especially size, size distribution, morphology, and dispersion of the particles. These parameters are mainly responsible for the catalytic activity of the prepared composite material. Additionally to the choice of the preparation method, one can also tune the nanoparticle synthesis by (i) modification of the support surface, (ii) the use of specific solvents, agents, or surfactants, and (iii) confining nanoparticles inside the support.

Methods for the preparation of MNP/carbon composites

In the synthesis of carbon-supported metal nanoparticles a variety of different methods were applied in the past. The major ones are: impregnation, deposition-precipitation, electrochemical deposition, and sol or polyol processes. Despite these major methods there are also some others recently described in the literature which were applied in the synthesis of MNP/carbon composites, including laser synthesis,[9] chemical vapor deposition,[10,11] atomic layer deposition,[12] plasma synthesis,[13,14] substrate enhanced electroless deposition (SEED),[15] galvanic displacement,[16] a reduction-etching-reduction sequence,[17] thermolytic pathways,[18,19] or the application of redox/disproportionation processes.[20a,21,20b–d] In the following we discuss the major preparation methods and give recent examples

with focus on size, distribution, and dispersion of the generated carbon-supported MNPs.

In the impregnation method, the support is stirred in a solution of the metal precursor and is subsequently aged and dried. After the drying process the support is either calcined under flexible conditions (rate of heating, temperature, atmosphere, time) or the metal is simply reduced applying a H_2 atmosphere. Two types of impregnation can be distinguished: (i) the “incipient-wetness impregnation”, where the solution volume is smaller or equal to the pore volume and (ii) the “wet impregnation”, where an excess of solution is applied and removed afterwards. Size, morphology, and dispersion of the MNPs in the composite material strongly depend on metal concentration, calcine conditions, and the choice of support. A nice example was recently shown, where platinum particles on porous carbon had a mean size of 5 nm with narrow distribution after reduction at 200 °C and much larger size (up to 100 nm) and wider distribution at 500 °C.[22] Furthermore, Song *et al.*[23] demonstrated that palladium nanoparticles generated by an incipient wetness impregnation method were much smaller on an activated carbon aerogel (average particle size of 11.5 nm) than on commercial activated carbon (28.1 nm). The size difference also greatly effects the catalytic activity, which they demonstrated for the decomposition of 4-phenoxyphenol.

The deposition-precipitation method differs from the impregnation method, as the support stays in solution/dispersion. The carbon-support is stirred in a solution of the metal precursor with subsequent reduction (metal salt precursor) or decomposition (organometallic metal(0) precursor) of the metal compound. For the reduction method a lot of different agents were used in the past, e.g. H_2,[24] $NaBH_4$,[25] hydrazine,[26] formaldehyde,[27] coffee as natural reducing agent,[28] and also photochemical reduction[29] is possible. For the decomposition of an organometallic precursor two different methods were shown in the literature. The decomposition could be done either by thermal or microwave-assisted heating. Urriolabeitia *et al.*[30] showed that microwave heating is not only a faster synthesis method, but also leads to smaller palladium nanoparticles (Fig. 2C) and a more narrow size distribution than with conventional heating (Fig. 2B). Furthermore, a novel effective microwave approach was very recently shown using a solvothermal route under nitrogen overpressure in an autoclave in the presence of low-boiling point alcohols.[31] To our opinion, the microwave synthesis is very promising for the

future synthesis of MNPs on carbon supports. In our group we could also demonstrate the facile microwave synthesis of palladium nanoparticles on magnetic carbon nanobeads exhibiting extremely good catalytic properties (see chapter 3). [32,33]

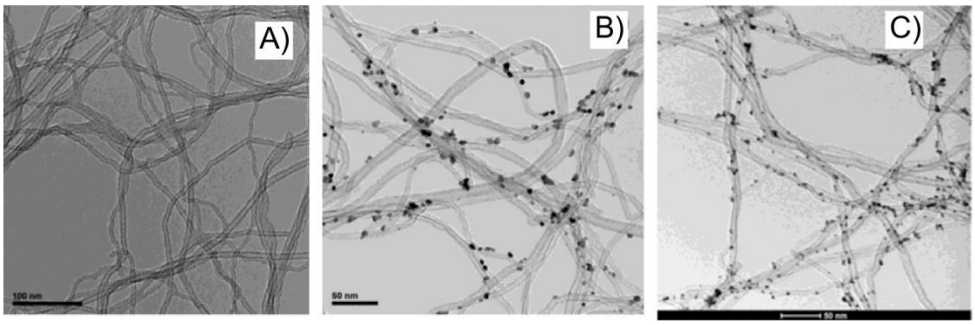

Fig. 2 TEM micrographs of A) pristine MWCNTs and Pd/MWCNT samples prepared in B) conventional heating (21.8 wt% Pd) and C) under microwave irradiation (19.8 wt% Pd). Micrographs show the homogeneous distribution of Pd NPs, with most of the particles in the range of 4-6 nm for conventional heating and in the range of 2-5 nm for microwave heating. Figure adapted with permission from ref [30]. Copyright 2011, Elsevier.

Another method which is applied for the deposition of MNPs on carbon nanotubes, nanodiamonds, and graphene or graphene-like carbon materials is the electrochemical deposition. In this method metal ions are reduced from an electrolyte solution on a substrate which works as an electrode. The substrate could be either the sole carbon material[34] or the carbon material deposited on e.g. silicon wafer substrates.[35,36] Size, size distribution, and dispersion of the nanoparticles can be easily controlled in this method varying the electrolyte concentration and the electrochemical parameters (potential, deposition time). Lemay and coworkers[35] showed that they can obtain small metal clusters (≈6 nm) at low coverage of nanotube side walls at a potential of 0.2 V. However, if they use a negative potential of –0.8 V the coverage with nanoparticles and the size (60-90 nm) increases significantly.

Moreover, the immobilization of MNPs on carbon substrates via the sol process is also widely applied. In this method the nanoparticles are pre-formed in a solvent as a stabilized, metallic sol and subsequently immobilized on the carbon support. The sol can be synthesized from an electrolyte solution containing a capping agent (e.g. sodium dodecyl sulfate (SDS), poly(vinylalcohol) (PVA), or

poly(vinylpyrrolidone) (PVP)) by photochemical reduction[37] or the reduction with e.g. H_2[38] or $NaBH_4$.[39] As the nanoparticles were already pre-formed in this process, the size and distribution in the composite MNP/carbon material is mainly independent of the support.[39] However, there are some exceptions due to agglomeration.[40] To enhance adsorption of the colloid on the carbon support, the solution has to be acidified during the immobilization process.[38] The right choice of acid plays an important role for the accessibility of the metal, thus affecting the catalytic performance (see chapter 3).

Another method which is often applied for various kinds of MNP/carbon nanocomposites is the deposition of nanoparticles via the polyol process. In this process the metal precursor is dissolved in a polyol (usually ethylene glycol), which acts both as the solvent and the reductant. The nanoparticles are usually deposited on the support by thermal[41] or microwave[42] heating. With the polyol process MNPs on carbon materials can be synthesized with small size and narrow distribution. Furthermore, the composite properties are not very much dependent on the carbon support. Platinum nanoparticles on chemically converted graphene showed similar values for the average MNP size (2.75 nm) as well as for the electrochemically surface area (36.27 $m^2 g^{-1}$) compared to platinum NPs on multi-walled carbon nanotubes (3.5 nm and 33.43 $m^2 g^{-1}$).[41]

Surface modification

Despite the choice of the preparation method, it is also possible to tune the nanoparticle synthesis by simply modifying the surface of the carbon support. Different examples are shown in literature to alter carbon surfaces for MNP deposition, e.g. the introduction of defects, a covalent, or a non-covalent functionalization of the carbon surface. These modifications can serve for a more efficient MNP synthesis and, furthermore, can lead to a stabilization of the MNPs for much better catalyst activity and recycling.

The introduction of defects for the synthesis of MNP/carbon composites is most often done by doping the carbon material (CNTs, graphene or graphene-like carbons) with nitrogen[43] or boron.[44] The doping process can be done either directly during the synthesis of the carbon material (“in situ” doping) or by the post-treatment of the material with nitrogen- or boron-containing precursors, e.g. N_2,

NH_3, or $B(OH)_3$ (“post” doping).[45] Generating multiple nitrogen- or boron-defect sites in CNTs or graphenes leads to an excellent environment for anchoring metal nanoparticles. The deposition of MNPs on such doped carbon materials not only enhances the dispersion of MNPs, but also impedes the particle migration, thus increasing the MNP-support interaction. Despite the generation of defects via doping, it is also possible to do this mechanically or by laser irradiation. El-Shall *et al.*[9] very recently showed that palladium nanoparticles on graphene nanosheets show an enhanced catalytic performance and recyclability due to the presence of multiple defect sites generated by laser irradiation. Furthermore, they could demonstrate that defect sites can play an important role for the synthesis of important Fischer-Tropsch synthesis (FTS) catalysts with very high activity and selectivity towards higher hydrocarbons.[46] The importance of defect sites can also be demonstrated by *ab initio* calculations[47] as well as a combination of in situ transmission electron microscopy (TEM), electron tomography (ET), and molecular dynamics (MD) calculations.[48]

Another way for tuning the nanoparticle synthesis is the functionalization of the carbon surface in a covalent or non-covalent way. The simplest way for covalently introducing functional groups on carbon supports is by the use of strong oxidants (e.g. HNO_3, $KMnO_4$, or H_2O_2). However, it is hard to study the real stabilization effect for MNPs using such harsh oxidation agents as a structural collapse of the carbon material is not avoidable. Li and Wang *et al.*[49] overcame this problem using a milder hydrothermal method to oxidize activated carbon without attacking the structure of the carbon material itself. They found out that especially phenolic groups have a high stabilization effect on palladium nanoparticles and, furthermore, enhance the binding energy between the palladium precursor and the carbon surface. After the oxidation process it is also possible to regulate the type and amount of surface oxygen functional groups by simple thermal treatment at varying temperatures.[50] Additionally to phenolic groups, covalently bound amino groups,[51] ionic liquids,[24,33] and dendrimers[52] were shown to effectively stabilize metal nanoparticles. Moreover, they enhance the catalytic activity as well as the recycling ability of the MNP/carbon composite. Besides, it is possible to introduce stabilizing molecules in a non-covalent way taking advantage of hydrophobic or π-π-stacking interactions of oligomeric/aromatic scaffolds with the surface of the carbon support. Examples for oligomeric structures are cyclodextrines,[53]

poly(diallyldimethylammonium chloride) (PDDA),[54] poly[(2-ethyldimethylammonioethyl methacrylate ethyl sulfate)-*co*-(1-vinylpyrrolidone)] (PQ11),[55] or poly(amidoamine) (PAMAM) dendrimers.[56] In addition, poly(pyrrole)[42,57] and poly(aniline) (PANI)[58] were used for a non-covalent functionalization, however, the interaction with the support in these cases relies more on a π-π-stacking interaction as it is the case for phenyl acetic acid,[59] phthalocyanine,[60] and pyrene derivatives.[5,61]

Solvents, agents, and surfactants for stabilization, coordination, linking, and structure-directing purposes

Additionally to the modification of the support, multiple examples are described in the literature where solvents, agents, or surfactants are used for tuning MNP/carbon composite materials. A nice method to form stable dispersions of graphene is by using ionic liquids (e.g. 1-butyl-3-methylimidazolium cholate[62] or 2-hydroxyethanaminium formate[63]) as the solvent which can be done by exfoliating graphite under ultrasound irradiation. Thereby the ionic liquid not only acts as a stabilizing solvent, but it is also beneficial for the formation of extremely small nanoparticles with very narrow size distribution. Furthermore, the resulting composites can exhibit superior catalytic activity and recycling ability.[62]

The MNP stabilization by ionic liquids can also be done by using them as a stabilizing agent in aqueous solution. Liu and Li *et al.*[64] demonstrated the synthesis of well-crystallized noble metal nanoparticles on MWCNTs with tunable diameter, very narrow size distribution (e.g. 1.8-3 nm), and uniform dispersion on the nanotubes. Furthermore, the composite materials exhibit excellent catalytic performances and remarkable size-dependent activity and selectivity. Another way for using ionic liquids as a stabilizing solvent/agent is the application of supported ionic liquid phases (SILPs).[65] Additionally to ionic liquids, sugars or polymers can be used as agents for the stabilization of metal nanoparticles. Jena and coworkers[66] showed the preparation of branched platinum nanostructures on graphene using glucose in aqueous solution as stabilizing agent. The glucose plays an important role by selectively binding to the platinum surface and constructing branched nanostructures from tiny nanoparticles. The platinum nanostructures had an average size of 5.8 nm with high dispersion on the graphene surface and a great num-

ber of branches. Recently, the group of Zhang also published an interesting example combining a polymer as stabilizing agents with *L*-lysine as a linking agent.[67] They deposited noble metal nanoparticles on a magnetic carbon material (magnetite/graphene composite) using *L*-lysine for the linking of nanoparticles to the surface and PVP as stabilizer for the composite in solution. The polymer is additionally crucial for the formation of very small nanoparticles (3-5 nm) and a high dispersion on the support. However, one has to mention that the majority of the nanoparticles are dispersed on magnetite and less on the graphene. Nevertheless, the material shows superior catalytic activity and magnetic recycling ability. Another method to ensure the linking of stabilized metal nanoparticles on a carbon support is the use of alkanethiolates for gold nanoparticles. Zhong *et al.*[68] demonstrated that alkanethiolate monolayer-capped Au NPs form a molecularly mediated assembly on MWCNTs via a combination of hydrophobic and hydrogen-bonding interactions between the capping shell and the nanotube surface (Scheme 1). Using this method an easy control of loading and distribution of MNPs on the support is possible by varying the concentrations of MNPs, MWCNTs, and the stabilizing/linking agent. Another impressive method for the synthesis of gold nanoparticles on a carbon support was most recently published by the group of Wan.[69] They synthesized gold nanoparticles in a “rigid” mesoporous carbon framework applying *co*-polymer F127 as structure-directing and a thiol-containing silane as coordinating agent. In doing so, they got monodispersed Au NPs with small size (≈9 nm) which are highly exposed due to the excellent properties of the carbon framework, thus showing excellent catalytic properties.

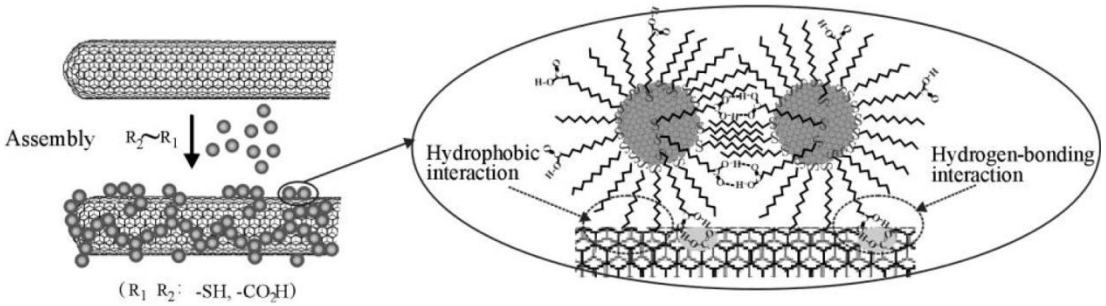

Scheme 1 Schematic illustrations of molecularly mediated assembly of monolayer-capped nanoparticles on CNT. Scheme adapted with permission from ref [68]. Copyright 2004, American Chemical Society.

Another possibility to tune the synthesis of MNP/carbon composites is the use of surfactants, e.g. sodium dodecyl sulfate (SDS). SDS has the interesting property to work as both a reducing agent and a surfactant. The reduction potential of SDS is caused by decomposition to 1-dodecanol upon heating, which is then able to reduce e.g. Pd(II) to Pd(0). SDS was shown to efficiently produce palladium nanoparticles on graphene[70,71] or a magnetite/graphene composite[72] forming Pd or Au NPs of controllable (by varying the SDS concentration) size and homogeneous distribution. Furthermore, the composites show excellent catalytic activity. Besides, there are also other surfactant molecules such as tetradecyltrimethylammonium bromide,[73] dodecanethiol, oleylamine, or 4-dimethylaminopyridine, where SDS in comparison does not always lead to the best results.[74]

Nanoparticle confinement

One additional possibility to tune the MNP synthesis in the case of carbon nanotube supports is by confining the nanoparticles inside the CNT channels. The usual way to adsorb MNPs on carbon nanotubes is on the outer wall of the CNTs (MNP-*out*-CNT) as they are usually closed by hemispherical caps. However, there is also the possibility to encapsulate the particles inside the nanotubes by opening the nanotube ends (MNP-*in*-CNT). This can lead to different properties and chemical reactivities compared to the MNP-*out*-CNT. As a lot of research was done in this area during the last years, it would be far beyond this review to discuss all findings about the confinement in carbon nanotubes. Furthermore, many excellent reviews were already published dealing with the adsorption inside SWCNTs,[75] catalysis in CNTs,[76] and reactions over catalysts confined in CNTs.[77] Therefore, we will just briefly show the possible synthetic methods for confined MNPs, the tuning abilities in the synthesis, and the major benefits of MNP-*in*-CNT for liquid-phase catalytic applications.

As already mentioned above, CNTs have to be opened at the end of the tube before being able to confine metal nanoparticles inside. This is done by oxidation of the CNTs using strong oxidants (e.g. a mixture of HNO_3/H_2SO_4 and subsequently H_2O_2/H_2SO_4), followed by heating of the etched material to high temperatures to remove functional groups from the oxidation process. Without this an-

nealing process, the entering ports for MNPs are hindered. Afterwards, the MNPs can be confined inside the CNTs by (i) wet chemistry methods, (ii) filling of volatile metal precursors, or (iii) in situ filling during arc-discharge growth of CNTs. Wet chemistry methods turned out to be the most simple and versatile ones. Another nice method to drive MNPs inside the CNTs was recently demonstrated by Serp *et al.* (Fig. 3).[78] They introduced hexadecylamine (HAD) on oxidized CNTs via amide bond formation to block the outer wall for π-π-interactions due to the long alkyl-chains. After depositing π-ligand coordinated PtRu NPs on the CNTs, the majority of MNPs was observed on the inner wall of the tubes due to steric hindrance of the alkyl chains combined with hampered π-stacking possibility on the outer wall.

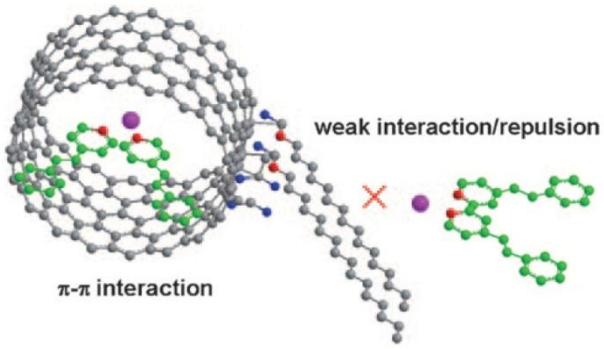

Fig. 3 Strategy adopted to drive NPs into CNTs. PtRu NPs pink, N red, O blue, C gray and green. Figure adapted with permission from ref [78]. Copyright 2009, WILEY-VCH Verlag GmbH & Co. KGaA, Weinheim.

The main advantage of confined MNPs is the restricted space inside the carbon nanotubes. This restricted space and additionally the rigidity of nanotubes is beneficial for the synthesis of particles on the nanoscale or even the sub-nanoscale. Taking advantage of this spatial restriction, one is able to tune the size of MNPs inside nanotube channels by simply choosing CNTs with different diameters (e.g. single-walled CNTs (SWCNT) or double-walled CNTs (DWCNT) with smaller diameter and MWCNTs with larger diameter). Furthermore, this restriction can also hamper the aggregation of the nanoparticles during the synthesis as well as under different reaction conditions. This is crucial regarding the application in catalysis, as nanoparticle aggregation usually leads to a deactivation of the catalytic activity. An interesting example was shown by Bao *et al.*,[79] comparing the

catalytic activity of RhMn NPs inside CNTs (RhMn-*in*-CNT) with RhMn NPs outside CNTs (RhMn-*out*-CNT) in the ethanol production from syngas at 320 °C and 5 MPa. The nanopartilces of RhMn-*in*-CNT with a diameter of 1-3 nm showed a continuous performance in ethanol production even after 112 h time on stream and, furthermore, the nanoparticle size was limited to 4-5 nm which reflects the inner diameter of the CNT. In contrast, NPs of RhMn-*out*-CNT lost in activity and the particles aggregated to a size distribution of 8-10 nm due to the lack of space restriction. Similar observations were found for nanoparticles in Fe-*in*-CNT in the Fischer-Tropsch synthesis.[80] After a reaction time of 125 h at 270 °C the particles on the inner wall remained in the range of 6-11 nm with a very slight shift to larger ones. However, the NPs in Fe-*out*-CNT aggregated significantly to a maximum size of 24 nm. The tuning of MNP-in-CNT by using nanotubes with a small diameter was demonstrated by the group of Pan and Bao.[81] They used DWCNTs with an inner diameter from 1.0 nm to 1.5 nm for the dispersion of titania subnanoclusters. The Ti-*in*-DWCNT composite showed a much higher activity in the epoxidation of propylene by H_2O_2 compared to Ti-*out*-DWCNT.

The possibility to confine metal nanoparticles in a carbon support with restricted space clearly shows an additional advantage for the generation of highly active MNP/carbon composites. Therefore, it seems to be an extremely interesting and promising field for future investigations.

3. Application of various carbon materials for MNP/carbon composites in liquid-phase catalysis

Carbon nanotubes/nanofibres

Besides electrocatalysis and gas-phase reactions (e.g. Fischer-Tropsch synthesis, direct H_2O_2 synthesis, or ammonia decomposition) the main application of MNP/CNT or MNP/CNF composites is in liquid-phase catalysis. Various examples are shown in the literature where the composite materials were applied in oxidation, hydrogenation, or cross-coupling reactions. Especially in hydrogenation reactions selectivity often plays an important role.

E.g. the reduction of phenol (Scheme 2A) is an important challenge in synthetic chemistry as it is often used as a raw material or intermediate in industry.

Ma *et al.*[58] reported the synthesis of palladium nanoparticles on polyaniline-functionalized CNTs or CNFs (Pd-PANI/CNT, Pd-PANI-CNF) for the direct hydrogenation of phenol to cyclohexanone. Compared to palladium nanoparticles supported on activated carbon or solely on PANI or CNTs the activity and selectivity of the reaction towards cyclohexanone was enhanced a lot. While conversions for Pd/AC, Pd/CNT, and Pd/PANI of down to 51% and selectivities down to 87% were observed, both composites Pd-PANI/CNT and Pd-PANI/CNF lead to a excellent conversion and selectivity of >99%.

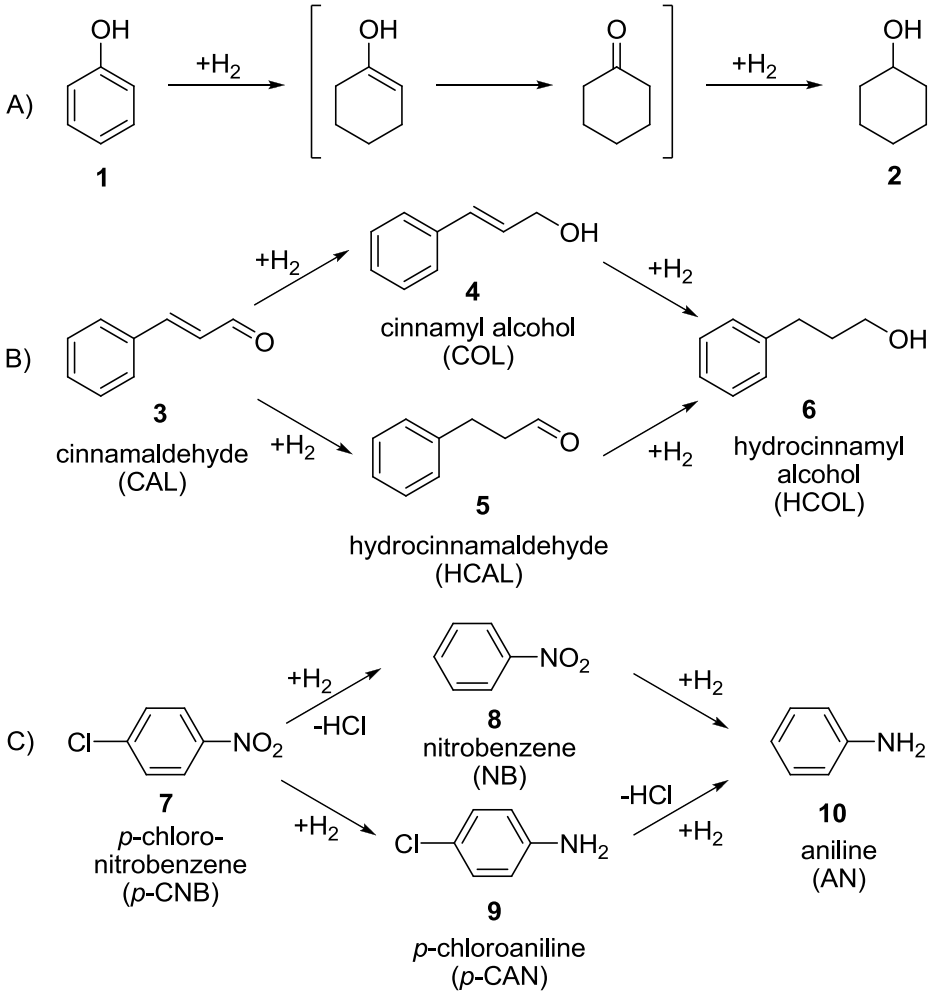

Scheme 2 Hydrogenation pathways of A) phenol, B) cinnamaldehyde, and C) *p*-chloronitrobenzene.

Another basic challenge for industrial synthetic chemistry is the reduction of α,β-unsaturated aldehydes. The hydrogenation of cinnamaldehyde **3** (CAL) was shown in the literature as a typical example due to its two partial hydrogenation products where either the C=O bond (cinnamyl alcohol **4** (COL)) or the C=C bond

(hydrocinnamaldehyde **5** (HCAL)) is selectively reduced (Scheme 2B). Planeix *et al.*[82] reported the first example for a MNP/CNT composite to selectively reduce CAL to COL using ruthenium nanoparticles on CNTs. The nanoparticles with a size range of 3-7 nm on CNTs showed a selectivity of 92% for the C=O reduction at a conversion of 80% of CAL. Most recently, Liu and coworkers[83] also showed an excellent example for the selective hydrogenation of cinnamaldehyde **3**. They prepared Pt/MWCNT as well as Pd/MWCNT composites with average NP sizes of 2.87 nm (Pt NPs) and 3.49 nm (Pd NPs) and investigated the hydrogenation reaction in a CO_2-expanded alcoholic medium. While the Pt/MWCNT nanocatalyst showed a very high selectivity for unsaturated alcohol **4** (97.3% COL at 99.3% CAL conversion), Pd/MWCNT was found to selectively reduce the C=C bond to saturated aldehyde **5** (91.3% HCAL at 98.6% CAL conversion). Furthermore, they could demonstrate that an enhanced CO_2 pressure leads to a better C=O than a C=C reducing performance.

Another class of substrates which are quite often studied for hydrogenations with MNP/CNT hybrids are nitro compounds. Palladium, ruthenium, silver, as well as bimetallic palladium-platinum MNPs were reported for the reduction of various nitro-substrates. p-Chloronitrobenzene **7** (p-CNB) is one example where selectivity of the hydrogenation again plays an important role (Scheme 2C). The groups of Raspolli-Galetti and Serp[84] showed the synthesis of ruthenium NPs on CNTs and CNFs with particle sizes of 4 nm (Ru/CNT) and 3 nm (Ru/CNF) for the hydrogenation of *p*-CNB at 35 bar and 60 °C. Both catalysts showed excellent activity in the reduction reaction compared to commercially available supported Ru-catalysts (Ru/Al_2O_3, Ru/C), while selectivities were slightly lower (92-94% against 96-100%). However, if the CNTs were pretreated with HNO_3, selectivity could be increased to 100% due to a more homogeneous Ru NP dispersion on the support and a stronger interaction of Ru NPs with the surface functional groups.[31] Another example for the selective reduction of nitro compounds was most recently demonstrated by Kim *et al.*[85] who used palladium-platinum bimetallic NPs on functionalized multi-wall carbon nanotubes. Compared to the monometallic catalyst the bimetallic composite shows an enhanced activity as well as excellent chemoselectivity even in the presence of various H_2 labile functional groups. Furthermore, the catalyst could be reused for ten times without significant loss of activity.

Table 1 Hydrogenation of olefins **11** using Pd/IL-MWCNT in [bmim][SbF_6] and recycling of Pd/IL-MWCNT / [bmim][SbF_6].[a]

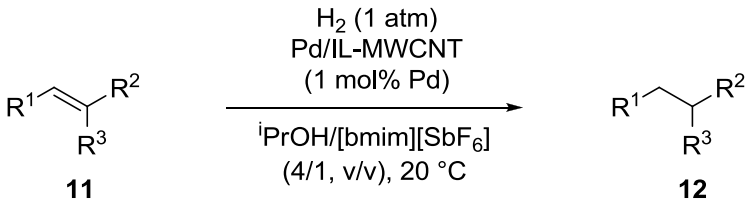

Entry	R^1	R^2	R^3	Reaction time [min]	Runs[b]	Conversion [%][c]
1	Ph	Ph	H	10	1-10	100
2[d]	Ph	H	H	5	11-20	100
3[d]	Ph	Me	H	10	21-30	100
4[d]	Ph	Me	Me	10	31-40	100
5[d]	4-$MeOC_6H_4$	H	H	10	41-50	100
6[d]	4-$MeOC_6H_4$	H	H	10	51	65
7	4-$CF_3C_6H_4$	H	H	5	1-10	100
8	4-ClC_6H_4	H	H	10	1-10	100
9	Ph	CO_2Me	H	15	1-10	100
10	4-Pyridyl	H	H	10	1-10	100

[a] Substrate **11** (1.0 mmol) in ^{i}PrOH-[bmim][SbF_6] (8 mL-2 mL) was hydrogenated under 1 atm of H_2 pressure at 20 °C in the presence of Pd/IL-MWCNT (1 mol% of Pd). [b] The Pd/IL-MWCNT / [bmim][SbF_6] recovered from previous run was used. [c] Determined by GC. [d] Pd/IL-MWCNT / [bmim][SbF_6] recovered from previous run was used and 0.3 mL of [bmim][SbF_6] was additionally added every 20 times reusing.

Moreover, also bimetallic CNT composites are very efficient in the hydrogenation of benzene.[59] Pt-Ru NPs supported on phenylacetic acid functionalized SWCNTs showed a much better catalytic performance than Pt/SWCNT and Ru/SWCNT. Furthermore, the Pt-Ru/SWCNT nanocatalyst was still active after five cycles. A much better recycling ability and probably the best reported for MNP/CNT or MNP/CNF composites so far, was reported for the hydrogenation of alkenes using imidazolium IL stabilized palladium NPs on the surface of MWCNTs

(Pd/IL-MWCNT).[24] The catalytic composite in combination with an ionic liquid in the solvent mixture could be reused 50 times without any loss of activity changing the substrate every 10 runs (Table 1). This amazing stability of the palladium NPs over time is probably due to an extremely good stabilizing effect of imidazolium ionic liquids, which we also observed in our group for palladium NPs on ionic-liquid modified magnetic carbon nanobeads.[33] Besides, there are also examples of transfer hydrogenations,[12] glycerol hydrogenolysis,[86] or the hydrogenation of challenging natural products.[87]

Additionally to hydrogenations MNP/CNT and MNP/CNF composites were also shown to efficiently work in hydroformylations,[10] cross-coupling reactions,[30,74,14] or a cross-coupling/hydrogenation sequence.[65] Rance and Khlobystov *et al.*[74] did interesting investigations about the influence of different CNTs (SWCNTs, DWCNTs, MWCNTs) and CNF as well as different surfactants used in the MNP synthesis on the activity in the Suzuki reaction between 1-iodo-4-nitrobenzene and phenylboronic acid. They found out that a composite material synthesized from MWCNTs and thiolate-stabilized palladium nanoparticles exhibits the best catalytic performance and recyclability with a turn over frequency (TOF) of 51.1 h^{-1} and three recycling runs without significant loss of activity. The group of Urriolabeitia[30] even reported TOFs of up to 80000 h^{-1} in the Heck reaction between iodobenzene and methylacrylate using Pd/MWCNT hybrid materials synthesized in a one-step microwave procedure.

Besides examples with MNP/CNT and MNP/CNF composites with metal nanoparticles on the outer wall, there are a lot of applications of hybrid materials with confined metal nanoparticles used in gas-phase (Fischer-Tropsch synthesis, NH_3 decomposition) and liquid-phase catalysis (hydrogenation, oxidation, and hydroxylation reactions). MNP-*in*-CNT composites can also play an important role for the selective hydrogenation of cinnamaldehyde **3** with very amazing results. Pd-*in*-MWCNT[88] showed the same selectivity as Pd-*out*-MWCNT[83] (reduction of the C=C bond to HCAL) and was furthermore more active and selective compared to Pd NPs on activated carbon. Moreover, Au NPs show the same selectivity as Pd NPs inside carbon nanotubes (91% HCAL at 95% CAL conversion).[89] However, using platinum nanoparticles leads to different results depending on the position of the metal. While Pt-*in*-CNT selectively hydrogenates the C=O bond, Pt-*out*-CNT leads to complete reduction of CAL to HCOL.[90] This is opposite to the observa-

tions of Liu's group who observed just the hydrogenation of the C=C bond for Pt NPs on the outer wall.[89] Bimetallic PtRu NPs inside CNTs also show the selective reduction of the C=O bond as described for Pt-*in*-CNT.[78] In this case selectivity to COL could be even tuned to 100% by increasing the amount of NPs on the inner wall and the loading of NPs. For the relationship of NPs on the inner wall to the COL-selectivity a linear increase could be described.

The group of Tsubaki reported the confinement of copper nanoparticles inside CNTs for the reduction of methyl acetate to ethanol and methanol.[91] They could show that Cu-*in*-CNT is much more active than Cu-*out*-CNT. Furthermore, they demonstrated that especially pre-heated composites with small diameter CNTs lead to an optimal catalytic performance.[92] Not only the diameter but also the length of CNTs plays an important role for the catalytic activity of MNP-in-CNT composites. Li and Li reported an example for Ru-*in*-MWCNT in the hydrogenation of D-glucose, where composites with short length and small diameter MWCNTs are the most active ones.[93]

Despite the higher activity of MNPs on the inner wall compared to MNPs on the outer wall in lots of examples, there is one more big advantage of the NP confinement regarding the metal leaching. Ran *et al.*[94] compared the Ru leaching of Ru-*in*-CNT and Ru-*out*-CNT in the conversion of cellobiose. The starting values for both catalyst with 2.05 wt% for Ru-*in*-CNT and 2.09 wt% for Ru-*out*-CNT were quite close to each other. However, after a reaction time of 3 h the Ru content of Ru-*in*-CNT only slightly decreases (1.73 wt%), whereas the content of Ru-*out*-CNT shows a drop to 1.15 wt% which is almost half of the starting content.

One can clearly see that a lot of impressive results in liquid-phase catalysis of MNP/CNT and MNP/CNF composites were reported in the past. However, there is still a lot of space for the future, regarding especially the use of confined metal nanoparticles with all its beneficial properties for catalytic applications.

Graphene and graphene-like materials

Graphene and related materials were used for catalytic applications numerous times. Especially during the last five years electrochemistry became the main field where MNP/graphene composites were applied for fuel cell or sensor purposes. However, there are also a lot of examples using MNPs on graphene or related ma-

terials in liquid-phase for hydrogenation, cross-coupling, oxidation, or photochemical reactions.

A widely studied reaction using palladium, platinum, gold, or silver nanoparticles on graphene materials is the reduction of 4-nitrophenol **13**. Zhang and Yin[95] most recently showed a nice example of graphene nanosheet (GN) supported Pt NPs which are encapsulated by thin mesoporous silica layers (Table 2). Due to the encapsulation, the Pt/GN hybrid has an isolated and confined space which avoids an aggregation via π-π-stacking of the graphene sheets. Therefore, it exhibits extremely high activity, stability, and recycling ability of the composite material. If the catalyst is deactivated upon feedstock poisoning, it can be even fully recovered by calcination at 350 °C for 1 h in air (Table 2, entry 5). Pd, Ag, and Au NPs on reduced graphene oxide (rGO) furthermore showed excellent activity in the reduction of various nitroaromatic compounds.[21,96] Interestingly, for Pd/rGO composite material on silicium, an increase in activity was observed for a higher palladium loading.[96] Additionally, an activity dependence of the different materials in the order Pd/rGO > Ag/rGO > Au/rGO was reported.[21] However, this observation is not attributed to the kind of metal, but on the size of the nanoparticles with Pd = 0.5-3 nm, Ag = 3-10 nm, and Au = 1-20 nm. Ag nanoparticles on graphite grafted poly(amidoamine) (PAMAM) dendrimers are also extremely active in the reduction of nitrophenols and especially selective in the reduction of halonitroarenes (Scheme 2C) without the dehalogenation to nitrobenzene **8** (NB) or aniline **10** (AN).[56] For gold nanoparticles supported on GN[55] and graphene oxide (GO)[97] two interesting effects could be observed in the hydrogenation reaction of 4-nitrophenol. While Au/rGO modified with temperature-responsive poly(*N*-isopropylacrylamide) (PNIPAM) leads to a thermo-sensitive catalytic activity, the graphene nanosheets of Au/GN enhance the catalytic activity via a synergistic effect. Such an enhanced activity through graphene was also most recently demonstrated by the group of Maser.[98] They synthesized palladium nanoparticles on the surface of rGO for the hydrogenation of acetophenone. Acetophenone is first reduced to 1-phenylethanol, subsequently dehydrated to styrene and in a third step reduced to ethylbenzene. Due to the acidic properties of rGO, the support can play an active role in the dehydratation which leads to a remarkable activity and selectivity of the Pd/rGO hybrid material in this reaction.

Table 2 Conversion of 4-nitrophenol **13** over catalysts containing Pt nanoparticles.[a]

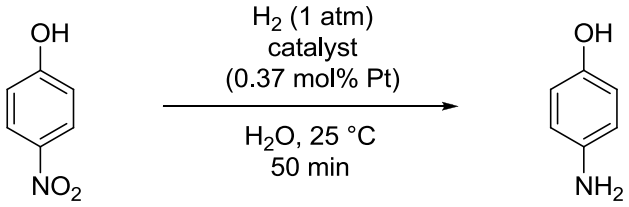

13 **14**

Entry	Catalyst	Conversion [%]
1	Pt/rGO@mSiO$_2$	100
2	Pt/rGO (etched)	87
3	Pt/rGO	25
4	poisoned Pt/rGO@mSiO$_2$[b]	16
5	regenerated Pt/rGO@mSiO$_2$[c]	100

[a] Reaction conditions: catalyst containing Pt nanoparticles (0.002 mmol), 4-nitrophenol **13** (0.54 mmol), and H_2O (25 mL) were mixed and then reacted at 25 °C under H_2 (1 atm) for 50 min. [b] Pt/rGO@mSiO$_2$ was poisoned with MPA. [c] The poisoned Pt/rGO@SiO$_2$ was calcined at 350 °C for 1 h in air.

Another important reaction is the hydrogenation of benzene or other arenes. Platinum, palladium, rhodium, and ruthenium hybrid materials can be used for this transformation. Graphene in this case again turns out to be an excellent support as it exceeds other carbon supports in the catalytic performance.[99] Ru on ionic liquid stabilized graphene is an excellent example for a highly active (TOF = 6000 h^{-1} at 110 °C and 8 MPa) and recyclable (6 runs) hybrid material in the hydrogenation of benzene.[62] The reduction of arenes can be also carried out under green solvent-free conditions.[100]

Mastalir *et al.*[73] reported interesting findings for hydrogenations of alkynes using palladium nanoparticles in graphite oxide. Pd-*in*-graphite oxide can be called a shape-selective catalyst due to the reactant size dependent activity and *cis*-selectivity. While the support is readily accessible for 3-hexyne giving high TOFs (64800-129600 h^{-1}) and *cis*-alkene selectivities (93-98.4%), the reaction for 4-octyne is strongly controlled by mass transport limitations.[101] Furthermore, the

catalytic activity can be modulated by the ratio of interlamellar to external Pd NPs, as the interlamellar particles participate as the active sites.[102]

In addition, Pt NPs were described in hybrid materials with graphite oxide as well as graphene. Applying high pressure in the hydrogenation of styrene, the Pt/graphene composite exhibits high activity compared to Pt/C, however, Pd/C is even more active.[63] An asymmetric variant of alkene hydrogenation is also possible using a chiral modifier. In the hydrogenation of α,β-unsaturated carboxylic acids, Pd NPs on graphene lead to enantioenriched products with *ee*'s up to 49% using cinchonidine as chiral modifier.[25]

Additionally to hydrogenation reactions, graphene hybrid materials were described as catalysts in cross-coupling reactions. Fan *et al.* reported Pd/graphene[71] as well as Au/graphene[70] hybrids in the Suzuki-Miyaura coupling of iodobenzene with phenyl boronic acid under aerobic conditions. In both cases they observed strong particle size dependence for the catalytic activity. The Pd/graphene hybrid furthermore showed excellent activity and recycling ability over 8 runs without significant loss of activity. The group of El-Shall used Pd/graphene[103] and Pd/rGO[9] composites for the Suzuki-Miyaura coupling of bromobenzene with phenyl boronic acid. While Pd/graphene already shows excellent performance with a TOF of 108000 h^{-1}, Pd/rGO even leads to a TOF of 230000 h^{-1} at 120 °C under microwave irradiation. This effect is probably due to the hybrid material synthesis by pulsed laser irradiation, generating defect sites in the graphene which enhances the metal-graphene interaction and therefore play a major role for the catalytic property (see chapter 2). Palladium NPs on graphite oxide were also reported for the use in Suzuki-Miyaura couplings. With TOFs up to 39000 h^{-1} and metal leaching <1 ppm this material exhibits extremely good features compared to Pd/C.[104] In some cases Pd/graphite oxide can even be reused for 16 runs due to the strong interaction of surface functional groups with the nanoparticles.[18] Moreover, graphene oxide can be used to form a 3-dimensional macroporous assembly for palladium NP incorporation.[105] These excellent hybrid materials are shown to be highly active composites in the Heck reaction of iodobenzene with methyl acrylate. Pd NPs synthesized in a facile coreduction with GO work highly active and selective in the Suzuki-Miyaura coupling of aryliodides with arylboronic acids.

Besides hydrogenation and cross-coupling reactions, another application for mainly Au-graphene composites is in oxidation reactions. Au NPs on rGO work very efficiently in the aerobic oxidation of benzyl alcohols,[106] showing even a higher activity than Au/AC and Au/graphite composites mainly due to the presence of surface functional groups.[39] A bimetallic Au-Pd/graphene composite was also reported for the oxidation of methanol to methyl formate at 70 °C exhibiting high acitivity (TOF = 1357 h^{-1}) and selectivity (100%).[107] One example using Ru NPs on GNS is also shown for the aerobic oxidation of various alcohols including aliphatic, aromatic, alicyclic, benzylic, allylic, amino, and heterocyclic alcohols.[108] With an extremely low amount of Ru hybrid material an excellent catalytic performance was observed with high chemoselectivity and recyclability (4 runs).

A last catalytic application of hybrid composites using graphene materials as support is in photocatalysis. Lu *et al.*[109] described the use of platinum nanoparticles on rGO in the photochemical reduction of H_2O. While Eosin Y is used as an additional photo sensitizer, rGO plays a crucial role in the catalytic process. The reduced graphene oxide transfers the electrons from Eosin Y to the metal, preventing a recombination of photoexcited pairs which enhances the photocatalytic activity significantly. Another example was described by Sun *et al.*[29] using a ternary nanohybrid photocatalyst. The hybrid material consists of tin(IV)porphyrin, Ag NPs and rGO and shows excellent activity in the degradation of rhodamin B pollutant and in the reduction of 4-nitrophenol under visible light irradiation.

MNPs on graphene materials can be used in various reaction types and show excellent results in liquid-phase catalysis. Regarding the multiple examples shown above MNP/graphene composites can lead to important applications in future organic synthesis.

Amorphous carbon

Amorphous carbons, including charcoal or activated carbon, are widely known for the deposition of metal clusters and the use of the MNP/carbon composites for catalytic applications. It would be far beyond the scope of this review to discuss all findings and applications of especially palladium on charcoal (Pd/C) in liquid-phase catalysis. Furthermore, the application of Pd/C in Heck, Stille, Suzuki-

Miyaura, Sonogashira, and Negishi couplings was already highlighted in many excellent reviews in the past. Therefore, we will focus on recent investigations of MNP/activated carbon (AC) composites and highlight results which, to our opinion, can play an important role in the future and can lead to new strategies in catalysis and catalyst design.

The activity of MNP/carbon composites which are synthesized via sol process is often decreased due to a hampered accessibility of the MNP surface atoms. Furthermore, the metal-support interaction can be limited if the pH of the sol solution is not acidic enough leading to a decrease in catalytic activity and reusability. Lefferts *et al.*[38] described the immobilization of MNPs on AC via sol process using PVA stabilized Pd NPs and investigated the influence of different acids in the synthetic process. They found out that HCl efficiently suppresses blocking of the Pd surface by PVA and, therefore, highly active Pd/AC composites can be achieved after H_2 reduction at 200 °C. In contrast, H_2SO_4 does not show such a suppressing effect and consequently a remarkable part of the metal surface remains blocked. This leads to an almost 4 times higher reaction rate for HCl pre-treated compared to H_2SO_4 pre-treated Pd/AC in the liquid-phase hydrogenation of nitrite. In gas-phase catalysis this effect is even more significant. Another surface effect in case of Pd/C was recently demonstrated by the group of Shimizu.[110] They studied the effect of oxygen adatoms (O_{ad}) on the surface of Pd with regard to the catalytic activity of Pd/C. Using Pd/C where the palladium was freshly reduced by hydrogen, no activity of the catalyst was observed in the hydration of acetonitrile. However, after air-exposure of Pd/C (now covered with O_{ad}) the hybrid material works as a highly active (TOF up to 82 h^{-1}), recyclable (4 runs), and selective catalyst for various nitriles to the corresponding amides. DFT calculations demonstrated a cooperative mechanism between Pd and O_{ad}, where Bronsted-acidic O_{ad} can dissociate H_2O via hydrogen bonding, being the critical step in this transformation. Besides, O_{ad} does not play a specific role when Ni/C is used as the catalyst.[111] The hybrid material shows excellent activity, selectivity, and recyclability for the hydration of silanes without the need of oxygen adatoms.

Another nice method for tuning Pd/C catalysts for hydrogenation reactions is by modifying the composite with CeO_2.[112] Ceria can enable the reduction of PdO_2 in the synthetic process and promotes the high dispersion of Pd as well as the hydrogen adsorption strength. On the other side, Pd can lower the reduction

temperature of CeO_2, facilitating an easier reduction step of ceria. This synergistic effect leads to a high catalytic performance of the hybrid material compared to sole Pd/C which was demonstrated for the hydrogenation purification of crude caprolactam. The nanocatalyst leads to high-quality ε-caprolactam with 99.9955% purity and a permanganate number of 24000 s. High permanganate numbers indicate a low amount of unsaturated impurities which can be oxidized by $KMnO_4$.

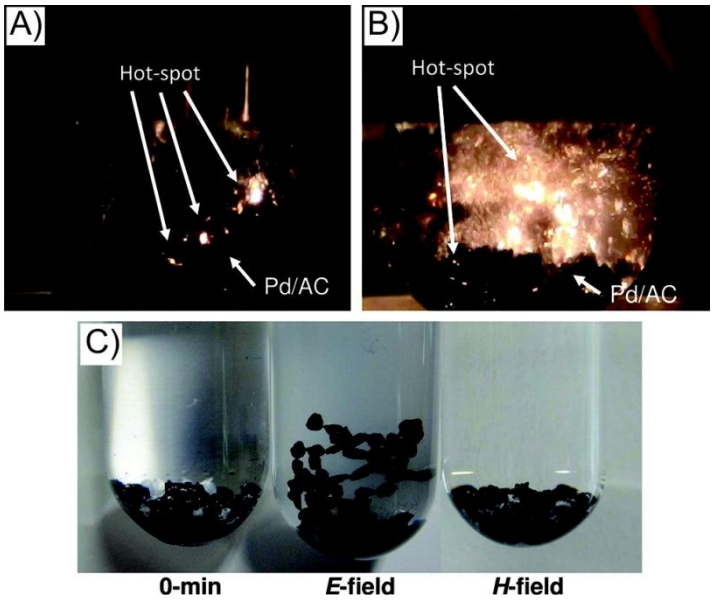

Fig. 4 High-speed camera photographs of the electric discharges occurring on the Pd/AC catalyst surface during the Suzuki-Miyaura coupling reaction under *E*-field conditions: A) 40 s irradiation and B) 120 s irradiation. C) Appearance of the Pd/AC catalyst in solution at 0 min and after 30 min of microwave irradiation under *E*-field and *H*-field conditions. Figure adapted with permission from ref [113]. Copyright 2011, American Chemical Society.

However, not just the material itself can influence the catalytic activity, but also the reaction conditions.[113] Different microwave fields (magnetic, electric) can have a surprising effect on the activity of a Pd/AC catalyst. Microwave irradiation using an electric-field (*E*-field) leads to the generation of multiple hot-spots (electric discharges) at AC (Fig. 4A and 4B), while magnetic-field (*H*-field) irradiation scarcely leads to the formation of hot-spots. These hot-spots can lead to the aggregation of the hybrid material (Fig. 4C), thus leading to a reduced catalytic activity. Pd/AC shows a two times higher activity in the Suzuki-Miyaura coupling of 4-bromotoluene with phenylboronic acid using *H*-field microwave irradiation com-

pared to *E*-field irradiation. Hence, if hot-spots have a negative effect on a catalytic reaction using *E*-field irradiation, one can simply change the conditions to a *H*-field.

Mesoporous carbon

Mesoporous carbon materials have attracted much attention for the synthesis of MNP/carbon composites as they exhibit beneficial properties including periodic micropores, uniform pore size, high surface areas, adequate pore volume, and high stability. These properties reveal mesoporous carbon as an excellent support for metal nanoparticles and their application in catalysis.

Li *et al.*[114] demonstrated an excellent example of ruthenium nanoparticles in ordered mesoporous carbons (CMK-3) for the hydrogenation of benzaldehydes to the corresponding benzylalcohols in H_2O. The material was highly active (TOF up to 947.5 h^{-1}), selective (up to >99.0%), and could be recycled for at least 5 times without significant loss of activity. Due to the outstanding stabilization by CMK-3, the ruthenium leaching was even under the detection limit of inductively coupled plasma optical emission spectrometry (ICP-OES). Furthermore, the composite material exceeded commercial Ru/C and self-prepared Ru/AC.

Mesoporous carbon beads (MBs) can also be used for the preparation of highly active nanocomposites. Pd NPs were synthesized on various MBs displaying different surface properties.[115] The catalysts were tested in the Suzuki-Miyaura coupling between *p*-bromobenzaldehyde and phenylboronic acid under conventional heating. Nanohybrids prepared from MBs with a hydrophilic surface character and less surface microporosity showed the best performance in the cross coupling reaction (TOF up to 649.5 h^{-1}). A significant increase of activity can be achieved by using microwave instead of conventional heating (TOF up to 3236 h^{-1}). Recycling with this novel catalytic system is possible for 10 runs (conventional heating) or 5 runs (microwave heating), respectively.

An excellent example for the oxidation of benzylalcohols by Au nanoparticles in mesoporous carbon materials was recently demonstrated by the group of Wan.[69] They synthesized AuNPs in a “rigid” mesoporous carbonaceous framework via coordination assisted approach (see chapter 2). The novel nanocatalyst showed high selectivity, reusability (5 runs), and poison resistance. If the reaction

is carried out with a molar ratio of thiocyanate:Au of 33, the catalyst still shows 37% activity. The extremely good catalytic performance of the hybrid system can be explained through the aggregation-free MNPs, the highly exposed surface atoms, and the confinement of MNPs inside the mesoporous carbon framework.

The catalytic examples of different MNPs in mesoporous carbon framework clearly show the advantages of such support materials for catalytic applications. Hence, they have enormous perspectives for the future.

Diamond nanoparticles and carbon quantum dots

Nanosized diamond materials reached great interest for catalytic applications especially during the last three years. The diamond nanoparticles (npD) consist of sp^3-hybridized carbon atoms, are crystalline, highly chemically stable, and affordable. Commercial nanodiamond is usually purified prior to use, e.g. by Fenton treatment or light combustion.[116] While the Fenton treatment needs large amounts of H_2O_2 and Fe(II) salts, light combustion is a much milder method. Through this purification, amorphous carbonaceous soot is removed, particles deagglomerate, and the population of surface hydroxyl groups is greatly increased (HO-npD). Hydrogen annealing of the purified nanodiamond leads to an even higher amount of surface hydroxyl groups by the reduction of C=O bonds, thus generating more anchoring sites for MNPs.[117] For the application of MNP/npD hybrid materials in catalysis mainly Cu and Au nanoparticles were used so far.

One main application of MNP/HO-npD hybrid materials is in the degradation of organic pollutants by hydroxyl radicals (Fenton reaction). The generation of hydroxyl radicals from hydrogen peroxide is usually done with Fe(II) or Cu(II). However, Garcia *et al.*[118] reported that Au NPs on HO-npD can also efficiently reduce hydrogen peroxide to hydroxyl radicals, which can be used for the degradation of e.g. phenol (Scheme 3). The generated Au^{3+} is then simply reoxydized by another hydrogen peroxide molecule. Au/HO-npD composites show extremely high activity (TON up to 458759) and selectivity (up to 79%) in the Fenton reaction, working in a pH range between 3.5 and 4.0.[119] However, below a pH of 3.5 gold leaching is considerably high and above a pH of 4.0 the catalytic activity is dramatically decreased. This problem can be solved by the use of visible light irradiation for electron injection, avoiding the need of an acidic pH.[120] The irradiation with light fur-

thermore decreases the amount of hydrogen peroxide which is needed for the Fenton reaction being another crucial point. This effect can be even strengthened by the combination of a catalytic Fenton reaction with biological degradation, requiring just 4 equivalents of hydrogen peroxide.[121]

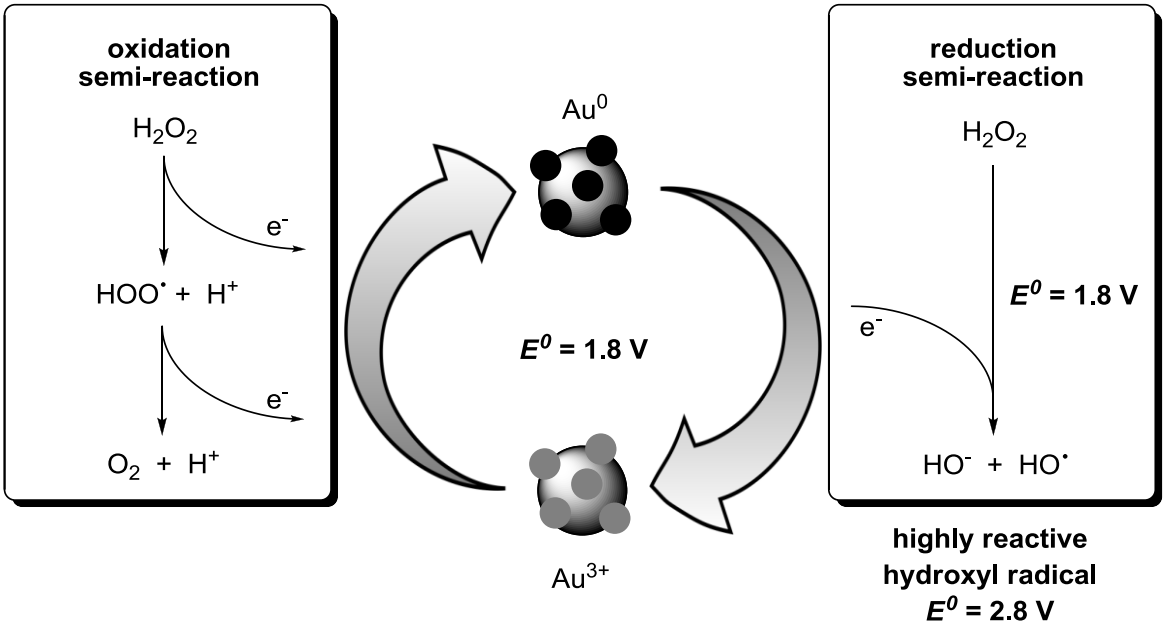

Scheme 3 Proposed mechanism for phenol degradation with Au/HO-npD and H_2O_2.[118]

The group of Garcia further showed the use Cu/HO-npD as efficient and cheap catalyst for the hydrogenation of alkenes[122] and the oxidation of aromatic thiols.[123] Hydrogen annealing of the catalyst was demonstrated to play a beneficial role for the catalyst activity due to the before mentioned enhancement of surface hydroxyl groups. Furthermore, Cu/HO-npD turned out to be more active in the hydrogenation of styrene than analogous Au- and Pd-composites and Cu-composites of activated carbon, graphene, or multi-walled carbon nanotubes. However, in the aerobic oxidation of aromatic thiols to the corresponding disulfides, Au/HO-npD exhibited somewhat a higher catalytic activity. As the Cu-nanocatalyst also shows good recyclability, this catalytic system is an extremely good alternative compared to expensive Pd- or Au-catalysts.

A Pd/npD nanocatalyst was reported by the group of Golubina for the hydrodechlorination of 1,3,5-trichlorbenzene.[124] This nanocomposite showed high activity and selectivity towards benzene compared to selfmade Pd/C as well as commercial Pd/C. The excellent activity is again based on the high amount of sur-

face hydroxyl groups, thus leading to an excellent coordination of the metal nanoparticles.

Besides diamond nanoparticles, carbon quantum dots (CQDs) were used as a nano-support for the deposition of MNPs. Kang *et al.*[125] developed a green photocatalytic system applying a Au/CQD composite material. This nanocatalyst shows an impressive efficiency (63.8% conversion) and selectivity (>99.9%) in the visible light driven oxidation of cyclohexane to cyclohexanone using hydrogen peroxide as oxidant. Au/CQD exceeded other nanocatalysts including Au/SiO_2, Au/CNT, Au/graphene, and Au/graphite in activity and selectivity by far. The remarkable activity of the Au/CQD composite is explained by the enhanced absorption capacity of the MNP by surface plasmon resonance, an efficient hydroxyl radical production by H_2O_2 decomposition (Scheme 3), and a particular interaction between CQDs and the metal nanoparticle under visible light.

Results with diamond nanoparticles and carbon quantum dots clearly demonstrate benefits of these nanosupports for their use in MNP/carbon composites. Therefore, these novel nanomaterials will play a major role in future applications for liquid-phase catalysis.

“Magnetic carbon”

For the separation and recycling of carbon materials usually filtration or centrifugation techniques are needed. These methods are not only time-consuming, but on larger scale also energy- and cost-intense. One possibility to solve this problem is the use of a “magnetic carbon” material, which can be easily separated from the reaction mixture by simple magnetic decantation. Especially in the last three years such “magnetic carbon” materials were reported for the preparation of MNP/carbon composites and their application in liquid-phase catalysis.

Fe_3O_4-graphene composite materials are examples for such magnetic carbons (Fig. 5, **15**). The preparation of a MNP hybrid material of these magnetic carbons could be done in two possible ways. Either magnetite is first deposited on graphene with subsequent NP synthesis on the surface (MNP/Fe_3O_4@graphene), or the nanoparticles are first generated on the graphene surface with subsequent deposition of Fe_3O_4 (Fe_3O_4/MNP@graphene). While MNPs in case of Fe_3O_4/MNP@graphene are directly adsorbed on the carbon surface,[126] they are

mostly deposited around[127] or even directly on[67] the magnetite surface in MNP/Fe_3O_4@graphene composites. Nanocatalysts of Pd, Pt, PdPt, Ag, and Au were applied in hydrogenation,[128,127,67,126] cross-coupling,[72] and oxidation[129] reactions with good catalytic performances and recycling ability. The latter is due to the high saturation magnetization (e.g. 37.84 emu g^{-1} for Fe_3O_4@rGO),[129] however, if the Fe_3O_4 loading is very low the magnetic separation ability is apparently weakened.[72] A Au/Fe_3O_4@GO composite for example could be magnetically recycled for 10 times and was even more active than corresponding Au hybrids with GO, Fe_3O_4, or Fe_3O_4/SiO_2.[127] Comparing Pd and bimetallic PdPt on Fe_3O_4@graphene, the Pd composite showed higher catalytic activity (TOF up to 5294 h^{-1}), however, the recycling ability of PdPt/Fe_3O_4@graphene is much better due to a better poisoning resistance.[67]

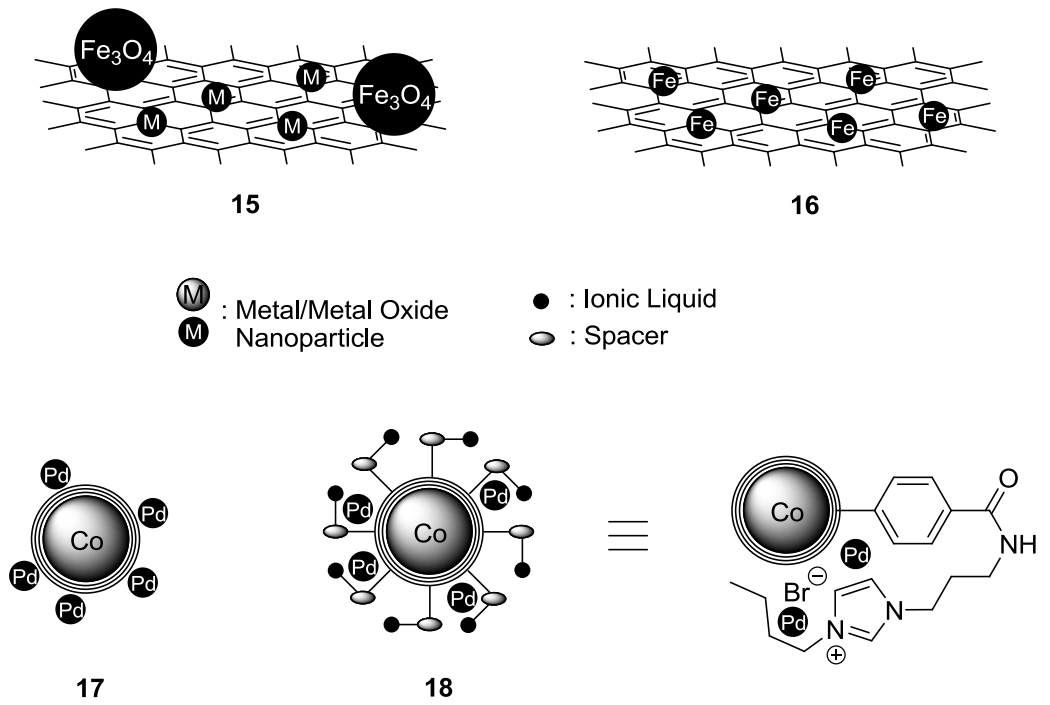

Fig. 5 Various “magnetic carbon” materials: MNPs on magnetite modified graphene **15**, Fe NPs on graphene **16**, and Pd NPs supported on Co/C nanobeads **17** or ionic-liquid-modified Co/C nanobeads **18**.

Another example of a “magnetic graphene” composite is FeNPs on the surface of graphene (Fig. 5, **16**), which act both as the catalytic species as well as the magnetic species. Fe/CDG composites were efficiently used for the hydrogenation of olefins[130] and the oxidative cyanation of tertiary amines.[131] In hydrogenation

reactions the hybrid material showed good results for terminal and cyclic olefins under 20 bar H_2 pressure and 100 °C. However, internal double bonds of acyclic systems were not or little hydrogenated and recycling was just demonstrated for 2 runs. In the oxidative cyanation of tertiary amines to the corresponding α-aminonitriles using hydrogen peroxide with sodium cyanide, the hybrid system gave excellent yields, was easily recyclable and no leaching was observed.

Li *et al.*[132] also reported a nice example of a magnetic carbon material, using Fe@Pd core-shell nanoparticles on activated carbon. They first synthesized Fe NPs on activated carbon, which are in a second step coated with Pd NPs leading to a hybrid catalyst with high saturation magnetization (14 emu g^{-1}). The material showed good results in the Suzuki-Miyaura coupling of phenylboronic acid with various aryliodides and –bromides. Magnetic recycling was possible for 5 times without significant loss of activity and minor metal leaching. After 5 runs still 92% of the metal was retained on the support.

Besides the immobilization of a magnetic species on the surface of carbon materials, there is also the possibility to obtain a “magnetic carbon” by simply coating magnetic particles with a carbon shell. The magnetic core is thereby protected against oxidation, acids, bases, and high temperature. Wang et al.[133] demonstrated an example where they used carbon coated Fe_3O_4 microspheres, synthesized from Fe_3O_4 by hydrothermal treatment using glucose as the carbon source. The hybrid material has a saturation magnetization of 9.7-13 emu g^{-1} depending on the thickness of the carbon shell. Pd NPs on the Fe_3O_4/C hybrid work efficiently in the reduction of methyl orange with $NaBH_4$. The composite even gave better results than Pd/C, however, due to catalyst loss and NP aggregation the reaction time had to be increased during recycling.

In our group we established the use of carbon coated cobalt nanoparticles as a magnetic carbon support.[134] The material exhibits excellent magnetic properties with a saturation magnetization of 158 emu g^{-1}, being almost the same as for bulk cobalt. Furthermore, the material can be synthesized on a very large-scale (>30 g h^{-1}) in a reducing flame synthesis. We applied those Co/C nanoparticles for the deposition of Pd NPs (Fig. 5, **17**) using two different methods, where the microwave synthesis via decomposition of $Pd_2(dba)_3 \cdot CHCl_3$ leads to the best results.[32] For the hydrogenation of *trans*-stilbene in ^{i}PrOH it turned out that a low loading of Pd leads to the best catalytic performance and even exceeds common

Pd/C by far (Table 3). The catalyst shows extremely high activity (TOF up to 11095 h^{-1}) in the hydrogenation of various di- or trisubstituted alkenes and nitro-compounds, is separable within seconds, and showed just little metal leaching (≤6 ppm/cycle). However, the composite material suffers from agglomeration of the Pd NPs over time, which allows only small Pd loadings (<1 wt%) and decreases activity upon recycling and reuse.

Table 3 Hydrogenation of *trans*-stilbene **11a** using Pd@Co/C **17** or Pd/C.[a]

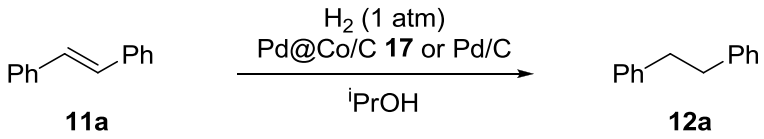

11a **12a**

Entry	Catalyst	Pd [wt%]	Catalyst [mol%]	t [min]	Conversion [%][b]	TOF [h^{-1}][c]
1	**17**	8.8	0.1	60	30	300
2	**17**	4.4	0.1	60	67	670
3	**17**	1.6	0.1	60	98	980
4	**17**	0.8	0.1	40	96	2015
5	**17**	0.2	0.1	10	64	3845
6[d]	**17**	0.2	0.01	60	100	11095
7	Pd/C	1.8	0.1	60	59	585

[a] Stilbene **11a** (0.5 mmol) in ^{i}PrOH (5 mL) was hydrogenated by 0.5 µmol (0.1 mol%) or 0.05 µmol (0.01 mol%) of catalyst using dodecane as internal GC standard. [b] Determined by GC analysis using internal standard. [c] Mol of substrate transformed per mol catalyst per hour. [d] 10 bar of H_2 pressure.

Therefore, we covalently introduced stabilizing ionic liquids on the surface of the supports to further stabilize Pd nanoparticles (Fig. 5, **18**).[33] Indeed, we could demonstrate that a quite flexible ionic liquid leads to an excellent stabilization of Pd NPs allowing much higher metal loadings (up to 43 wt%) and recycling runs (12 times). Furthermore, recycling experiments are possible by changing the substrate after each run. This high-capacity system is especially attractive for large-scale applications as one can produce 30 mol of product applying just 1 g of the catalyst.

The use of MNPs on “magnetic carbon” materials clearly shows the advantages of those hybrid materials regarding the ease of separation and the high recycling ability. This seems to our opinion a very promising field of research and would be especially attractive for the use in industrial applications, reducing time and costs for intense filtration/centrifugation techniques.

4. Conclusion and perspectives

This review clearly shows the unique benefits of carbon materials for their use as MNP supports. The chemical properties of MNP/carbon composites which are crucial for their use in catalysis can be controlled by the choice of carbon support, the preparation method, and additional synthetic skills. These include the modification of the carbon surface, the use of specific agents, solvents or surfactants in the MNP synthesis, and the confinement of MNPs inside the carbon material. Some excellent features are described for the generation of highly active hybrid materials including especially the use of microwave irradiation or the confinement of MNPs in CNTs. Applying these possibilities, one can tune the size, size distribution, morphology, and dispersion of the MNPs on the carbon supports. In the second part we demonstrate how these specific composite properties effect the applications in liquid-phase catalysis with focus on activity, stability and recyclability of the hybrid catalysts. The results show that not just the preparation method for the MNPs is an important factor, but also the choice of the support. Especially the use of novel materials like nanodiamond or “magnetic carbon” materials demonstrate excellent performance in catalysis and will probably play a very important role in catalysis in the future.

5. References

[1] M. Zahmakıran, S. Özkar, *Nanoscale* **2011**, *3*, 3462–3481.

[2] a) A. Schaetz, M. Zeltner, W. J. Stark, *ACS Catal.* **2012**, *2*, 1267–1284; b) D. S. Su, S. Perathoner, G. Centi, *Chem. Rev.* **2013**, *113*, 5782–5816.

[3] a) H. Gao, Y. Wang, F. Xiao, C. B. Ching, H. Duan, *J. Phys. Chem. C* **2012**, *116*, 7719–7725; b) B. Seger, P. V. Kamat, *J. Phys. Chem. C* **2009**, *113*, 7990–7995; c) E. Yoo, T. Okada, T. Akita, M. Kohyama, I. Honma, J. Nakamura, *J. Power Sources* **2011**, *196*, 110–115.

[4] S. Guo, D. Wen, Y. Zhai, S. Dong, E. Wang, *ACS Nano* **2010**, *4*, 3959–3968.

[5] W. Hong, H. Bai, Y. Xu, Z. Yao, Z. Gu, G. Shi, *J. Phys. Chem. C* **2010**, *114*, 1822–1826.

[6] a) B. Jiang, M. Wang, Y. Chen, J. Xie, Y. Xiang, *Biosens. Bioelectron.* **2012**, *32*, 305–308; b) J. Lu, I. Do, L. T. Drzal, R. M. Worden, I. Lee, *ACS Nano* **2008**, *2*, 1825–1832.

[7] F. Xiao, J. Song, H. Gao, X. Zan, R. Xu, H. Duan, *ACS Nano* **2012**, *6*, 100–110.

[8] L. Prati, A. Villa, *Catalysts* **2012**, *2*, 24–37.

[9] S. Moussa, A. R. Siamaki, B. F. Gupton, M. S. El-Shall, *ACS Catal.* **2012**, *2*, 145–154.

[10] H. Zhang, J. Qiu, C. Liang, Z. Li, X. Wang, Y. Wang, Z. Feng, C. Li, *Catal. Lett.* **2005**, *101*, 211–214.

[11] a) J. P. O'Byrne, R. E. Owen, D. R. Minett, S. I. Pascu, P. K. Plucinski, M. D. Jones, D. Mattia, *Catal. Sci. Technol.* **2013**, *3*, 1202–1207; b) M. Ran, Y. Liu, W. Chu, Z. Liu, A. Borgna, *Catal. Commun.* **2012**, *27*, 69–72.

[12] C. Jiang, X. Liang, *Catal. Commun.* **2014**, *46*, 41–45.

[13] J. Kang, O. L. Li, N. Saito, *Nanoscale* **2013**, *5*, 6874–6882.

[14] F. Yang, Y. Li, T. Liu, K. Xu, L. Zhang, C. Xu, J. Gao, *Chem. Eng. J.* **2013**, *226*, 52–58.

[15] L. Qu, L. Dai, *J. Am. Chem. Soc.* **2005**, *127*, 10806–10807.

[16] L. Qu, L. Dai, E. Osawa, *J. Am. Chem. Soc.* **2006**, *128*, 5523–5532.

[17] J. Yang, C. Tian, L. Wang, T. Tan, J. Yin, B. Wang, H. Fu, *ChemPlusChem* **2012**, *77*, 301–307.

[18] S. Santra, P. K. Hota, R. Bhattacharyya, P. Bera, P. Ghosh, S. K. Mandal, *ACS Catal.* **2013**, *3*, 2776–2789.

[19] X. Ni, B. Zhang, C. Li, M. Pang, D. Su, C. T. Williams, C. Liang, *Catal. Commun.* **2012**, *24*, 65–69.

[20] a) K. Y. Lee, M. Kim, Y. W. Lee, J.-J. Lee, S. W. Han, *Chem. Phys. Lett.* **2007**, *440*, 249–252; b) X. Zhou, X. Huang, X. Qi, S. Wu, C. Xue, Boey, Freddy Y. C., Q. Yan, P. Chen, H. Zhang, *J. Phys. Chem. C* **2009**, *113*, 10842–10846; c) H. Sharghi, R. Khalifeh, M. M. Doroodmand, *Adv. Synth. Catal.* **2009**, *351*, 207–218; d) H. Sharghi, R. Khalifeh, S. G. Mansouri, M. Aberi, M. M. Eskandari, *Catal. Lett.* **2011**, *141*, 1845–1850.

[21] M.-Q. Yang, X. Pan, N. Zhang, Y.-J. Xu, *CrystEngComm* **2013**, *15*, 6819–6828.

[22] F. Alonso, P. Riente, F. Rodríguez-Reinoso, J. Ruiz-Martínez, A. Sepúlveda-Escribano, M. Yus, *ChemCatChem* **2009**, *1*, 75–77.

[23] H. W. Park, U. G. Hong, Y. J. Lee, I. K. Song, *Appl. Catal., A* **2011**, *409-410*, 167–173.

[24] Y. S. Chun, J. Y. Shin, C. E. Song, S.-g. Lee, *Chem. Commun.* **2008**, 942–944.

[25] K. Szőri, R. Puskás, G. Szőllősi, I. Bertóti, J. Szépvölgyi, M. Bartók, *Catal. Lett.* **2013**, *143*, 539–546.

[26] R. Wojcieszak, M. Zieliński, S. Monteverdi, M. M. Bettahar, *J. Colloid Interface Sci.* **2006**, *299*, 238–248.

[27] S. Bawaked, Q. He, N. F. Dummer, A. F. Carley, D. W. Knight, D. Bethell, C. J. Kiely, G. J. Hutchings, *Catal. Sci. Technol.* **2011**, *1*, 747–759.

[28] P. Duffy, L. A. Reynolds, S. E. Sanders, K. M. Metz, P. E. Colavita, *Mater. Chem. Phys.* **2013**, *140*, 343–349.

[29] H. Li, Y. Zhang, G. Chang, S. Liu, J. Tian, Y. Luo, A. M. Asiri, A. O. Al-Youbi, X. Sun, *ChemPlusChem* **2012**, *77*, 545–550.

[30] M. Cano, A. Benito, W. K. Maser, E. P. Urriolabeitia, *Carbon* **2011**, *49*, 652–658.

[31] C. Antonetti, M. Oubenali, A. M. Raspolli Galletti, P. Serp, G. Vannucci, *Appl. Catal., A* **2012**, *421-422*, 99–107.
[32] Q. M. Kainz, R. Linhardt, R. N. Grass, G. Vilé, J. Pérez-Ramírez, W. J. Stark, O. Reiser, *Adv. Funct. Mater.* **2013**, DOI: 10.1002/adfm.201303277.
[33] R. Linhardt, Q. M. Kainz, R. N. Grass, W. J. Stark, O. Reiser, *RSC Adv.* **2014**, *4*, 8541–8549.
[34] T. Maiyalagan, X. Dong, P. Chen, X. Wang, *J. Mater. Chem.* **2012**, *22*, 5286–5290.
[35] B. M. Quinn, C. Dekker, S. G. Lemay, *J. Am. Chem. Soc.* **2005**, *127*, 6146–6147.
[36] L. La-Torre-Riveros, K. Soto, M. A. Scibioh, C. R. Cabrera, *J. Electrochem. Soc.* **2010**, *157*, B831–B836.
[37] Z. Li, D. Huang, R. Xiao, W. Liu, C. Xu, Y. Jiang, L. Sun, *Curr. Nanosci.* **2012**, *8*, 26–28.
[38] Y. Zhao, L. Jia, J. A. Medrano, Ross, Julian R. H., L. Lefferts, *ACS Catal.* **2013**, *3*, 2341–2352.
[39] X. Yu, Y. Huo, J. Yang, S. Chang, Y. Ma, W. Huang, *Appl. Surf. Sci.* **2013**, *280*, 450–455.
[40] M. Sankar, N. Dimitratos, D. W. Knight, A. F. Carley, R. Tiruvalam, C. J. Kiely, D. Thomas, G. J. Hutchings, *ChemSusChem* **2009**, *2*, 1145–1151.
[41] Y. Li, W. Gao, L. Ci, C. Wang, P. M. Ajayan, *Carbon* **2010**, *48*, 1124–1130.
[42] S. Yang, C. Shen, Y. Liang, H. Tong, W. He, X. Shi, X. Zhang, H.-j. Gao, *Nanoscale* **2011**, *3*, 3277–3284.
[43] a) R. Lv, T. Cui, M.-S. Jun, Q. Zhang, A. Cao, D. S. Su, Z. Zhang, S.-H. Yoon, J. Miyawaki, I. Mochida et al., *Adv. Funct. Mater.* **2011**, *21*, 999–1006; b) R. Imran Jafri, N. Rajalakshmi, S. Ramaprabhu, *J. Mater. Chem.* **2010**, *20*, 7114–7117; c) L.-S. Zhang, X.-Q. Liang, W.-G. Song, Z.-Y. Wu, *Phys. Chem. Chem. Phys.* **2010**, *12*, 12055–12059.
[44] X. Bo, M. Li, C. Han, L. Guo, *Electrochim. Acta* **2013**, *114*, 582–589.
[45] L. F. Mabena, S. Sinha Ray, S. D. Mhlanga, N. J. Coville, *Appl. Nanosci.* **2011**, *1*, 67–77.
[46] S. O. Moussa, L. S. Panchakarla, M. Q. Ho, M. S. El-Shall, *ACS Catal.* **2014**, *4*, 535–545.
[47] G. Kim, S.-H. Jhi, *ACS Nano* **2011**, *5*, 805–810.
[48] M. S. Moldovan, H. Bulou, Y. J. Dappe, I. Janowska, D. Bégin, C. Pham-Huu, O. Ersen, *J. Phys. Chem. C* **2012**, *116*, 9274–9282.
[49] T.-y. Xu, Q.-f. Zhang, H.-f. Yang, X.-n. Li, J.-g. Wang, *Ind. Eng. Chem. Res.* **2013**, *52*, 9783–9789.
[50] C. Li, Z. Shao, M. Pang, C. T. Williams, C. Liang, *Catal. Today* **2012**, *186*, 69–75.
[51] a) D.-j. Guo, H.-l. Li, *Electrochem. Commun.* **2004**, *6*, 999–1003; b) Y. N. Jeong, M. Y. Choi, H. C. Choi, *Electrochim. Acta* **2012**, *60*, 78–84.
[52] E. Murugan, G. Vimala, *J. Colloid Interface Sci.* **2013**, *396*, 101–111.
[53] A. Denicourt-Nowicki, A. Roucoux, F. Wyrwalski, N. Kania, E. Monflier, A. Ponchel, *Chem. Eur. J.* **2008**, *14*, 8090–8093.
[54] a) Y. Shao, S. Zhang, C. Wang, Z. Nie, J. Liu, Y. Wang, Y. Lin, *J. Power Sources* **2010**, *195*, 4600–4605; b) S. Wang, X. Wang, S. P. Jiang, *Phys. Chem. Chem. Phys.* **2011**, *13*, 6883–6891; c) J.-D. Qiu, G.-C. Wang, R.-P. Liang, X.-H. Xia, H.-W. Yu, *J. Phys. Chem. C* **2011**, *115*, 15639–15645.
[55] X. Qin, W. Lu, Y. Luo, G. Chang, A. M. Asiri, A. O. Al-Youbi, X. Sun, *J. Nanosci. Nanotech.* **2012**, *12*, 2983–2989.
[56] R. Rajesh, R. Venkatesan, *J. Mol. Catal. A: Chem.* **2012**, *359*, 88–96.
[57] Y. Zhao, L. Zhan, J. Tian, S. Nie, Z. Ning, *Electrochim. Acta* **2011**, *56*, 1967–1972.
[58] J. Chen, W. Zhang, L. Chen, L. Ma, H. Gao, T. Wang, *ChemPlusChem* **2013**, *78*, 142–148.
[59] Y.-J. Liao, H.-B. Pan, C. M. Wai, *J. Nanosci. Nanotech.* **2011**, *11*, 8580–8585.
[60] J.-P. Zhong, Y.-J. Fan, H. Wang, R.-X. Wang, L.-L. Fan, X.-C. Shen, Z.-J. Shi, *Electrochim. Acta* **2013**, *113*, 653–660.
[61] L. Li, J. Zhang, Y. Liu, W. Zhang, H. Yang, J. Chen, Q. Xu, *ACS Sustainable Chem. Eng.* **2013**, *1*, 527–533.
[62] W. Xiao, Z. Sun, S. Chen, H. Zhang, Y. Zhao, C. Huang, Z. Liu, *RSC Adv.* **2012**, *2*, 8189–8193.
[63] J.-Y. Lee, T.-Y. Yung, L.-K. Liu, *Nanoscale Res. Lett.* **2013**, *8*, 414–419.

[64] H. Chu, Y. Shen, L. Lin, X. Qin, G. Feng, Z. Lin, J. Wang, H. Liu, Y. Li, *Adv. Funct. Mater.* **2010**, *20*, 3747–3752.
[65] L. Rodríguez-Pérez, C. Pradel, P. Serp, M. Gómez, E. Teuma, *ChemCatChem* **2011**, *3*, 749–754.
[66] S. C. Sahu, A. K. Samantara, B. Satpati, S. Bhattacharjee, B. K. Jena, *Nanoscale* **2013**, *5*, 11265–11274.
[67] X. Li, X. Wang, S. Song, D. Liu, H. Zhang, *Chem. Eur. J.* **2012**, *18*, 7601–7607.
[68] L. Han, W. Wu, F. L. Kirk, J. Luo, M. M. Maye, N. N. Kariuki, Y. Lin, C. Wang, C.-J. Zhong, *Langmuir* **2004**, *20*, 6019–6025.
[69] S. Wang, Q. Zhao, H. Wei, J.-Q. Wang, M. Cho, H. S. Cho, O. Terasaki, Y. Wan, *J. Am. Chem. Soc.* **2013**, *135*, 11849–11860.
[70] Y. Li, X. Fan, J. Qi, J. Ji, S. Wang, G. Zhang, F. Zhang, *Mater. Res. Bull.* **2010**, *45*, 1413–1418.
[71] Y. Li, X. Fan, J. Qi, J. Ji, S. Wang, G. Zhang, F. Zhang, *Nano Res.* **2010**, *3*, 429–437.
[72] J. Hu, Y. Wang, M. Han, Y. Zhou, X. Jiang, P. Sun, *Catal. Sci. Technol.* **2012**, *2*, 2332–2340.
[73] Á. Mastalir, Z. Király, M. Benkő, I. Dékány, *Catal. Lett.* **2008**, *124*, 34–38.
[74] B. Cornelio, G. A. Rance, M. Laronze-Cochard, A. Fontana, J. Sapi, A. N. Khlobystov, *J. Mater. Chem. A* **2013**, *1*, 8737–8744.
[75] P. Kondratyuk, J. T. Yates, *Acc. Chem. Res.* **2007**, *40*, 995–1004.
[76] P. Serp, E. Castillejos, *ChemCatChem* **2010**, *2*, 41–47.
[77] X. Pan, X. Bao, *Chem. Commun.* **2008**, 6271–6281.
[78] E. Castillejos, P.-J. Debouttière, L. Roiban, A. Solhy, V. Martinez, Y. Kihn, O. Ersen, K. Philippot, B. Chaudret, P. Serp, *Angew. Chem.* **2009**, *121*, 2567–2571; *Angew. Chem. Int. Ed.* **2009**, *48*, 2529–2533.
[79] X. Pan, Z. Fan, W. Chen, Y. Ding, H. Luo, X. Bao, *Nat. Mater.* **2007**, *6*, 507–511.
[80] Abbaslou, Reza M. Malek, A. Tavassoli, J. Soltan, A. K. Dalai, *Appl. Catal., A* **2009**, *367*, 47–52.
[81] H. Zhang, X. Pan, Liu , Jingyue Jimmy, W. Qian, F. Wei, Y. Huang, X. Bao, *ChemSusChem* **2011**, *4*, 975–980.
[82] J. M. Planeix, N. Coustel, B. Coq, V. Brotons, P. S. Kumbhar, R. Dutartre, P. Geneste, P. Bernier, P. M. Ajayan, *J. Am. Chem. Soc.* **1994**, *116*, 7935–7936.
[83] B.-H. Zhao, J.-G. Chen, X. Liu, Z.-W. Liu, Z. Hao, J. Xiao, Z.-T. Liu, *Ind. Eng. Chem. Res.* **2012**, *51*, 11112–11121.
[84] M. Oubenali, G. Vanucci, B. Machado, M. Kacimi, M. Ziyad, J. Faria, A. Raspolli-Galetti, P. Serp, *ChemSusChem* **2011**, *4*, 950–956.
[85] E. Kim, H. S. Jeong, Kim, B. Moon, *Catal. Commun.* **2014**, *45*, 25–29.
[86] Z. Wu, Y. Mao, X. Wang, M. Zhang, *Green Chem.* **2011**, *13*, 1311–1316.
[87] M. Cano, A. M. Benito, W. K. Maser, E. P. Urriolabeitia, *New J. Chem.* **2013**, *37*, 1968–1972.
[88] J.-P. Tessonnier, L. Pesant, G. Ehret, M. J. Ledoux, C. Pham-Huu, *Appl. Catal., A* **2005**, *288*, 203–210.
[89] X. Zhang, Y. C. Guo, Z. Cheng Zhang, J. S. Gao, C. M. Xu, *J. Catal.* **2012**, *292*, 213–226.
[90] H. Ma, L. Wang, L. Chen, C. Dong, W. Yu, T. Huang, Y. Qian, *Catal. Commun.* **2007**, *8*, 452–456.
[91] D. Wang, X. Sun, C. Xing, G. Yang, K. Tao, T. Kawabata, K. Matsuda, Y. Tan, N. Tsubaki, *J. Nanosci. Nanotech.* **2013**, *13*, 1274–1277.
[92] D. Wang, G. Yang, Q. Ma, M. Wu, Y. Tan, Y. Yoneyama, N. Tsubaki, *ACS Catal.* **2012**, *2*, 1958–1966.
[93] S. Xu, P. Zhang, H. Li, H. Wei, L. Li, B. Li, X. Wang, *RSC Adv.* **2014**, *4*, 7079–7083.
[94] M. Ran, Y. Liu, W. Chu, A. Borgna, *Catal. Lett.* **2013**, *143*, 1139–1144.
[95] L. Shang, T. Bian, B. Zhang, D. Zhang, L.-Z. Wu, C.-H. Tung, Y. Yin, T. Zhang, *Angew. Chem.* **2014**, *126*, 254–258; *Angew. Chem. Int. Ed.* **2014**, *53*, 250–254.
[96] K. Bramhaiah, N. S. John, *RSC Adv.* **2013**, *3*, 7765–7773.
[97] A. Chen, J. Qi, Q. Zhao, Y. Li, G. Zhang, F. Zhang, X. Fan, *RSC Adv.* **2013**, *3*, 8973–8977.

[98] M. Cano, A. M. Benito, E. P. Urriolabeitia, R. Arenal, W. K. Maser, *Nanoscale* **2013**, *5*, 10189–10193.
[99] K. X. Yao, X. Liu, Z. Li, C. C. Li, H. C. Zeng, Y. Han, *ChemCatChem* **2012**, *4*, 1938–1942.
[100] D. Marquardt, C. Vollmer, R. Thomann, P. Steurer, R. Mülhaupt, E. Redel, C. Janiak, *Carbon* **2011**, *49*, 1326–1332.
[101] Á. Mastalir, Z. Király, Á. Patzkó, I. Dékány, P. L'Argentiere, *Carbon* **2008**, *46*, 1631–1637.
[102] Á. Mastalir, T. Szabó, Z. Király, I. Dékány, *Catal. Commun.* **2012**, *17*, 104–107.
[103] A. R. Siamaki, A. E. R. S. Khder, V. Abdelsayed, M. S. El-Shall, B. F. Gupton, *J. Catal.* **2011**, *279*, 1–11.
[104] G. M. Scheuermann, L. Rumi, P. Steurer, W. Bannwarth, R. Mülhaupt, *J. Am. Chem. Soc.* **2009**, *131*, 8262–8270.
[105] Z. Tang, S. Shen, J. Zhuang, X. Wang, *Angew. Chem.* **2010**, *122*, 4707–4711; *Angew. Chem. Int. Ed.* **2010**, *49*, 4603–4607.
[106] P. Sharma, G. Darabdhara, T. M. Reddy, A. Borah, P. Bezboruah, P. Gogoi, N. Hussain, P. Sengupta, M. R. Das, *Catal. Commun.* **2013**, *40*, 139–144.
[107] R. Wang, Z. Wu, C. Chen, Z. Qin, H. Zhu, G. Wang, H. Wang, C. Wu, W. Dong, W. Fan et al., *Chem. Commun.* **2013**, *49*, 8250–8252.
[108] M. Gopiraman, S. Ganesh Babu, Z. Khatri, W. Kai, Y. A. Kim, M. Endo, R. Karvembu, I. S. Kim, *J. Phys. Chem. C* **2013**, *117*, 23582–23596.
[109] S. Min, G. Lu, *J. Phys. Chem. C* **2011**, *115*, 13938–13945.
[110] K.-i. Shimizu, T. Kubo, A. Satsuma, T. Kamachi, K. Yoshizawa, *ACS Catal.* **2012**, *2*, 2467–2474.
[111] K.-i. Shimizu, K. Shimura, N. Imaiida, A. Satsuma, *J. Mol. Catal. A: Chem.* **2012**, *365*, 50–54.
[112] C. Tu, S. Cheng, *ACS Sustainable Chem. Eng.* **2014**, DOI: 10.1021/sc400501w.
[113] S. Horikoshi, A. Osawa, M. Abe, N. Serpone, *J. Phys. Chem. C* **2011**, *115*, 23030–23035.
[114] Y. Ding, X. Li, H. Pan, P. Wu, *Catal. Lett.* **2014**, *144*, 268–277.
[115] E. J. García-Suárez, P. Lara, A. B. García, M. Ojeda, R. Luque, K. Philippot, *Appl. Catal., A* **2013**, *468*, 59–67.
[116] D. Sempere, S. Navalon, M. Dančíková, M. Alvaro, H. Garcia, *Appl. Catal., B* **2013**, *142–143*, 259–267.
[117] S. Navalon, D. Sempere, M. Alvaro, H. Garcia, *ACS Appl. Mater. Interfaces* **2013**, *5*, 7160–7169.
[118] S. Navalon, R. Martin, M. Alvaro, H. Garcia, *Angew. Chem.* **2010**, *122*, 8581–8585; *Angew. Chem. Int. Ed.* **2010**, *49*, 8403–8407.
[119] R. Martin, S. Navalon, J. J. Delgado, J. J. Calvino, M. Alvaro, H. Garcia, *Chem. Eur. J.* **2011**, *17*, 9494–9502.
[120] S. Navalon, M. de Miguel, R. Martin, M. Alvaro, H. Garcia, *J. Am. Chem. Soc.* **2011**, *133*, 2218–2226.
[121] a) R. Martín, S. Navalon, M. Alvaro, H. Garcia, *Appl. Catal., B* **2011**, *103*, 246–252; b) S. Navalon, R. Martin, M. Alvaro, H. Garcia, *ChemSusChem* **2011**, *4*, 650–657.
[122] A. Dhakshinamoorthy, S. Navalon, D. Sempere, M. Alvaro, H. Garcia, *Chem. Commun.* **2013**, *49*, 2359–2361.
[123] A. Dhakshinamoorthy, S. Navalon, D. Sempere, M. Alvaro, H. Garcia, *ChemCatChem* **2013**, *5*, 241–246.
[124] E. V. Golubina, E. S. Lokteva, A. G. Majouga, M. V. Lobanov, V. V. Lunin, *Diamond Relat. Mater.* **2011**, *20*, 960–964.
[125] R. Liu, H. Huang, H. Li, Y. Liu, J. Zhong, Y. Li, S. Zhang, Z. Kang, *ACS Catal.* **2014**, *4*, 328–336.
[126] J.-c. Qu, C.-l. Ren, Y.-l. Dong, Y.-p. Chang, M. Zhou, X.-g. Chen, *Chem. Eng. J.* **2012**, *211–212*, 412–420.
[127] J. Hu, Y.-l. Dong, X.-j. Chen, H.-j. Zhang, J.-m. Zheng, Q. Wang, X.-g. Chen, *Chem. Eng. J.* **2014**, *236*, 1–8.

[128] S. Chandra, S. Bag, P. Das, D. Bhattacharya, P. Pramanik, *Chem. Phys. Lett.* **2012**, *519-520*, 59–63.
[129] S. Wu, Q. He, C. Zhou, X. Qi, X. Huang, Z. Yin, Y. Yang, H. Zhang, *Nanoscale* **2012**, *4*, 2478–2483.
[130] M. Stein, J. Wieland, P. Steurer, F. Tölle, R. Mülhaupt, B. Breit, *Adv. Synth. Catal.* **2011**, *353*, 523–527.
[131] D. Verma, S. Verma, A. K. Sinha, S. L. Jain, *ChemPlusChem* **2013**, *78*, 860–865.
[132] W. Tang, J. Li, X. Jin, J. Sun, J. Huang, R. Li, *Catal. Commun.* **2014**, *43*, 75–78.
[133] L. Kong, X. Lu, X. Bian, W. Zhang, C. Wang, *ACS Appl. Mater. Interfaces* **2011**, *3*, 35–42.
[134] R. N. Grass, E. K. Athanassiou, W. J. Stark, *Angew. Chem.* **2007**, *119*, 4996–4999; *Angew. Chem. Int. Ed.* **2007**, *46*, 4909–4912.

B. Main Part

1. Carbon-coated, magnetic nanobeads for the synthesis of high-density catalytic systems

1.1 The requirement of efficient and economic catalytic systems

With the synthesis of carbon-coated metal nanobeads Stark *et al.* developed a versatile tool for magnetic separations in organic synthesis (Fig. 6A).[1] The reported magnetic nanoparticles with a graphene-like coating offer multiple advantages including high chemical and thermal stability, excellent magnetic properties, and a large surface area enabling facile functionalization. This allows the nanobeads to serve as an outstanding support for catalysts allowing the recovery and recycling by an external magnetic field (Fig. 6B). In our group we successfully demonstrated the possibility to covalently and non-covalently immobilize catalysts on the carbon surface, thus using them as highly recyclable catalytic systems.

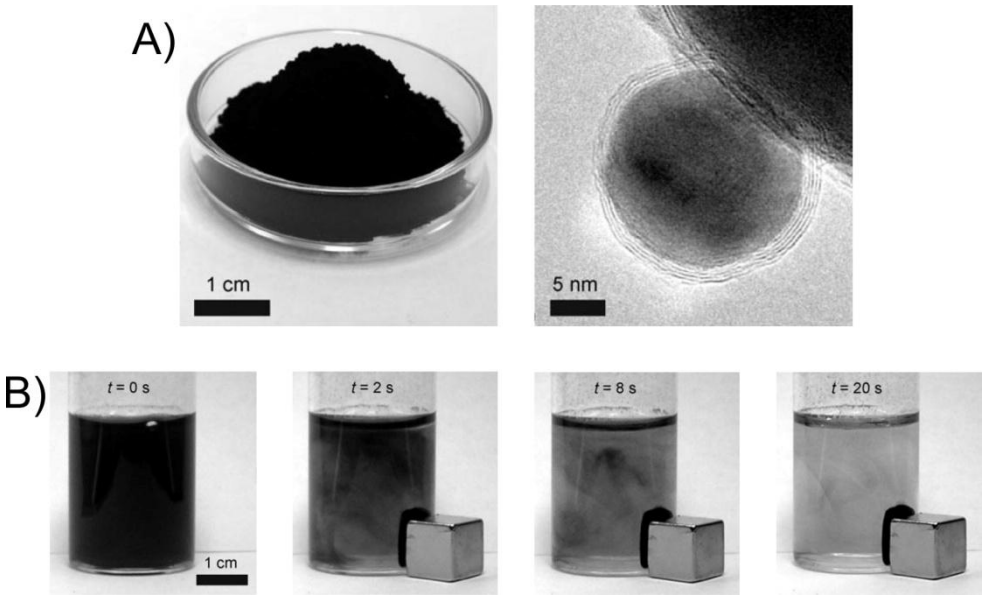

Fig. 6 A) Left: Photograph of about 5 g of the air-stable, carbon-coated nanomaterial. Right: Transmission electron microscopic image of the powder shows two to four homogeneous graphene layers coating the metallic cobalt core. B) Separation of cobalt nanoparticles from a suspension (1 g L^{-1}) in water by a commercial neodymium magnet (B = 1.4 T). Photographs were taken at indicated times after placement of the magnet. Figures adapted with permission from ref [1]. Copyright 2007, WILEY-VCH Verlag GmbH & Co. KGaA, Weinheim.

The application of magnetic TEMPO **19**[2] as well as a magnetic Pd-NHC complex **20**[3] (Fig. 7) leaded to excellent catalytic performances in oxidation or hydroxycarbonylation reactions, respectively. Furthermore, the catalysts could be easily recovered from the reaction mixture and reused for multiple runs. However, in terms of efficiency and economy, one also has to consider the amount of magnetic support which is required for the recycling of a specific amount of a catalyst. With catalyst loadings of 0.1-0.2 mmol g^{-1} and required catalyst amounts of 2.0-2.5 mol% for each reaction, one can calculate masses between 100-125 mg of the catalytic material for a reaction on a 1 mmol scale. Certainly this is not a significant amount on the laboratory scale. However, one has also to consider a possible use for large-scale applications and for catalytic reactions where a larger quantity of catalyst is required, e.g. multiple organocatalytic reactions. Furthermore, if one is interested in the recycling of expensive transition metal catalysts, it would not be very convenient to use an enormous quantity of a cobalt support to recycle just minimal amounts of e.g. platinum, palladium, or gold.

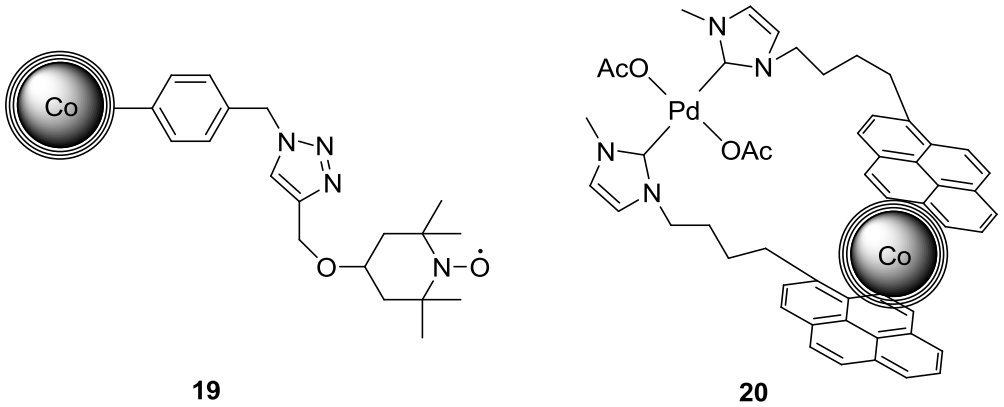

19 **20**

Fig. 7 Covalently immobilized TEMPO catalyst **19** and non-covalently immobilized Pd-NHC complex **20** on carbon-coated cobalt nanoparticles.

1.2 Outline

The following chapters demonstrate possibilities to increase the amount of catalysts loaded onto magnetic supports. Especially the synthesis and application of magnetic organocatalysts (chapter 2 and 3) and transition metal catalysts (chapter 4) will be discussed. Special attention will be paid on the tuning of activity, efficiency, and recyclability of the catalytic systems. Furthermore, chapter 3 compares magnetic nanobeads and phosphorous dendrimers as globular catalyst supports, highlighting the benefits of both for a convenient and recyclable catalytic system. In chapter 5 studies towards recyclable catalysts for C-H activation and olefin metathesis are discussed.

1.3 References

[1] R. N. Grass, E. K. Athanassiou, W. J. Stark, *Angew. Chem.* **2007**, *119*, 4996–4999; *Angew. Chem. Int. Ed.* **2007**, *46*, 4909–4912.

[2] A. Schätz, R. N. Grass, W. J. Stark, O. Reiser, *Chem. Eur. J.* **2008**, *14*, 8262–8266.

[3] S. Wittmann, A. Schätz, R. N. Grass, W. J. Stark, O. Reiser, *Angew. Chem.* **2010**, *122*, 1911–1914; *Angew. Chem. Int. Ed.* **2010**, *49*, 1867–1870.

2. *N*-Alkylimidazole immobilized on high-loading, carbon-coated iron nanobeads as recyclable organocatalyst

Graphene-coated iron nanobeads have been grafted with polymer shells and functionalized with *N*-alkylimidazole. The high-loading imidazole catalyst (1.6 mmol g^{-1}) is applied in the Baylis-Hillman reaction of nitro benzaldehyde and methyl vinyl ketone. Activity of the catalyst is compared to a monomeric *N*-alkylimidazole and a low-density co-polymeric catalyst (0.9 mmol g^{-1}). The high-loading catalyst could be reused for 7 consecutive runs after tuning of the recycling conditions. Furthermore, we could show an interesting dendritic-like effect from the monomeric to the high-loading catalyst.

2.1 Introduction

Carbon-carbon bond forming reactions are one of the most important tools in today's organic synthesis. Various natural carbon frameworks could be generated through these useful transformations, e.g. polyketides,[1,2] terpenoids,[2] or alkaloids.[3] One major difference between various C-C bond forming reactions is the point of atom-economy.[4] Atom-economic reactions such as aldol, Diels-Alder, Michael, or Baylis-Hillman reactions are more attractive than non atom-economic reactions like Grignard, Wittig, Friedel-Crafts, or Suzuki/Heck coupling reactions.

The Baylis-Hillman reaction needs three essential components. In earlier years, these components were limited to an activated alkene, a carbon electrophile and a tertiary amine as catalyst. During the last 10 to 15 years this atom-economic reaction got more and more attraction and the variety of substrates and catalysts increased dramatically.[5] However, there are still some drawbacks described in literature regarding this powerful reaction.

One major drawback is the slow reaction rate of the Baylis-Hillman reaction. It often takes days to weeks to reach full completion depending on the substrates and catalysts. Although the reaction is atom-economically, the catalyst is not reused in most cases. A few examples exist in literature where Baylis-Hillman catalysts are supported on silica,[6] polymers,[7a–c,8,7d–f] hairy particles,[9] or ions.[10] However, just in very few cases recycling of the catalyst is possible. One interesting example regarding the activity of a supported catalyst was recently shown by Portnoy.[11] They used Wang resin supported *N*-alkylimidazole-decorated dendrons in the Baylis-Hillman reaction of 4-nitro benzaldehyde with methyl vinyl ketone, exhibiting high activities and short reaction times. However, recycling of this supported organocatalyst, which would make the catalytic system much more attractive, was not possible at all. Having catalysts immobilized on solid supports also causes problems if the catalytic system needs ultra-/filtration methods for an efficient recycling. Filters or membranes are often blocked and/or the filtration process is time- and energy-intense.[12] One concept to solve this problem is the application of a magnetic support, allowing the separation by simple magnetic decantation.[13]

Hence, the aim of our study was to immobilize an *N*-alkylimidazole catalyst – similar to Portnoy *et al.*[11] – on a magnetic support achieving a catalytic system which is easy to synthesize, highly active, easily recyclable and, therefore, makes

the Baylis-Hillman reaction even more economic. To achieve this goal, we use carbon-coated iron (Fe/C) nanoparticles, which are functionalized with a polymeric shell, on which an *N*-alkylimidazole is immobilized. The catalytic system is applied in the Baylis-Hillman reaction and different reaction/recycling conditions are screened. Furthermore, cooperative effects of the imidazole units are examined comparing the catalyst with a lower-density co-polymeric catalyst and a homogeneous, monomeric catalyst.

2.2 Results and discussion

Stark *et al.*[14] recently reported the synthesis of highly stable, carbon-coated iron or cobalt nanobeads. The material is synthesized on large scale (>30 g h^{-1}) via reducing flame synthesis. Carbon-coated nanomagnets exhibit extremely high magnetization and provide high thermal, air, and moisture stability. As the carbon coating of the beads is chemically related to graphene, graphite or carbon nanotubes, the surface functionalization could be established in a similar way. Several examples are shown in literature where ligands,[15] catalysts,[16,17–20] polymers/dendrimers,[21a,22,17–20,21b] scavengers,[23] reagents,[23,24] or fluorescent dyes[22] are immobilized applying covalent or non-covalent strategies. With the introduction of a polymeric resin on the particle surface a much higher loading of functional groups can be achieved. Hence, we introduced such a polymeric structure for the immobilization of our catalyst with the intention of generating a high-loading catalyst material.

The synthesis of the catalyst is shown in Scheme 4. Iron nanobeads **21** are tagged with styrene moieties using diazonium chemistry followed by Suzuki coupling.[25] Subsequent polymerization of 4-chloromethylstyrene on styrene modified beads **22** leads to the magnetic, Merrifield-like resin **23**. **23** then reacts with 3-aminopropyl imidazole in a substitution reaction to high-density catalyst **24**. The loading of **24** was determined by elemental microanalysis to 1.6 mmol g^{-1}.

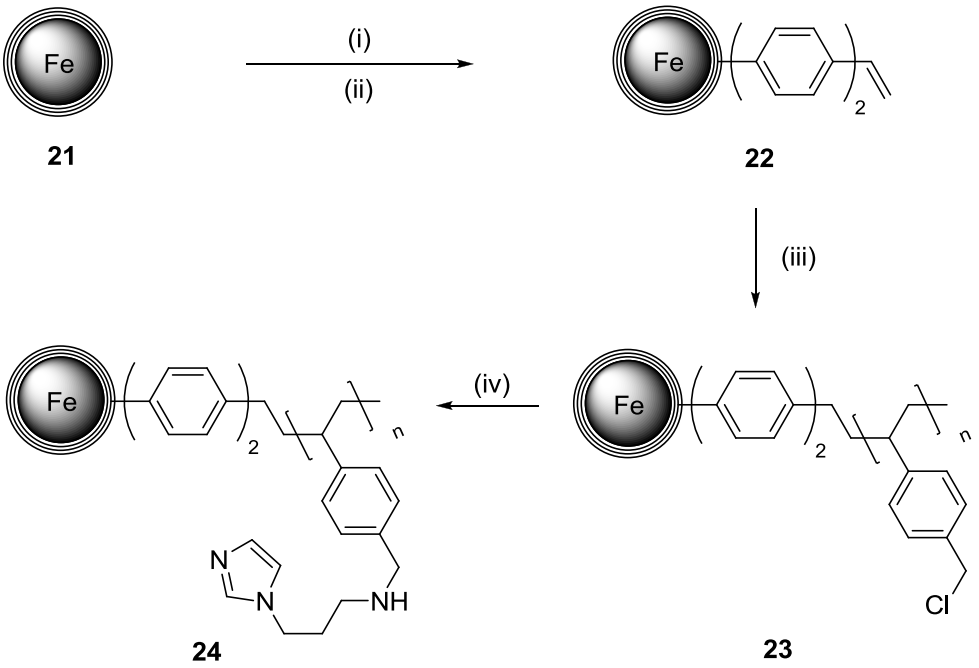

Scheme 4 Synthesis of high-density *N*-alkyl imidazolium catalyst **24** from Fe/C nanobeads **21**. Reagents and conditions: (i) 4-iodo aniline, $NaNO_2$, HCl, H_2O, ultrasound, 25 °C, 30 min; (ii) 4-vinyl phenyl boronic acid, $Pd(OAc)_2$, PPh_3, $^{i}PrOH/H_2O$, Na_2CO_3, 65 °C, 16 h; (iii) 4-chloro methyl styrene, AIBN, DMF, 100 °C, 12 h; (iv) 3-amino propyl imidazole, DMF, 85 °C, 16 h.

Having synthesized the novel material **24**, the activity as well as the recycling ability of the catalyst was explored. Imidazole catalysts were frequently applied in Baylis-Hillman reactions in the past. Either sole imidazole catalysts,[26,27,8] *N*-alkylimidazole catalysts[27,28,11] or *L*-proline with an imidazole co-catalyst.[29,30] However, these reactions often suffer from long reaction times and bad yields.

Recently, Portnoy *et al.*[11] reported a Wang resin supported *N*-alkyl imidazole in the Baylis-Hillman reaction of 4-nitro benzaldehyde with methyl vinyl ketone with short reaction times and good yields. However, they were not able to recycle the catalyst, which would make it much more attractive. Hence, we also carried out tests with our nanomagnetic catalysts. Additionally to catalyst **24** we further synthesized a co-polymeric catalyst **25** with a lower density of imidazole on the surface and a monomeric imidazole catalyst **26** with a similar structure (Fig. 8). With these three catalysts we carried out the Baylis-Hillman reaction of 4-nitro benzaldehyde and methyl vinyl ketone with focus on activity, recycling ability and cooperative effects of the imidazole moiety.

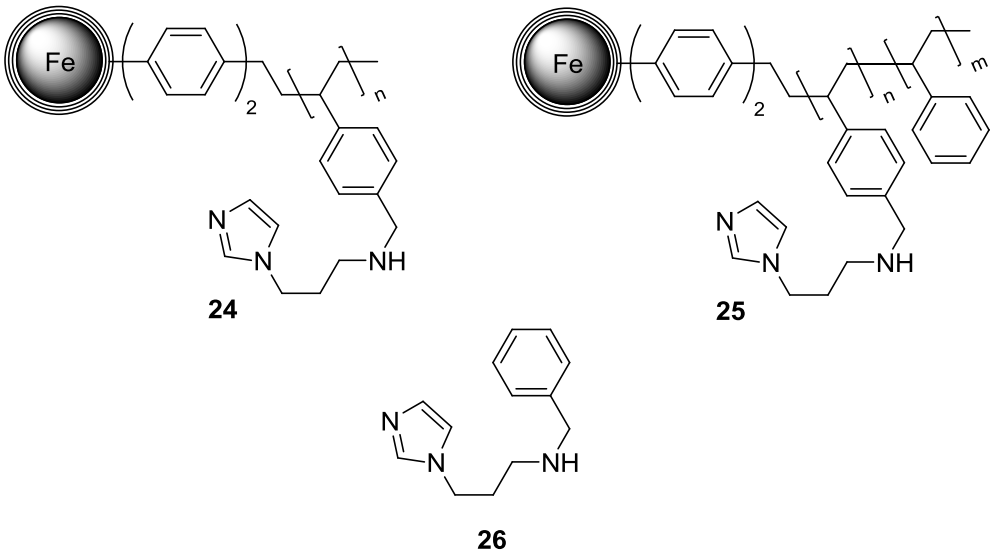

Fig. 8 The three different *N*-alkyl imidazole catalysts: heterogeneous nanocatalysts **24** and **25** and homogeneous catalyst **26**.

First, we screened different reaction conditions with catalyst **24** in the Baylis-Hillman reaction between 4-nitro benzaldehyde **27** and methyl vinyl ketone **28**. The results are shown in Table 4. DMF and THF were compared as solvents and additionally the effect of water was evaluated which is known to be able to enhance the reaction speed.[27,30,11] In cases of pure DMF and THF the reaction did not reach full conversion, even after a reaction time of 7 d. The yield of the Baylis-Hillman product was 32% (Table 4, entry 1) or 74% (Table 4, entry 5), respectively. Using organic solvent/water mixtures, the reaction time could be dramatically decreased and full conversion was reached. In case of a THF/H_2O 9:1 mixture the reaction time was reduced to 96 h, whereas for a 1:1 mixture the time even decreases to 24 h. However multiple side products[31,6] were observed in these cases, appearing in higher quantities with an enhanced amount of water. In comparison of the two different solvents, the results obtained with THF or THF/H_2O mixtures turned out to be much better than the ones with DMF and DMF/H_2O. The best solvent conditions for the Baylis-Hillman reaction with catalyst **24** were found to be a mixture of THF/H_2O 19:1 with a yield of 83% (Table 4, entry 6). By decreasing the amount of methyl vinyl ketone from three to two equivalents we could even reach a yield of 90% (Table 4, entry 7).

Table 4 Baylis-Hillman reaction of 4-nitro benzaldehyde **27** with methyl vinyl ketone **28** using high-density catalyst **24**.[a]

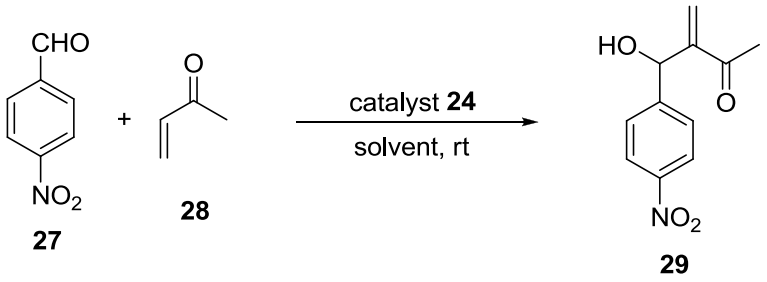

Entry	Solvent	Reaction time [h][b]	Yield [%][c]
1[d]	DMF	7 d	32
2	DMF/H_2O 9:1	72	48
3	DMF/H_2O 1:1	24	53
4	DMF/H_2O 1:1	24	61
5[d]	THF	7 d	74
6	THF/H_2O 19:1	120	83
7[e]	THF/H_2O 19:1	120	90
8	THF/H_2O 9:1	96	76
9	THF/H_2O 7:3	48	71
10	THF/H_2O 1:1	24	63

[a] 4-Nitro benzaldehyde **27** (0.5 mmol) was reacted with methyl vinyl ketone **28** (1.5 mmol) in 1 mL of solvent using 0.05 mmol (10 mol%) of catalyst **24**. [b] Reaction monitored by TLC control and stopped at full conversion. [c] Determined by ^{1}H NMR analysis using diphenyl methane as internal standard. [d] Full conversion could not be reached. [e] Two equivalents of methyl vinyl ketone were used instead of three.

Previous results with polymer-coated nanobeads showed in some cases a prolonged time to separate the catalyst from the reaction mixture compared to the sole magnetic nanobeads.[32] However in case of **24** the separation of the catalyst takes just a few seconds under the reported reaction conditions (Fig. 9).

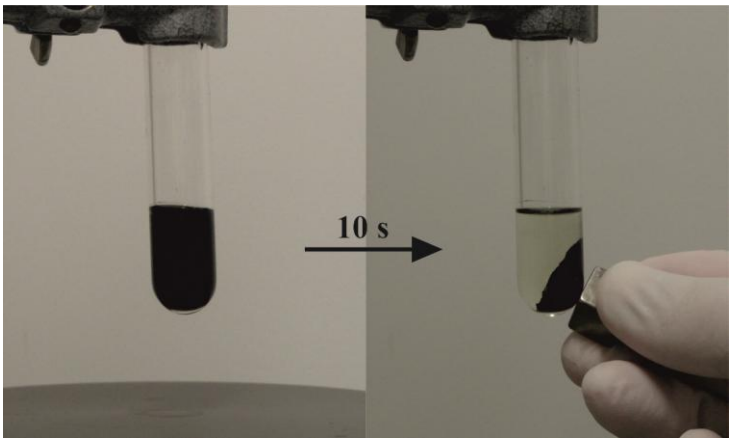

Fig. 9 Collecting nanocatalyst **24** from the reaction mixture by an external magnet.

We then also carried out catalytic experiments with co-polymeric catalyst **25** to exemplify a possible dendritic-like effect which was described by Portnoy *et al.*[11]. The results clearly demonstrate an increase in yield from the lower-density imidazole catalyst **25** to the high-density catalyst **24** in the range of 4 to 13% (Table 5).

Table 5 Baylis-Hillman reaction of 4-nitro benzaldehyde **27** with methyl vinyl ketone **28** using high-density catalyst **24** and the lower-density catalyst **25**.[a]

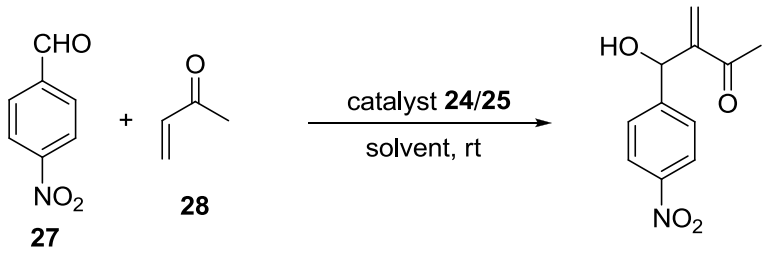

Entry	Solvent	Reaction time [h][b]	Yield [%][c]	
			Cat. **24**	Cat. **25**
1	THF/H_2O 19:1	120	83	75
2[d]	THF/H_2O 19:1	120	90	77
3	THF/H_2O 7:3	48	71	60
4	THF/H_2O 1:1	24	63	59

[a] 4-Nitro benzaldehyde **27** (0.5 mmol) was reacted with methyl vinyl ketone **28** (1.5 mmol) in 1 mL of solvent using 0.05 mmol (10 mol%) of catalyst **24** or **25**. [b] Reaction monitored by TLC control and stopped at full conversion. [c] Determined by ^{1}H NMR analysis using diphenyl methane as internal standard. [d] Two equivalents of methyl vinyl ketone were used instead of three.

To further exemplify this effect we additionally carried out catalytic experiments with the monomeric aminopropyl imidazole catalyst **26** (Table 6). The results clearly show that the reaction under homogeneous conditions works even worse than under the previously described heterogeneous ones. With catalyst **26** the reaction times had to be increased to reach full conversion and the yields were either worse or equal to the heterogeneous reactions. The effects of water were the same as in the heterogeneous case. An increase of the H_2O amount speeds up the reaction and leads to higher quantities of side products. These results again demonstrate the cooperative effect of the imidazole units described before.

Table 6 Baylis-Hillman reaction of 4-nitro benzaldehyde **27** with methyl vinyl ketone **28** using homogeneous model catalyst **26**.[a]

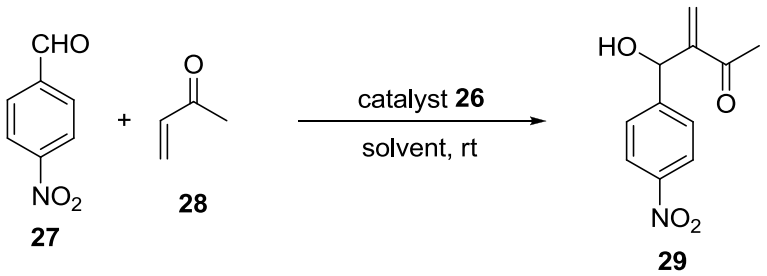

Entry	Solvent	Reaction time [h][b]	Yield [%][c]
1[d]	THF	7 d	11
2	THF/H_2O 19:1	6 d	87
3	THF/H_2O 7:3	96	24
4	THF/H_2O 1:1	72	22

[a] 4-Nitro benzaldehyde **27** (0.5 mmol) was reacted with methyl vinyl ketone **28** (1.5 mmol) in 1 mL of solvent using 0.05 mmol (10 mol%) of catalyst **26**. [b] Reaction monitored by TLC control and stopped at full conversion. [c] Determined by ^{1}H NMR analysis using diphenyl methane as internal standard. [d] Full conversion could not be reached.

To further decrease the reaction time of our catalytic system we also investigated the effect of additional proline in the reaction (Table 7). Entry 2 shows a decrease from 120 h to 72 h in reaction time while sole proline does not catalyze the reaction under these conditions at all. Furthermore, the yield was improved from 90% to 96% applying the combined proline/imidazole system.

Table 7 Baylis-Hillman reaction of 4-nitro benzaldehyde **27** with methyl vinyl ketone **28** using model catalyst **24** and optional *L*-proline.[a]

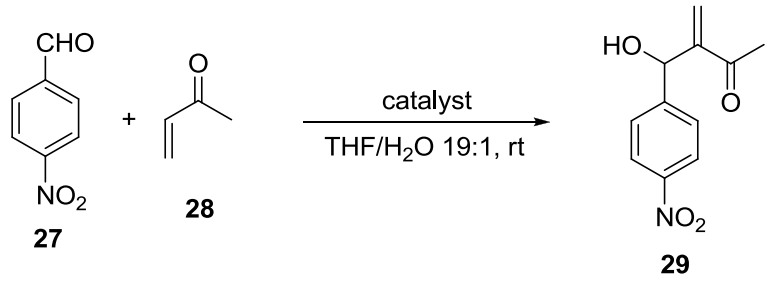

Entry	Catalyst	Reaction time [h][b]	Yield [%][c]
1	**24**	120	90
2	**24** + *L*-proline	72	96
3	*L*-proline	72	0

[a] 4-Nitro benzaldehyde **27** (0.5 mmol) was reacted with methyl vinyl ketone **28** (1.0 mmol) in 1 mL of THF/H_2O 19:1 using 0.05 mmol (10 mol%) of catalyst **24** and optional 0.05 mmol (10 mol%) *L*-proline. [b] Reaction monitored by TLC control and stopped at full conversion. [c] Determined by ^1H NMR analysis using diphenyl methane as internal standard.

As Portnoy *et al.*[11] reported a gradual deterioration in the catalyst activity during recycling experiments we next investigated the recycling ability of our catalytic system (Fig. 10). Applying catalyst **24** under the best reaction conditions we also see a gradual decrease in activity from the 1st (90%) to the 7th (28%) run, keeping the reaction time constant. However, we can reduce this gradual decrease by washing the catalyst after each run with a 1M solution of Et_3N in dichloromethane. Here, the decrease is just from 90% (1st run) to 59% (7th run). Applying our combined proline/imidazole catalyst system we can even keep the yields constant for at least 6 runs without increasing the reaction time.

Even if our catalytic system is not as active compared to literature results with dendron-decorated Wang resin, we could show the effective recycling ability of the system simply by basic washing of the catalyst before the reuse.

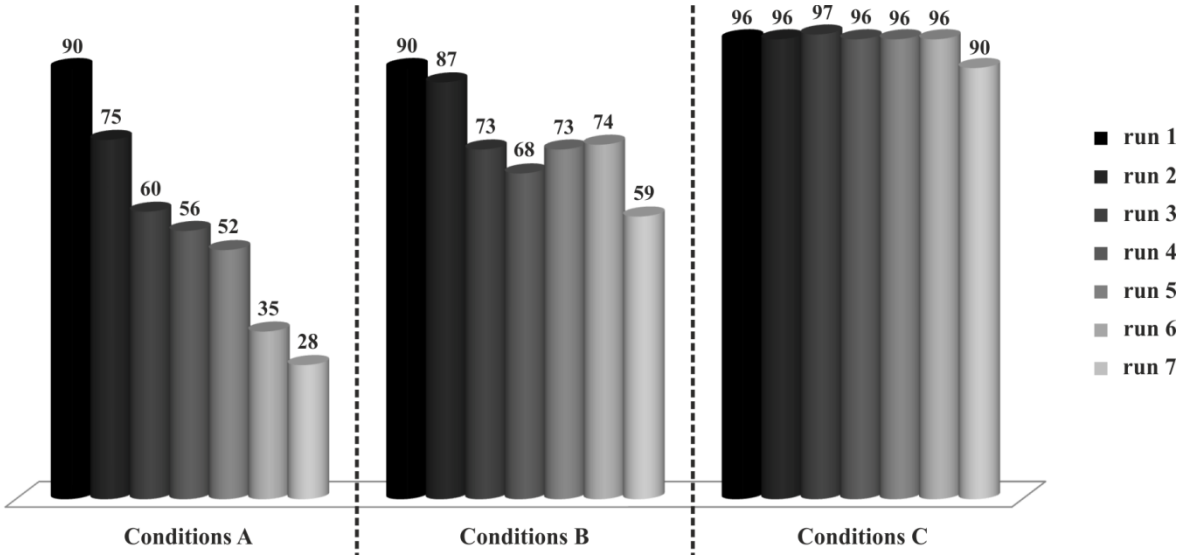

Fig. 10 Recycling experiments with catalyst **24** in the Baylis-Hillman reaction of 4-nitro benzaldehyde with methyl vinyl ketone under different reaction/recycling conditions. Reaction was stirred to full conversion in the 1. run. For the following runs the reaction time was held constant. Yields are given in % above every single column. Conditions: A) reaction with catalyst **24**; catalyst was washed with dichloromethane after each run; B) reaction with catalyst **24**; catalyst was washed with Et_3N in dichloromethane (1M) after each run; C) reaction with catalyst **24** and additional *L*-proline; catalyst was washed with Et_3N in dichloromethane (1M) after each run.

Additionally to the recycling experiments in Fig. 10, we also carried out recycling experiments on a 1 mmol scale isolating the product after each run. The reaction in this case worked with the same reaction time (Table 8, entry 1-6) and excellent yields (87-92%). In the 7^{th} run reaction time had to be increased to 80 h to reach again full conversion (Table 8, entry 7).

Table 8 Recycling experiments with catalyst **24** in the Baylis-Hillman reaction of 4-nitro benzaldehyde **27** with methyl vinyl ketone **28**.[a]

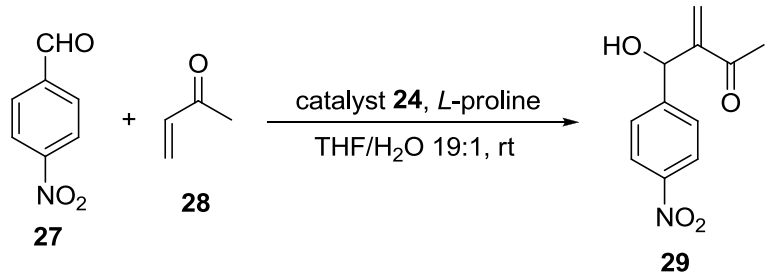

Entry	Run	Reaction time [h][b]	Yield [%][c]
1	1	72	92
2	2	72	88
3	3	72	87
4	4	72	89
5	5	72	91
6	6	72	90
7	7	80	92

[a] 4-Nitro benzaldehyde **27** (1.0 mmol) was reacted with methyl vinyl ketone **28** (2.0 mmol) in 2 mL of THF/H_2O 19:1 using 0.1 mmol (10 mol%) of catalyst **24** and 0.1 mmol (10 mol%) *L*-proline. [b] Reaction was monitored by TLC control and stopped at full conversion. [c] Isolated yield after column chromatography.

2.3 Conclusion

We successfully developed a novel, magnetic Baylis-Hillman catalyst with *N*-alkylimidazole units on the surface. The material is easily synthesized, shows reasonable reaction times and excellent recyclability. Furthermore, we could demonstrate a dendritic-like effect of imidazole units by comparing two heterogeneous catalysts with different catalyst density on the surface with a homogeneous one.

Regarding the atom-economy of the Baylis-Hillman reaction, this easily synthesized and highly recyclable catalyst system makes the Baylis-Hillman reaction even more economically and, therefore, very attractive in terms of sustainability.

2.4 Experimental section

Materials and methods

Carbon coated iron nanomagnets (Fe/C) were purchased from Turbobeads Llc, Switzerland. Prior to use, they were washed in a concentrated HCl/water mixture 1:1 (5x) for 24 h. Acid residuals were removed by washing with millipore water (5x) and the particles were dried at 50 °C in a vacuum oven.[33] All other commercially available compounds were used as received.

The magnetic nanobeads were dispersed using an ultrasound bath (Sonorex RK 255 H-R, Bandelin) and recovered with the aid of a neodymium based magnet (15 x 30 mm). They were characterized by IR-ATR spectroscopy (Biorad Excalibur FTS 3000), and elemental microanalysis (LECO CHN-900).

Poly(benzylchloride)styrene functionalized iron nanoparticles **23** and poly(benzylchloride-*co*-phenyl)styrene functionalized iron nanoparticles were prepared on the gram scale following a previously reported procedure.[34,25]

NMR spectra were recorded with a Bruker AV 300 spectrometer with $CHCl_3$ as standard. Chemical shifts (δ) are reported in ppm and coupling constants (*J*) are reported in Hertz (Hz). The signals in the spectra are described as s (singlet), d (doublet), t (triplet), quin (quintet) and m (multiplet).

Synthesis of the catalysts

Poly(*N*-benzyl-3-(1H-imidazol-1-yl)propan-1-amine)styrene functionalized carbon coated iron nanoparticles (24)

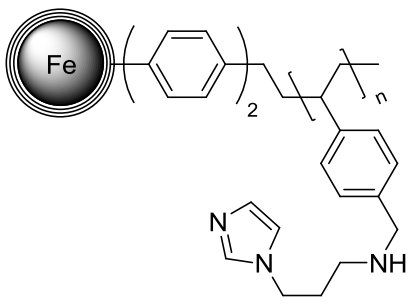

500 mg (1.6 mmol of benzylchloride units) Poly(benzylchloride)styrene functionalized Fe/C nanoparticles **23** were sonicated in 10 mL DMF for 10 min. 590 μL (5 mmol) 1-(3-Aminopropyl)imidazole were added and the reaction mixture stirred

at 80 °C for 16 h. After magnetic decantation, the particles were washed with DMF (3 x 5 mL), Et_3N in dichloromethane (1M, 3 x 5 mL) and dichloromethane (3 x 5 mL) and subsequently dried in vacuo to obtain 505 mg of **24** with a loading of 1.77 mmol g^{-1}.

IR (ν/cm^{-1}): 2920, 2837, 1645, 1604, 1563, 1506, 1442, 1419, 1342, 1227, 1152, 1105, 1077, 1014, 967, 914, 812, 733, 659; elemental microanalysis (%): C, 48.75; H, 5.07; N, 7.44; Cl, 3.05.

Poly(*N*-benzyl-3-(1H-imidazol-1-yl)propan-1-amine-*co*-phenyl)styrene functionalized carbon coated iron nanoparticles (25)

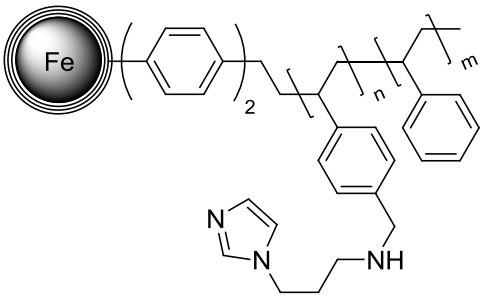

500 mg (0.8 mmol of benzylchloride units) Poly(benzylchloride-*co*-phenyl)styrene functionalized Fe/C nanoparticles were sonicated in 10 mL DMF for 10 min. 295 μL (2.5 mmol) 1-(3-Aminopropyl)imidazole were added and the reaction mixture stirred at 80 °C for 16 h. After magnetic decantation, the particles were washed with DMF (3 x 5 mL), Et_3N in dichloromethane (1M, 3 x 5 mL) and dichloromethane (3 x 5 mL) and subsequently dried in vacuo to obtain 503 mg of **25** with a loading of 0.94 mmol g^{-1}.

IR (ν/cm^{-1}): 2918, 2842, 1599, 1492, 1450, 1356, 1226, 1106, 1076, 1018, 967, 905, 817, 754, 696, 661; elemental microanalysis (%): C, 58.46; H, 5.18; N, 3.96.

N-Benzyl-3-(1H-imidazol-1-yl)propan-1-amine (26)

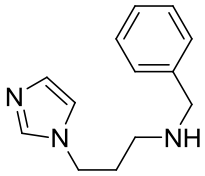

A solution of 142.3 μL (1.25 mmol) 1-(3-aminopropyl)imidazole in 3 mL dry DMF was stirred at rt under N_2-atmosphere. 60.3 μL (0.5 mmol) Benzylchloride in 2 mL dry DMF was added over 30 min and the reaction mixture stirred for 2 h. After evaporation of the solvent 10 mL NaOH solution (1M) was added and the mixture extracted three times with 10 mL dichloromethane. After the organic layer was dried over $MgSO_4$ the solvent was removed and the crude product purified by column chromatography (R_f (EE/MeOH 95:5) = 0.2) to obtain 87 mg (81%) of the product.

^{1}H NMR (300 MHz, $CDCl_3$): δ = 7.29 (d, *J* = 12.0 Hz, 1H), 7.26 – 7.10 (m, 5H), 6.93 (s, 1H), 6.77 (s, 1H), 3.91 (t, *J* = 6.9 Hz, 2H), 3.64 (s, 2H), 2.49 (t, *J* = 6.7 Hz, 2H), 1.79 (quin, *J* = 6.8 Hz, 2H), 1.55 (s, 2H); ^{13}C NMR (75 MHz, $CDCl_3$): δ = 140.2, 137.2, 129.3, 128.4, 128.1, 127.0, 118.9, 53.9, 45.6, 44.6, 31.3; IR (ν/cm^{-1}): 2934, 2828, 1667, 1645, 1507, 1454, 1358, 1266, 1229, 1109, 1078, 1027, 912, 820, 735, 700, 665, 642, 619; ESI-HRMS: 216.1497 (MH^+), calc.: 216.1495.

General procedures for catalytic experiments

General procedure for the Baylis-Hillman reaction with heterogeneous catalysts 24 and 25

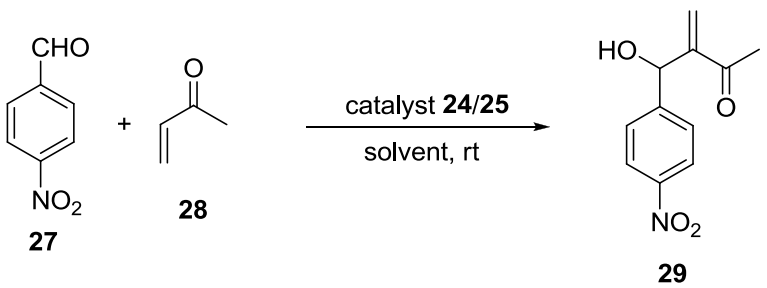

75.6 mg (0.5 mmol) *p*-Nitrobenzaldehyde **27** and 31.4 mg (0.05 mmol) **24** or 53.2 mg (0.05 mmol) **25** were predispersed for 10 min in 1 mL of solvent using an ultrasonic bath. After adding 41.6 μL (0.25 mmol) diphenylmethane as internal

standard, 126.8 μL (1.5 mmol) methylvinylketone **28** were added via syringe and the reaction mixture stirred at room temperature. After magnetic decantation, the nanoparticles were washed with ethyl acetate (5 x 2 mL). To the combined phase 10 mL H_2O and 10 mL saturated NH_4Cl solution were added and the reaction mixture was extracted with ethyl acetate (3 x 10 mL). The organic phase was dried over $MgSO_4$ and the solvent evaporated under vacuum to give the crude material for ^1H NMR analysis.

For recycling experiments the particles were washed with dichloromethane (3 x 3 mL) or Et_3N in dichloromethane (1M, 3 x 3 mL) and dichloromethane (2 x 3 mL) and subsequently dried under vacuum.

For isolation of the product the crude mixture was purified by column chromatography (R_f (PE/EE 2:1) = 0.3).

General procedure for the Baylis-Hillman reaction with heterogeneous catalyst 24 and additional *L*-proline

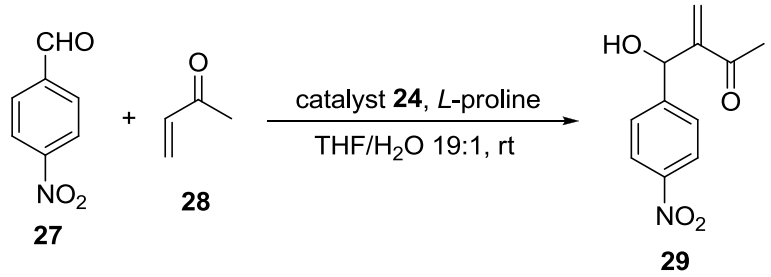

75.6 mg (0.5 mmol) *p*-Nitrobenzaldehyde **27**, 31.4 mg (0.05 mmol) **24** and 5.8 mg (0.05 mmol) *L*-proline were predispersed for 10 min in 1 mL of solvent using an ultrasonic bath. After adding 41.6 μL (0.25 mmol) diphenylmethane as internal standard, 126.8 μL (1.5 mmol) methylvinylketone **28** were added via syringe and the reaction mixture stirred at room temperature. After magnetic decantation, the nanoparticles were washed with ethyl acetate (5 x 2 mL). To the combined phase 10 mL H_2O and 10 mL saturated NH_4Cl solution were added and the reaction mixture was extracted with ethyl acetate (3 x 10 mL). The organic phase was dried over $MgSO_4$ and the solvent evaporated under vacuum to give the crude material for ^1H NMR analysis.

For recycling experiments the particles were washed with dichloromethane (3 x 3 mL) or Et_3N in dichloromethane (1M, 3 x 3 mL) and dichloromethane (2 x 3 mL) and subsequently dried under vacuum.

For isolation of **29** the crude mixture was purified by column chromatography (R_f (PE/EE 2:1) = 0.3).

General procedure for the Baylis-Hillman reaction with homogeneous catalyst 26

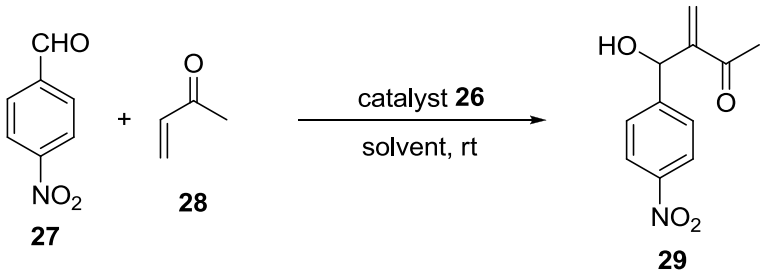

75.6 mg (0.5 mmol) p-Nitrobenzaldehyde **27** and 10.8 mg (0.05 mmol) *N*-benzyl-3-(1H-imidazol-1-yl)propan-1-amine **26** were dissolved in 1 mL of solvent. After adding 41.6 µL (0.25 mmol) diphenylmethane as internal standard, 126.8 µL (1.5 mmol) methylvinylketone **28** were added via syringe and the reaction mixture stirred at room temperature. After adding 10 mL H_2O and 10 mL saturated NH_4Cl solution, the reaction mixture was extracted with ethyl acetate (3 x 10 mL). The organic phase was dried over $MgSO_4$ and the solvent evaporated under vacuum to give the crude material for ^1H NMR analysis.

2.5 References

[1] S. M. Dalby, I. Paterson, *Curr. Opin. Drug Discovery Dev.* **2010**, *13*, 777–794.

[2] J. C. Morris, A. J. Phillips, *Nat. Prod. Rep.* **2010**, *27*, 1186–1203.

[3] Z. Jin, *Nat. Prod. Rep.* **2005**, *22*, 196–229.

[4] B. M. Trost, *Science* **1991**, *254*, 1471–1477.

[5] a) D. Basavaiah, A. J. Rao, T. Satyanarayana, *Chem. Rev.* **2003**, *103*, 811–892; b) D. Basavaiah, K. V. Rao, R. J. Reddy, *Chem. Soc. Rev.* **2007**, *36*, 1581–1588; c) D. Basavaiah, B. S. Reddy, S. S. Badsara, *Chem. Rev.* **2010**, *110*, 5447–5674; d) D. Basavaiah, G. Veeraraghavaiah, *Chem. Soc. Rev.* **2011**, *41*, 68–78.

[6] H.-T. Chen, S. Huh, J. W. Wiench, M. Pruski, V. S.-Y. Lin, *J. Am. Chem. Soc.* **2005**, *127*, 13305–13311.

[7] a) K. Akagawa, S. Sakamoto, K. Kudo, *Synlett* **2011**, *2011*, 817–820; b) A. Corma, H. García, A. Leyva, *Chem. Commun.* **2003**, 2806–2807; c) V. D'Elia, Y. Liu, H. Zipse, *Eur. J. Org. Chem.* **2011**, *2011*, 1527–1533; d) J.-W. Huang, M. Shi, *Adv. Synth. Catal.* **2003**, *345*, 953–958; e) L.-J. Zhao, H. S. He, M. Shi, P. H. Toy, *J. Comb. Chem.* **2004**, *6*, 680–683; f) L.-J. Zhao, C. K.-W. Kwong, M. Shi, P. H. Toy, *Tetrahedron* **2005**, *61*, 12026–12032.

[8] F. Giacalone, M. Gruttadauria, A. M. Marculescu, F. D'Anna, R. Noto, *Catal. Commun.* **2008**, *9*, 1477–1481.

[9] B. Zhao, X. Jiang, D. Li, X. Jiang, T. G. O'Lenick, B. Li, C. Y. Li, *J. Polym. Sci. Part A: Polym. Chem.* **2008**, *46*, 3438–3446.

[10] Y. Imura, N. Shimojuh, K. Moriyama, H. Togo, *Tetrahedron* **2012**, *68*, 2319–2325.

[11] K. Goren, M. Portnoy, *Chem. Commun.* **2010**, *46*, 1965–1967.

[12] W. T. Ford, *Polymeric reagents and catalysts*, American Chemical Society, Washington, D.C, **1986**.

[13] S. Luo, X. Zheng, H. Xu, X. Mi, L. Zhang, J.-P. Cheng, *Adv. Synth. Catal.* **2007**, *349*, 2431–2434.

[14] R. N. Grass, E. K. Athanassiou, W. J. Stark, *Angew. Chem.* **2007**, *119*, 4996–4999; *Angew. Chem. Int. Ed.* **2007**, *46*, 4909–4912.

[15] a) F. M. Koehler, M. Rossier, M. Waelle, E. K. Athanassiou, L. K. Limbach, R. N. Grass, D. Günther, W. J. Stark, *Chem. Commun.* **2009**, 4862–4864; b) R. Fuhrer, I. K. Herrmann, E. K. Athanassiou, R. N. Grass, W. J. Stark, *Langmuir* **2011**, *27*, 1924–1929.

[16] a) A. Schätz, R. N. Grass, W. J. Stark, O. Reiser, *Chem. Eur. J.* **2008**, *14*, 8262–8266; b) A. Schätz, R. N. Grass, Q. Kainz, W. J. Stark, O. Reiser, *Chem. Mater.* **2010**, *22*, 305–310; c) S. Wittmann, A. Schätz, R. N. Grass, W. J. Stark, O. Reiser, *Angew. Chem.* **2010**, *122*, 1911–1914; *Angew. Chem. Int. Ed.* **2010**, *49*, 1867–1870.

[17] M. Keller, A. Perrier, R. Linhardt, L. Travers, S. Wittmann, A.-M. Caminade, J.-P. Majoral, O. Reiser, A. Ouali, *Adv. Synth. Catal.* **2013**, *355*, 1748–1754.

[18] A. Schätz, T. R. Long, R. N. Grass, W. J. Stark, P. R. Hanson, O. Reiser, *Adv. Funct. Mater.* **2010**, *20*, 4323–4328.

[19] S. Wittmann, J.-P. Majoral, R. N. Grass, W. J. Stark, O. Reiser, *Green Proc. Synth.* **2012**, *1*, 275–279.

[20] M. Zeltner, A. Schätz, M. L. Hefti, W. J. Stark, *J. Mater. Chem.* **2011**, *21*, 2991–2996.

[21] a) M. Rossier, F. M. Koehler, E. K. Athanassiou, R. N. Grass, M. Waelle, K. Birbaum, D. Günther, W. J. Stark, *Ind. Eng. Chem. Res.* **2010**, *49*, 9355–9362; b) M. Keller, V. Collière, O. Reiser, A.-M. Caminade, J.-P. Majoral, A. Ouali, *Angew. Chem.* **2013**, *125*, 3714–3717; *Angew. Chem. Int. Ed.* **2013**, *52*, 3626–2629.

[22] Q. M. Kainz, A. Schätz, A. Zöpfl, W. J. Stark, O. Reiser, *Chem. Mater.* **2011**, *23*, 3606–3613.

[23] Q. M. Kainz, M. Zeltner, M. Rossier, W. J. Stark, O. Reiser, *Chem. Eur. J.* **2013**, *19*, 10038–10045.

[24] Q. M. Kainz, R. Linhardt, P. K. Maity, P. R. Hanson, O. Reiser, *ChemSusChem* **2013**, *6*, 721–729.

[25] A. Schaetz, M. Zeltner, T. D. Michl, M. Rossier, R. Fuhrer, W. J. Stark, *Chem. Eur. J.* **2011**, *17*, 10566–10573.
[26] R. Gatri, M. M. El Gaïed, *Tetrahedron Lett.* **2002**, *43*, 7835–7836.
[27] S. Luo, B. Zhang, J. He, A. Janczuk, P. G. Wang, J.-P. Cheng, *Tetrahedron Lett.* **2002**, *43*, 7369–7371.
[28] a) J. E. Imbriglio, M. M. Vasbinder, S. J. Miller, *Org. Lett.* **2003**, *5*, 3741–3743; b) C. E. Aroyan, M. M. Vasbinder, S. J. Miller, *Org. Lett.* **2005**, *7*, 3849–3851; c) M. M. Vasbinder, J. E. Imbriglio, S. J. Miller, *Tetrahedron* **2006**, *62*, 11450–11459; d) K. Asano, S. Matsubara, *Synlett* **2009**, *2009*, 35–38.
[29] M. Shi, J.-K. Jiang, C.-Q. Li, *Tetrahedron Lett.* **2002**, *43*, 127–130.
[30] H. J. Davies, A. M. Ruda, N. C. Tomkinson, *Tetrahedron Lett.* **2007**, *48*, 1461–1464.
[31] a) M. Shi, C.-Q. Li, J.-K. Jiang, *Chem. Commun.* **2001**, 833–834; b) M. Shi, C.-Q. Li, J.-K. Jiang, *Tetrahedron* **2003**, *59*, 1181–1189.
[32] R. Linhardt, Q. M. Kainz, R. N. Grass, W. J. Stark, O. Reiser, *RSC Adv.* **2014**, *4*, 8541–8549.
[33] M. Rossier, F. M. Koehler, E. K. Athanassiou, R. N. Grass, B. Aeschlimann, D. Günther, W. J. Stark, *J. Mater. Chem.* **2009**, *19*, 8239–8243.
[34] M. Rossier, A. Schaetz, E. K. Athanassiou, R. N. Grass, W. J. Stark, *Chem. Eng. J.* **2011**, *175*, 244–250.

3. Dendrimers or nanoparticles as supports for the design of efficient and recoverable organocatalysts?[i]

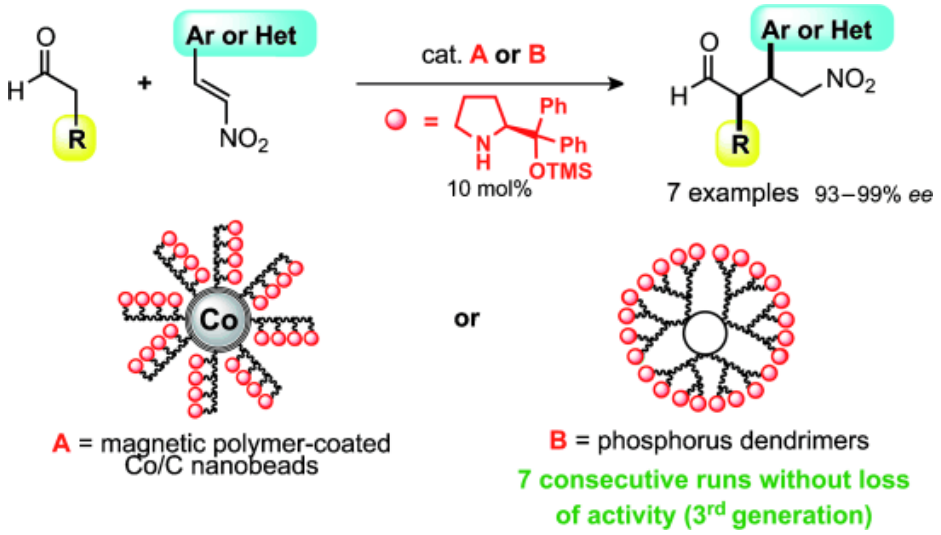

The Jørgensen-Hayashi catalyst [(*S*)-α,α-diphenylprolinol trimethylsilyl ether] was grafted onto the surface of two different supports: phosphorus dendrimers (generations 1 to 3) and magnetic, polymer-coated cobalt/carbon (Co/C) nanobeads. These new supported catalysts displayed high activities and selectivities in the Michael additions of a wide range of aldehydes to different nitroolefins. Moreover, the dendrimer of the third generation displayed excellent recycling abilities since it could be recovered and reused in 7 consecutive runs without loss of activity.[ii]

[i] Reproduced with permission from: M. Keller, A. Perrier, R. Linhardt, L. Travers, S. Wittmann, A.-M. Caminade, J.-P. Majoral, O. Reiser, A. Ouali, Adv. Synth. Catal. 2013, 355, 1748-1754. Copyright © 2013 WILEY-VCH Verlag GmbH & Co. KGaA, Weinheim.

[ii] The synthesis of compounds **33-M**, **33-G$_1$**, **33-G$_2$**, and **33-G$_3$** and all experiments with compounds **33-M**, **33-G$_1$**, **33-G$_2$**, and **33-G$_3$** were carried out by M. Keller, A. Perrier, and L. Travers. The synthesis of **32**, and **33-NP** and all experiments with **33-NP** were carried out by R. Linhardt.

3.1 Introduction

α,α-Diarylprolinol silyl ethers, introduced as organocatalysts by Jørgensen and Hayashi independently in 2005,[1,2] have proved to be versatile organocatalysts, displaying high efficiency, selectivity, and robustness.[3] Major drawbacks of these systems concern the high catalyst loading required as well as the tedious purification processes necessary to separate the organocatalyst from the products. Catalyst immobilization may allow us to overcome both limitations and moreover holds the promise for organocatalyst recovery and reuse.[4] Along these lines, various supports have been proposed for immobilizing the Jørgensen-Hayashi catalyst. They involve polymers,[5,6–9] magnetic nanoparticles (MNPs)[10,11] or dendrons.[12] To the best of our knowledge, the influence of the support's nature on the catalytic performances and recycling abilities of these immobilized organocatalysts has not been studied so far. We thus planned to compare Jørgensen-Hayashi catalysts grafted onto dendrimers and MNPs, two supports that have proved to be very useful in a wide range of reactions. Indeed, dendritic catalysts[13a–c,14,13d,15] can be recycled by precipitation and besides this advantage, dendritic supports may also strongly enhance the catalytic activity ("dendritic effect").[14,15] MNPs are also increasingly recognized as appealing supports since they can be easily recovered by simple magnetic decantation.[16] Herein we report the preparation of (*S*)-α,α-diphenylprolinol trimethylsilyl ether grafted onto phosphorus dendrimers[17] and polystyrene functionalized Co/C MNPs[18a–f,19,18g,20] by using the copper-catalyzed azide-alkyne [3+2] cycloaddition[21] (CuAAC). The latter is an attractive ligation method regarding atom economy and the beneficial effect of the triazole ring on the efficiency of the catalyst which was highlighted in the case of polymeric supports (PEG[8] and polystyrene[6,9]). The catalytic activities and recyclabilities of the nano-organocatalysts obtained were compared in Michael addition reactions of various aldehydes to nitroolefins in conditions comparable to those previously reported by Pericàs and involving a polystyrene resin as the support.[5,6]

3.2 Results and discussion

Azide-functionalized phosphorus dendrimers **31-G_n**[22] (n = 1-3) and carbon coated Co-MNPs with high-loading polymer shells **31-NP**[20] were obtained from the corresponding chloride compounds **30-G_n** and **30-NP**[19] (Scheme 5). The immobilization of α,α-diphenylprolinol trimethylsilyl ethers onto azido-terminated dendrimers **31-G_n** (n = 1-3) and poly(benzyl azide) styrene-functionalized Co/C MNP **31-NP** was per-formed on the gram scale via CuAAC by using acetylenic prolinol **32** (Scheme 6).[8] The loadings of Jørgensen–Hayashi catalysts were in the same order of magnitude for all nano-catalysts: 1.55 mmol g^{-1} for **33-G_1**, 1.45 mmol g^{-1} for **33-G_2**, 1.40 mmol g^{-1} for **33-G_3** and 1.34 mmol g^{-1} for **33-NP**.

However, in the case of dendrimers, functional groups are located on the surface while for MNPs, they are partially inside the polymer shells. Furthermore, a monomeric organocatalyst **33-M** involving the triazole moiety was prepared by reaction between **32** and 4-methoxybenzyl azide. All of these “click” chemistry protocols were monitored by IR tracking the vanishing azide peak at 2085 cm^{-1} (see addendum). Dendrimers **33-G_n** and **33-M** were characterized by ^{1}H, ^{13}C and ^{31}P NMR and the composition of **33-NP** was confirmed by elemental analysis.

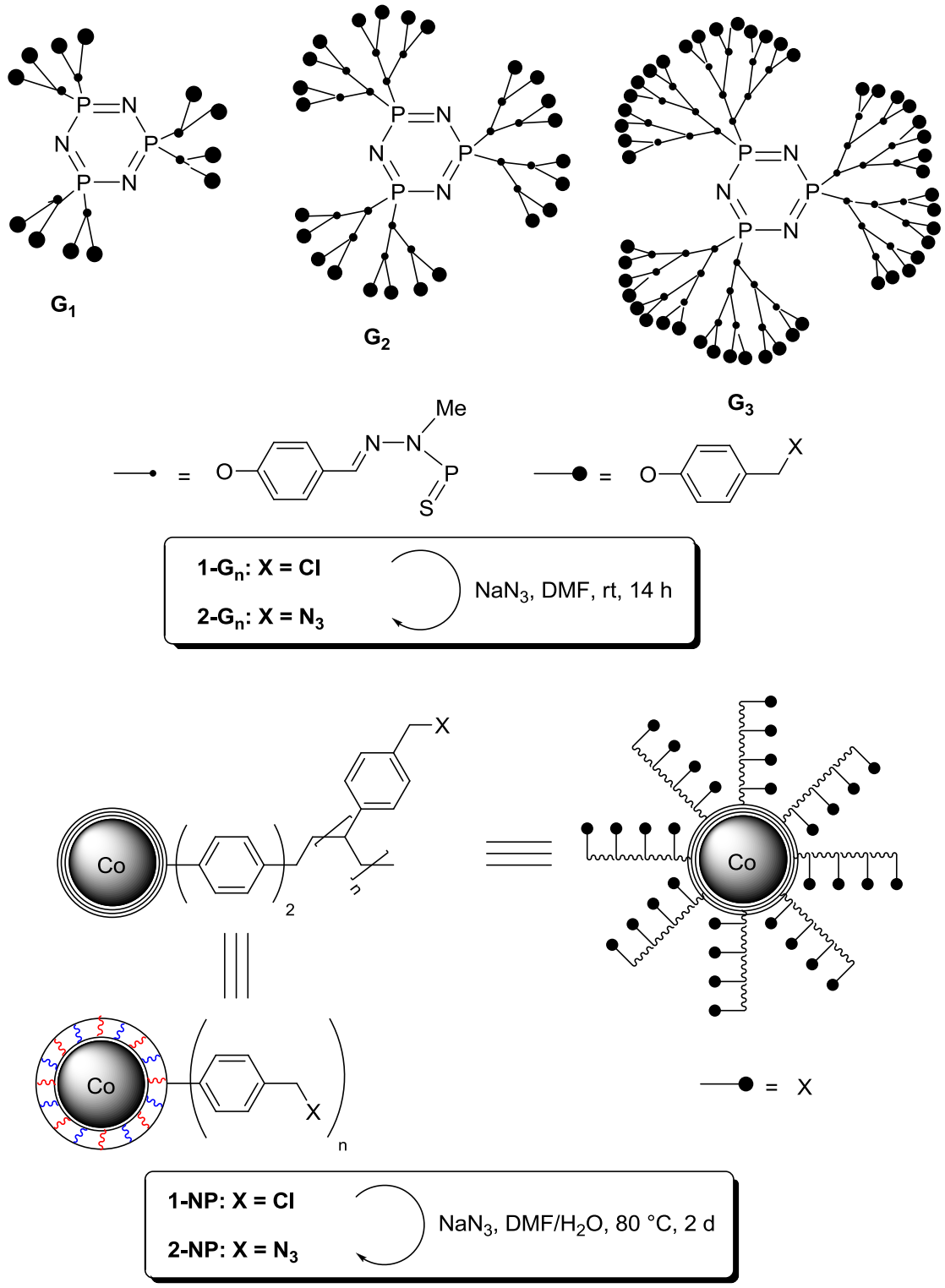

Scheme 5 Preparation of azido-terminated phosphorus dendrimers and Co/C MNP with high-loading polymer shells.

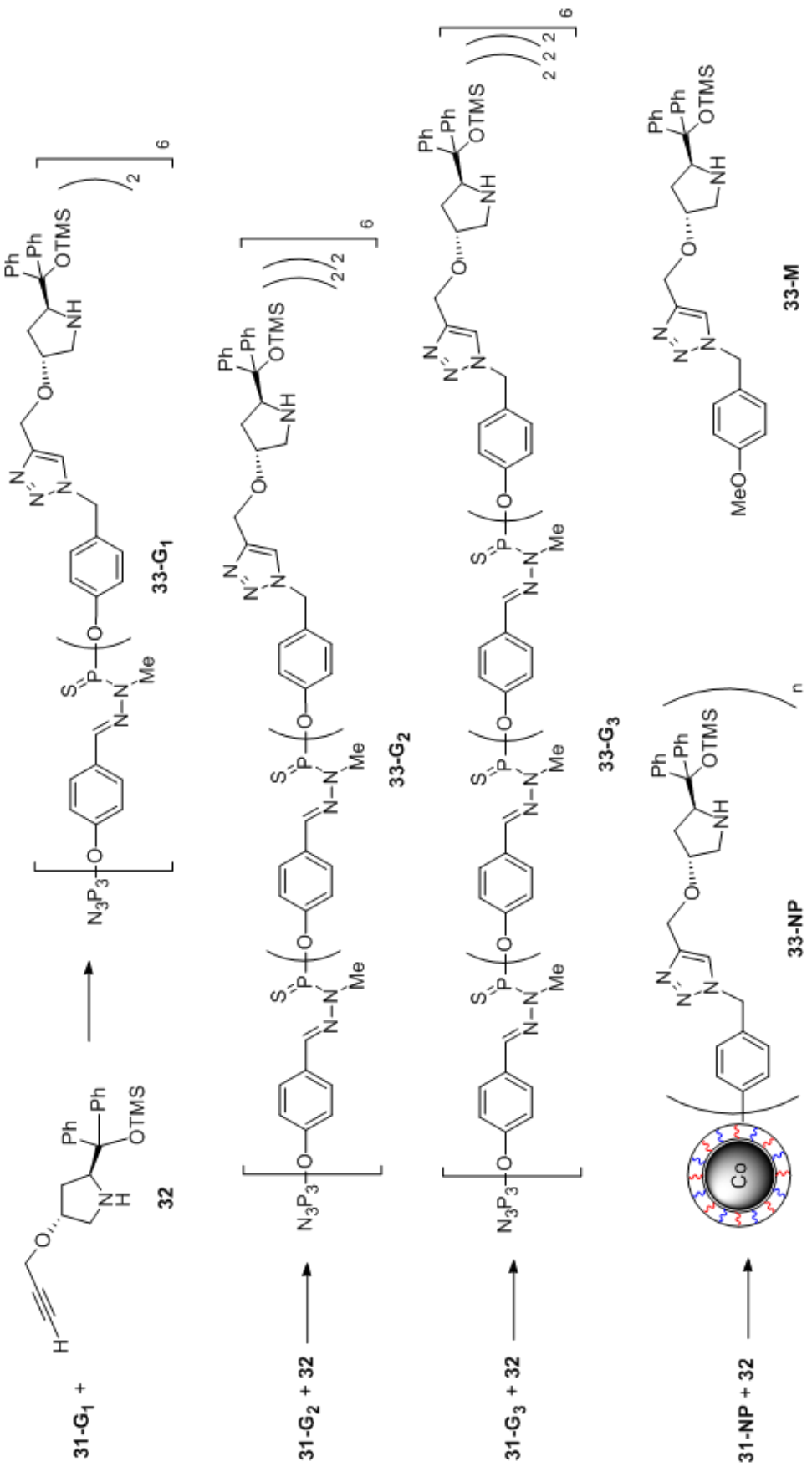

Scheme 6 Preparation of Jørgensen–Hayashi catalysts supported onto dendrimers (**33-G$_n$**, n = 1-3) and magnetic nanoparticles (**33-NP**).

Nano-organocatalysts **33-G_n** (n = 1-3) and **33-NP** were tested in Michael addition reactions under conditions analogous to those previously reported for polystyrene-supported Jørgensen-Hayashi catalyst.[6,9] To the best of our knowledge, this system appears as one of the most efficient to date in terms of activity, selectivity and recyclability (5 times without significant loss of activity in Michael additions).[6,9]

The Michael addition of propanal **34a** to β-nitrostyrene **35a** in CH_2Cl_2 at 10 °C with a **34a**/**35a** ratio of 1.6:1 was selected as the model reaction (Table 9). After 14 h, adduct **36a** could be obtained in fair yield (53%) in the presence of the monomer **33-M** involving the triazole linker. The dendritic supports allowed us to significantly improve the performances since the yield of **36a** reached 80% with **33-G_1** and became quantitative with **33-G_2** and **33-G_3** (entries 2-4). The superiority of 2nd and 3rd generation dendrimers might be rationalized in terms of catalytic site accessibility, the latter being likely more available in the highest generations. Noteworthy, it was checked that 14 h were necessary and sufficient to get complete conversion of **35a** using **33-G_2** and **33-G_3**. Therefore, 14 h was chosen as the reaction time for the following experiments involving dendrimers. Additionally, MNP-based organocatalyst **33-NP** required 22 h to complete the addition, **36a** being obtained in 80% yield after 14 h (entries 5 and 6). This lower activity may be due to a lower availability of the catalysts partially located inside the polymer shell. The *syn* product was almost exclusively formed regardless of the nature of the support, but the best *syn*-to-*anti* ratios were obtained with dendritic organocatalysts **33-G_n** (97:3). In each case, excellent *ee*s (>99%) could be reached and **36a** was quantitatively isolated on the mmol scale without the need for chromatographic purification (entries 4 and 6).

Table 9 Addition of propanal **34a** to β-nitrostyrene **35a** in the presence of dendrimer- and MNP-supported catalysts.[a]

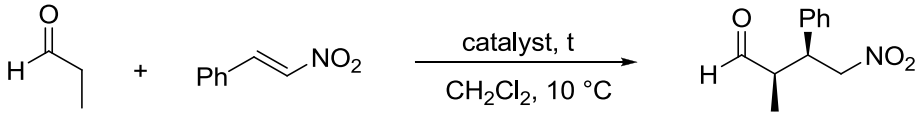

34a **35a** **36a**

Entry	Catalyst	t [h]	Yield [%][c]	*syn/anti*[d]	*ee* [%][e]
1	**33-M**	14	53	98:2	> 99
2	**33-G_1**	14	80	97:3	> 99
3	**33-G_2**	14[b]	> 99	97:3	> 99
4	**33-G_3**	14[b]	> 99 (99)	97:3	> 99
5	**33-NP**	14	80	93:7	> 99
6	**33-NP**	22	> 99 (99)	92:8	> 99

[a] All reactions were performed with β-nitrostyrene **35a** (0.2 mmol), propanal **34a** (0.32 mmol, 1.6 equiv.), CH_2Cl_2 (2 mL) and (S)-α,α-diphenylprolinol trimethylsilyl ether moiety (0.02 mmol): **33-G_1** (12.9 mg, 1.666 mmol), **33-G_2** (13.8 mg, 0.833 mmol), **33-G_3** (14.3 mg, 0.416 mmol), **33-NP** (15.0 mg). [b] 14 h = time required to get complete conversion of **35a** with **33-G_2** and **33-G_3**. [c] The ^{1}H NMR yields were determined with 1,3,5-trimethoxybenzene as the standard/isolated yields in brackets (1 mmol scale, see experimental section). [d] Determined by ^{1}H NMR of the crude reaction mixture. [e] Determined by chiral HPLC.

One of the main advantages to design supported catalysts is the opportunity to recover and reuse them. Recycling experiments were thus carried out with **33-G_n** (n = 1-3) and **33-NP** by precipitation with pentane or magnetic decantation respectively (Fig. 11). The reaction time required for complete conversion of **35a** with **33-G_2** and **33-G_3** (14 h, Table 9) was chosen. Recycling abilities of dendritic catalysts **33-G_1** and **33-G_2** revealed disappointing, yields of **36a** decreasing significantly from the 1st run. On the contrary, catalyst **33-G_3** could be successfully used 4 times while a significant loss of activity was observed from the 3rd run when recycling MNPs **33-NP**. The better recyclability of **33-G_3** compared to **33-G_2** may be rationalized by its lower solubility in pentane which likely enables quantitative recovery. Selectivities remained constantly high during recycling experiments in case of dendrimers as well as MNPs in contrast to literature data.[10,11] As a result,

dendrimer **33-G_3**, recovered by straightforward precipitation that does not require any specific equipment, appeared as the most promising organocatalyst in terms of recycling capabilities. Noteworthy, this is the first time that a supported Jørgensen-Hayashi catalyst can be recycled without increasing the reaction time or resorting to reactivation of the catalyst between two runs.[7,6,9,10] Indeed, the system involving polystyrene as the support could be recycled but required a reconditioning in the presence of non-commercially available trimethylsilyl *N*,*N*-dimethylcarbamate to transform the inactive diphenylprolinol formed during the reaction into the catalytically active silyl ethers.[6,9] Besides, when grafting the Jørgensen-Hayashi catalyst onto MeOPEGs, a deactivation via product inhibition required washings with the aldehyde to restore the catalyst activity.[7] Both methods did not increase the recycling activity in the case of **33-NP**. The scope of nano-organocatalysts **33-G_3** and **33-NP** was next investigated in the Michael addition of various aldehydes **34** to nitroolefins **35** (Table 10).

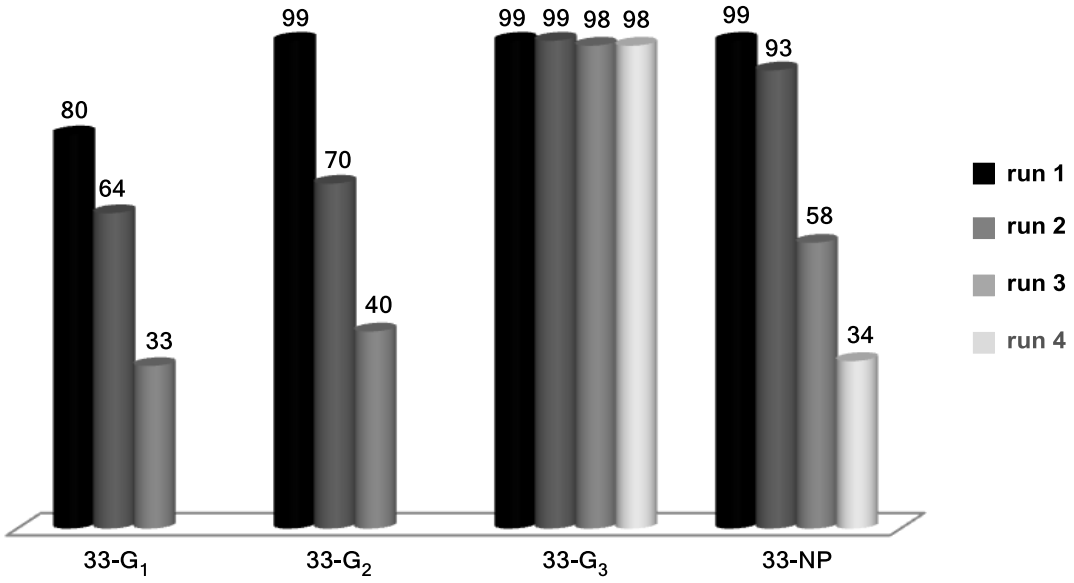

Fig. 11 Michael addition of propanal **34a** to β-nitrostyrene **35a**: Yields of **36a** [%] in recycling experiments. Reaction conditions: see Table 1 (14 h for **33-G_n** and 22 h for **33-NP**). ^{1}H NMR yields were determined by using 1,3,5-trimethoxybenzene as the standard. The *syn*/*anti* ratios for **33-G_n** were 97:3 to 96:4, for **33-NP**: 92:8 to 90:10 as determined by ^{1}H NMR of the crude reaction mixture. The *ee*s were determined by chiral HPLC analysis: >99% for all supported catalysts.

Table 10 Scope of supported organocatalysts **33-NP** and **33-G$_3$**.[a]

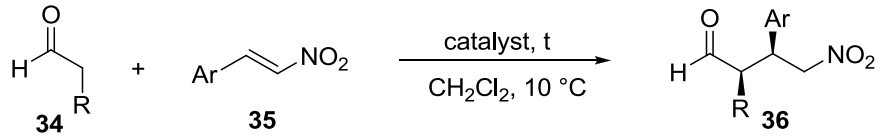

Entry	R^1	R^2	Product	Yield [%][b]	*syn/anti*[c]	*ee* [%][d]	Yield [%][b]	*syn/anti*[c]	*ee* [%][d]
				33-NP			**33-G$_3$**		
1	Me (**5a**)	Ph (**6a**)	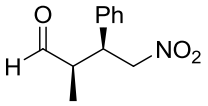 **36a**	>99	92:8	99	>99	97:3	99
2	Et (**5b**)	Ph (**6a**)	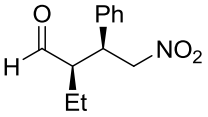 **36b**	98	80:20	98	>99	94:6	98
3	Pr (**5c**)	Ph (**6a**)	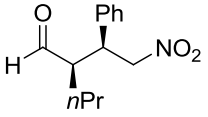 **36c**	99	79:21	99	>99	97:3	>99
4	*n*-pent (**5d**)	Ph (**6a**)	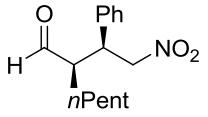 **36d**	42	78:22	98	>99	90:10	>99
5	Me (**5a**)	4-Br-C_6H_4 (**6b**)	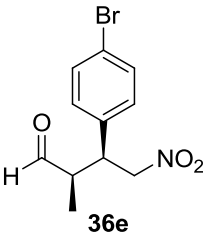 **36e**	97	91:9	98	>99	95:5	98
6	Me (**5a**)	4-MeO-C_6H_4 (**6c**)	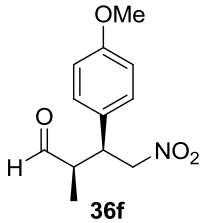 **36f**	98	91:9	97	>99	90:10	97
7	Me (**5a**)	2-furyl (**6d**)	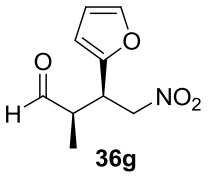 **36g**	96	91:9	93	99	90:10	94

[a] All reactions performed with nitroolefins **35** (0.2 mmol), aldehydes **34** (0.32 mmol, 1.6 equiv.), CH_2Cl_2 (2 mL) and (S)-α,α-diphenylprolinol trimethylsilyl ether moiety (0.02 mmol): **33-G$_3$** (14.3 mg, 0.416 mmol, 14 h), **33-NP** (15.0 mg, 22 h). [b] The ^{1}H NMR yields were determined by using 1,3,5-trimethoxybenzene as the standard. [c] Determined by ^{1}H NMR of the crude reaction mixture. [d] Determined by chiral HPLC analysis.

The Michael additions of various aldehydes differing by the length of the alkyl chain were first performed (entries 1-4). n-Butanal (entry 2) and valeraldehyde (entry 3) reacted with β-nitrostyrene to give adducts **36b** and **36c**, respectively, in quantitative yields within 22 h for **33-NP** and 14 h for **33-G_3** with excellent *ee*s. In terms of diastereoselectivity, dendritic catalyst **33-G_3** proved to be more efficient since *syn*-to-*anti* ratios of 97:3 could be reached against 80:20 in the case of **33-NP**.

Michael additions of less reactive heptanal were found to proceed sluggishly in the presence of **33-NP** (42% yield after 22 h, entry 4) while dendritic catalyst **33-G_3** allowed us to obtain enantiopure **36d** in 99% yield within 14 h. Noteworthy, with the polystyrene supported Jørgensen-Hayashi catalyst, the same reaction required 48 h to go to completion.[6,9] With respect to Michael acceptor, nitroolefins **35b**, **35c** and **35d** bearing substituted aryl or heteroaryl substituents (entries 5-7) led to the expected adducts **36e-g** in quantitative yields, very good *ee*s and diastereoselectivities comparable to those reported for homogeneous[23] and supported[6,9] catalysts in the same process.

Recycling tests of **33-G_3** were finally achieved by changing the substrate at each run (Table 11). Therefore, Michael adducts **36a-g** could successfully be prepared in 7 consecutive runs with very high yields and selectivities. To the best of our knowledge, such a study has never been carried out previously to illustrate the robustness of other supported organocatalysts.

Table 11 Recyclings of **33-G_3** in changing the substrates at each run.[a]

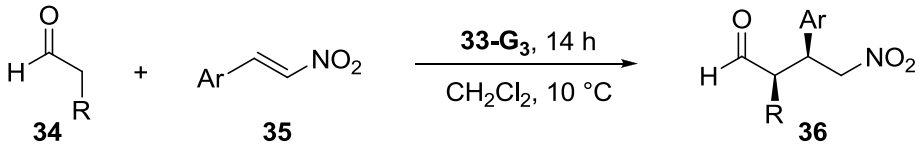

Entry	Run	Adduct	Yield [%][b]	*ee* [%][d]
1	1	**36b**	99	99
2	2	**36d**	99	99
3	3	**36c**	99	99
4	4	**36a**	99	97
5	5	**36f**	98	96
6	6	**36g**	97	93
7	7	**36e**	98	95

[a] All reactions performed with nitroolefins **35** (0.2 mmol), aldehydes **34** (0.32 mmol, 1.6 equiv.), CH_2Cl_2 (2 mL) and **33-G_3** (14.3 mg, 0.416 mmol). [b] Isolated yields. [c] The *syn*/*anti* ratio was determined by ^{1}H NMR of the crude reaction mixture. [d] Determined by chiral HPLC analysis.

3.3 Conclusion

In summary, the Jørgensen-Hayashi organocatalyst was grafted via triazole linkers onto two supports, phosphorus dendrimers and MNPs with high-loading polymer shells. Performances of both catalysts were tested in Michael additions of various aldehydes onto nitroolefins regarding activity, selectivity and recycling ability. Dendrimers turned out to be more active than MNPs since they required 14 h to allow full conversions of all nitroolefins tested instead of 22 h. The catalytic performances of **33-G_3** were generally found to be analogous to those reported for the best homogeneous[22] and supported[6,7] catalysts in the same reaction. Enantio- and diastereoselectivities were high in cases of **33-NP** compared to literature reports while **33-G_3** led to excellent results. In terms of recycling ability, MNPs **33-NP** could be recovered by straightforward magnetic decantation but their activity significantly decreased from the 3rd run. The performances of dendritic catalysts

were found to greatly depend on the generation: 1st and 2nd generations were poorly efficient whereas **33-G_3** could be successfully recovered by precipitation/filtration and reused at least 7 times to yield 7 different adducts in very high yields and selectivities. Noteworthy, this straightforward recovery method does not require any specific equipment contrary to more tedious nanofiltration, for example. **33-G_3** thus constitutes one of the most competitive recyclable supported systems reported so far for organocatalyzed Michael reactions. Lastly, the comparative study reported in this paper illustrates the crucial role of the support on the performances of the catalyst. Structural modifications aiming at further improving efficiencies of reported nano-organocatalysts in terms of activities, selectivities and recyclabilities are ongoing in our laboratories. The extension of their scope to other reactions is also being explored.

3.4 Addendum

The synthesis of the propargylated (*S*)-α,α-diphenylprolinol trimethylsilyl ether was carried out according to a procedure described by Zeitler *et al.* (Scheme 7).[8] It starts from commercially available *trans*-*L*-hydroxy proline **37**. In the first step the amine (as its ethyl carbamate) and the carboxylic acid (as a methyl ester) are protected in a one pot reaction forming **38**. Subsequently, the addition of two equivalents of a phenyl Grignard reagent leads to the formation of tertiary alcohol **39**. Propargylation of **39** additionally leads to the in situ protection of the tertiary alcohol under basic conditions forming a five membered carbamate ring **40**. Opening of the carbamate with KOH again leads to the tertiary alcohol **41**, which is then silyl protected leading to the propargylated Jørgensen-Hayashi catalyst **32**.

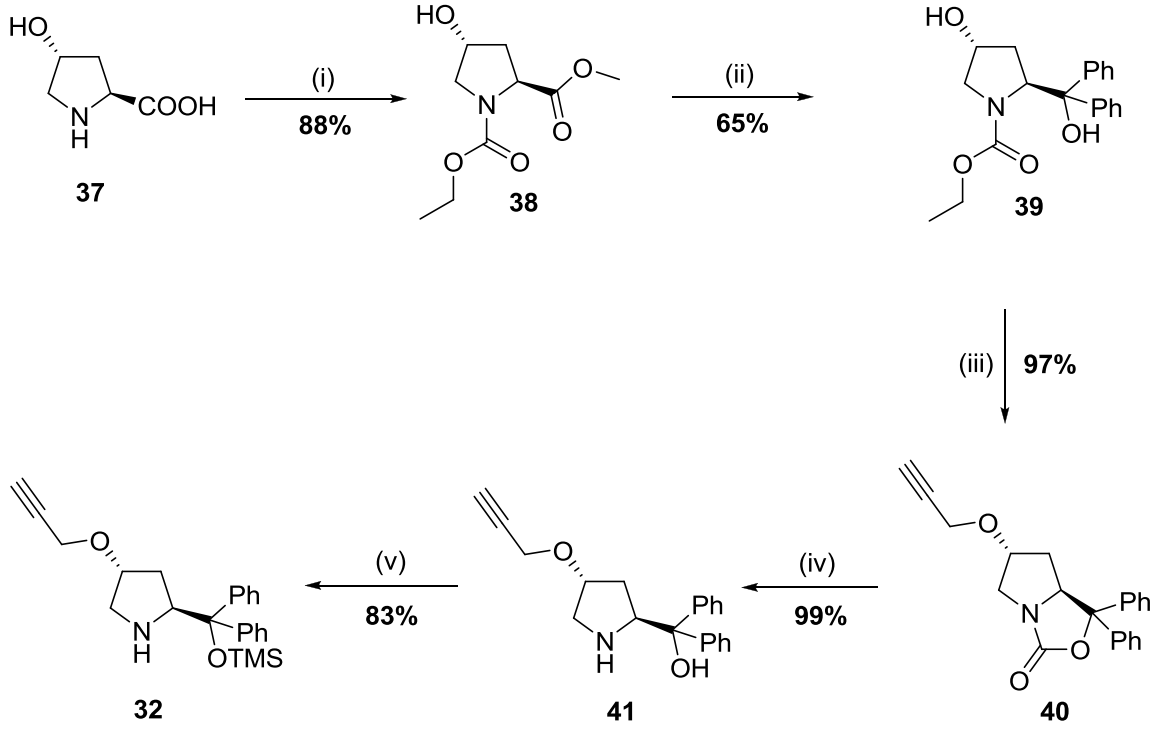

Scheme 7 Synthesis of propargylated (*S*)-α,α-diphenylprolinol trimethylsilyl ether **32** from (2*S*,4*R*)-4-hydroxyprolin **37** according to a literature procedure.[8] Reagents and conditions: (i) $ClCO_2Et$, K_2CO_3, MeOH, 16 h; (ii) PhMgBr, THF, 0 °C, 20 h; (iii) NaH, propargyl bromide, DMF, 0 °C → rt, 18 h; (iv) KOH, EtOH/H_2O, 50 °C, 20 h; (v) TMSOTf, Et_3N, CH_2Cl_2, 0 °C, 22 h.

The immobilization of propargylated Jørgensen-Hayashi organocatalyst was followed by IR spectroscopy (Fig. 12). Poly(benzylchloride)styrene functionalized MNPs **30-NP** clearly show the specific peak for the benzyl chloride at 1260 cm^{-1}. After substitution reaction to azide **31-NP** vanishing of the benzyl chloride peak and the appearance of a azide peak at 2085 cm^{-1} is observed. In the subsequent copper-catalyzed azide-alkyne [3+2] cycloaddition to MNPs **33-NP** the azide peak vanishes completely and the characteristic peaks of the Jørgensen-Hayashi organocatalyst **32** at 1025 cm^{-1}, 1075 cm^{-1}, 1250 cm^{-1}, 1446 cm^{-1}, and 1495 cm^{-1} could be observed.

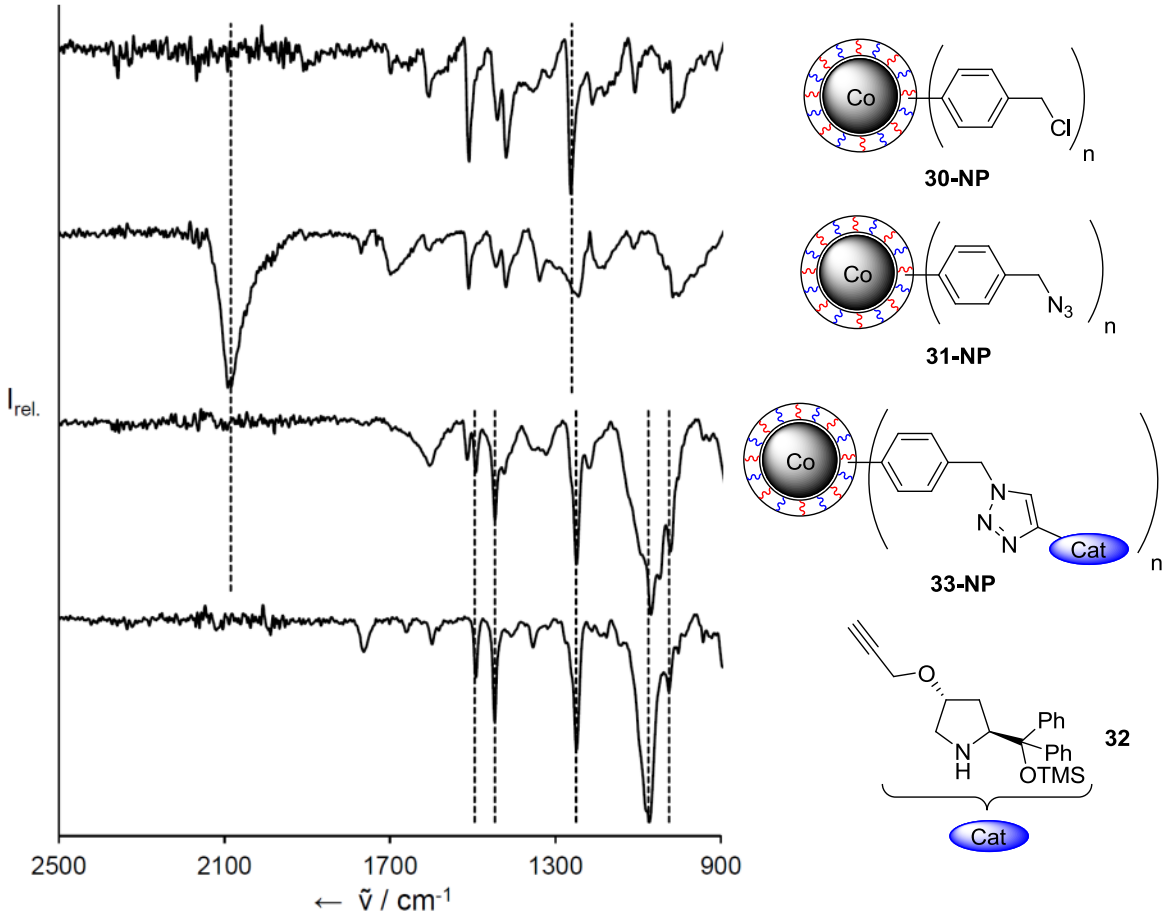

Fig. 12 IR spectra of poly(benzylchloride)styrene functionalized MNPs **30-NP**, poly-(benzylazide)styrene functionalized MNPs **31-NP**, diphenylprolinol trimethylsilyl ether functionalized MNPs **33-NP**, and propargylated diphenylprolinol trimethylsilyl ether **32**.

The catalytic cycle for the Michael addition reaction with the Jørgensen-Hayashi catalyst was already described in literature (Scheme 8).[24] The cycle starts with the condensation of organocatalyst **42** and the respective aldehyde **34** forming enamine **A**. Subsequently, enamine **A** attacks the nitroalkene **35** leading to the zwitterionic species **B**. Protonation of the zwitterionic intermediate **B** first leads to iminium ion **C** which is then hydrolysed regenerating catalyst **42** and releasing the Michael addition product **36**.

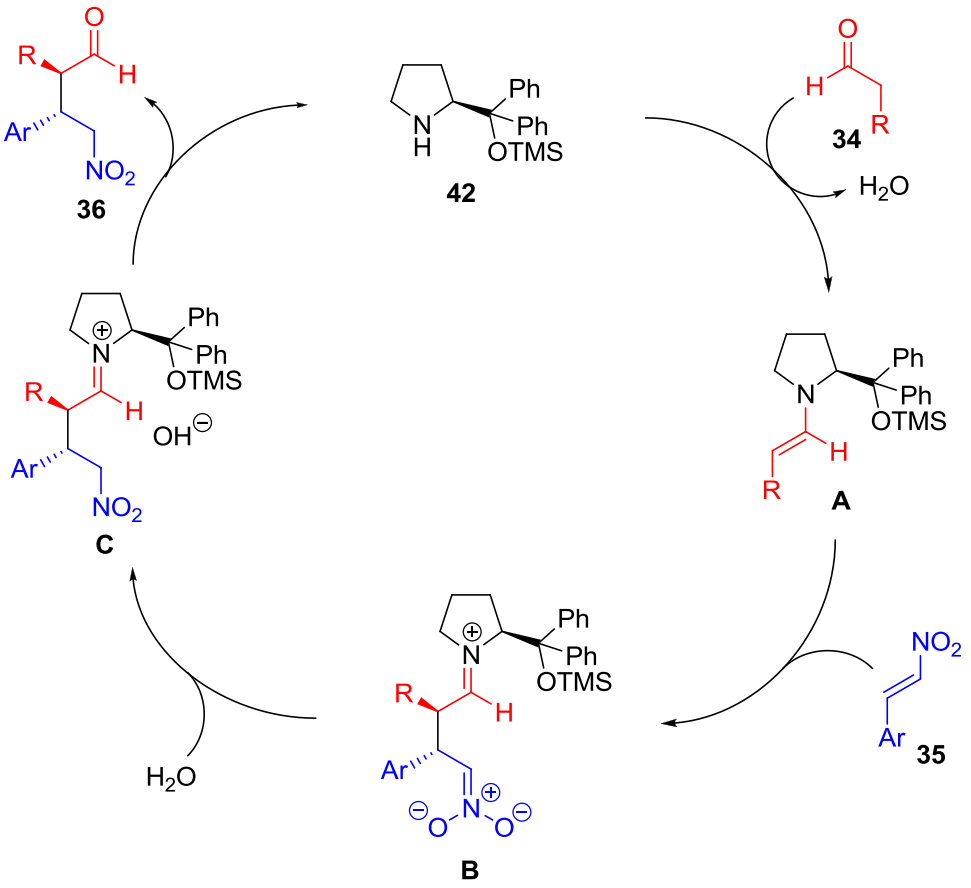

Scheme 8 Catalytic cycle of the Michael addition reaction between aldehydes **34** and nitroalkenes **35** using the Jørgensen-Hayashi catalyst.[24]

3.5 Experimental section

Materials and methods

NMR spectra were recorded with Bruker DPX 300, AV 300, AV 400 spectrometers. All spectra were measured at 25 °C in the indicated deuterated solvents. References for NMR chemical shifts are H_3PO_4 (85%) for ^{31}P NMR, and $SiMe_4$ for ^{1}H and ^{13}C NMR spectroscopies.^{1}H, ^{13}C and ^{31}P chemical shifts (δ) are reported in ppm and coupling constants (*J*) are reported in Hertz (Hz). The signals in the spectra are described as s (singlet), d (doublet), t (triplet), m (multiplet) and br (broad resonances). Attribution was carried out thanks to two-dimensional experiments when necessary (COSY, HMBC, HMQC).

IR Spectra were recorded with a Bio-Rad FT-IR Excalibur FTS 3000 equipped with a Specac *Golden Gate* Diamond Single Reflection ATR-System. Catalytic reactions were performed on a Radley carousel „Reaction station RR 98030“.

Liquid chromatographies (HPLC) were recorded on a Shimadzu instrument with a Shimadzu LC-2010 HT and using IA, IC or AD-H columns.

Chemicals were purchased from Aldrich, Acros, Fluka, Alfa Aesar and Strem, and were used without further purification, except for $P_3N_3Cl_6$ which was recrystallized from hexane and 4-hydroxybenzaldehyde which was recrystallized from diethyl ether. Organic solvents were dried and distilled according to usual procedures.[25] Purifications by column chromatography were performed on silica gel (50 µm). TLCs were performed on silica gel 60 F254 plates and detection was carried out under UV light. Dendrimers $\mathbf{G_n}$ were synthesized according to published procedures.[26,22]

The carbon coated cobalt nanomagnets (Co/C, 20.5 m^2/g, mean particle size ≈ 25 nm) were purchased from Turbobeads Llc, Switzerland. Prior to use, they were washed in a concentrated HCl / water mixture (1:1) 5 times for 24 h. Acid residuals were removed by washing with millipore water (5x) and the particles were dried at 50 °C in a vacuum oven.[27] The magnetic nanobeads were dispersed using an ultrasound bath and recovered with the aid of a neodymium based magnet (15 x 30 mm). They were characterized by IR-ATR spectroscopy and elemental microanalysis (LECO CHN-900). Poly(benzylchloride)styrene coat-

ed cobalt nanoparticles **30-NP**[19] and poly(benzylazide)styrene functionalized cobalt nanoparticles **31-NP**[20] were prepared on the gram scale following previously reported procedures.

(2*S*,4*R*)-2-(Diphenyl(trimethylsilyloxy)methyl)-4-(prop-2-ynyloxy)pyrrolidine was synthesized according to a literature procedure.[8]

Azido-terminated dendrimers **31-G_1**, **31-G_2** and **31-G_3** have also been previously described.[22] The latter were identified in each case by ^{1}H NMR and ^{31}P NMR spectroscopy and the data obtained matched literature values.

For all "click reactions" (copper-catalyzed 1,3-cycloadditions) solvent was degassed before use.

Synthesis of the nanoparticles

Co/C-PS supported diphenylprolinol trimethylsilyl ether (33-NP)

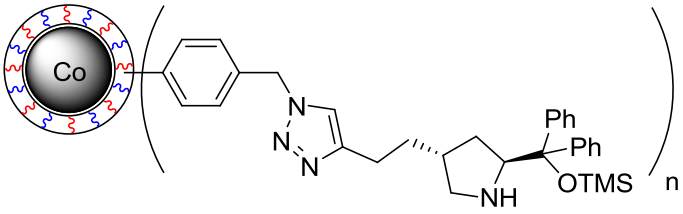

150 mg (0.51 mmol) of Co/C-PS-N_3 **31-NP**, 81 mg (0.15 mmol) TBTA and 18 mg (0.10 mmol) CuI were predispersed in 10 mL degassed dichloromethane for 10 min using ultrasonic bath. 387 mg (1.02 mmol) propargylated catalyst **32** and 63 µL (0.51 mmol) diisopropyl ethylamine were added and the reaction mixture was stirred for 2 d at room temperature. The particles were separated from the mixture by an external magnet, washed with dichloromethane (3 x 5 mL), aqueous EDTA (3 x 5 mL), H_2O (3 x 5 mL) and acetone (3 x 5 mL). After drying in vacuum 291 mg of **33-NP** were obtained.

IR ($\tilde{\nu}$/cm^{-1}): 2916, 1604, 1513, 1492, 1446, 1323, 1249, 1218, 1069, 1022, 874, 836, 751, 700; elemental microanalysis (%): C, 59.22; H, 5.76; N, 7.53.

General procedures for catalytic experiments

Catalysis: Michael reaction

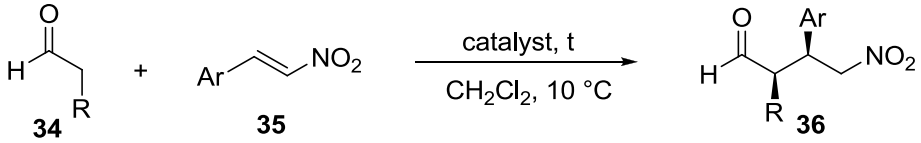

Catalytic reactions were carried out under argon atmosphere using Radley Carousel "reaction station RR98030". The yields and disatereoisomer proportions of final products are calculated by ^{1}H NMR using 1,3,5-trimethoxybenzene as the standard and *ee*'s were measured by HPLC.

General procedure for the Michael addition with using dendritic organocatalysts

After standard cycles of evacuation and back-filling with argon, a Radley tube equipped with a magnetic stirring bar was charged with catalyst (0.838 µmol for **33-G$_1$**, 0.419 µmol for **33-G$_2$**, 0.210 µmol for **33-G$_3$**) and nitroolefin **35** (0.2 mmol). CH_2Cl_2 (2 mL) was introduced, the mixture was cooled to 0 °C and aldehyde **34** (0.32 mmol) was added. The mixture was stirred at 10 °C for 22 h. An aliquot was used for HPLC analysis and the mixture. Solvent was concentrated under vacuum, 1,3,5-trimethoxybenzene (0.18 mmol) and pentane (10 mL) were added. The precipitate was filtered and washed once with pentane (5 mL). The combined filtrates were dried under vacuum and used for NMR analysis (yield and diastereoisomeric ratio). After standard cycles of evacuation and back-filling with argon, the precipitate was directly used for a new catalytic run.

General procedure for the Michael addition with Co/C-PS supported organocatalysts

After standard cycles of evacuation and back-filling with argon, a Radley tube (Carousel "reaction station RR98030") was charged with 15.0 mg of **33-NP** (0.02 mmol of α,α-diphenylprolinol trimethylsilyl ether moieties) and nitroolefin **35** (0.2 mmol). After adding 2 mL of dry dichloromethane, the reaction mixture was predispersed for 10 min using an ultrasonic bath. The mixture was cooled to 10 °C, aldehyde **34** (0.32 mmol) was added and the mixture was stirred at 10 °C

for 22 h. Then 30 mg of 1,3,5-trimethoxybenzene (0.18 mmol) was added as standard. An aliquot was used for HPLC analysis and the reaction mixture was separated from the catalyst by an external magnet. After washing the particles with dichloromethane (5 x 3 mL), the combined washing solutions were evaporated and the product mixture dried for NMR analysis (yield and diastereomeric ratio). For recycling experiments the particles **33-NP** were again washed with dichloromethane (3 x 3 mL), dried in vacuo and reused for further runs.

HPLC for Michael adducts

All products are known and all spectroscopic data matched with those reported in the literature.

(2*R*, 3*S*)-2-Methyl-4-nitro-3-phenylbutanal (36a)[2]

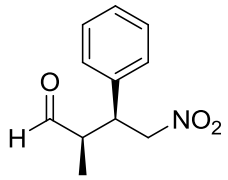

(2*R*,3*S*)-2-Methyl-4-nitro-3-phenylbutanal **36a** was prepared from *trans*-β-nitrostyrene (29.8 mg, 0.2 mmol) and propionaldehyde (23 µL, 0.32 mmol) according to the General Procedures. The enantiomeric excess was determined by HPLC using an IC column (hexane-ethanol 95:5, 0.8 mLmin^{-1}, 214 nm): t_R = 16.9 min (major, *anti*), 20.2 min (minor, *syn*), 23.4 min (major, *syn*), 24.5 min (minor, *anti*).

(2*R*, 3*S*)-2-Ethyl-4-nitro-3-phenylbutanal (36b)[1]

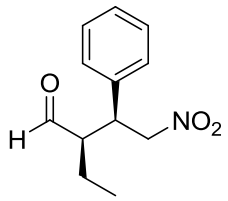

(2*R*,3*S*)-2-Ethyl-4-nitro-3-phenylbutanal **36b** was prepared from *trans*-β-nitrostyrene (29.8 mg, 0.2 mmol) and butanal (29 µL, 0.32 mmol) according to the General Procedures. The enantiomeric excess was determined by HPLC using an IA column (hexane-*i*PrOH 99:1, 0.4 mLmin^{-1}, 254 nm): t_R = 47.6 min (major, *syn*), 54.4 min (major, *anti*), 66.1 min (minor, *anti*), 74.4 min (minor, *syn*).

(2*R*)-((*S*)-2-Nitro-1-phenylethyl)-pentanal (36c)[1]

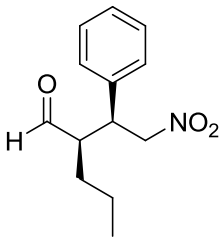

(2*R*)-((*S*)-2-Nitro-1-phenylethyl)-pentanal **36c** was prepared from *trans*-β-nitrostyrene (29.8 mg, 0.2 mmol) and valeraldehyde (34 µL, 0.32 mmol) according to the General Procedures. The enantiomeric excess was determined by HPLC using an IA column (hexane-ethanol 99:1, 0.8 mLmin^{-1}, 214 nm): t_R = 23.8 min (minor, *anti*), 26.7 min (major, *anti*), 36.7 min (minor, *syn*), 39.3 min (major, *syn*).

(2*R*)-((*S*)-2-Nitro-1-phenylethyl)-heptanal (36d)[28]

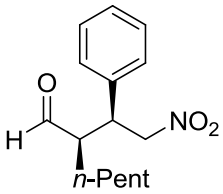

(2*R*)-((*S*)-2-Nitro-1-phenylethyl)-heptanal **36d** was prepared from *trans*-β-nitrostyrene (29.8 mg, 0.2 mmol) and heptaldehyde (45 µL, 0.32 mmol) according to the General Procedures. The enantiomeric excess was determined by HPLC using an IA column (hexane-*i*PrOH 99:1, 0.4 mLmin^{-1}, 254 nm): t_R = 28.9 min (major, *syn*), 36.5 min (minor, *syn*), 47.8 min (minor, *anti*), 53.1 min (major, *anti*).

(2*R*, 3*S*)-(4-Bromophenyl)-2-methyl-4-nitrobutyraldehyde (36e)[1]

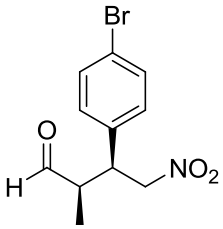

(2*R*,3*S*)-(4-Bromophenyl)-2-methyl-4-nitrobutyraldehyde **36e** was prepared from *trans*-4-bromo-β-nitrostyrene (45.6 mg, 0.2 mmol) and propionaldehyde (23 µL, 0.32 mmol) according to the General Procedures. The enantiomeric excess was determined by HPLC using an AD-H column (hexane-*i*PrOH 99:1, 0.6 mLmin^{-1},

254 nm): t_R = 22.4 min (major, *syn*), 25.3 min (major, *anti*), 41.7 min (minor, *anti*), 49.4 min (minor, *syn*).

(2*R*, 3*S*)-2-Methyl-4-nitro-3-(4-methoxyphenyl)-butanal (36f)[1]

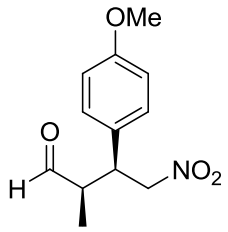

(2*R*,3*S*)-2-Methyl-4-nitro-3-(4-methoxyphenyl)-butanal **36f** was prepared from *trans*-4-methoxy-β-nitrostyrene (35.8 mg, 0.2 mmol) and propionaldehyde (23 µL, 0.32 mmol) according to the General Procedures. The enantiomeric excess was determined by HPLC using an IC column (hexane-ethanol 80:20, 0.6 mLmin^{-1}, 254 nm): t_R = 8.7 min (major, *anti*), 12.1 min (major, *syn*), 12.8 min (minor, *syn*), 14.7 min (minor, *anti*).

(2*R*, 3*S*)-3-Furyl-2-methyl-4-nitrobutyraldehyde (36g)[1]

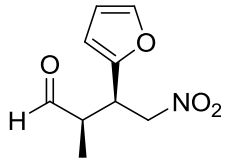

(2*R*,3*S*)-3-Furyl-2-methyl-4-nitrobutyraldehyde **36g** was prepared from 2-(2-nitrovinyl)-furan (27.8 mg, 0.2 mmol) and propionaldehyde (23 µL, 0.32 mmol) according to the General Procedures. The enantiomeric excess was determined by HPLC using an IC column (hexane-*i*PrOH 95:5, 0.6 mLmin^{-1}, 230 nm): t_R = 23.2 min (minor, *anti*), 23.6 min (minor, *syn*), 30.0 min (major, *syn*), 31.8 min (major, *anti*).

TEM picture

Transmission electron microscopy (TEM) picture of Co/C-PS supported diphenylprolinol trimethylsilyl ether **33-NP**:

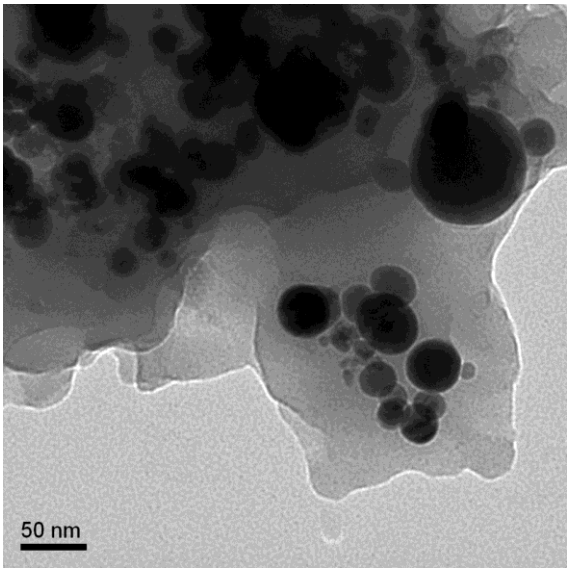

3.6 References

[1] M. Marigo, T. C. Wabnitz, D. Fielenbach, K. A. Jørgensen, *Angew. Chem.* **2005**, *117*, 804–807; *Angew. Chem. Int. Ed.* **2005**, *44*, 4212–4215.

[2] Y. Hayashi, H. Gotoh, T. Hayashi, M. Shoji, *Angew. Chem.* **2005**, *117*, 4284–4287; *Angew. Chem. Int. Ed.* **2005**, *44*, 794–797.

[3] a) C. Palomo, A. Mielgo, *Angew. Chem.* **2006**, *118*, 8042–8046; *Angew. Chem. Int. Ed.* **2006**, *45*, 7876–7880; b) A. Mielgo, C. Palomo, *Chem. Asian J.* **2008**, *3*, 922–948; c) L.-W. Xu, L. Li, Z.-H. Shi, *Adv. Synth. Catal.* **2010**, *352*, 243–279; d) K. L. Jensen, G. Dickmeiss, H. Jiang, Ł. Albrecht, K. A. Jørgensen, *Acc. Chem. Res.* **2012**, *45*, 248–264.

[4] a) S. Bräse, F. Lauterwasser, R. E. Ziegert, *Adv. Synth. Catal.* **2003**, *345*, 869–929; b) A. Corma, H. Garcia, *Adv. Synth. Catal.* **2006**, *348*, 1391–1412; c) B. M. L. Dioos, I. F. J. Vankelecom, P. A. Jacobs, *Adv. Synth. Catal.* **2006**, *348*, 1413–1446; d) M. Benaglia, *New J. Chem.* **2006**, *30*, 1525; e) M. Benaglia in *Handbook of Asymmetric Heterogeneous Catalysis* (Eds.: K. Ding, Y. Uozumi), Wiley-VCH Verlag GmbH & Co. KGaA, Weinheim, Germany, **2008**; f) M. Gruttadauria, F. Giacalone, R. Noto, *Chem. Soc. Rev.* **2008**, *37*, 1666–1688; g) F. Giacalone, M. Gruttadauria, R. Noto in *Ideas in Chemistry and Molecular Sciences* (Ed.: B. Pignataro), Wiley-VCH Verlag GmbH & Co. KGaA, Weinheim, Germany, **2010**; h) T. E. Kristensen, T. Hansen, *Eur. J. Org. Chem.* **2010**, *2010*, 3179–3204; i) A.-M. Caminade, A. Ouali, M. Keller, J.-P. Majoral, *Chem. Soc. Rev.* **2012**, *41*, 4113–4125.

[5] a) C. Röben, M. Stasiak, B. Janza, A. Greiner, J. Wendorff, A. Studer, *Synthesis* **2008**, *2008*, 2163–2168; b) M. C. Varela, S. M. Dixon, K. S. Lam, N. E. Schore, *Tetrahedron* **2008**, *64*, 10087–10090.

[6] E. Alza, M. A. Pericàs, *Adv. Synth. Catal.* **2009**, *351*, 3051–3056.

[7] T. E. Kristensen, K. Vestli, M. G. Jakobsen, F. K. Hansen, T. Hansen, *J. Org. Chem.* **2010**, *75*, 1620–1629.

[8] I. Mager, K. Zeitler, *Org. Lett.* **2010**, *12*, 1480–1483.

[9] E. Alza, S. Sayalero, P. Kasaplar, D. Almaşi, M. A. Pericàs, *Chem. Eur. J.* **2011**, *17*, 11585–11595.

[10] B. G. Wang, B. C. Ma, Q. Wang, W. Wang, *Adv. Synth. Catal.* **2010**, *352*, 2923–2928.

[11] P. Riente, C. Mendoza, M. A. Pericás, *J. Mater. Chem.* **2011**, *21*, 7350–7355.

[12] Y. Li, X.-Y. Liu, G. Zhao, *Tetrahedron: Asymmetry* **2006**, *17*, 2034–2039.

[13] a) D. A. Tomalia, P. R. Dvornic, *Nature* **1994**, *372*, 617–618; b) R. van Heerbeek, P. C. J. Kamer, P. W. N. M. van Leeuwen, J. N. H. Reek, *Chem. Rev.* **2002**, *102*, 3717–3756; c) A.-M. Caminade, J.-P. Majoral, *Coord. Chem. Rev.* **2005**, *249*, 1917–1926; d) R. Andrés, E. de Jesús, J. C. Flores, *New J. Chem.* **2007**, *31*, 1161.

[14] B. Helms, J. M. J. Fréchet, *Adv. Synth. Catal.* **2006**, *348*, 1125–1148.

[15] A. Ouali, R. Laurent, A.-M. Caminade in *Dendrimers: Towards catalytic, material, and biomedical uses*.

[16] a) S. Roy, M. A. Pericàs, *Org. Biomol. Chem.* **2009**, *7*, 2669–2677; b) S. Shylesh, V. Schünemann, W. R. Thiel, *Angew. Chem.* **2010**, *122*, 3504–3537; *Angew. Chem. Int. Ed.* **2010**, *49*, 3428–3459; c) A. Schätz, O. Reiser, W. J. Stark, *Chem. Eur. J.* **2010**, *16*, 8950–8967; d) V. Polshettiwar, R. Luque, A. Fihri, H. Zhu, M. Bouhrara, J.-M. Basset, *Chem. Rev.* **2011**, *111*, 3036–3075; e) A. Schaetz, M. Zeltner, W. J. Stark, *ACS Catal.* **2012**, *2*, 1267–1284.

[17] a) A. Ouali, R. Laurent, A.-M. Caminade, J.-P. Majoral, M. Taillefer, *J. Am. Chem. Soc.* **2006**, *128*, 15990–15991; b) M.-A. Lacour, M. Zablocka, C. Duhayon, J.-P. Majoral, M. Taillefer, *Adv. Synth. Catal.* **2008**, *350*, 2677–2682; c) M. Keller, M. Ianchuk, S. Ladeira, M. Taillefer, A.-M. Caminade, J.-P. Majoral, A. Ouali, *Eur. J. Org. Chem.* **2012**, *2012*, 1056–1062; d) M. Keller, A. Hameau, G. Spataro, S. Ladeira, A.-M. Caminade, J.-P. Majoral, A. Ouali, *Green Chem.* **2012**, *14*, 2807–2815; e) M. Keller, V. Collière, O. Reiser, A.-M. Caminade, J.-P. Majoral, A. Ouali, *Angew. Chem.* **2013**, *125*, 3714–3717; *Angew. Chem. Int. Ed.* **2013**, *52*, 3626–3629.

[18] a) R. N. Grass, E. K. Athanassiou, W. J. Stark, *Angew. Chem.* **2007**, *119*, 4996–4999; *Angew. Chem. Int. Ed.* **2007**, *46*, 4909–4912; b) A. Schätz, R. N. Grass, W. J. Stark, O. Reiser, *Chem. Eur. J.* **2008**, *14*, 8262–8266; c) S. Wittmann, A. Schätz, R. N. Grass, W. J. Stark, O. Reiser, *Angew. Chem.* **2010**, *122*, 1911–1914; *Angew. Chem. Int. Ed.* **2010**, *49*, 1867–1870; d) A. Schätz, T. R. Long, R. N. Grass, W. J. Stark, P. R. Hanson, O. Reiser, *Adv. Funct. Mater.* **2010**, *20*, 4323–4328; e) A. Schätz, R. N. Grass, Q. Kainz, W. J. Stark, O. Reiser, *Chem. Mater.* **2010**, *22*, 305–310; f) M. Zeltner, A. Schätz, M. L. Hefti, W. J. Stark, *J. Mater. Chem.* **2011**, *21*, 2991–2996; g) M. Rossier, A. Schaetz, E. K. Athanassiou, R. N. Grass, W. J. Stark, *Chem. Eng. J.* **2011**, *175*, 244–250.

[19] A. Schaetz, M. Zeltner, T. D. Michl, M. Rossier, R. Fuhrer, W. J. Stark, *Chem. Eur. J.* **2011**, *17*, 10566–10573.

[20] Q. M. Kainz, A. Späth, S. Weiss, T. D. Michl, A. Schätz, W. J. Stark, B. König, O. Reiser, *ChemistryOpen* **2012**, *1*, 125–129.

[21] R. Huisgen, *Pure Appl. Chem.* **1989**, *61*, 613–628.

[22] A. Gissibl, C. Padié, M. Hager, F. Jaroschik, R. Rasappan, E. Cuevas-Yañez, C.-O. Turrin, A.-M. Caminade, J.-P. Majoral, O. Reiser, *Org. Lett.* **2007**, *9*, 2895–2898.

[23] a) P. García-García, A. Ladépêche, R. Halder, B. List, *Angew. Chem.* **2008**, *120*, 4797–4799; *Angew. Chem. Int. Ed.* **2008**, *47*, 4719–4721; b) Y. Hayashi, T. Itoh, M. Ohkubo, H. Ishikawa, *Angew. Chem.* **2008**, *120*, 4800–4802; *Angew. Chem. Int. Ed.* **2008**, *47*, 4722–4724.

[24] K. Patora-Komisarska, M. Benohoud, H. Ishikawa, D. Seebach, Y. Hayashi, *Helv. Chim. Acta* **2011**, *94*, 719–745.

[25] D. D. Perrin, W. L. F. Armarego, *Purification of laboratory chemicals*, Pergamon Press, Oxford, **1998**.

[26] N. Launay, A.-M. Caminade, J. P. Majoral, *J. Organomet. Chem.* **1997**, *529*, 51–58.

[27] M. Rossier, F. M. Koehler, E. K. Athanassiou, R. N. Grass, B. Aeschlimann, D. Günther, W. J. Stark, *J. Mater. Chem.* **2009**, *19*, 8239–8243.

[28] C. Palomo, S. Vera, A. Mielgo, E. Gómez-Bengoa, *Angew. Chem.* **2006**, *118*, 6130–6133; *Angew. Chem. Int. Ed.* **2006**, *45*, 5984–5987.

4. Palladium nanoparticles supported on ionic liquid modified, magnetic nanobeads – recyclable, high-capacity catalysts for alkene hydrogenation[i]

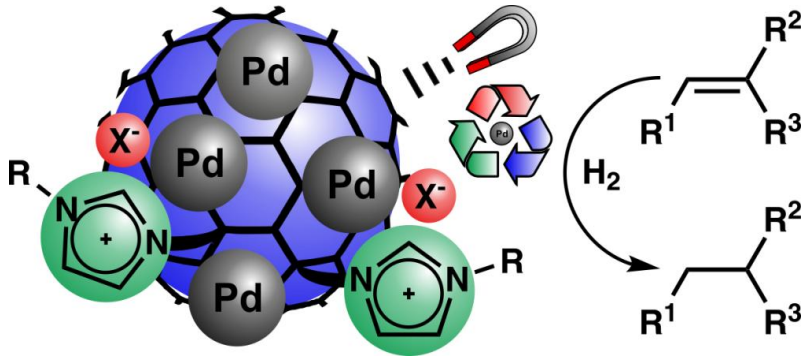

Magnetic hybrid materials have been synthesized as recyclable catalysts for alkene hydrogenation. The materials consist of magnetic nanobeads functionalized with imidazolium-based ionic liquids and optional polymer shells. Palladium nanoparticles (NPs) were synthesized on the surface of these supports by two different methods and evaluated as catalysts for alkene hydrogenation. Deposition of palladium(0) onto the magnetic nanobeads by microwave decomposition of $Pd_2(dba)_3 \cdot CHCl_3$ leads to more efficient catalysts than the reduction of a Pd(II) precursor. Reactivity, recycling ability and ease of separation of the catalysts are compared. A hybrid material without polymer shells and a quite flexible ionic liquid was identified as the most promising for stabilizing Pd NPs resulting in a catalyst that shows high activity (TOF up to 330 h^{-1}), good recycling ability, and minor metal leaching into the product. Notably, the activity of this catalyst increases with an enhanced Pd loading, contrasting related systems for which a decrease of activity is observed due to agglomeration. Therefore, this recyclable, high-capacity system is especially attractive for large-scale applications, requiring just a minimal amount of supporting material for the recycling of expensive Pd that is readily achieved by magnetic decantation.[ii]

[i] Reproduced with permission from: R. Linhardt, Q. M. Kainz, R. N. Grass, W. J. Stark, O. Reiser, RSC Adv. 2014, 4, 8541-8549. Copyright © 2014 The Royal Society of Chemistry.
[ii] TEM was carried out by R. Grass. XRD was performed by P. Peter and ICP-OES was carried out by J. Rewitzer. All other synthesis and experiments were carried out by R. Linhardt.

4.1 Introduction

Pd-catalyzed reactions are widely applied in today's organic synthesis.[1] The variety of reactions is enormous ranging from alkylations, oxidations and carbonylations to coupling reactions or hydrogenations. Especially palladium promoted hydrogenations[2] and coupling reactions[3] play a very important role in pharmaceutical, agrochemical and fine chemical industries. Therefore, the reuse and recycling of palladium and other expensive metals like platinum or gold is a major concern in organic chemistry and especially in industry.[4]

In recent years, the application of palladium nanoparticles became of strong interest owing to their extremely high surface to volume ratio compared to the bulk phase. Metal nanoparticles exceed the catalytic activity of the bulk metal by far, and consequently, the use of nanoparticles as catalysts can reduce the amount of metal needed in organic synthesis. However, aggregation of the nanomaterial to the bulk phase often causes problems during catalysis. To overcome these difficulties, nanoparticles can be stabilized by their immobilization on solid supports[5a,6,5b,5c,7] or their coating with ionic liquids (ILs).[8] Additionally a combination of both strategies is also possible using supported ionic liquids (SILs).[9]

Ionic liquids can stabilize nanoparticles electrostatically or by coordination of the metal.[10] During recent years, palladium NPs were frequently stabilized by ILs applying either sole ILs,[11] supported ionic liquid phases (SILPs)[12] or ILs covalently supported on polymers,[13] silica,[14] and carbon nanotubes.[15] Activity and recycling ability of these Pd NPs is often significantly increased. However, the ease of recycling often suffers from the need of cost- and time-intensive filtration methods. One concept to solve this problem is the application of magnetic supports allowing the recovery of Pd NPs by simple magnetic decantation.[16] We recently reported Pd NPs deposited on magnetic carbon coated cobalt nanoparticles as catalysts for alkene hydrogenation. However, these catalysts suffered from agglomeration of the Pd NPs on the carbon surface of the magnetic support over time, allowing only small loadings of Pd (<1 wt%) to achieve high activity. Moreover, a significant decrease of activity of these catalysts was observed upon recycling and reuse.[17] Hence, the overall aim of this study is to generate a high-loading Pd nanocatalyst by the introduction of stabilizing IL groups and, furthermore, to take advantage of a magnetic support allowing simple magnetic separation.

Herein, we describe the synthesis of novel hybrid systems consisting of a magnetic core (carbon-coated Co nanobeads), covalently attached imidazolium ILs and Pd nanoparticles immobilized on the surface. The attachment of ILs on the particles was performed in three different ways: (i) directly on the surface of the nanobeads; (ii) on a polymer coating the nanobeads; (iii) on a flexible spacer which is attached to the nanoparticles (Fig. 13). Our study includes the synthesis and characterization of the novel hybrid materials, comparison of different Pd sources for the nanoparticle synthesis, influence of the different materials on activity/recycling ability, leaching tests, and recycling studies.

4.2 Results and discussion

Carbon-coated cobalt nanobeads (Co/C) were used as magnetic support for our studies. The highly magnetic material (158 emu/g) is synthesized on large scale via reducing flame spray pyrolysis (>30 g/h).[18] The graphene-like coating of the beads provides high stability against acids, air/moisture, high temperature and, furthermore, enables facile functionalization of the surface analogous to carbon nanotubes (CNTs). We successfully demonstrated covalent as well as non-covalent methods to immobilize catalysts,[19,20] scavengers,[21] reagents[21,22] or fluorescent dyes[23] on the graphene-like surface. While the loading via direct immobilization is limited to ≈0.2 mmol/g,[16] the introduction of polymer-shells can lead to a higher loading of up to 3 mmol/g.[24,25] This reduces the amount of required support and can even lead to higher activities due to a dendritic-like effect.[25] Most recently, we reported the deposition of Pd nanoparticles on the carbon surface of Co/C NPs.[17] This novel material (Fig. 13, **17**) showed extremely high activity in alkene hydrogenation reactions (TOF up to 11095 h^{-1}) and exceeded other Pd catalysts, especially common Pd/C catalysts, by far. These catalysts could be reused for six consecutive runs, however, a loss of activity was observed from the second run indicating agglomeration of the nanoparticles deposited on the Co/C support. Furthermore, a quite large amount of supporting material is needed due to the necessity of low palladium loading onto the support in order to achieve high catalytic activities.

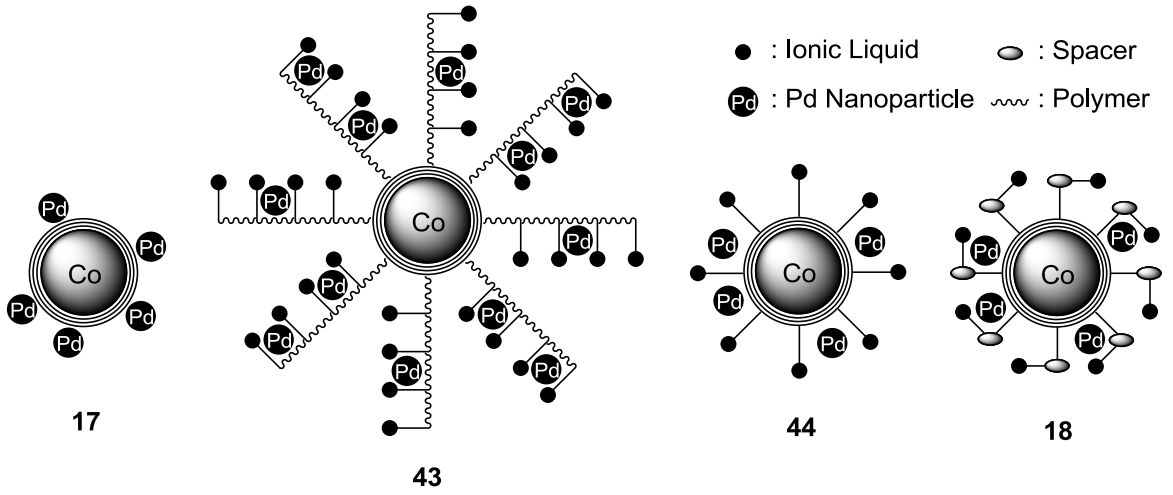

Fig. 13 Novel Pd@Co/C hybrid systems: Pd@Co/C **17**,[17] Pd@PS-IL@Co/C **43**, Pd@Bz-IL@Co/C **44**, and Pd@Spacer-IL@Co/C **18**.

Synthesis of Co/C-supported ionic liquids

Since ILs are known to effectively stabilize metal nanoparticles through electrostatic interactions and coordination of the metal,[8] Co/C-supported ILs could serve as a stabilizing material for Pd nanoparticles and therefore enhance the recycling ability of Pd catalysts. Hence, we synthesized different Co/C nanobeads with ILs covalently bound to the surface: PS-IL@Co/C **45** having a polymer shell between the Co/C beads and the IL (Scheme 9), Bz-IL@Co/C **48** bearing an IL directly on the Co/C surface, and Spacer-IL@Co/C **51**, having a small, flexible spacer between the Co/C core and the IL (Scheme 10).

The synthesis of PS-IL@Co/C **45** started from poly(benzyl-chloride)styrene functionalized Co/C NPs **30-NP** (3.1 mmol/g chloride)[20,21] via microwave reaction with methyl imidazole (Scheme 9). The loading of IL on the surface was determined by elemental microanalysis as 2.1 mmol/g, indicating a 88% displacement of chloride with the imidazolium moiety.

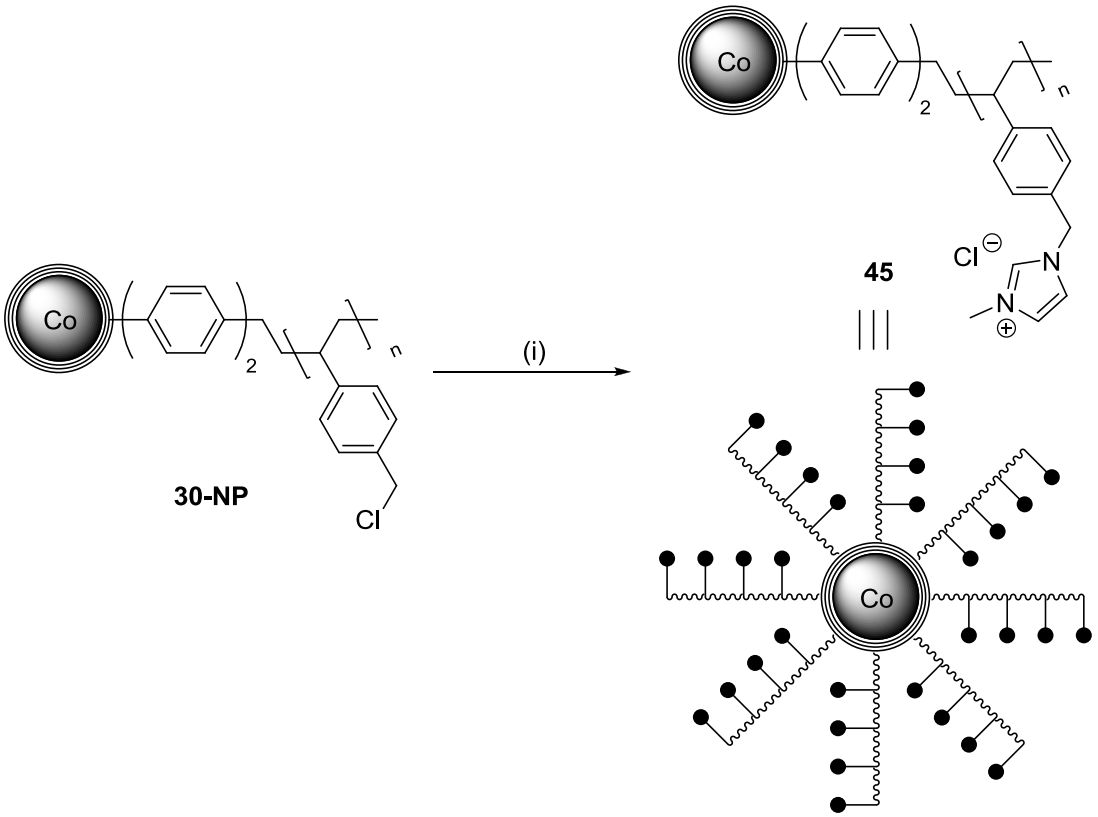

Scheme 9 Synthesis of PS-IL@Co/C **45** from poly(benzyl-chloride)styrene functionalized Co/C NPs **30-NP**. Reagents and conditions: (i) methyl imidazole, toluene, microwave heating, 150 °C, 30 min.

Bz-IL@Co/C **48** and Spacer-IL@Co/C **51** were synthesized from benzyl-alcohol functionalized Co/C NPs **46** (Scheme 10).[19] Benzyl-chloride modified Co/C NPs **47** were generated by substitution reaction of **46** (0.11 mmol/g benzyl alcohol) with $SOCl_2$. To obtain Bz-IL@Co/C **48**, **47** was subsequently heated under microwave irradiation with methyl imidazole. The loading of IL on the surface was 0.09 mmol/g, reflecting 83% of the maximum loading. Spacer-IL@Co/C **51** were synthesized by oxidation of **46**, followed by amide formation of the benzoic acid functionalized Co/C NPs **47** with 1-(3-aminopropyl)imidazole. After substitution with 1-bromobutane following the lead of Lee *et al.*[15] Spacer-IL@Co/C **51** were generated with a loading of 0.05 mmol/g, reflecting 47% of the maximum loading after three steps.

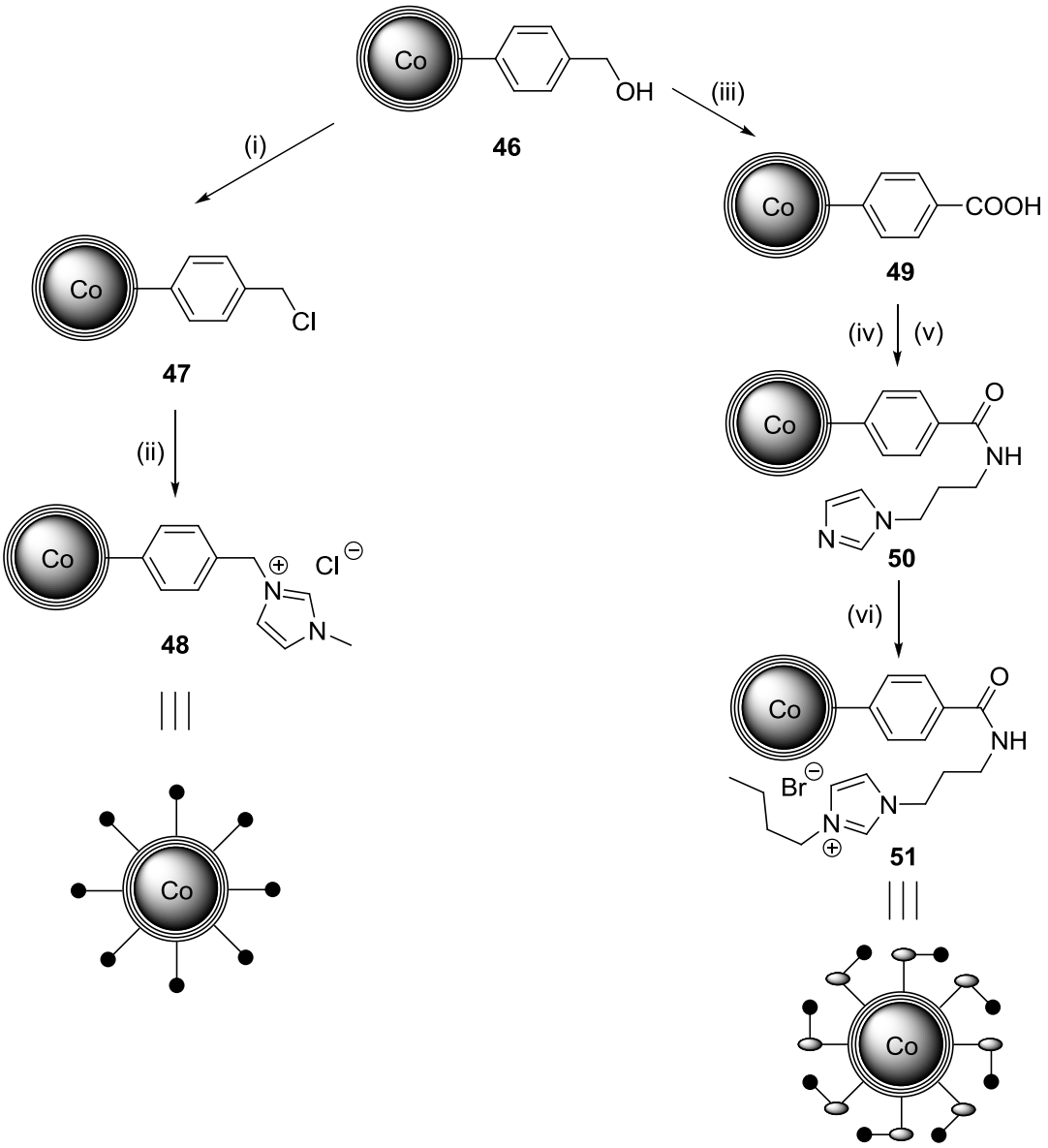

Scheme 10 Synthesis of Bz-IL@Co/C **48** and Spacer-IL@Co/C **51** from benzyl-alcohol functionalized Co/C NPs **46**. Reagents and conditions: (i) $SOCl_2$, DMF, DCM, 0 °C → rt, 12 h; (ii) methyl imidazole, toluene, microwave heating, 150 °C, 30 min; (iii) $KHSO_5$, $MeCN/H_2O$, reflux, 24 h; (iv) $SOCl_2$, reflux, 24 h; (v) amino propyl imidazole, 120 °C, 24 h; (vi) bromo butane, 80 °C, 24 h.

Synthesis of Pd@IL@Co/C with varying Pd loadings

In a second step palladium NPs were deposited on IL modified Co/C NPs (IL@Co/C). Different mass ratios of palladium to IL@Co/C were used in the synthesis to determine an effect of the palladium loading on the catalytic activity.

The deposition of palladium NPs on IL@Co/C was carried out using two different methods. Urriolabeitia *et al.*[7] reported a procedure to immobilize palladium NPs on CNTs using $Pd_2(dba)_3{\cdot}CHCl_3$ as Pd(0) source in dry toluene under

microwave heating in just two minutes. Alternatively Lee *et al.*[15] reported a procedure reducing Na_2PdCl_4 under hydrogen atmosphere to deposit palladium NPs on ionic liquid functionalized CNTs.

The tendency of $Pd_2(dba)_3 \cdot CHCl_3$ to rapidly form Pd NPs upon decomposition was recently intensely discussed by the group of Ananikov.[26] The nanoparticles are not just formed under heating conditions, but also at room temperature upon storing for longer time. The amount of decomposed complex furthermore depends on the commercial source or the applied method of synthesis, respectively. The nanoparticles formed at room temperature were found to have a size of 60-200 nm with minor amounts of smaller ones (10-20 nm). The complex we used for our studies was commercially available (see experimental section), which was determined by the method of Ananikov to contain 68% of $Pd_2(dba)_3 \cdot CHCl_3$ along with Pd NPs, being in good agreement with the results reported for commercial sources.[26]

Applying the two described methods we synthesized catalysts with varying palladium loadings for PS-IL@Co/C **45**, Bz-IL@Co/C **48**, and Spacer-IL@Co/C **51** (Table 12). For PS-IL@Co/C **45** dry toluene was replaced by a mixture of dry toluene/MeOH in order to increase the swelling of the polystyrene coating. The amount of palladium used in the synthesis is given as the mass ratio of ionic-liquid functionalized Co/C NPs to Pd. E.g. a mass ratio of 1:0.1 means 100 mg NPs to 10 mg Pd. The Pd content for the resulting hybrid materials was determined by ICP-OES analysis.

Table 12 Synthesis of Pd@PS-IL@Co/C **43**, Pd@Bz-IL@Co/C **44**, and Pd@Spacer-IL@Co/C **18** with varying Pd loadings.

Entry	Index	Pd source	Method of synthesis[a]	Mass ratio[b]	Pd incorporated [%][c]	Pd loading [mmol/g][c]	Pd content [wt%][c]
1	**43a**	$Pd_2(dba)_3{\cdot}CHCl_3$	A	1:1	56	2.6	28
2	**43b**	$Pd_2(dba)_3{\cdot}CHCl_3$	A	1:0.6	64	2.3	24
3	**43c**	$Pd_2(dba)_3{\cdot}CHCl_3$	A	1:0.2	74	1.2	12
4	**43d**	$Pd_2(dba)_3{\cdot}CHCl_3$	A	1:0.1	69	0.6	6
5	**43e**	$Pd_2(dba)_3{\cdot}CHCl_3$	A	1:0.01	81	0.08	0.8
6	**43f**	Na_2PdCl_4	B	1:1	100	4.8	50
7	**43g**	Na_2PdCl_4	B	1:0.6	90	3.2	34
8	**43h**	Na_2PdCl_4	B	1:0.2	85	1.3	14
9	**44a**	$Pd_2(dba)_3{\cdot}CHCl_3$	A	1:1	91	4.3	45
10	**44b**	$Pd_2(dba)_3{\cdot}CHCl_3$	A	1:0.6	83	2.9	31
11	**44c**	$Pd_2(dba)_3{\cdot}CHCl_3$	A	1:0.2	100	1.6	17
12	**44d**	$Pd_2(dba)_3{\cdot}CHCl_3$	A	1:0.1	86	0.7	8
13	**44e**	$Pd_2(dba)_3{\cdot}CHCl_3$	A	1:0.01	96	0.09	0.9
14	**18a**	$Pd_2(dba)_3{\cdot}CHCl_3$	A	1:1	86	4.0	43
15	**18b**	$Pd_2(dba)_3{\cdot}CHCl_3$	A	1:0.6	90	3.2	34
16	**18c**	$Pd_2(dba)_3{\cdot}CHCl_3$	A	1:0.2	81	1.3	14
17	**18d**	$Pd_2(dba)_3{\cdot}CHCl_3$	A	1:0.1	90	0.8	8
18	**18e**	$Pd_2(dba)_3{\cdot}CHCl_3$	A	1:0.01	100	0.09	1

[a] Method A: heating under microwave irradiation; method B: reduction with H_2. [b] Mass ratio of NPs to Pd in the synthesis. [c] Determined by ICP-OES.

Thus, hybrid materials were obtained with Pd contents ranging from 0.8-50 wt% (Pd@PS-IL@Co/C, **43a-h**), 0.9-45 wt% (Pd@Bz-IL@Co/C, **44a-e**) and 1-43 wt% (Pd@Spacer-IL@Co/C, **18a-e**). The palladium incorporation into the polystyrene coated platforms PS-IL@Co/C **45** is not as effective as the deposition on Bz-IL@Co/C **48** and Spacer-IL@Co/C **51** (Fig. 14A). Especially with an increasing amount of palladium used in the synthesis the gap of Pd incorporation between polymeric and non-polymeric NPs is increasing. Furthermore, the results with PS-IL@Co/C **45** show that the palladium incorporation starting from a Pd(II) source is much more effective than starting from a Pd(0) source (Fig. 14B). This is probably due to the higher polarity of the solvent used in the synthesis, being consistent with the synthesis of **43** starting from $Pd_2(dba)_3 \cdot CHCl_3$, where a solvent mixture of dry toluene/MeOH leads to a better swelling and dispersibility than in pure toluene.

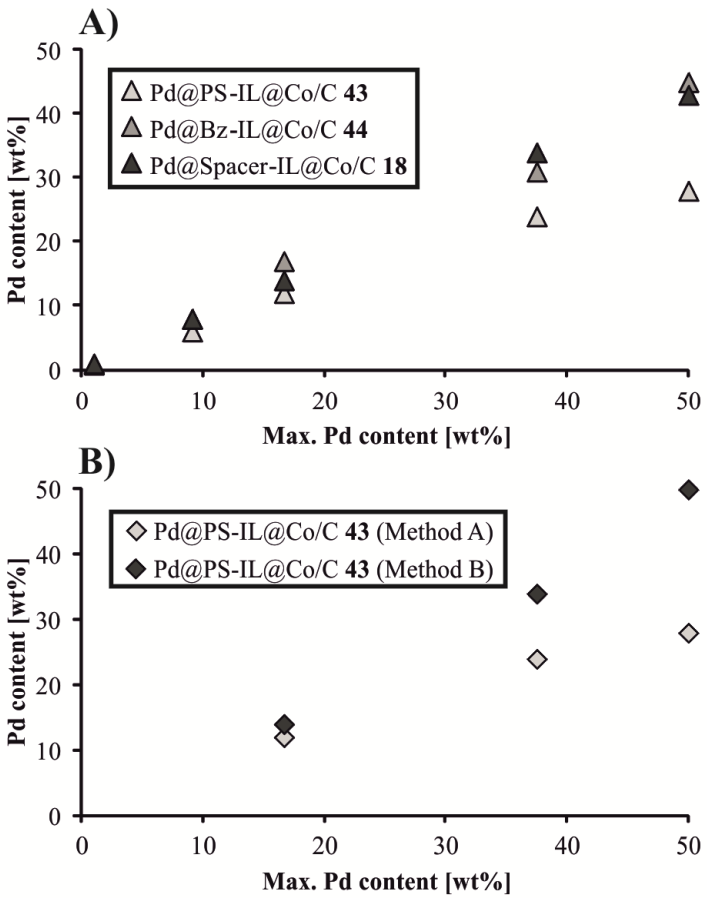

Fig. 14 Comparison of Pd incorporation depending on A) the support (Method A) and B) the deposition method.

The novel hybrid materials were characterized using transmission electron microscopy (TEM) and x-ray powder diffraction (XRD) techniques. TEM pictures clearly show the existence of Pd nanoparticles (5-15 nm) on the surface of the Co/C nanobeads (see experimental section), while XRD proves the presence of Pd and Co both in oxidation state ±0: For Co(0) the characteristic peaks at 2θ of 44.25°, 51.50°, and 75.81° and for Pd the characteristic peaks at 2θ of 40.06°, 46.49°, 67.94°, and 81.85° were observed (see experimental section). However, at Pd contents lower than 10 wt% the characteristic Pd(0) peaks could not be distinguished from the background any longer.

As the nanoparticles we observed on the surface of the supports are between 5-15 nm, we can conclude that Pd NPs which were already present in the $Pd_2(dba)_3 \cdot CHCl_3$ complex (10-200 nm)[26] were crushed under the high temperature microwave conditions applied.

Hydrogenation of *trans*-stilbene

To evaluate the activity of the different catalysts and the effects of varying Pd loading the hydrogenation of *trans*-stilbene **11a** with molecular hydrogen was chosen as test reaction. The amount of catalyst was adjusted to ensure either 0.1 mol% or 1 mol% of Pd in each reaction.

Table 13 shows the results of the catalytic tests. Starting with catalyst **43**, we observed a higher acitivity of those stemming from the Pd(0) source.[iii] For example, comparing catalyst **43c** (12 wt% Pd, Table 13, entry 4) with **43h** (14 wt% Pd, Table 13, entry 9) the activity is almost four times higher in case of the material prepared from the Pd(0) precursor. In both cases the activity of the materials increases with a higher Pd content on the surface which is opposite to what was observed in case of carbon stabilized Pd NPs (Pd@Co/C).[17] The maximum turn over frequency for the polymeric material **43** was 100 h^{-1}.

[iii] The same trend was observed for Pd@Co/C nanobeads.[17]

Table 13 Hydrogenation of *trans*-stilbene **11a** using Pd@PS-IL@Co/C **43**, Pd@Bz-IL@Co/C **44** and Pd@Spacer-IL@Co/C **18**.[a]

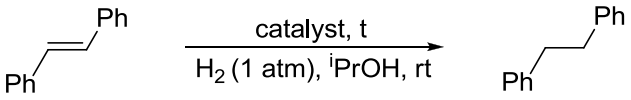

11a **12a**

Entry	Catalyst	Pd [wt%]	Catalyst [mol%]	t [min]	Conversion [%][b]	TOF [h^{-1}][c]
1	**43a**	28	1.0	60	87	87
2	**43b**	24	1.0	60	100	100
3	**43b**	24	0.1	60	5	50
4	**43c**	12	1.0	60	91	91
5	**43d**	6	1.0	60	52	52
6	**43e**	0.8	1.0	60	1	1
7	**43f**	50	1.0	60	48	48
8	**43g**	34	1.0	60	22	22
9	**43h**	14	1.0	60	23	23
10	**44a**	45	0.1	60	15	150
11	**44b**	31	0.1	60	19	190
12	**44c**	17	0.1	60	33	330
13	**44d**	8	0.1	60	61	610
14	**44e**	0.9	0.1	60	88	880
15[d]	**44e**	0.9	0.1	15	100	4000
16	**18a**	43	0.1	90	50	333
17	**18a**	43	1.0	75	100	80
18	**18b**	34	0.1	90	34	200
19[d]	**18b**	34	0.1	90	58	387
20	**18b**	34	1.0	120	100	50
21	**18c**	14	0.1	90	16	107
22	**18d**	8	0.1	90	10	93
23	**18e**	1	0.1	90	1	7

[a] Stilbene **11a** (2 mmol) in ^{i}PrOH (20 mL) was hydrogenated by 2 µmol (0.1 mol%) or 20 µmol (1 mol%) of catalyst using dodecane as internal GC standard. [b] Determined by GC analysis using internal standard. [c] Mol of substrate transformed per mol catalyst per hour. [d] 10 bar of H_2 pressure.

Using the non-polymer coated catalyst Pd@Bz-IL@Co/C **44** we observed an increase in activity by a factor of nine (Table 13, entry 14) and could even reach a turn over frequency of 4000 h^{-1} applying a hydrogen pressure of 10 bar (Table 13, entry 15). The loading/activity relationship in this case is reversed compared to the polystyrene coated catalyst **43**. The material with the lowest loading shows the highest activity in the hydrogenation (Table 13, entry 14). The activity of Pd@Spacer-IL@Co/C **18** turned out to be in between **43** and **44**, the maximum TOF was observed for **18a** (333 h^{-1}, Table 13, entry 16). Activity increases again with an increase in loading as previously seen for the polystyrene coated particles **43**.

Generally, we observed also differences during the catalytic tests regarding the ease of separation of the materials (Fig. 15). Magnetic separation in case of polystyrene coated particles **43**, especially the ones with high Pd content, took several minutes applying a 1.2 T neodymium based magnet (Fig. 15A). However, hybrid materials **44** (Fig. 15B) and **18** (Fig. 15C) were separated from the reaction mixture within seconds.

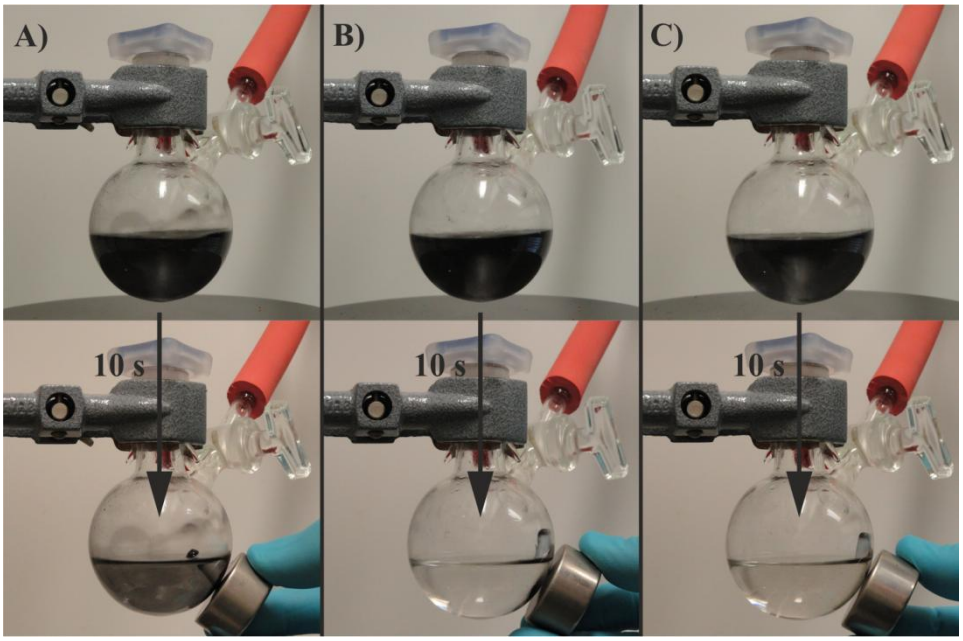

Fig. 15 Collecting the nanocatalysts from the reaction mixture by an external magnet. A) Pd@PS-IL@Co/C **43b**, B) Pd@Bz-IL@Co/C **44b**, C) Pd@Spacer-IL@Co/C **18b**.

Recycling studies

We next investigated the recycling ability of the three different hybrid materials (Fig. 16). Recycling experiments in all cases were performed with the two high-loading catalysts of each material, i.e. with Pd@PS-IL@Co/C **43a** and **43b**, Pd@Bz-IL@Co/C **44a** and **44b**, and Pd@Spacer-IL@Co/C **18a** and **18b**. Reactions were carried out with an initial palladium amount of 1 mol% and stopped in each case after reaching full conversion in the first run. For further runs the reaction time was held constant.

In cases of **43** and **44** a drop of activity is observed after the first or the second run, respectively. This indicates that these materials are not effectively stabilizing the Pd NPs on the surface resulting in aggregation of the Pd NPs and/or leaching of Pd. However, the material with the more flexible ionic liquid on the surface shows much better results. In case of **18a** we also see a decrease in yield after the first run, whereas for **18b** recycling is possible for at least five runs without loss of activity demonstrating the efficient stabilization of Pd NPs on the surface of the hybrid material. The observation of a slight decrease for catalyst **18a** is probably caused by agglomeration due to higher Pd contents. From now on **18b** was used as catalyst for further leaching/recycling studies.

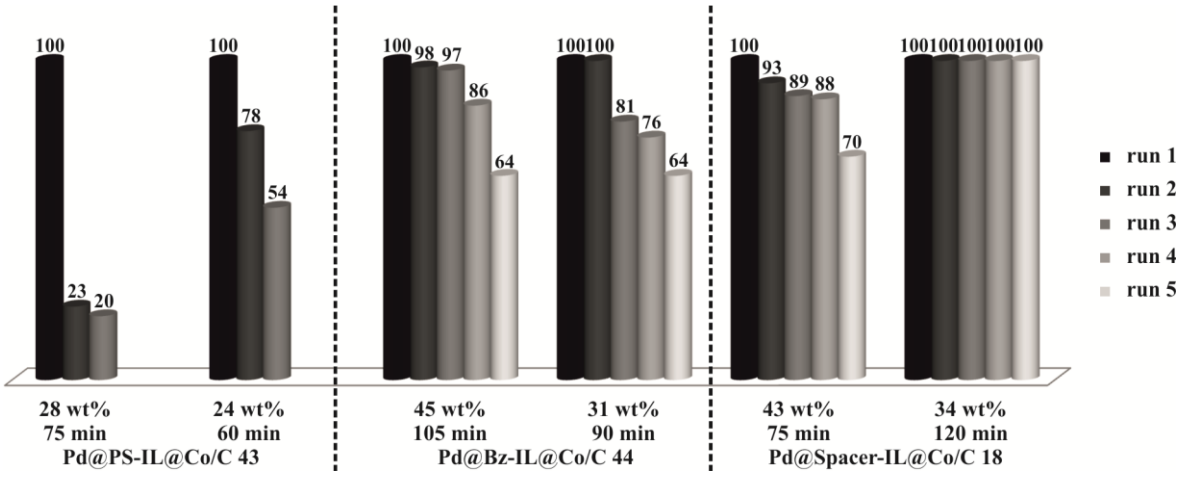

Fig. 16 Recycling studies with Pd@PS-IL@Co/C (**43a**, **43b**), Pd@Bz-IL@Co/C (**44a**, **44b**) and Pd@Spacer-IL@Co/C (**18a**, **18b**). Reaction times are given below the columns; yields in % are given above every single column.

Next, another reaction batch with **18b** was run without internal standard in order to determine the contents of Pd and Co in the product by ICP-OES analysis

(Table 14). Contamination of the product is possible either by leaching of Pd or Co from the catalyst or by particles that are not separated from the reaction mixture effectively. The material was recycled for 11 runs without any need of increasing the reaction time (120 min). In run 12 the reaction time had to be increased to 150 min to reach full conversion. After these 12 runs the Pd retained on the hybrid material was determined as 87% of the starting value. TEM pictures do not show any significant change of the nanocatalysts (see experimental section). The Pd and Co contents in the products were in the first 10 runs between 8 and 28 ppm, whereas the Pd content increases in run 11 and 12 to 64 and 48 ppm.

Table 14 Recycling studies of Pd@Spacer-IL@Co/C (34 wt%, **18b**) in the hydrogenation of *trans*-stilbene **11a**.[a]

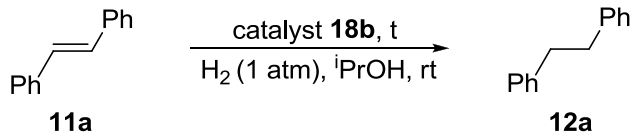

11a **12a**

Run	Reaction time to full conversion [min][b]	Pd leaching [ppm][c]	Co leaching [ppm][c]
1	120	9	17
2	120	11	9
3	120	20	13
4	120	11	8
5	120	16	17
6	120	28	14
7	120	19	17
8	120	8	21
9	120	11	14
10	120	28	13
11	120	64	22
12	150	48	15

[a] Stilbene **11a** (2 mmol) in ^{i}PrOH (20 mL) was hydrogenated by 20 µmol (1 mol%) of catalyst **18b**. [b] Reaction was monitored by GC analysis and stopped at full conversion. [c] In µg per g of product. Determined by ICP-OES.

We also carried out leaching studies with **18b** using 0.1 mol% Pd under additional 10 bar of hydrogen pressure (Table 15). The particles could be recycled for 10 consecutive runs with reaction times from 180 to 300 mins. In this case, we observed Pd contents of <10 ppm and Co contents of <8 ppm with two exceptions (17 ppm Pd in run 7 and 14 ppm Co in run 8). These results are also promising for industrial uses as the acceptable palladium limits are reported to be between 10 and 20 ppm.[27]

Catalyst **18b** is additionally attractive due to its very high capacity in palladium, requiring only little amounts of supporting material, which is also important for the recycling of expensive metals like Pd. For experiments using a Pd content of 0.1 mol% only 0.7 mg of catalyst **18b** were needed in order to generate 20 mmol of product within 10 runs. This would in scale up lead to 30 mol of product (or 5 kg in case of *trans*-stilbene) applying 1 g of catalyst **18b**.

Table 15 Recycling studies of Pd@Spacer-IL@Co/C (34 wt%, **18b**) in the hydrogenation of *trans*-stilbene under 10 bar H_2-pressure.[a]

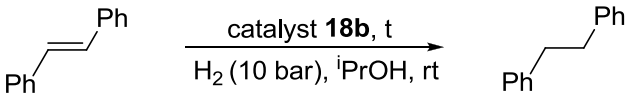

11a **12a**

Run	Reaction time to full conversion [min][b]	Pd leaching [ppm][c]	Co leaching [ppm][c]
1	180	10	2
2	180	2	1
3	180	4	2
4	210	6	3
5	210	6	4
6	210	5	3
7	210	17	7
8	240	8	14
9	240	3	4
10	300	6	7

[a] Stilbene **11a** (2 mmol) in ^{i}PrOH (20 mL) was hydrogenated by 2 µmol (0.1 mol%) of catalyst **18b** under 10 bar of H_2-pressure. [b] Reaction was monitored by GC analysis and stopped at full conversion. [c] In µg per g of product. Determined by ICP-OES.

Recycling experiments varying the substrate

We also investigated the scope of the reaction with catalyst **18b** by reusing the particles and changing the substrate after each run (Table 16). Various styrene derivatives **11** were hydrogenated in short reaction times of 15-60 minutes (Table 16, run 2-6) bearing electron withdrawing (Table 16, run 5) as well as electron donating functional groups (Table 16, run 6). Additionally, chalcones and cinnamic esters were hydrogenated selectively (Table 16, run 7+8), which was additionally proved by ^{1}H NMR and ^{13}C NMR. Furthermore, strained compounds like norbornene were hydrogenated in very short reaction times (Table 16, run 9) as well as nitro compounds bearing electron donating (Table 16, run 10) or electron withdrawing groups (Table 16, run 11).

4.3 Conclusion

In this report, we successfully developed novel hybrid materials consisting of magnetic ionic liquids and stabilized Pd nanoparticles. The catalyst with a quite flexible ionic liquid on the surface turned out to be the most promising regarding the stabilization of Pd NPs. It showed high activity in the hydrogenation of *trans*-stilbene, is easily separable, and furthermore was recycled for at least 11 runs without significant loss of activity. Furthermore, we could show that the leaching of Pd and Co into the product was not noticeably high if a Pd amount of 0.1 mol% was used. Recycling of the catalyst was also possible varying the substrate after each run.

This novel catalyst is especially interesting regarding the point of sustainability as one can recycle expensive Pd with a very small amount of supporting material. This makes it especially attractive for industry where not only costs of catalyzing metal but also of supporting material play a very important role.

Table 16 Recycling of catalyst Pd@Spacer-IL@Co/C (34 wt%, **18b**) in the hydrogenation of olefins and nitro compounds.[a]

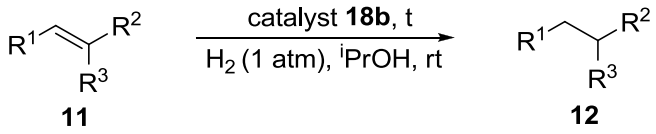

11 **12**

Run	Substrate	Product	t [min]	Conversion [%][b]
1	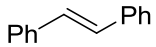 **11a**	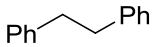 **12a**	120	100
2	**11b**	**12b**	15	100
3	**11c**	**12c**	50	100
4	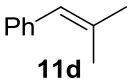 **11d**	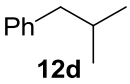 **12d**	60	100
5	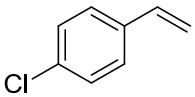 **11e**	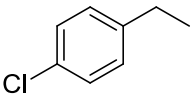 **12e**	15	100
6	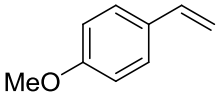 **11f**	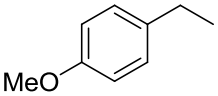 **12f**	15	100
7	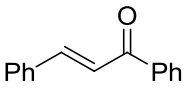 **11g**	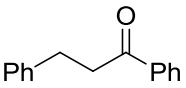 **12g**	420	100
8	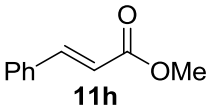 **11h**	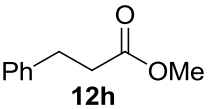 **12h**	40	100
9	**11i**	**12i**	10	100
10	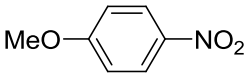 **11j**	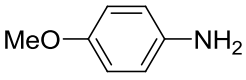 **12j**	20	100
11	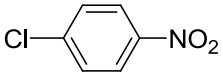 **11k**	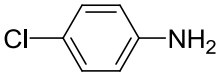 **12k**	20	100

[a] Substrate **11** (2 mmol) in ^{i}PrOH (20 mL) was hydrogenated by 20 µmol (1 mol%) of catalyst **18b** using dodecane as internal GC standard. [b] Determined by GC analysis using internal standard.

4.4 Addendum

Additionally to polymer-coated catalysts Pd@PS-IL@Co/C we synthesized other nanocatalysts with a poly(*N*-isopropylacrylamide) (PNIPAM) coating (Pd@PNIPAM@Co/C **13**, Fig. 17). PNIPAM is also known to stabilize palladium nanoparticles. The synthesis of PNIPAM@Co/C was reported by Stark *et al*.[28] However, for the synthesis of palladium nanoparticles only method B can be utilized as PNIPAM undergoes a phase transition and shrunks at temperatures above 32 °C. Hence, method A cannot be applied as the reaction temperature is 110 °C under microwave heating.

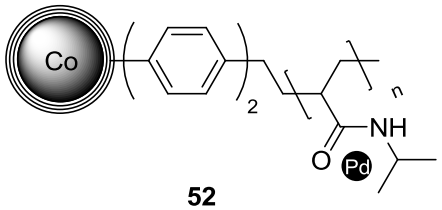

52

Fig. 17 Novel Pd@Co/C hybrid system: Pd@PNIPAM@Co/C **52**.

The nanobeads PNIPAM@Co/C were donated from the Stark group (ETH Zürich). On these particles we also deposited palladium nanoparticles with a mass ratio of 1:0.2. Table 17 shows the results and comparison with polymer-coated nanocatalysts Pd@PS-IL@Co/C. The incorporation of palladium is slightly more effective than for polymer-coated nanocatalysts **43**. Using the reduction of Na_2PdCl_4 for the nanoparticle synthesis we observed a Pd incorporation of 90% (Table 17, entry 3) instead of 85% for **43h** (Table 17, entry 2).

Table 17 Synthesis of Pd@PS-IL@Co/C **43** and Pd@PNIPAM@Co/C **52**.

Entry	Index	Pd source	Method of synthesis[a]	Mass ratio[b]	Pd incorporated [%][c]	Pd loading [mmol/g][c]	Pd content [wt%][c]
1	**43c**	$Pd_2(dba)_3{\cdot}CHCl_3$	A	1:0.2	74	1.2	12
2	**43h**	Na_2PdCl_4	B	1:0.2	85	1.3	14
3	**52a**	Na_2PdCl_4	B	1:0.2	90	1.4	15

[a] Method A: heating under microwave irradiation; method B: reduction with H_2. [b] Mass ratio of NPs to Pd in the synthesis. [c] Determined by ICP-OES.

We further investigated the activity of **52a** in the hydrogenation of *trans*-stilbene compared to catalysts **43c** and **43h** (Table 18). The results clearly show that there is no difference observable in the acitivity of **43h** (Table 18, entry 2) and **52a** (Table 18, entry 3). Compared to catalyst **43c** (synthesized from $Pd_2(dba)_3 \cdot CHCl_3$) the activity again is decreased by almost one forth. Hence, Pd@PNIPAM@Co/C **52** was not further applied in catalytic tests.

Table 18 Hydrogenation of *trans*-stilbene **11a** using Pd@PS-IL@Co/C **43**, and Pd@PNIPAM@Co/C **52**.[a]

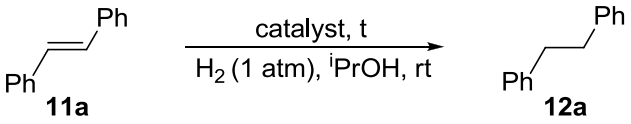

Entry	Catalyst	Pd [wt%]	Catalyst [mol%]	t [min]	Conversion [%][b]	TOF [h^{-1}][c]
1	**43c**	12	1.0	60	91	91
2	**43h**	14	1.0	60	23	23
3	**52a**	15	1.0	60	22	22

[a] Stilbene **11a** (0.5 mmol) in ^{i}PrOH (5 mL) was hydrogenated by 5 µmol (1 mol%) of catalyst using dodecane as internal GC standard. [b] Determined by GC analysis using internal standard. [c] Mol of substrate transformed per mol catalyst per hour.

4.5 Experimental section

Materials and methods

Carbon coated cobalt nanomagnets (Co/C, 20.5 m^2/g, mean particle size ≈ 25 nm) were purchased from Turbobeads Llc, Switzerland. Prior to use, they were washed in a concentrated HCl / water mixture (1:1) 5 times for 24 h. Acid residuals were removed by washing with millipore water (5x) and the particles were dried at 50 °C in a vacuum oven.[29] All other commercially available compounds were used as received.

The magnetic nanobeads were dispersed using an ultrasound bath (Sonorex RK 255 H-R, Bandelin) and recovered with the aid of a neodymium based magnet (15 x 30 mm). They were characterized by IR-ATR spectroscopy (Biorad Excalibur FTS 3000), elemental microanalysis (LECO CHN-900), transmission electron microscopy (CM30 ST-Philips, LaB_6cathode, operated at 300 kV point resolution ~4 Å), x-ray powder diffraction, and inductively coupled plasma optical emission spectrometry (Spectro Analytical Instruments ICP Modula EOP).
Poly(benzylchloride)styrene coated cobalt nanoparticles **30-NP**[30] and benzylalcohol functionalized cobalt nanoparticles **46**[19] were prepared on the gram scale following previously reported procedures.

$Pd_2(dba)_3 \cdot CHCl_3$ was purchased (Sigma-Aldrich) and used as received. As determined by the procedure reported by Ananikov *et al.*[26], the ratio of $Pd_2(dba)_3$:dba was 1:0.46, which reflects that 68% of the Pd content is present as $Pd_2(dba)_3$, while 32% of the Pd content are already present as Pd nanoparticles.

A solution of Na_2PdCl_4 in water (conc. 1 mg Pd per mL) was freshly prepared by mixing $PdCl_2$ (1 equiv.) with NaCl (2 equiv.) in H_2O using an ultrasound bath for 30 min.

NMR spectra were recorded with a Bruker AV 300 spectrometer with $CHCl_3$ as standard. Chemical shifts (δ) are reported in ppm and coupling constants (*J*) are reported in Hertz (Hz). The signals in the spectra are described as d (doublet), t (triplet), and m (multiplet).

Gas chromatography was recorded on Fisons Instruments GC8000 equipped with a capillary (30 m x 250 µm x 0.25 µm) and flame ionization detector.

Nomenclature of the nanobeads

The nomenclature of the nanobeads is as follows:

Co/C	carbon coated cobalt nanoparticles
PS-IL@Co/C	poly(benzyl-methyl imidazolium chloride)styrene functional-ized carbon coated cobalt nanoparticles
Bz-IL@Co/C	benzyl-methyl imidazolium chloride functionalized carbon coated cobalt nanoparticles
Spacer-IL@Co/C	benzamidopropyl-butyl-imidazolium bromide functionalized carbon coated cobalt nanoparticles
IL@Co/C	PS-IL@Co/C, Bz-IL@Co/C, and Spacer-IL@Co/C
Pd@PS-IL@Co/C	Pd NPs deposited on PS-IL@Co/C
Pd@Bz-IL@Co/C	Pd NPs deposited on Bz-IL@Co/C
Pd@Spacer-IL@Co/C	Pd NPs deposited on Spacer-IL@Co/C
Pd@IL@Co/C	Pd NPs deposited on IL@Co/C

Synthesis of the nanoparticles

Benzyl-chloride functionalized carbon coated cobalt nanoparticles (47, Bz-Cl@Co/C)

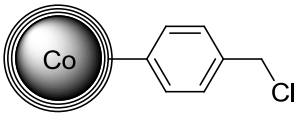

450 mg (0.12 mmol/g) Bz-OH@Co/C **46** and 1.4 µL (18 µmol) dry DMF were predispersed in 4.5 mL dry dichloromethane for 10 min under N_2-atmosphere using an ultrasonic bath. The dispersion was cooled to 0 °C and 65.3 µL (0.9 mmol) $SOCl_2$ was added slowly. The reaction mixture was allowed to warm to rt and stirred over night. After magnetic decantation the particles were washed with dichloromethane (5 x 5 mL) and dried in vacuo to obtain Bz-Cl@Co/C **47** (440.8 mg, 0.11 mmol/g).

IR ($\tilde{\nu}$/cm^{-1}): 1676, 1596, 1503, 1263, 1015, 778; elemental microanalysis (%): C, 8.54; H, 0.14; N, 0.07; Cl, 0.40.

Benzyl-methyl imidazolium chloride functionalized carbon coated cobalt nanoparticles (48, Bz-IL@Co/C)

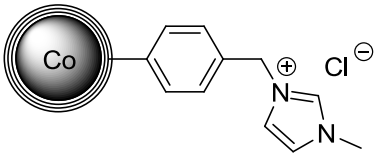

400 mg (0.12 mmol/g) Bz-Cl@Co/C **47** and 4 mL dry toluene were introduced to a microwave vial and sonicated for 10 min under N_2-atmosphere using an ultrasonic bath. After adding 24 µL (0.3 mmol) *N*-methyl-imidazole the reaction mixture was heated in a focused microwave oven to 150 °C for 30 min. After removing the supernatant by magnetic decantation the particles were washed with toluene (5 x 5 mL), and dichloromethane (3 x 5 mL) and dried under vacuum at 80 °C yielding **9** (397.6 mg, 0.09 mmol/g).
IR ($\tilde{\nu}$/cm^{-1}): 2920, 2852, 2363, 1214, 1161, 1014, 814, 654; elemental microanalysis (%): C, 8.98; H, 0.16; N, 0.23; Cl, 0.27.

Poly(benzyl-methyl imidazolium chloride)styrene functionalized carbon coated cobalt nanoparticles (45, PS-IL@Co/C)

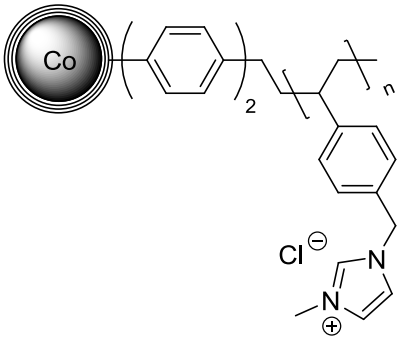

500 mg (3.1 mmol/g) PS-Cl@Co/C **30-NP** and 5 mL dry toluene were introduced to a microwave vial and sonicated for 10 min under N_2-atmosphere using ultrasonic bath. 309 µL (3.88 mmol) *N*-methyl-imidazole was added and the reaction mixture heated in a focused microwave oven to 150 °C for 30 min. After magnetic decantation the particles were washed with toluene (5 x 5 mL), dichloromethane (3 x 5 mL) and dried under vacuum at 80 °C yielding **45** (637.2 mg, 2.1 mmol/g).
IR ($\tilde{\nu}$/cm^{-1}): 3373, 2927, 2851, 1562, 1511, 1449, 1422, 1158, 1018; elemental microanalysis (%): C, 43.95; H, 4.62; N, 5.75; Cl, 7.41.

Benzoic acid functionalized carbon coated cobalt nanoparticles (49, Ph-COOH@Co/C)

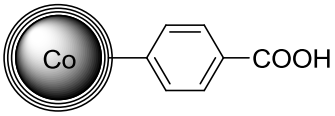

1.3 g (0.26 mmol of benzylalcohol units) Bz-OH@Co/C **46** were sonicated in 30 mL MeCN/H_2O (1:1) for 10 min using an ultrasonic bath. After adding 479.5 mg (0.78 mmol) oxone the mixture was refluxed for 24 h. Another portion of oxone (479.5 mg, 0.78 mmol) was added after 12 h. After magnetic decantation the particles were washed with MeCN/H_2O (3 x 20 mL), MeCN (3 x 20 mL) and dried under vacuum to obtain Ph-COOH@Co/C **49** (1.18 g).

IR ($\tilde{\nu}$/cm^{-1}): 2358, 2330, 1731, 1360, 1219; elemental microanalysis (%): C, 8.71; H, 0.28; N, 0.30.

(*N*-Imidazole)propyl-benzamide functionalized carbon coated cobalt nanoparticles (50)

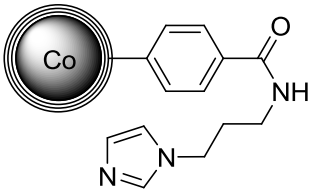

1.0 g Ph-COOH@Co/C **49** were stirred in 5.0 mL $SOCl_2$ under N_2-atmosphere for 24 h. After magnetic decantation the particles where washed with dry THF (5 x 5 mL) and dried under vacuum. Subsequently 5.0 mL 1-(3-aminopropyl)imidazole were introduced under N_2-atmosphere and the mixture heated to 120 °C for another 24 h. After magnetic decantation the particles were washed with THF (3 x 5 mL), 1M HCl (1 x 5 mL), saturated $NaHCO_3$ solution (1 x 5 mL), H_2O (1 x 5 mL) and EtOH (3 x 5 mL). After drying the particles in vacuo **50** (934.7 mg, 0.07 mmol/g) was obtained.

IR ($\tilde{\nu}$/cm^{-1}): 2893, 2840, 1564, 973, 867, 848, 835, 819, 752, 698, 689, 656; elemental microanalysis (%): C, 9.32; H, 0.19; N, 0.60.

Benzamidopropyl-butyl-imidazolium bromide functionalized carbon coated cobalt nanoparticles (51, Spacer-IL@Co/C)

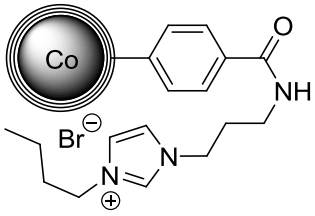

900 mg (0.063 mmol of imidazole units) of **50** were sonicated in 15 mL freshly distilled 1-bromobutane under N_2-atmosphere using an ultrasonic bath. The reaction mixture was stirred for 24 h at 80 °C. The particles were separated by an external magnet and washed with dry THF (5 x 10 mL) and dried under vacuum to obtain **51** (909.2 mg, 0.05 mmol/g).

IR ($\tilde{\nu}$/cm^{-1}): 2913, 2850, 1738, 1455, 1366, 1222, 1217, 1160, 753; elemental microanalysis (%): C, 9.40; H, 0.24; N, 0.51.

Representative procedure for the microwave deposition of Pd nanoparticles on PS-IL@Co/C nanobeads (Method A)

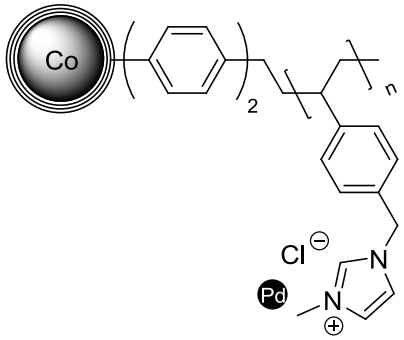

100 mg PS-IL@Co/C **45** and 1 mL of a mixture dry toluene/MeOH were introduced to a microwave vial and sonicated in an ultrasonic bath for 10 min under N_2-atmosphere. 4.9 mg (4.7 µmol) $Pd_2(dba)_3 \cdot CHCl_3$ was added and the reaction mixture heated in a focused microwave oven to 110 °C for 2 min. After magnetic decantation the particles were washed with dichloromethane (5 x 5 mL) and dried under vacuum to obtain Pd@PS-IL@Co/C **43e** (96.9 mg). The loading of Pd was determined by ICP-OES (0.08 mmol/g, 81%).

Representative procedure for the microwave deposition of Pd nanoparticles on Bz-IL@Co/C nanobeads (Method A)

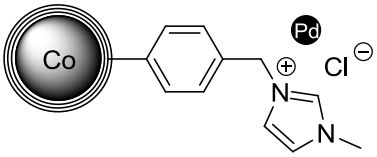

100 mg Bz-IL@Co/C **48** and 1 mL dry toluene were introduced to a microwave vial and sonicated in an ultrasonic bath for 10 min under N_2-atmosphere. 4.9 mg (4.7 µmol) $Pd_2(dba)_3 \cdot CHCl_3$ was added and the reaction mixture heated in a focused microwave oven to 110 °C for 2 min. After magnetic decantation the particles were washed with dichloromethane (5 x 5 mL) and dried under vacuum to obtain Pd@Bz-IL@Co/C **44e** (99.8 mg). The loading of Pd was determined by ICP-OES (0.089 mmol/g, 96%).

Representative procedure for the microwave deposition of Pd nanoparticles on Spacer-IL@Co/C nanobeads (Method A)

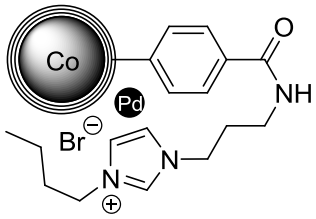

50 mg Spacer-IL@Co/C **51** and 1 mL dry toluene were introduced to a microwave vial and sonicated in an ultrasonic bath for 10 min under N_2-atmosphere. 2.5 mg (2.4 µmol) $Pd_2(dba)_3 \cdot CHCl_3$ was added and the reaction mixture heated in a focused microwave oven to 110 °C for 2 min. After magnetic decantation the particles were washed with dichloromethane (5 x 5 mL) and dried under vacuum to obtain Pd@Spacer-IL@Co/C **18e** (50.1 mg). The loading of Pd was determined by ICP-OES (0.093 mmol/g, 100%).

Representative procedure for the deposition of Pd nanoparticles on PS-IL@Co/C nanobeads by H_2-reduction (Method B)

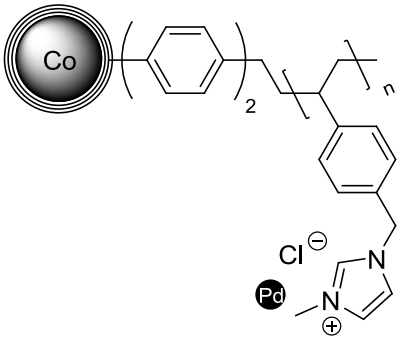

To a schlenk tube 20 mg PS-IL@Co/C **45** and 4 mL of a freshly prepared Na_2PdCl_4 solution (Pd conc. 1 mg/mL) were introduced. The reaction mixture was stirred vigorously for 30 min followed by 30 min under 1 atm H_2 pressure (balloon). After magnetic decantation the particles were washed with H_2O (5 x 3 mL), MeOH (3 x 3 mL), and acetone (2 x 3 mL) and dried under vacuum to obtain Pd@PS-IL@Co/C **43h** (15.8 mg). The loading of Pd was determined by ICP-OES (1.3 mmol/g, 85%).

General procedure for the hydrogenation using Pd@IL@Co/C catalysts

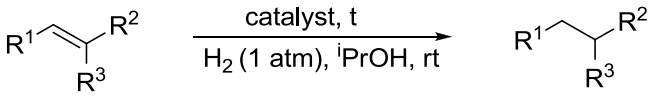

11 **12**

To a schlenk tube Pd@IL@Co/C (1 mol% Pd, 20 µmol), substrate (2 mmol), iPrOH (20 mL), and dodecane (1 mmol) as internal standard were introduced. The reaction mixture was sonicated in an ultrasonic bath for 10 min and subsequently stirred vigorously under 1 atm H_2-pressure (balloon). The progress of the reaction was monitored by GC analysis. For recycling experiments the particles were separated by an external magnet and after magnetic decantation washed with ^{i}PrOH (2 x 5 mL) and dichloromethane (2 x 5 mL). After drying in vacuo the catalyst was reused for further runs.

GC data

All products are literature-known and all spectroscopic data matched with those reported in the literature.

1,2-Diphenylethane (12a)[6]

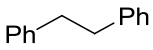

1,2-Diphenylethane **12a** was prepared from *trans*-stilbene **11a** (360.5 mg, 2 mmol) according to the general procedure. The progress of the reaction was monitored by GC analysis: 140 °C (3 min), 20 °C/min, 300 °C; t_R = dodecane (3.54 min), 1,2-diphenylethane (7.66 min), *trans*-stilbene (9.37 min).

Ethylbenzene (12b)[31]

Ethylbenzene **12b** was prepared from styrene **11b** (228.9 µL, 2 mmol) according to the general procedure. The progress of the reaction was monitored by GC analysis: 60 °C (3 min), 20 °C/min, 240 °C; t_R = ethylbenzene (4.29 min), styrene (4.65 min), dodecane (8.30 min).

Ethane-1,1-diyldibenzene (12c)[6]

Ethane-1,1-diyldibenzene **12c** was prepared from ethane-1,1-diyldibenzene **11c** (283.0 µL, 2 mmol) according to the general procedure. The progress of the reaction was monitored by GC analysis: 140 °C (3 min), 16 °C/min, 300 °C; t_R = dodecane (3.49 min), ethane-1,1-diyldibenzene (6.26 min), ethene-1,1-diyldibenzene (6.47 min).

Isobutylbenzene (12d)[15]

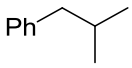

Isobutylbenzene **12d** was prepared from (2-methylprop-1-en-1-yl)benzene **11d** (293.5 µL, 2 mmol) according to the general procedure. The progress of the reaction was monitored by GC analysis: 60 °C (3 min), 24 °C/min, 300 °C; t_R = isobutylbenzene (6.01 min), (2-methylprop-1-en-1-yl)benzene (6.72 min), dodecane (7.80 min).

1-Chloro-4-ethylbenzene (12e)[30]

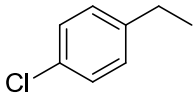

1-Chloro-4-ethylbenzene **12e** was prepared from 1-chloro-4-vinylbenzene **11e** (274.6 µL, 2 mmol) according to the general procedure. The progress of the reaction was monitored by GC analysis: 100 °C (5 min), 25 °C/min, 300 °C; t_R = 1-chloro-4-ethylbenzene (4.51 min), 1-chloro-4-vinylbenzene (4.88 min), dodecane (7.12 min).

1-Ethyl-4-methoxybenzene (12f)[30]

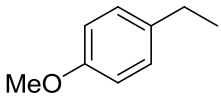

1-Ethyl-4-methoxybenzene **12f** was prepared from 1-methoxy-4-vinylbenzene **11f** (269.2 µL, 2 mmol) according to the general procedure. The progress of the reaction was monitored by GC analysis: 100 °C (5 min), 25 °C/min, 300 °C; t_R = 1-methoxy-4-vinylbenzene (4.90 min), 1-ethyl-4-methoxybenzene (5.64 min), dodecane (7.14 min).

1,3-Diphenylpropan-1-one (12g)[6]

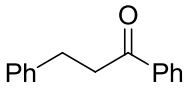

1,3-Diphenylpropan-1-one **12g** was prepared from chalcone **11g** (416.5 mg, 2 mmol) according to the general procedure. The progress of the reaction was monitored by GC analysis: 140 °C (3 min), 16 °C/min, 300 °C; t_R = dodecane (3.52 min), 1,3-diphenylpropan-1-one (9.19 min), chalcone (10.22 min). The selective hydrogenation of the C=C double bond was proved by ^{1}H NMR and ^{13}C NMR: ^{1}H NMR (300 MHz, $CDCl_3$): δ = 7.98 (d, *J* = 7.4 Hz, 2H), 7.57 (t, *J* = 7.3 Hz, 1H), 7.47 (t, *J* = 7.5 Hz, 2H), 7.41 – 7.14 (m, 5H), 3.32 (t, *J* = 7.6 Hz, 2H), 3.09 (t, *J* = 7.6 Hz, 2H); ^{13}C NMR (75 MHz, $CDCl_3$): δ = 199.3, 141.3, 136.9, 133.1, 128.7, 128.6, 128.5, 128.1, 126.2, 40.5, 30.2.

Methyl-3-phenylpropanoate (12h)[6]

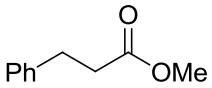

Methyl-3-phenylpropanoate **12h** was prepared from methyl cinnamate **11h** (324.4 mg, 2 mmol) according to the general procedure. The progress of the reaction was monitored by GC analysis: 100 °C (3 min), 20 °C/min, 300 °C; t_R = dodecane (5.95 min), methyl-3-phenylpropanoate (6.47 min), methyl cinnamate (7.43 min).

Bicyclo[2.2.1]heptanes (12i)[32]

Bicyclo[2.2.1]heptane **12i** was prepared from norbornene **11i** (188.3 mg, 2 mmol) according to the general procedure. The progress of the reaction was monitored by GC analysis: 60 °C (3 min), 30 °C/min, 300 °C; t_R = norbornene (2.53 min), bicyclo[2.2.1]heptane (2.87 min), dodecane (7.27 min).

4-Methoxyaniline (12j)[33]

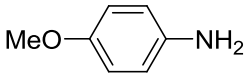

4-Methoxyaniline **12j** was prepared from 1-methoxy-4-nitrobenzene **11j** (306.3 mg, 2 mmol) according to the general procedure. The progress of the reaction was monitored by GC analysis: 70 °C (3 min), 13 °C/min, 200 °C; t_R = 4-methoxyaniline (8.81 min), dodecane (9.01 min), 1-methoxy-4-nitrobenzene (10.92 min).

4-Chloraniline (12k)[33]

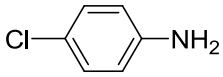

4-Chloraniline **12k** was prepared from 1-chloro-4-nitrobenzene **11k** (315.1 mg, 2 mmol) according to the general procedure. The progress of the reaction was monitored by GC analysis: 50 °C (3 min), 5 °C/min, 170 °C; t_R = 4-chloroaniline (15.73 min), 1-chloro-4-nitrobenzene (16.64 min), dodecane (16.91 min).

Preparation of samples for ICP-OES analysis

General procedure for the preparation of Pd samples to determine the Pd amount on Pd@Co/C catalysts

5.0 mg Pd@Co/C were heated in 3.2 mL aqua regia for 30 min. Upon cooling, the mixture was diluted with H_2O (millipore grade) and after collecting the particles with an external magnet the solution was filtrated in a 10 mL measuring flask. After washing the particles for three times with H_2O with subsequent filtration the measuring flask was filled to 10 mL. The Pd concentration was then determined by ICP-OES analysis.

General procedure for the preparation of Pd and Co samples to determine the Pd and Co amount in hydrogenated products

250.0 mg 1,2-Diphenylethane was heated in 3.2 mL aqua regia for 30 min. Upon cooling, the mixture was diluted with H_2O (millipore grade) and filtrated in a 10 mL measuring flask. After washing the vial for three times with H_2O with subsequent

filtration the measuring flask was filled to 10 mL. The Pd and Co concentration was then determined by ICP-OES analysis.

IR spectra

Example for following the reaction progress of the nanoparticle synthesis by IR spectroscopy. IR spectra of PS-Cl@Co/C **30-NP** and PS-IL@Co/C **45** are shown:

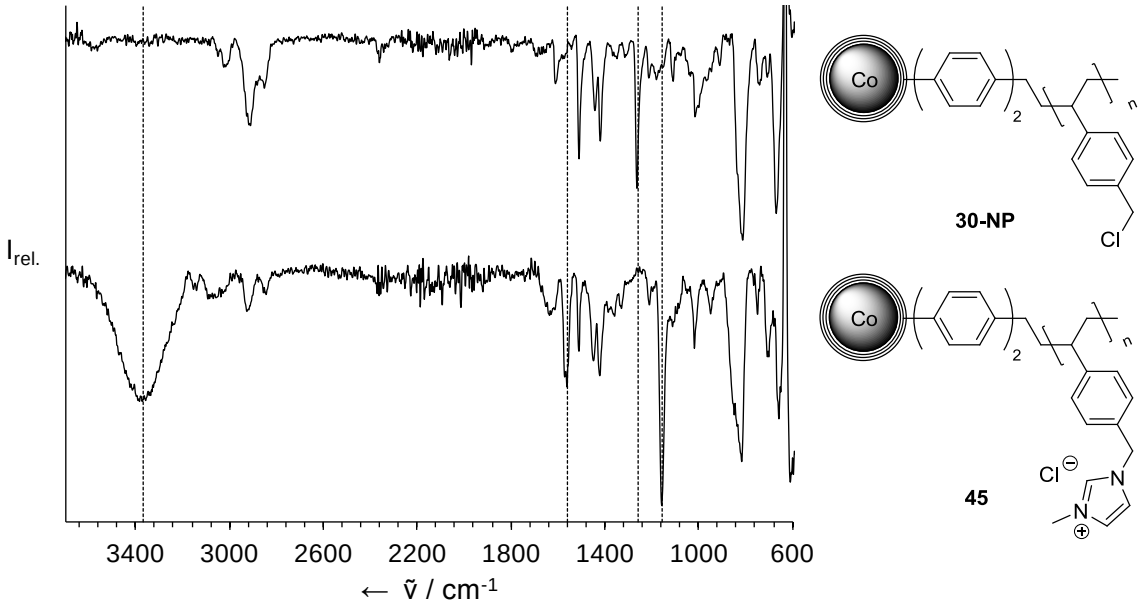

TEM pictures

Transmission electron microscopy (TEM) pictures of A) Pd@PS-IL@Co/C **43b** (24 wt%), B) Pd@Bz-IL@Co/C **44b** (31 wt%), C) Pd@Spacer-IL@Co/C **18b** (34 wt%), and D) Pd@Spacer-IL@Co/C **18b** (34 wt%) after 12 cycles:

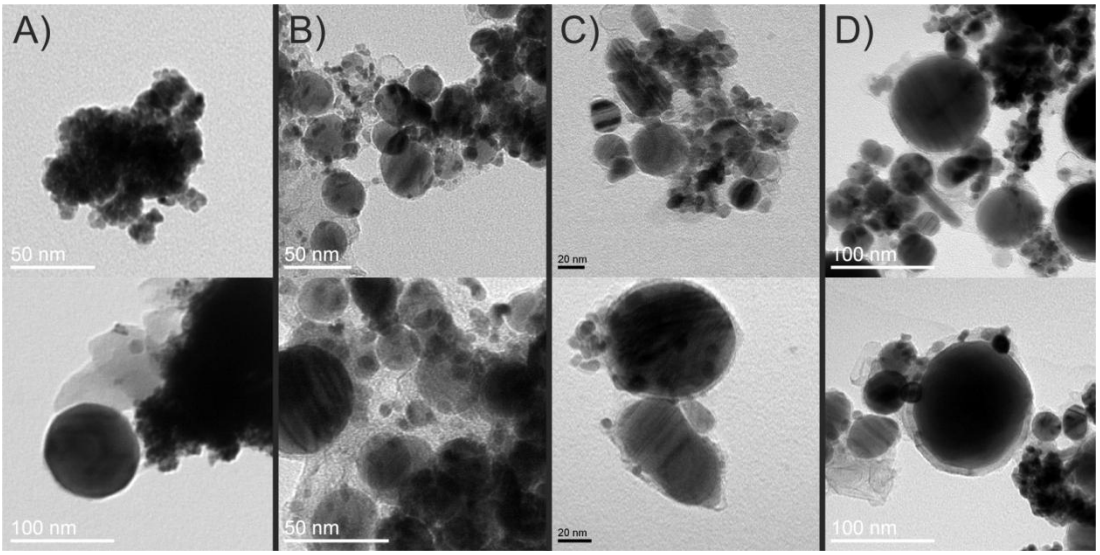

XRD measurements

X-ray diffraction spectrum of Pd@Spacer-IL@Co/C **18b** with a palladium content of 34 wt%. The characteristic peaks for Co and Pd are detected:

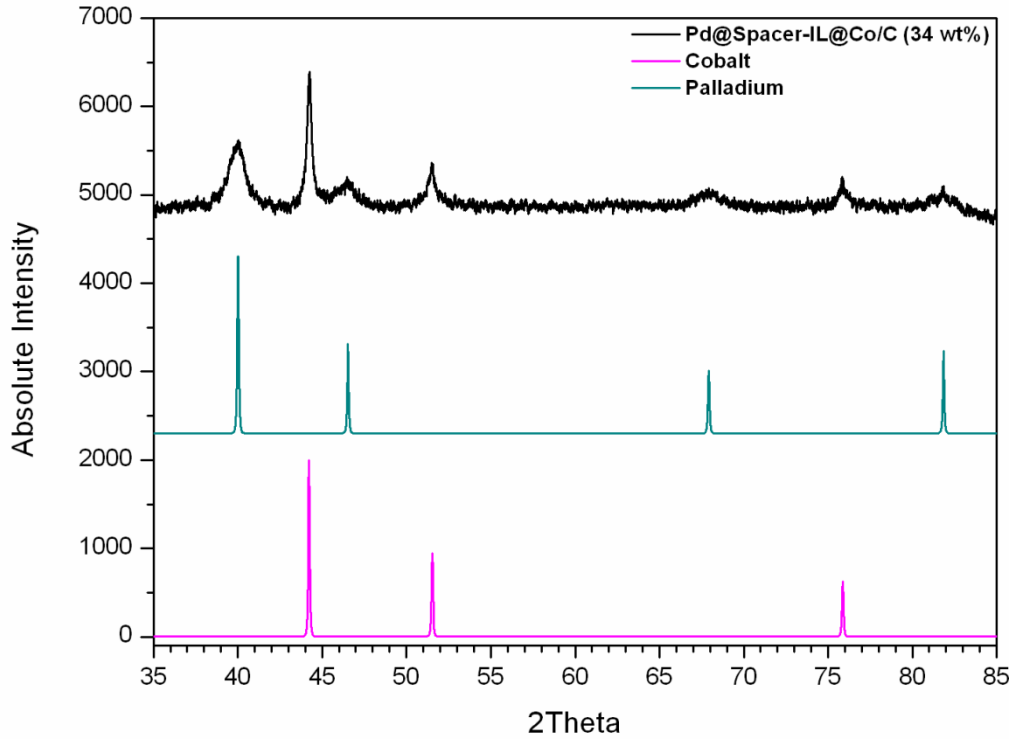

4.6 References

[1] G. Poli, G. Giambastiani, A. Heumann, *Tetrahedron* **2000**, *56*, 5959–5989.

[2] a) D. Duca, F. Frusteri, A. Parmaliana, G. Deganello, *Appl. Catal., A* **1996**, *146*, 269–284; b) E. Auer, A. Freund, J. Pietsch, T. Tacke, *Appl. Catal., A* **1998**, *173*, 259–271; c) B. Chen, U. Dingerdissen, J. G. E. Krauter, H. G. J. Lansink Rotgerink, K. Möbus, D. J. Ostgard, P. Panster, T. H. Riermeier, S. Seebald, T. Tacke et al., *Appl. Catal., A* **2005**, *280*, 17–46.

[3] a) M. Beller, A. Zapf, W. Mägerlein, *Chem. Eng. Technol.* **2001**, *24*, 575–582; b) M. Beller, A. Zapf in *Handbook of Organopalladium Chemistry for Organic Synthesis*, John Wiley & Sons, Inc, **2003**; c) C. Torborg, M. Beller, *Adv. Synth. Catal.* **2009**, *351*, 3027–3043; d) A. Dumrath, C. Lübbe, M. Beller in *Palladium-Catalyzed Coupling Reactions*, Wiley-VCH Verlag GmbH & Co. KGaA, **2013**.

[4] a) C. Nowottny, W. Halwachs, K. Schügerl, *Sep. Purif. Technol.* **1997**, *12*, 135–144; b) M. A. Barakat, M. H. H. Mahmoud, Y. S. Mahrous, *Appl. Catal., A* **2006**, *301*, 182–186.

[5] a) S. Mori, T. Ohkubo, T. Ikawa, A. Kume, T. Maegawa, Y. Monguchi, H. Sajiki, *J. Mol. Catal. A: Chem.* **2009**, *307*, 77–87; b) C. M. Cirtiu, A. F. Dunlop-Brière, A. Moores, *Green Chem.* **2011**, *13*, 288; c) M. Lim, K. A. de Castro, S. Oh, K. Lee, Y.-W. Chang, H. Kim, H. Rhee, *Appl. Organometal. Chem.* **2011**, *25*, 1–8.

[6] F.-X. Felpin, E. Fouquet, *Chem. Eur. J.* **2010**, *16*, 12440–12445.

[7] M. Cano, A. Benito, W. K. Maser, E. P. Urriolabeitia, *Carbon* **2011**, *49*, 652–658.

[8] a) J. Dupont, J. D. Scholten, *Chem. Soc. Rev.* **2010**, *39*, 1780; b) Z. Ma, J. Yu, S. Dai, *Adv. Mater.* **2010**, *22*, 261–285; c) C. Vollmer, C. Janiak, *Coord. Chem. Rev.* **2011**, *255*, 2039–2057.

[9] a) Y. Gu, G. Li, *Adv. Synth. Catal.* **2009**, *351*, 817–847; b) T. Selvam, A. Machoke, W. Schwieger, *Appl. Catal., A* **2012**, *445-446*, 92–101.

[10] a) N. D. Clement, K. J. Cavell, C. Jones, C. J. Elsevier, *Angew. Chem.* **2004**, *116*, 1297–1299; *Angew. Chem. Int. Ed.* **2004**, *43*, 1277–1279; b) J. Dupont, J. Spencer, *Angew. Chem.* **2004**, *116*, 5408–5409; *Angew. Chem. Int. Ed.* **2004**, *43*, 5296–5297; c) L. S. Ott, M. L. Cline, M. Deetlefs, K. R. Seddon, R. G. Finke, *J. Am. Chem. Soc.* **2005**, *127*, 5758–5759.

[11] a) J. Durand, E. Teuma, F. Malbosc, Y. Kihn, M. Gómez, *Catal. Commun.* **2008**, *9*, 273–275; b) J. H. Cha, K. S. Kim, H. Lee, *Korean J. Chem. Eng.* **2009**, *26*, 760–764; c) E. Raluy, I. Favier, A. M. López-Vinasco, C. Pradel, E. Martin, D. Madec, E. Teuma, M. Gómez, *Phys. Chem. Chem. Phys.* **2011**, *13*, 13579–13584.

[12] a) M. Ruta, G. Laurenczy, P. J. Dyson, L. Kiwi-Minsker, *J. Phys. Chem. C* **2008**, *112*, 17814–17819; b) K. V. Kovtunov, V. V. Zhivonitko, L. Kiwi-Minsker, I. V. Koptyug, *Chem. Commun.* **2010**, *46*, 5764–5766; c) L. Rodríguez-Pérez, C. Pradel, P. Serp, M. Gómez, E. Teuma, *ChemCatChem* **2011**, *3*, 749–754.

[13] a) D. Zhao, Z. Fei, W. H. Ang, P. J. Dyson, *Small* **2006**, *2*, 879–883; b) X. Yang, Z. Fei, D. Zhao, W. H. Ang, Y. Li, P. J. Dyson, *Inorg. Chem.* **2008**, *47*, 3292–3297; c) Y. Zeng, Y. Wang, Y. Xu, Y. Song, J. Jiang, Z. Jin, *Catal. Lett.* **2013**, *143*, 200–205; d) W. Zhu, Y. Yu, H. Yang, L. Hua, Y. Qiao, X. Zhao, Z. Hou, *Chem. Eur. J.* **2013**, *19*, 2059–2066.

[14] a) Y. Kume, K. Qiao, D. Tomida, C. Yokoyama, *Catal. Commun.* **2008**, *9*, 369–375; b) B. Karimi, D. Elhamifar, J. H. Clark, A. J. Hunt, *Org. Biomol. Chem.* **2011**, *9*, 7420–7426; c) M. Gruttadauria, L. F. Liotta, A. M. P. Salvo, F. Giacalone, V. La Parola, C. Aprile, R. Noto, *Adv. Synth. Catal.* **2011**, *353*, 2119–2130.

[15] Y. S. Chun, J. Y. Shin, C. E. Song, S.-g. Lee, *Chem. Commun.* **2008**, 942–944.

[16] a) A. J. Amali, R. K. Rana, *Green Chem.* **2009**, *11*, 1781–1786; b) Y. Kim, M.-J. Kim, *Bull. Korean Chem. Soc.* **2010**, *31*, 1368–1370; c) F. Zhang, J. Jin, X. Zhong, S. Li, J. Niu, R. Li, J. Ma, *Green Chem.* **2011**, *13*, 1238–1243.

[17] Q. M. Kainz, R. Linhardt, R. N. Grass, G. Vilé, J. Pérez-Ramírez, W. J. Stark, O. Reiser, *Adv. Funct. Mater.* **2013**, DOI: 10.1002/adfm.201303277.

[18] R. N. Grass, E. K. Athanassiou, W. J. Stark, *Angew. Chem.* **2007**, *119*, 4996–4999; *Angew. Chem. Int. Ed.* **2007**, *46*, 4909–4912.

[19] A. Schätz, R. N. Grass, W. J. Stark, O. Reiser, *Chem. Eur. J.* **2008**, *14*, 8262–8266.
[20] a) A. Schätz, R. N. Grass, Q. Kainz, W. J. Stark, O. Reiser, *Chem. Mater.* **2010**, *22*, 305–310; b) S. Wittmann, A. Schätz, R. N. Grass, W. J. Stark, O. Reiser, *Angew. Chem.* **2010**, *122*, 1911–1914; *Angew. Chem. Int. Ed.* **2010**, *49*, 1867–1870.
[21] Q. M. Kainz, M. Zeltner, M. Rossier, W. J. Stark, O. Reiser, *Chem. Eur. J.* **2013**, *19*, 10038–10045.
[22] Q. M. Kainz, R. Linhardt, P. K. Maity, P. R. Hanson, O. Reiser, *ChemSusChem* **2013**, *6*, 721–729.
[23] Q. M. Kainz, A. Schätz, A. Zöpfl, W. J. Stark, O. Reiser, *Chem. Mater.* **2011**, *23*, 3606–3613.
[24] S. Wittmann, J.-P. Majoral, R. N. Grass, W. J. Stark, O. Reiser, *Green Proc. Synth.* **2012**, *1*, 275–279.
[25] M. Keller, A. Perrier, R. Linhardt, L. Travers, S. Wittmann, A.-M. Caminade, J.-P. Majoral, O. Reiser, A. Ouali, *Adv. Synth. Catal.* **2013**, *355*, 1748–1754.
[26] S. S. Zalesskiy, V. P. Ananikov, *Organometallics* **2012**, *31*, 2302–2309.
[27] a) C. E. Garrett, K. Prasad, *Adv. Synth. Catal.* **2004**, *346*, 889–900; b) V. L. Budarin, P. S. Shuttleworth, J. H. Clark, R. Luque, *Curr. Org. Synth.* **2010**, *7*, 614–627.
[28] M. Zeltner, A. Schätz, M. L. Hefti, W. J. Stark, *J. Mater. Chem.* **2011**, *21*, 2991–2996.
[29] M. Rossier, F. M. Koehler, E. K. Athanassiou, R. N. Grass, B. Aeschlimann, D. Gunther, W. J. Stark, *J. Mater. Chem.* **2009**, *19*, 8239–8243.
[30] A. Schaetz, M. Zeltner, T. D. Michl, M. Rossier, R. Fuhrer, W. J. Stark, *Chem. Eur. J.* **2011**, *17*, 10566–10573.
[31] D. J. Frank, L. Guiet, A. Käslin, E. Murphy, S. P. Thomas, *RSC Adv.* **2013**, *3*, 25698–25701.
[32] B. Nguyen, J. M. Brown, *Adv. Synth. Catal.* **2009**, *351*, 1333–1343.
[33] E. Vasilikogiannaki, C. Gryparis, V. Kotzabasaki, I. N. Lykakis, M. Stratakis, *Adv. Synth. Catal.* **2013**, *355*, 907–911.

5. Towards magnetically recyclable catalysts for C-H activation and olefin metathesis

5.1 Palladium nanoparticles supported on Co/C nanobeads for C-H activation

The synthesis of arylated heterocycles is an important challenge in organic chemistry as they are present in numerous natural products.[1] They can be prepared via e.g. transition-metal catalyzed cross-coupling or C-H activation. While cross-coupling reactions require functionalized heterocycles and appropriate coupling partners, the direct C-H activation route is much more convenient and sustainable as it avoids a pre-functionalization of the heterocycle.

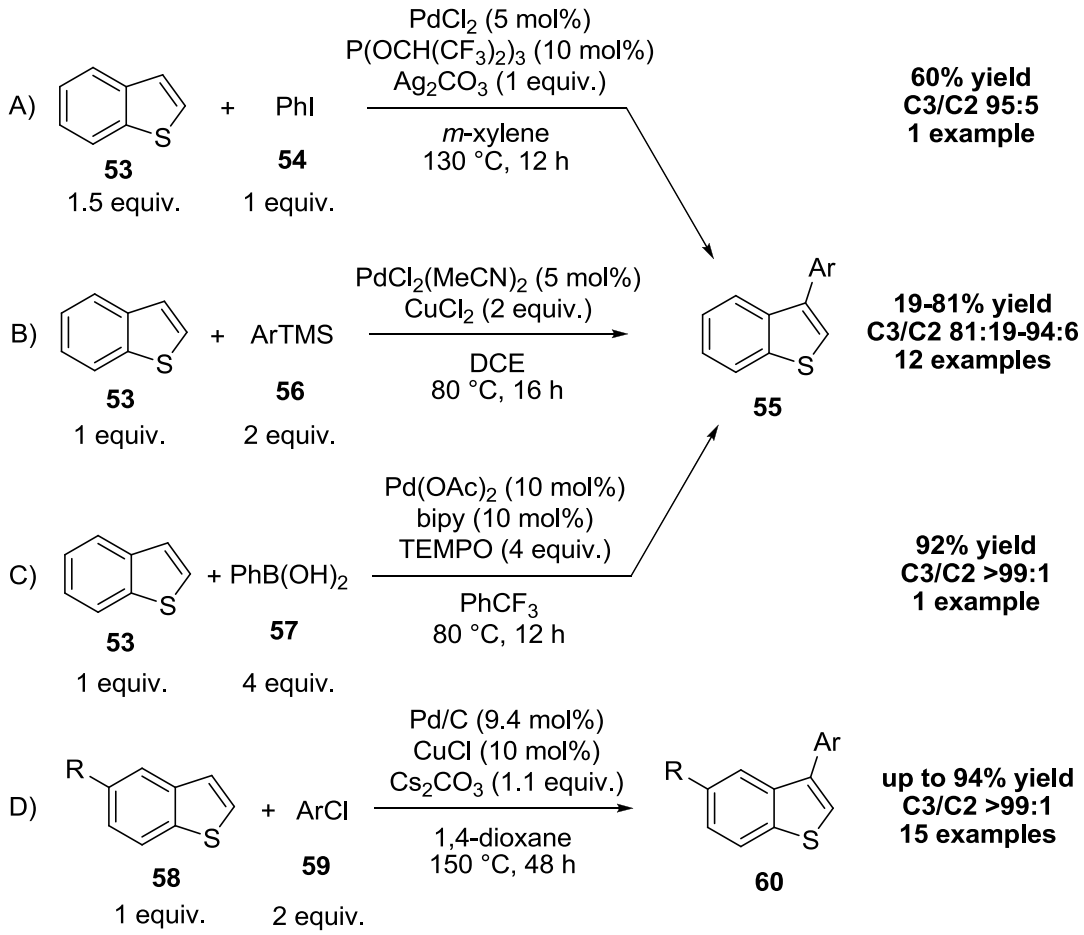

Scheme 11 Examples for C3-selective arylations of benzo[*b*]thiophenes by the groups of A) Itami,[2] B) Oi,[3] C) Itami and Studer,[4] and D) Glorius.[5]

Benzo[*b*]thiophenes represent a challenging structural scaffold regarding the selective arylation. While the direct arylation of the C2-position is well established, the selectivity towards the C3 position encounters difficulties. Reported examples for C3-selective arylations suffer from bad yields (Scheme 11A and 11B),[3,2] insufficient selectivities (Scheme 11B),[3] or the requirement of a large excess of reagents/oxidants (Scheme 11C).[4] Glorius *et al.*[5] most recently demonstrated a highly efficient and selective catalytic system for the C3-selective arylation of various benzo[*b*]thiophene derivatives (Scheme 11D). They could establish a method to couple benzo[*b*]thiophenes with inexpensive, easily available aryl chlorides using simple heterogeneous Pd/C with CuCl as co-catalyst. The reaction is insensitive to air and moisture, scalable, and does not need any additional ligand or directing group. However, for sustainable and economical chemical reactions one has also to regard other reaction parameters such as reaction time, temperature, and separation/recyclability of the catalyst. With a temperature of 150 °C for 48 h the reaction conditions in Glorius' example are quite harsh and, furthermore, the transition-metal catalyst is not shown to be recyclable.

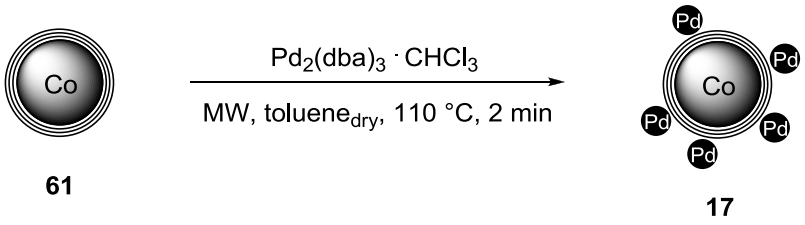

61 **17**

Scheme 12 Microwave synthesis of a Pd@Co/C nanocomposite.[6]

In our group, we could most recently demonstrate the synthesis and application of a magnetic alternative to Pd/C (Scheme 12).[6] Palladium nanoparticles deposited on the surface of carbon coated cobalt nanoparticles **61** showed excellent catalytic performances in the hydrogenation of alkenes, exceeding commercial Pd/C catalysts by far. Hence, our catalytic system could be an improvement in the C-H activation with respect to a higher catalytic activity, milder reaction conditions, and a convenient catalyst separation/reuse.

Therefore, we synthesized a Pd@Co/C catalyst **17** via microwave decomposition of $Pd_2(dba)_3 \cdot CHCl_3$ according to our reported procedure (Scheme 12). We could establish a Pd loading of 4.3 wt% which is quite similar to the commercially

available Pd/C catalyst reported by Glorius (5 wt%). To test our catalyst in the C-H activation, we carried out the arylation of benzo[*b*]thiophene with chlorobenzene under the same reaction conditions Glorius reported. However, after a reaction time of 48 h we could not observe any conversion of the starting material. Even a prolonged reaction time of 5 days did not show any conversion and the starting material could be fully recovered. This result is quite surprising as our catalyst showed superior results in the hydrogenation compared to commercial Pd/C. One reason could be the role of Pd in this C-H activation. The role of Pd/C and the mechanism of the reaction are still not completely clear and require further investigations.[5] Pd/C catalyzed reactions are often thought to include a homogeneous active species due to the leaching of Pd into solution.[7] However, the group of Glorius performed several experiments to determine the nature of the active species and all results so far strongly suggest a heterogeneous reaction.[5] Hence, our heterogeneous Pd@Co/C catalyst should also work in the C-H activation if this assumption is right.

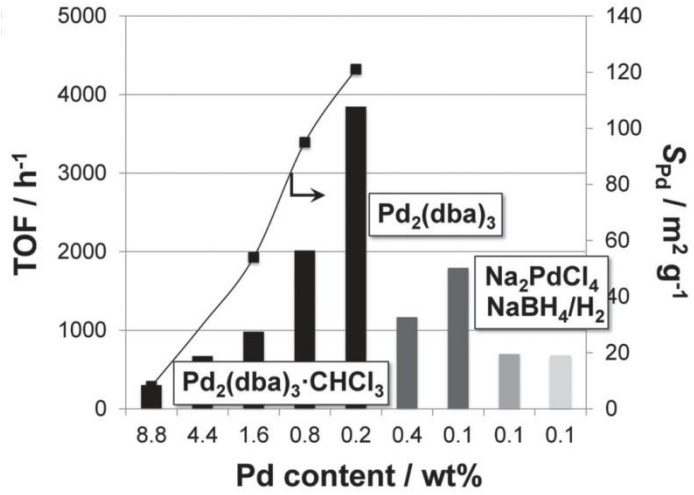

Fig. 18 Hydrogenation tests of *trans*-stilbene at a Pd catalyst amount of 0.1 mol%. The best results were obtained for Pd@Co/C particles with a low Pd content of 0.2 wt% synthesized by microwave decomposition of $Pd_2(dba)_3 \cdot CHCl_3$. Figure adapted with permission from ref [6]. Copyright 2013, WILEY-VCH Verlag GmbH & Co. KGaA, Weinheim.

Regarding the activity of our Pd@Co/C catalyst depending on the loading of Pd (Fig. 18),[6] we are at the moment testing a catalyst with a decreased Pd loading and, therefore, higher activity. However, a catalyst with a loading of 0.2 wt% (highest activity) would not make much sense due to the huge amount of required hy-

brid material. E.g. one would need around 5 g of hybrid material for a reaction on 1 mmol scale under the reported reaction conditions. Nevertheless, investigations will go further in our group achieving a potential magnetic C-H activation catalyst.

5.2 Ionic liquid modified Co/C nanobeads as Grubbs catalyst precursor for olefin metathesis

During the last ten to fifteen years olefin metathesis has become a major tool in organic and polymer synthesis.[8] The great success is mainly attributed to the development of well-defined alkylidene ruthenium complexes (Fig. 19) including first and second generation Grubbs catalysts (**62a**, **62b**) and the chelating Hoveyda-Grubbs catalysts (**63a**, **63b**). However, using a catalyst in a homogeneous way often entails deactivation through decomposition, difficult recycling, and time-consuming separation of the catalyst from the reaction mixture.

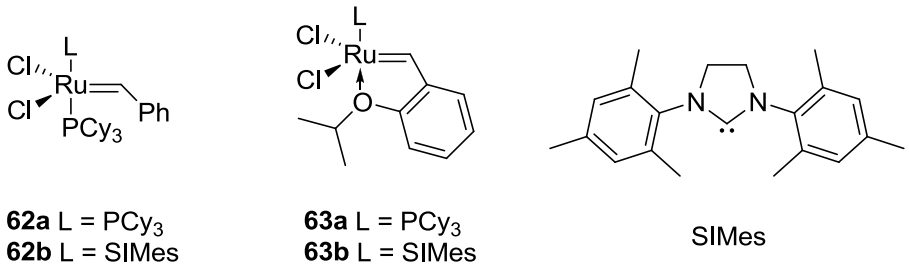

62a L = PCy_3
62b L = SIMes

63a L = PCy_3
63b L = SIMes

Fig. 19 Ruthenium alkylidene metathesis catalysts.

Hence, several attempts have been made to generate heterogeneous metathesis catalysts by immobilizing Grubbs or Hoveyda-Grubbs catalysts on silica,[9] polymers,[10] dendrimers,[11] or magnetic nanoparticles.[12] The support precursor for the immobilization could be phosphine ligand **64**, alkylidene ligand **65**, or NHC ligand **66** (Fig. 20).[13] However, the precursor is often synthesized over multiple steps which is time-consuming and uneconomically. Therefore, an inexpensive and easily available precursor would be a great advance for olefin metathesis, thus shortening the immobilization process and working more economically.

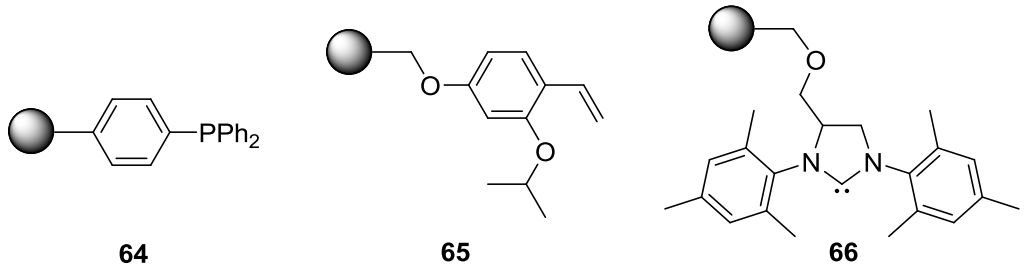

Fig. 20 Different types of support precursors for the immobilization of metathesis catalysts.[14]

In chapter 4 we demonstrated the facile synthesis of ionic liquid modified magnetic nanobeads PS-IL@Co/C **45** bearing a benzyl-methyl imidazolium moiety. This moiety differs from ionic liquid precursors for second generation Grubbs or Hoveyda-Grubbs catalysts, however, as the synthesis is extremely simple it would be worth to try the immobilization of an alkylidene ruthenium complex by deprotonation and ligand exchange. The deprotonation of a structural similar imidazolium salt was shown by Bolm *et al.*[14] using NaH and KO^{t}Bu in THF. They could also demonstrate the reactivity of the generated NHC via a subsequent reaction with a $[Rh(COD)Cl]_2$ complex by ligand exchange.

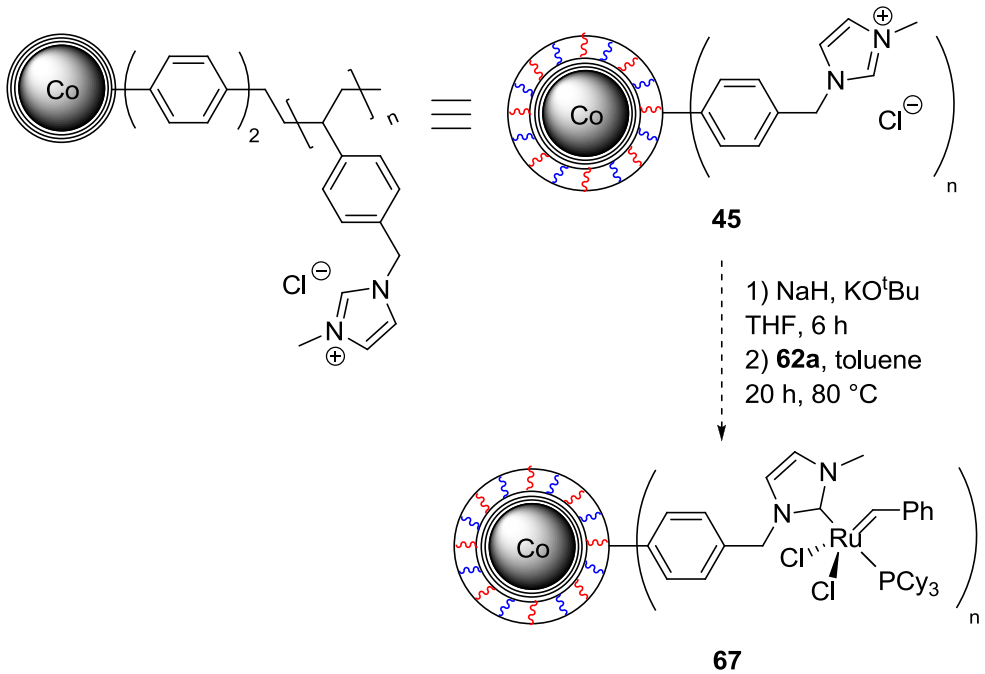

Scheme 13 A possible pathway to immobilize a metathesis catalyst on ionic liquid modified polystyrene coated Co/C nanoparticles **45**.

Hence, we also tried to deprotonate **45** using the procedure described by Bolm with subsequent reaction using first generation Grubbs catalyst (Scheme 13). After the two step reaction the nanoparticles were qualitatively analyzed by IR spectroscopy and quantitatively via ICP-OES analysis (Ru amount). Table 19 shows the screening of different reaction conditions. In entry 1 10 mol% KO^{t}Bu and 2 equiv. NaH were used for a reaction time of 6 h. Compared to Bolm (5 mol% KO^{t}Bu, 1.1 equiv. NaH, 60 min) reagent amounts and reaction time were enhanced as we work under heterogeneous conditions. However, no formation of the product was observed in the IR spectra. ICP-OES analysis gave a value of 0.012 mmol g^{-1} reflecting a Ru amount of 1.13% referred to the maximum. Due to the hygroscopic ionic liquid, we lyophilized the starting material for 4 days prior to use (entry 2 and 3), however, the characteristic H_2O-peak at 3050 cm^{-1} did not vanish completely. ICP-OES in entry 2 showed a value of 0.050 mmolg-1 (4.87%), being a little higher than in entry 1. However, one cannot make a certain statement about this difference as we are very close to the detection limit. Furthermore absolutely no difference was observed in the IR spectrum compared to **45**. In entry 3 we further enhanced the amounts of KO^{t}Bu (50 mol%) and NaH (5 equiv.) to see if a more significant change could be observed. Nevertheless, the Ru loading was again extremely low (0.004 mmol g^{-1}, 0.37%) and IR spectroscopy did not show any difference. Therefore, the Ru value of entry 2 was indeed not reliable.

Table 19 Immobilization of a metathesis catalyst on ionic liquid modified polymer coated Co/C nanoparticles **45**.[a]

Entry	Amount NaH [equiv.][b]	Amount KO^{t}Bu [mol%][b]	IR spectra[c]	Ru loading [mmolg^{-1}][d]
1	2	10	no change	0.012
2[e]	2	10	no change	0.050
3[e]	5	50	no change	0.004

[a] PS-IL@Co/C **45** (0.084 mmol) was reacted with NaH and KO^{t}Bu (1M in THF) in 2 mL of dry THF. After washing and drying, the product was heated with **62a** (0.126 mmol) at 80 °C for 20 h.
[b] Amounts of reagents used in the synthesis. [c] Observed changes in the IR spectra. [d] Loading of Ru in the product. Determined by ICP-OES analysis. [e] PS-IL@Co/C **45** was lyophilized for 4 d prior to use.

Unfortunately, the formation of a Ru complex on the heterogeneous support was not possible using the simple benzyl-methyl imidazolium scaffold as a precursor. To synthesize a recyclable catalyst based on Grubbs or Hoveyda-Grubbs catalysts, one probably also needs to follow a multiple step precursor synthesis mentioned above.

5.3 Conclusion

Attempts were made to establish a magnetically recyclable catalyst for C-H activation as well as alkene metathesis. The application of a Pd@Co/C catalyst failed in the arylation of benzo[*b*]thiophenes applying a catalyst with a Pd loading of 4.3 wt%. One reason could be that the commercially available Pd/C catalyst used by Glorius is simply more active than our catalyst. The activity of different commercially available Pd/C catalysts can vary a lot. Another reason would be that the active species is not a heterogeneous one as Glorius proposed, thus having just a high reactivity with major metal leaching. Therefore, further investigations are ongoing to test Pd@Co/C with higher activity to check if any conversion can be observed.

The formation of a Ru complex on the heterogeneous support with simple benzyl-methyl imidazolium scaffold as a precursor also failed. The reason could be the extremely hygroscopic nature of the heterogeneous support. Even after lyophilizing for multiple days the characteristic H_2O-peak did not vanish completely. Therefore, one probably also needs to follow a multiple step precursor synthesis mentioned above to synthesize a recyclable catalyst based on Grubbs or Hoveyda-Grubbs catalysts. In doing so, the best way would be via phosphine precursor **64** or alkylidene precursor **65**, thus avoiding a hygroscopic moiety on the support.

5.4 Experimental section

Synthesis of the catalysts

Co/C supported Pd nanoparticles (17, Pd@Co/C)

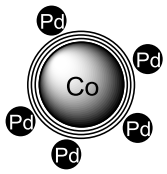

100 mg Co/C **61** and 2.5 mL dry toluene were introduced to a microwave vial and sonicated in an ultrasonic bath for 10 min under N_2-atmosphere. 24.4 mg (23.6 µmol) $Pd_2(dba)_3 \cdot CHCl_3$ was added and the reaction mixture heated in a focused microwave oven to 110 °C for 2 min. After magnetic decantation the particles were washed with dichloromethane (5 x 5 mL) and dried under vacuum to obtain Pd@Co/C **17** (104.4 mg). The loading of Pd was determined by ICP-OES (0.404 mmol g^{-1}, 90%).

Representative procedure towards the synthesis of Co/C supported alkene metathesis catalyst (67)

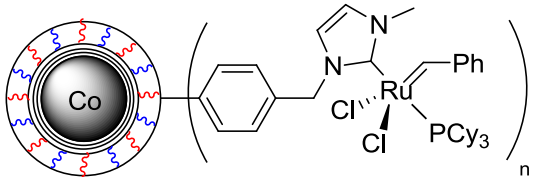

40 mg PS-IL@Co/C **45** in dry THF were predispersed in a pressure tube under nitrogen atmosphere for 10 min. 6.7 mg NaH (168 µmol, 60% in dispersion in mineral oil) and 8.4 µL KO^tBu (8.4 µmol, 1M in THF) were added and the reaction mixture stirred for 6 h. After magnetic decantation the particles were washed with dry THF (6 x 5 mL) and dried under vacuum. Subsequently 2 mL dry toluene and 104 mg **62a** (126 µmol) were added, the suspension predispersed using ultrasonic bath and stirred for 20 h at 80 °C under nitrogen atmosphere. After cooling and magnetic decantation the particles were washed with toluene (5 x 5 mL) and di-

chloromethane (3 x 5 mL) and dried in vacuo. Ruthenium loading was determined by ICP-OES (0.050 mmol g^{-1}, 4.87%).

General procedure for the arylation of benzo[*b*]thiophene

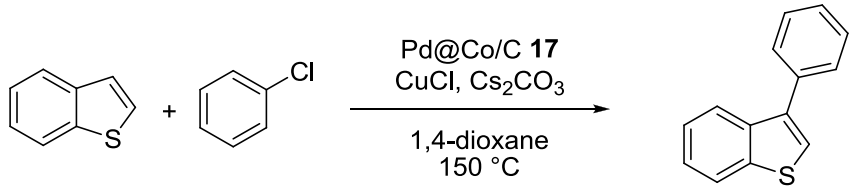

53 **59a** **55a**

46.5 mg (18.8 µmol) Pd@Co/C **17**, 26.8 mg (0.2 mmol) freshly distilled benzo[*b*]thiophene **53**, 71.7 mg (0.22 mmol) Cs_2CO_3, 2 mg (20 µmol) CuCl, and 28.0 µL (0.2 mmol) mesitylene as internal standard were predispersed for 10 min in 1 mL 1,4-dioxane using ultrasonic bath. 40.6 µL (0.4 mmol) freshly distilled chlorbenzene was added and the reaction mixture stirred at 150 °C for 5 d. GC samples were taken after various times (GC conditions: 50 °C (3 min), 40 °C/min, 290 °C).

5.5 References

[1] a) C. Lamberth, J. Dinges, *Bioactive heterocyclic compound classes*. *Agrochemicals*, Wiley-VCH; John Wiley, Weinheim, Chichester, **2012**; b) G. P. McGlacken, L. M. Bateman, *Chem. Soc. Rev.* **2009**, *38*, 2447; c) K. C. Nicolaou, C. R. H. Hale, C. Nilewski, H. A. Ioannidou, *Chem. Soc. Rev.* **2012**, *41*, 5185–5238.

[2] K. Ueda, S. Yanagisawa, J. Yamaguchi, K. Itami, Angew. Chem. 2010, 122, 9130–9133; *Angew. Chem. Int. Ed.* **2010**, *49*, 8946–8949.

[3] K. Funaki, T. Sato, S. Oi, *Org. Lett.* **2012**, *14*, 6186–6189.

[4] S. Kirchberg, S. Tani, K. Ueda, J. Yamaguchi, A. Studer, K. Itami, *Angew. Chem.* **2011**, *123*, 2435–2439; *Angew. Chem. Int. Ed.* **2011**, *50*, 2387–2391.

[5] D.-T. D. Tang, K. D. Collins, F. Glorius, *J. Am. Chem. Soc.* **2013**, *135*, 7450–7453.

[6] Q. M. Kainz, R. Linhardt, R. N. Grass, G. Vilé, J. Pérez-Ramírez, W. J. Stark, O. Reiser, *Adv. Funct. Mater.* **2013**, DOI: 10.1002/adfm.201303277.

[7] a) R. H. Crabtree, *Chem. Rev.* **2012**, *112*, 1536–1554; b) J. A. Widegren, R. G. Finke, *J. Mol. Catal. A: Chem.* **2003**, *198*, 317–341.

[8] G. C. Vougioukalakis, R. H. Grubbs, *Chem. Rev.* **2010**, *110*, 1746–1787.

[9] a) D. P. Allen, M. M. Van Wingerden, R. H. Grubbs, *Org. Lett.* **2009**, *11*, 1261–1264; b) M. Bru, R. Dehn, J. H. Teles, S. Deuerlein, M. Danz, I. B. Müller, M. Limbach, *Chem. Eur. J.* **2013**, *19*, 11661–11671; c) J. Cabrera, R. Padilla, M. Bru, R. Lindner, T. Kageyama, K. Wilckens, S. L. Balof, H.-J. Schanz, R. Dehn, J. H. Teles et al., *Chem. Eur. J.* **2012**, *18*, 14717–14724; d) J.-E. Jee, J. L. Cheong, J. Lim, C. Chen, S. H. Hong, S. S. Lee, *J. Org. Chem.* **2013**, *78*, 3048–3056; e) J. Lim, S. S. Lee, S. N. Riduan, J. Y. Ying, *Adv. Synth. Catal.* **2007**, *349*, 1066–1076; f) F. Michalek, D. Mädge, J. Rühe, W. Bannwarth, *Eur. J. Org. Chem.* **2006**, *2006*, 577–581; g) A. Monge-Marcet, R. Pleixats, X. Cattoën, M. Wong Chi Man, *J. Mol. Catal. A: Chem.* **2012**, *357*, 59–66; h) K. Vehlow, S. Maechling, K. Köhler, S. Blechert, *J. Organomet. Chem.* **2006**, *691*, 5267–5277.

[10] M. Al-Hashimi, C. Hongfa, B. George, H. S. Bazzi, D. E. Bergbreiter, *J. Polym. Sci. A Polym. Chem.* **2012**, *50*, 3954–3959.

[11] N. J. M. Pijnenburg, E. Tomás-Mendivil, K. E. Mayland, H. Kleijn, M. Lutz, A. L. Spek, G. van Koten, Klein Gebbink, Robertus J. M., *Inorg. Chim. Acta* **2014**, *409, Part A*, 163–173.

[12] a) C. Che, W. Li, S. Lin, J. Chen, J. Zheng, J.-c. Wu, Q. Zheng, G. Zhang, Z. Yang, B. Jiang, *Chem. Commun.* **2009**, 5990; b) Z. Yinghuai, L. Kuijin, N. Huimin, L. Chuanzhao, L. P. Stubbs, C. F. Siong, T. Muihua, S. C. Peng, *Adv. Synth. Catal.* **2009**, *351*, 2650–2656.

[13] I. Dragutan, V. Dragutan, *Platinum Met. Rev.* **2008**, *52*, 71–82.

[14] C. Bolm, M. Kesselgruber, G. Raabe, *Organometallics* **2002**, *21*, 707–710.

C. Summary

The present dissertation deals with the immobilization of organo- and transition metal catalysts on the surface of magnetic, carbon-coated Fe or Co nanoparticles. With the introduction of polymeric structures or stabilizing groups, the preparation of catalysts with an extremely high surface density (1.3-4.0 mmol g^{-1}) is possible. The high-density materials can be efficiently applied in catalysis including facile recovery and recycling due to its highly magnetic properties.

Chapter 1 demonstrates the need of high-loading catalysts in terms of sustainability and economy of catalytic reactions. A low catalyst loading can lead to the requirement of an exorbitant amount of supporting material. The recycling of small amounts of e.g. an expensive transition metal is not very effective if a high amount of a Co support is used. Hence, the synthesis of magnetic, high-density catalysts can diminish the waste of catalysts as well as supporting material.

In chapter 2 the synthesis of a novel, magnetic Baylis-Hillman catalyst is demonstrated (Scheme 14). Using a covalently immobilized polymeric resin on the surface of Fe/C nanobeads, a catalyst with a maximum loading of 1.6 mmol g^{-1} is obtained. The material bearing *N*-alkylimidazole units is easily synthesized, shows good yields after moderate reaction times, and exhibits excellent recyclability. Furthermore, we could demonstrate a dendritic-like effect of the catalyst units by comparing two heterogeneous catalysts (different catalyst density) and a homogeneous analogue.

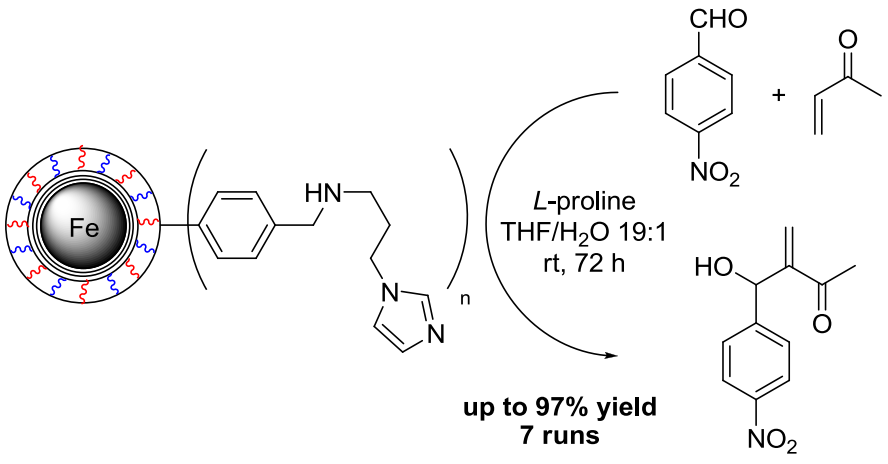

Scheme 14 Baylis-Hillman reaction with *N*-alkylimidazole immobilized on polymer-coated Fe/C nanobeads.

Chapter 3 deals with the immobilization of an asymmetric organocatalyst on polymer-functionalized Co/C nanobeads (Scheme 15). The magnetic Jørgensen-Hayashi catalyst with a loading of 1.34 mmol g^{-1} shows superior catalytic performance in Michael additions than a homogeneous analogue. In collaboration with the group of Caminade and Majoral we could very nicely compare our magnetic with a dendritic globular catalyst support. In terms of activity and recycling ability, the dendritic catalyst leads to a better performance, while enantio- and diastereoselectivities for both catalysts were good to excellent. Regarding catalyst recovery, our magnetic catalyst performed much better via simple magnetic decantation while the dendritic catalyst needs a circumstantial precipitation/filtration process.

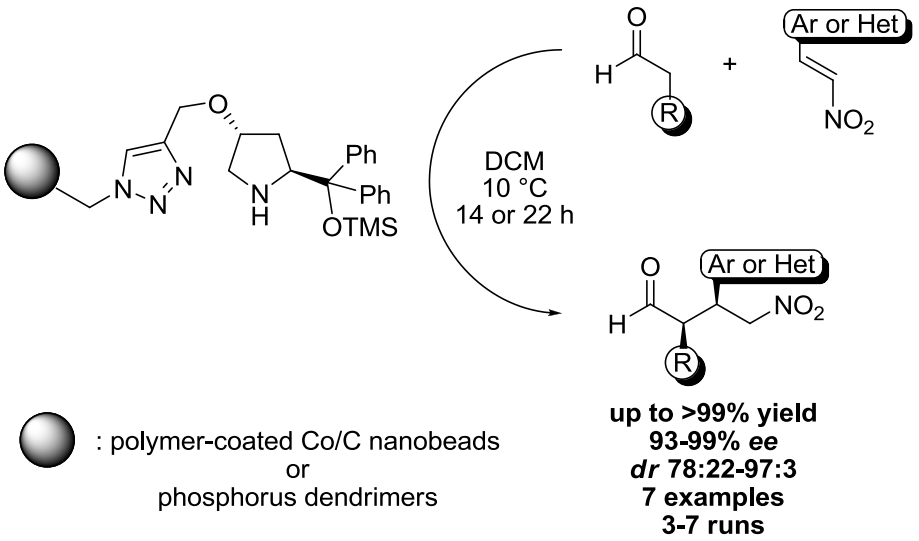

Scheme 15 Michael addition with Jørgensen-Hayashi catalyst immobilized on polymer-coated Co/C nanobeads and phosphorus dendrimers.

In chapter 4 magnetic hybrid materials are reported as recyclable, high-density catalysts for alkene hydrogenation (Scheme 16). The materials consist of magnetic nanobeads functionalized with imidazolium-based ionic liquids and optional polymer shells. Palladium nanoparticles were synthesized on the surface of these supports by two different methods. Deposition of palladium(0) onto the magnetic nanobeads by microwave decomposition of $Pd_2(dba)_3 \cdot CHCl_3$ leads to more efficient catalysts than the reduction of a Pd(II) precursor. The catalyst with a quite flexible ionic liquid on the surface turned out to be the most promising regarding the stabilization of Pd nanoparticles. It showed great catalyst density (up to 4.0 mmol g^{-1}), high activity in the hydrogenation of *trans*-stilbene (TOF up to

330 h^{-1}), easy separation, and furthermore was recycled for at least 11 runs without significant loss of activity. Moreover, we could show that the leaching of Pd and Co into the product was not noticeably high if a Pd amount of 0.1 mol% was used. Recycling of the catalyst was also possible varying the substrate after each run.

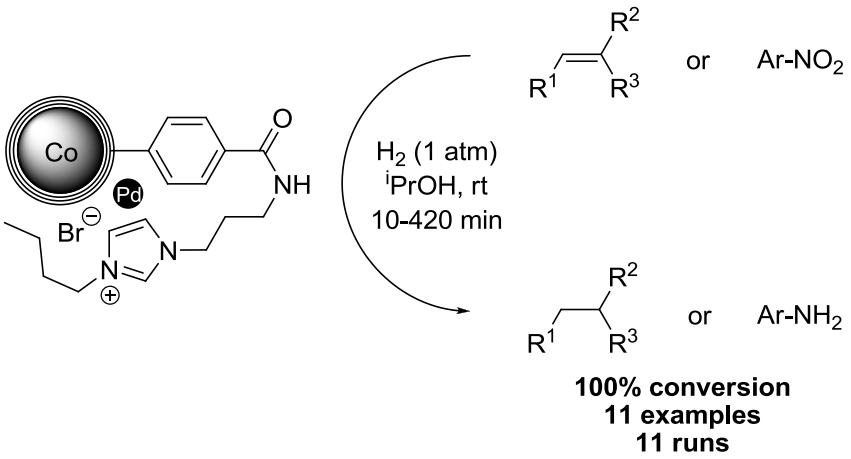

Scheme 16 Hydrogenation of alkenes and nitro compounds with Pd nanoparticles supported on ionic liquid modified Co/C nanobeads.

In chapter 5 studies towards recyclable catalysts for C-H activation and olefin metathesis are discussed. Palladium nanoparticles on the surface of Co/C nanobeads (Pd@Co/C) were applied in the arylation of benzo[*b*]thiophene. Unfortunately, no conversion could be observed for this C-H activation being remarkable compared to literature results with Pd/C. One reason could be the mechanism of the reaction, which is not completely proved so far. If the active catalytic species is not a heterogeneous one, the reaction will only work if a significant Pd(II) leaching into solution is present. The formation of a magnetic Ru complex for olefin metathesis unfortunately also failed. Using a simple benzyl-methyl imidazolium moiety as precursor on the Co/C surface, we tried to immobilize a Grubbs catalyst by simple ligand exchange. The problem for failing in this case could be the hygroscopic nature of our imidazolium support.

D. Zusammenfassung

Die vorliegende Dissertation beschäftigt sich mit der Immobilisierung von Organo- und Übergangsmetall-Katalysatoren auf magnetischen, Kohlenstoff-beschichteten Kobalt- oder Eisen-Nanopartikeln (Co/C, Fe/C). Mit Hilfe von Polymeren und stabilisierenden Gruppen war es möglich Katalysatoren mit einer sehr hohen Oberflächen-Beladung zu synthetisieren. Diese magnetischen, hoch-beladenen Katalysatoren konnten anschließend mit sehr guten Ergebnissen in der Katalyse eingesetzt werden. Dabei war durch die hohe Magnetisierung des Trägermaterials ein einfaches Abtrennen und Wiederverwerten möglich.

Kapitel 1 befasst sich mit der Notwendigkeit von Katalysatoren mit einer hohen Oberflächenbeladung um katalytische Reaktionen nachhaltiger und ökonomischer zu gestalten. Eine niedrige Beladung eines heterogenen Katalysators führt automatisch zu einem enormen Verbrauch an Trägermaterial. Das Recyceln einer geringen Menge an teuren Übergangs-Metallen wäre beispielsweise nicht sehr effektiv, wenn dafür große Mengen an Kobalt-Trägermaterial eingesetzt werden müssten. Die Verwendung von magnetischen, hoch-beladenen Katalysatoren würde daher nicht nur das Recyceln von Katalysatoren ermöglichen, sondern auch der Verschwendung von teurem Trägermaterial entgegenwirken.

In Kapitel 2 ist die Synthese eines neuen, magnetischen Baylis-Hillman Katalysators dargestellt (Schema 1). Dabei wurden Fe/C-Nanopartikel zunächst mit einem Polymer beschichtet, durch das der Katalysator anschließend mit einer sehr hohen Beladung (1.6 mmol g^{-1}) aufgebracht werden konnte. Das Material mit *N*-Alkylimidazol Einheiten ist sehr einfach herzustellen, zeigt hohe Ausbeuten (bis zu 97%) nach moderaten Reaktionszeiten und konnte effektiv recycelt werden (7 Zyklen). Des Weiteren war ein interessanter Effekt zu beobachten, der sehr häufig bei dendritischen Strukturen auftritt. Bei diesem Effekt nimmt die Aktivität eines Katalysators mit der Dichte an Katalysatoreinheiten zu. Das konnte in unserem Fall durch den Vergleich von zwei heterogenen Katalysatoren unterschiedlicher Beladung mit einem analogen, homogenen Katalysator gezeigt werden.

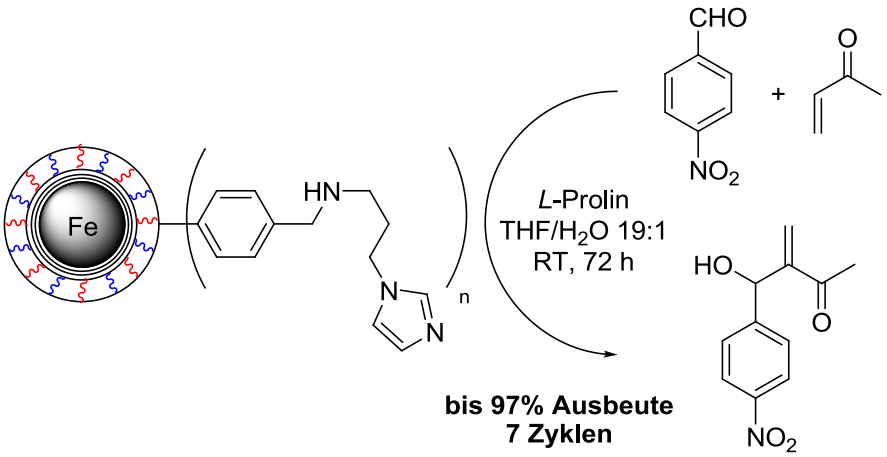

Schema 1 Baylis-Hillman Reaktion mit Hilfe von *N*-Alkylimidazol Einheiten, welche auf Polymer-beschichteten Fe/C Nanopartikeln immobilisiert sind.

In Kapitel 3 ist die Immobilisierung eines asymmetrischen Organokatalysators auf Polymer-beschichteten Co/C-Nanopartikeln gezeigt (Schema 2). Der magnetische Jørgensen-Hayashi Katalysator mit einer Beladung von 1.34 mmol g^{-1} stellte sich in der Michael-Addition als wesentlich aktiver verglichen mit einem analogen, homogenen Katalysator heraus. In Kooperation mit der Gruppe von Caminade und Majoral konnten wir an diesem Beispiel sehr schön unser sphärisches, magnetisches Trägermaterial mit einem ebenso sphärischen, dendritischen Trägermaterial vergleichen. Dabei stellte sich der Dendrimer-basierte Katalysator als effektiver und besser recycelbar heraus, während die Enantio- und Diastereoselektivität für beide Katalysatoren gut bis exzellent war. Bezogen auf die Abtrennung des Katalysators, konnte unser auf magnetischen Nanopartikeln basierter Katalysator überzeugen, da dies sehr schnell und effektiv durch das einfache Anhalten eines Magneten möglich ist. Der dendritische Katalysator muss hingegen erst umständlich aus der Lösung ausgefällt und anschließend abfiltriert werden, bevor er für den nächsten Lauf wieder verwendet werden kann.

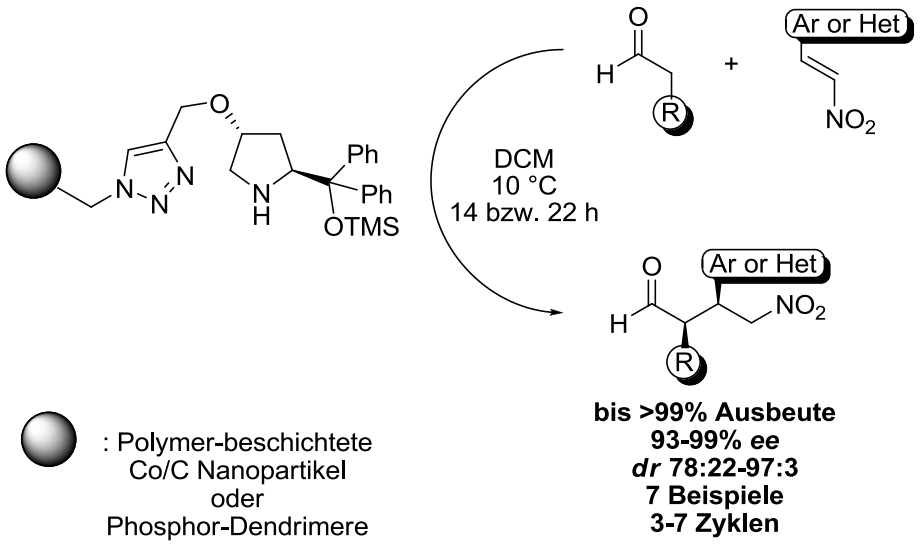

Schema 2 Michael-Addition mit Hilfe eines Jørgensen-Hayashi Katalysators, der sowohl auf Polymer-beschichteten Co/C-Nanopartikeln als auch auf Phosphor-Dendrimeren immobilisiert wurde.

In Kapitel 4 ist ein hoch-beladenes Hybrid-Material für die Hydrierung von Alkenen beschrieben (Schema 3). Das Material besteht aus Co/C Nanopartikeln, die mit auf Imidazolium-Ionen basierten ionischen Flüssigkeiten und optionaler Polymer-Hülle funktionalisiert sind. Auf der Oberfläche dieser funktionalisierten Trägermaterialien wurden Palladium-Nanopartikel mit Hilfe zweier unterschiedlicher Methoden abgeschieden. Dabei stellte sich heraus, dass eine Abscheidung von Palladium(0) durch Zersetzung von $Pd_2(dba)_3 \cdot CHCl_3$ unter Mikrowellen-Bedingungen zu effektiveren Katalysatoren führt als die Reduktion eines Pd(II)-Komplexes. Bei den Untersuchungen wurde festgestellt, dass ein Katalysator mit einer relativ flexiblen, ionischen Flüssigkeit am besten für eine Stabilisierung der Palladium-Nanopartikel auf der Oberfläche sorgen kann. Dieser Katalysator mit einer exzellenten Beladung (bis zu 4.0 mmol g^{-1}) zeigte sehr hohe Aktivität in der Hydrierung von *trans*-Stilben (Wechselzahl bis zu 330 h^{-1}), ist sehr leicht abzutrennen und konnte 11 Mal ohne Aktivitätsverlust wiederverwendet werden. Des Weiteren konnten wir feststellen, dass bei der verwendeten Katalysator-Menge von 0.1 mol% nur sehr wenig Palladium und Kobalt in das Reaktionsprodukt auslaugt. Das Recyceln des Katalysators war auch möglich, indem nach jedem Zyklus ein anderes Substrat für die Hydrierung zugesetzt wurde.

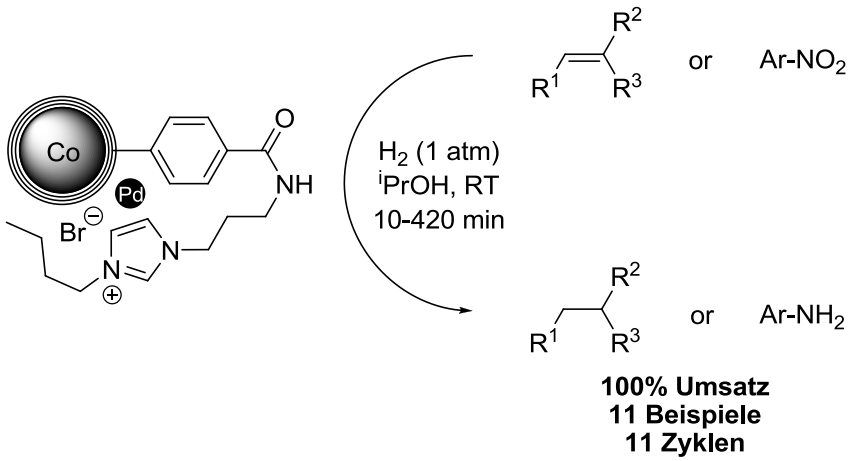

Schema 3 Hydrierung von Alkenen und Nitro-Verbindungen mit Hilfe von Palladium-Nanopartikeln, die auf Co/C-Nanopartikeln funktionalisiert mit einer ionischen Flüssigkeit, immobilisiert wurden.

In Kapitel 6 wurde versucht recycelbare Katalysatoren für die C-H Aktivierung und die Olefin Metathese herzustellen. Für die C-H Aktivierung wurden Palladium-Nanopartikel direkt auf der Oberfläche von Co/C-Nanopartikeln abgeschieden und in der Arylierung von Benzo[*b*]thiophen getestet. Leider konnte dabei jedoch kein Umsatz beobachtet werden, was uns aufgrund von Literatur-Ergebnissen mit Palladium auf Aktivkohle überraschte. Ein möglicher Grund dafür könnte darin liegen, dass der Mechanismus dieser Reaktion noch nicht komplett aufgeklärt ist. Falls die aktive Katalysator-Spezies nämlich nicht hetero- sondern homogen ist, würde die Reaktion nur bei einem enormen Auslaugen von Pd(II) in die Reaktionslösung funktionieren. Ein magnetischer Ruthenium-Komplex für die Olefin-Metathese konnte ebenso nicht dargestellt werden. Wir haben versucht einen Grubbs Katalysator durch einfachen Liganden-Austausch mit einem simplen Benzyl-Methyl-Imidazolium Baustein als Vorstufe auf der Nanopartikel-Oberfläche zu immobilisieren. Dies funktionierte vermutlich nicht, da sich das Imidazolium-Trägermaterial als extrem hygroskopisch herausstellte und somit das Herstellen der Carben-Zwischenstufe nahezu unmöglich ist.

E. List of abbreviations

AC	activated carbon
AIBN	*N*,*N*-azobisisobutyro-nitrile
AN	aniline
Ar	aryl
atm	atmosphere
ATR	attenuated total reflection
bipy	2,2'-bipyridine
bmim	butylmethylimidazolium
br	broad resonance
Bz	benzyl
CAL	cinnamaldehyde
CDG	chemically derived graphene
CNF	carbon nanofibre
CNT	carbon nanotube
Co/C	carbon-coated cobalt nanoparticles
COD	1,5-cyclooctadiene
COL	cinnamyl alcohol
CQD	carbon quantum dot
CuAAC	copper-catalyzed azide/ alkyne cycloaddition
Cy	cyclohexyl
d	day(s), doublet
DCE	dichloroethane
DCM	dichloromethane
dba	dibenzylidene acetone
DFT	density functional theory
DMF	dimethylformamide
dr	diastereomeric ratio
DWCNT	double-walled carbon nanotube
EDTA	ethylenediaminetetra-acetic acid
EE	ethyl acetate
ee	enantiomeric excess
E-field	electric field
equiv	equivalents
ESI	electrospray ionization
ET	electron tomography
Et	ethyl
EtOH	ethanol
Fe/C	carbon-coated iron nanoparticles
FT	Fourier transform
FTS	Fischer-Tropsch synthesis
GC	gas chromatography
GN	graphene nanosheet
G_n	dendrimer of generation n
GO	graphene oxide
h	hour(s)
HAD	hexadecylamine
HCAL	hydrocinnamaldehyde
HCOL	hydrocinnamyl alcohol
Het	heterocycle
H-field	magnetic field
HPLC	high-performance liquid chromatography
Hz	hertz
ICP	inductively coupled plasma
IL	ionic liquid

^{i}Pr	iso-propyl
IR	infrared
I_{rel}	relative intensity
J	coupling constant
L	ligand
M	metal, monomer
m	multiplet
m-	*meta*-
MD	molecular dynamics
Me	methyl
MeCN	acetonitrile
MeOH	methanol
MeOPEG	polyethylene glycol monomethyl ether
Mes	mesitylene
min	minute(s)
MNP	metal nanoparticle
MPA	mercaptopropionic acid
MS	mass spectrometry
$mSiO_2$	mesoporous silica
MW	microwave
MWCNT	multi-wall carbon nanotube
NB	nitrobenzene
NHC	*N*-heterocyclic carbene
NMR	nuclear magnetic resonance
NP	nanoparticle
npD	diamond nanoparticle
*n*Pent	*n*-pentyl
*n*Pr	*n*-propyl
o-	*ortho*-
O_{ad}	oxygen adatom
OES	optical emission spectrometry
OTf	triflate
p-	*para*-
PAMAM	poly(amidoamine)
PANI	polyaniline
p-CAN	*para*-chloroaniline
p-CNB	*para*-chloronitro-benzene
PDDA	poly(diallyldimethyl-ammonium chloride)
PE	hexanes
PEG	poly ethylene glycol
Ph	phenyl
ppm	part per million
PS	polystyrene
PVA	poly(vinylalcohol)
PVP	poly(vinylpyrrolidone)
quin	quintet
R^{x}	arbitrary rest
rGO	reduced graphene oxide
rt	room temperature
s	singlet, second(s)
SDS	sodium dodecyl sulfate
SEED	substrate enhanced electroless deposition
SIL	supported ionic liquid
SILP	supported ionic liquid phase
SWCNT	single-walled carbon nanotube
T	temperature
t	triplet, time
TBTA	tris(benzyltriazolyl-methyl)amine
^{t}Bu	*tert*-butyl
TEM	transmission electron microscopy
TEMPO	2,2,6,6-tetramethyl-piperidine-1-oxyl
THF	tetrahydrofurane

TLC	thin layer chromatography
TOF	turnover frequency
TON	turnover number
TMS	trimethyl silyl
t_R	retention time
UV	ultraviolet
$\tilde{\nu}$	wave number
wt%	weight percent
X	arbitrary anion
XRD	x-ray diffraction

F. Appendix

1. NMR spectra

^{1}H NMR (300 MHz)

^{13}C NMR (75 MHz)

Solvent: $CDCl_3$

N-Benzyl-3-(1H-imidazol-1-yl)propan-1-amine (26)

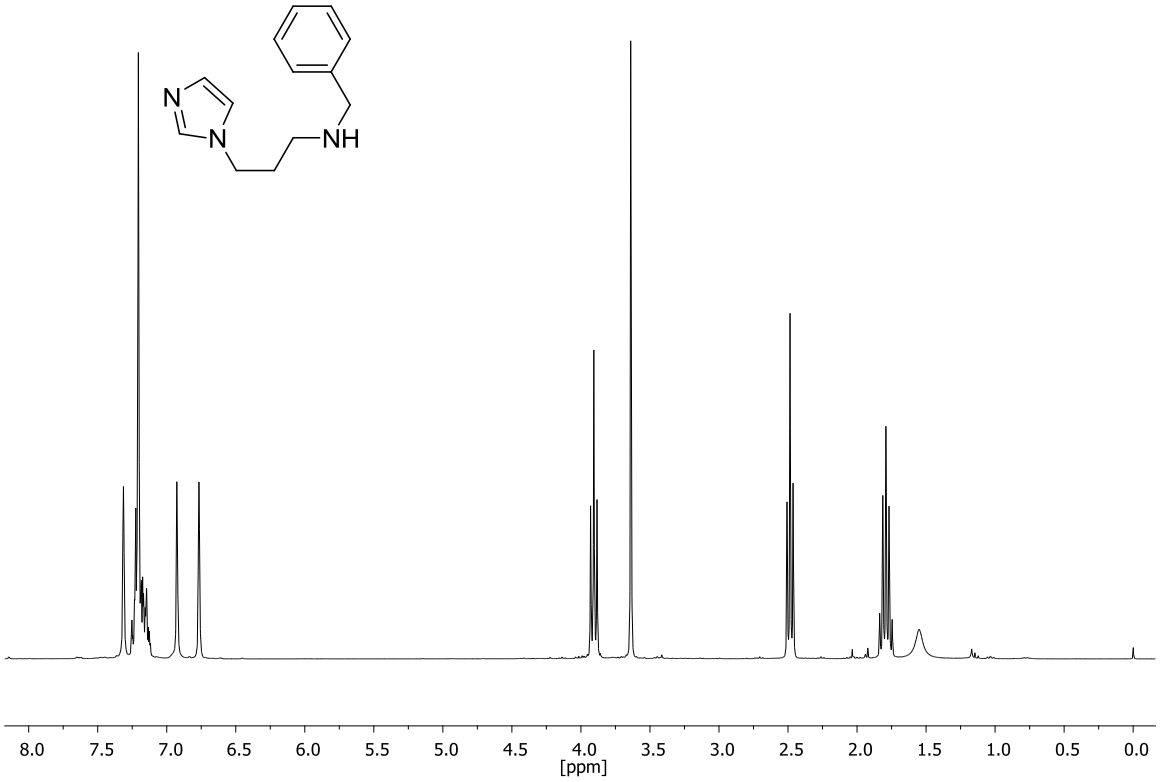

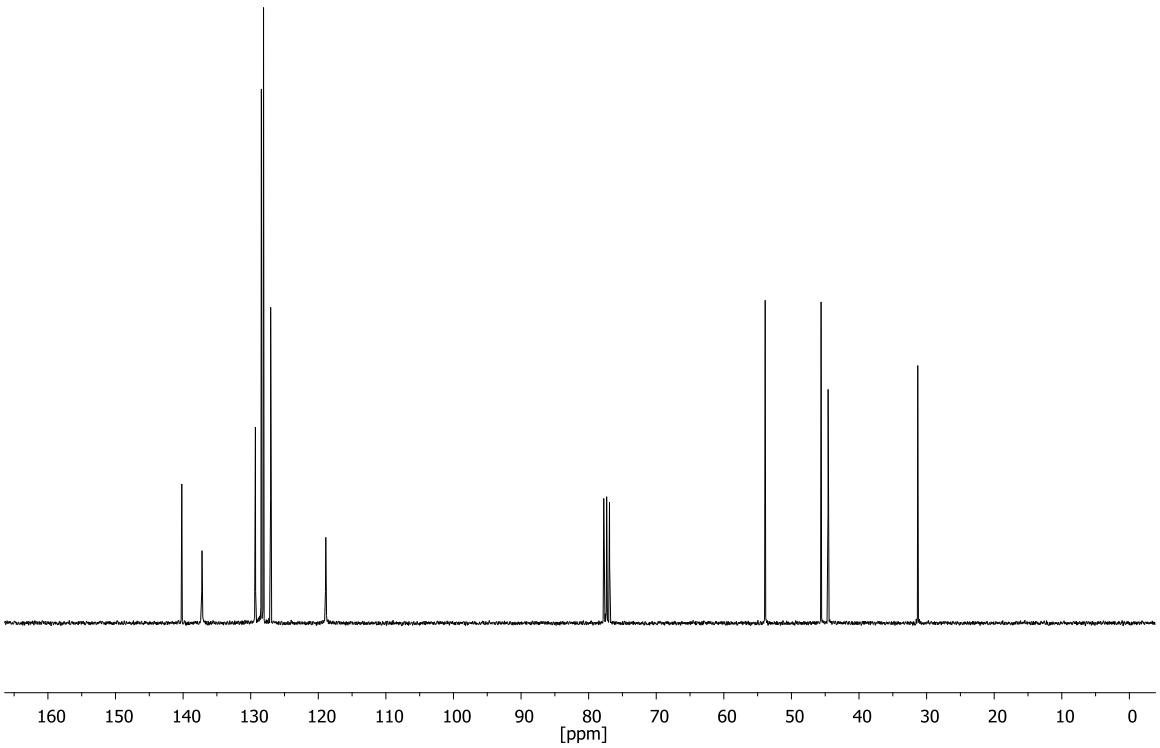

2-Methyl-4-nitro-3-phenylbutanal (36a) (*syn* and *anti*)

major diastereomer

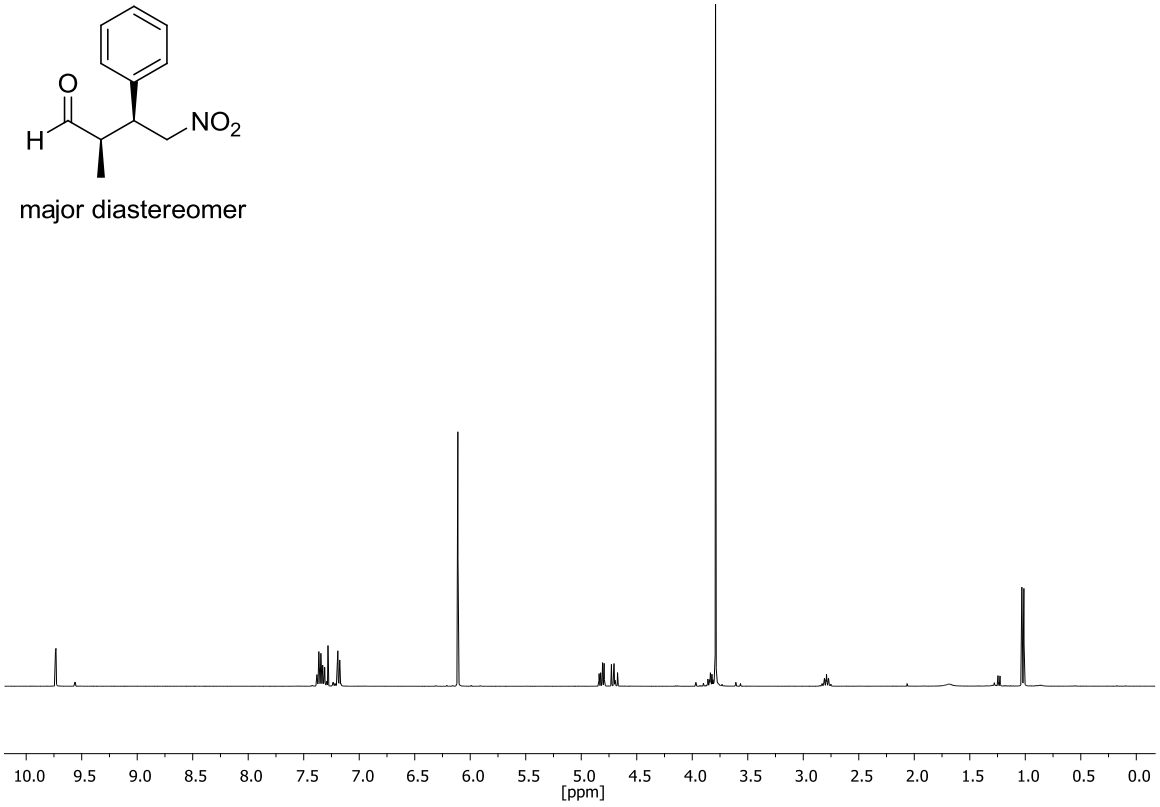

2-Ethyl-4-nitro-3-phenylbutanal (36b) (*syn* and *anti*)

major diastereomer

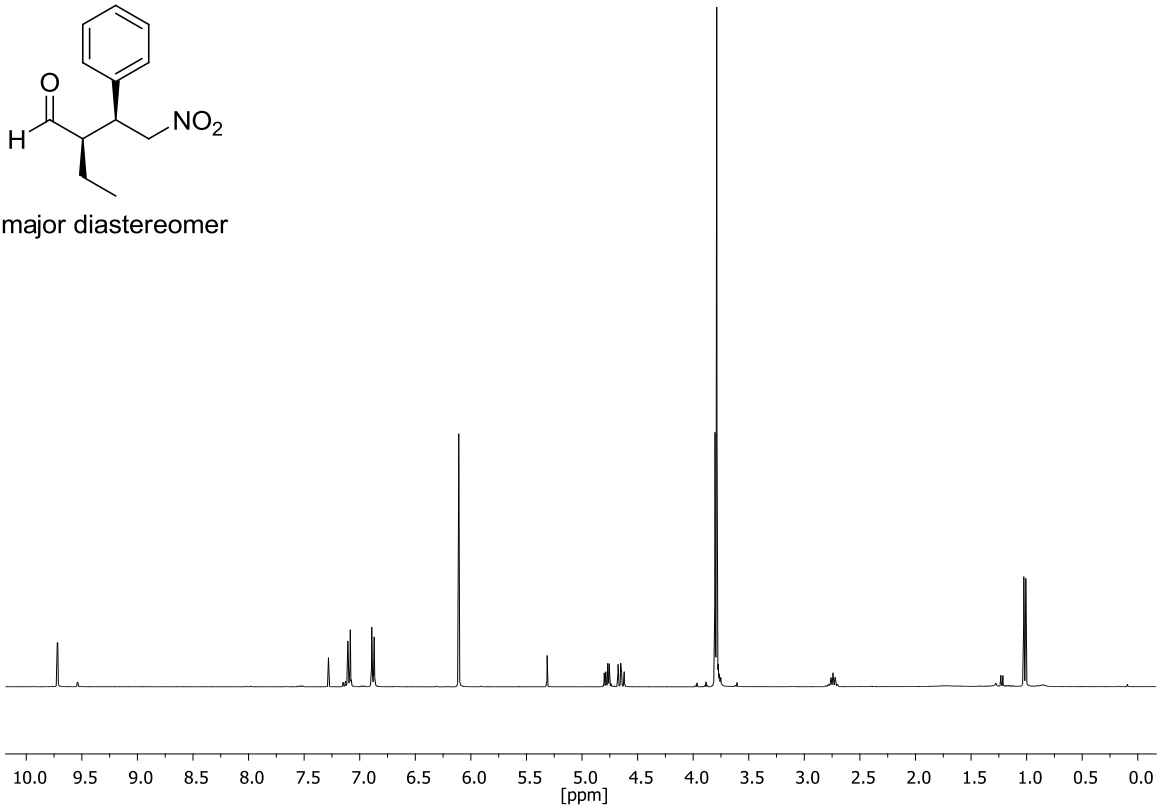

2-Nitro-1-phenylethyl)-pentanal (36c) (*syn* and *anti*)

major diastereomer

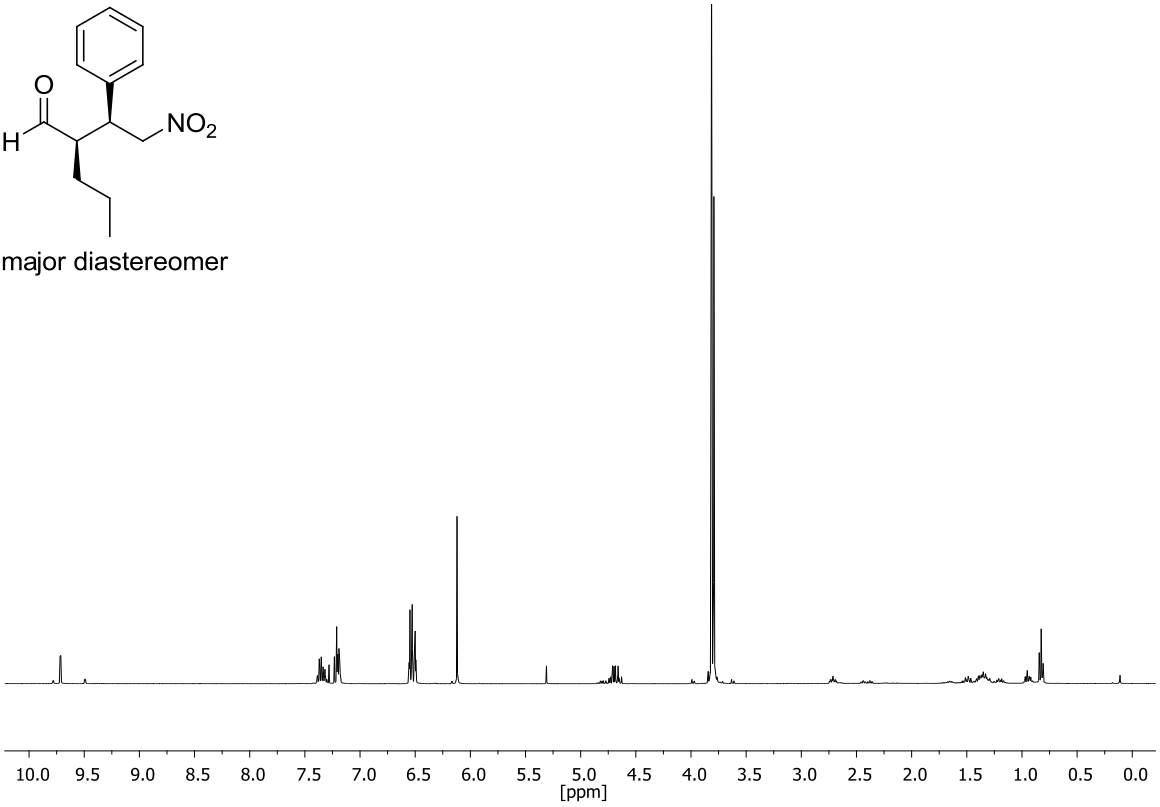

2-Nitro-1-phenylethyl)-heptanal (36d) (*syn* and *anti*)

major diastereomer

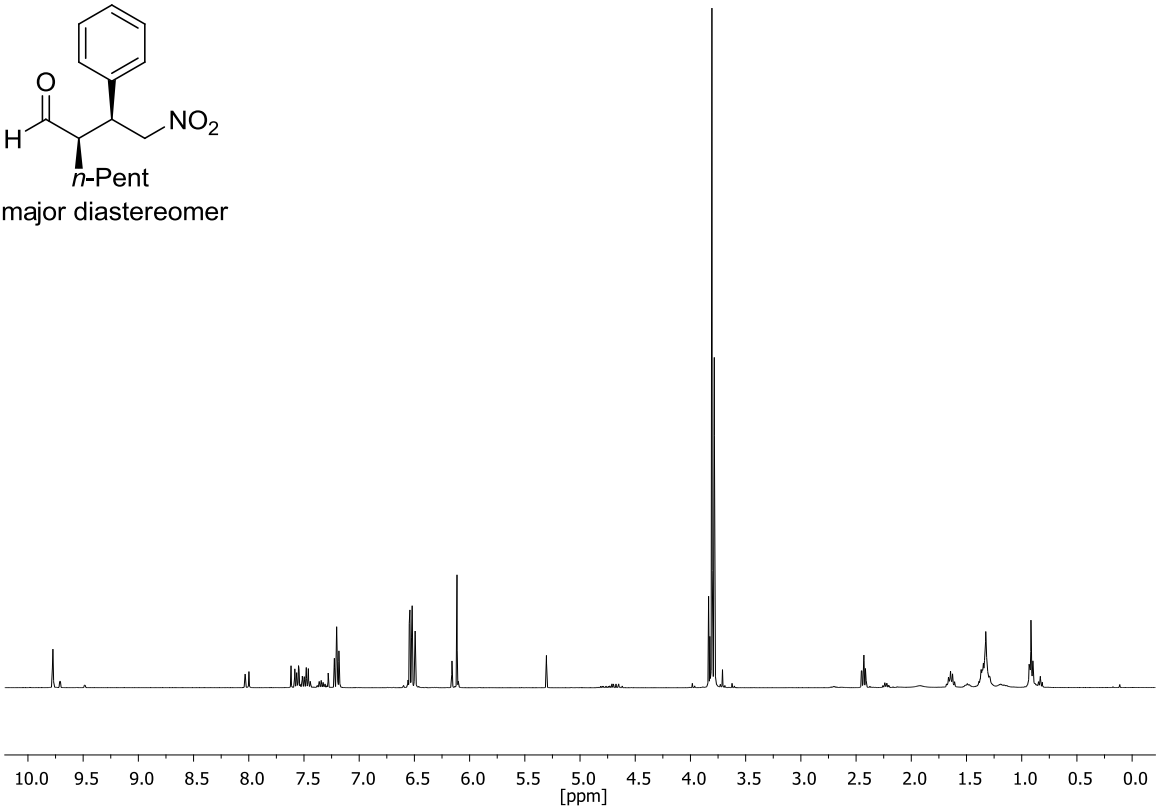

(4-Bromophenyl)-2-methyl-4-nitrobutyraldehyde (36e) (*syn* and *anti*)

major diastereomer

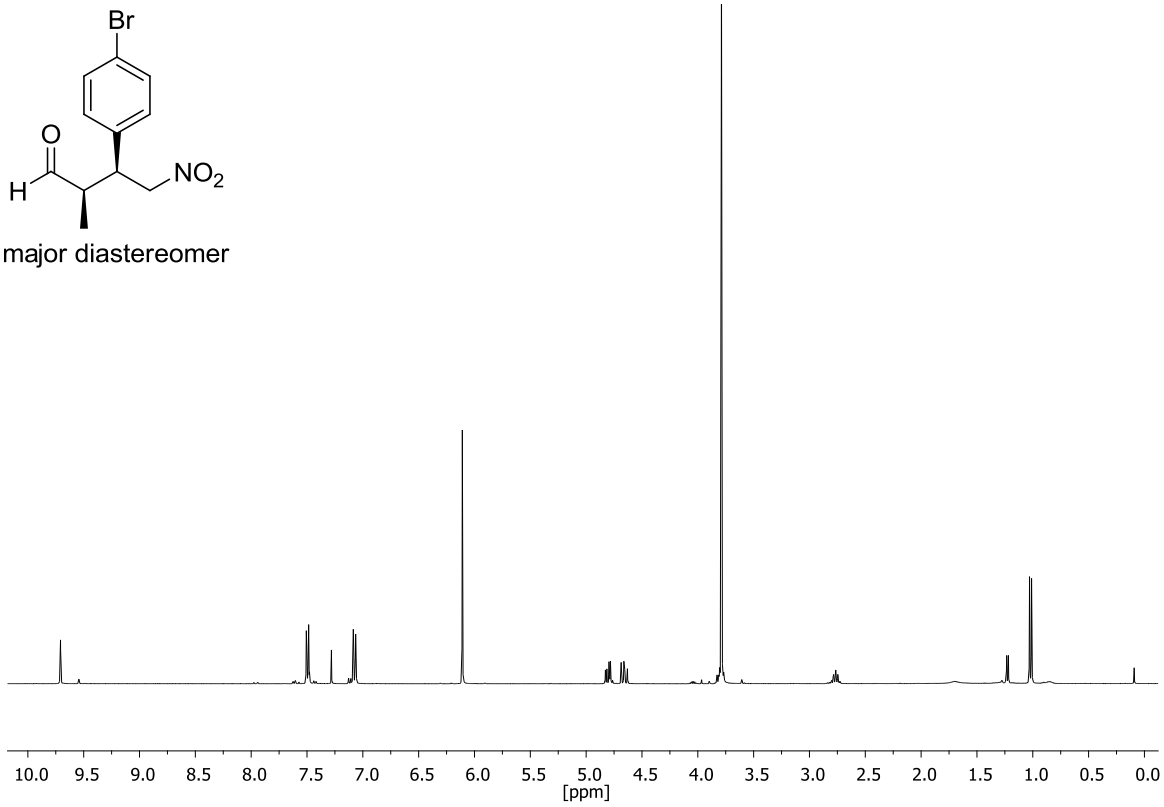

2-Methyl-4-nitro-3-(4-methoxyphenyl)-butanal (36f) (*syn* and *anti*)

major diastereomer

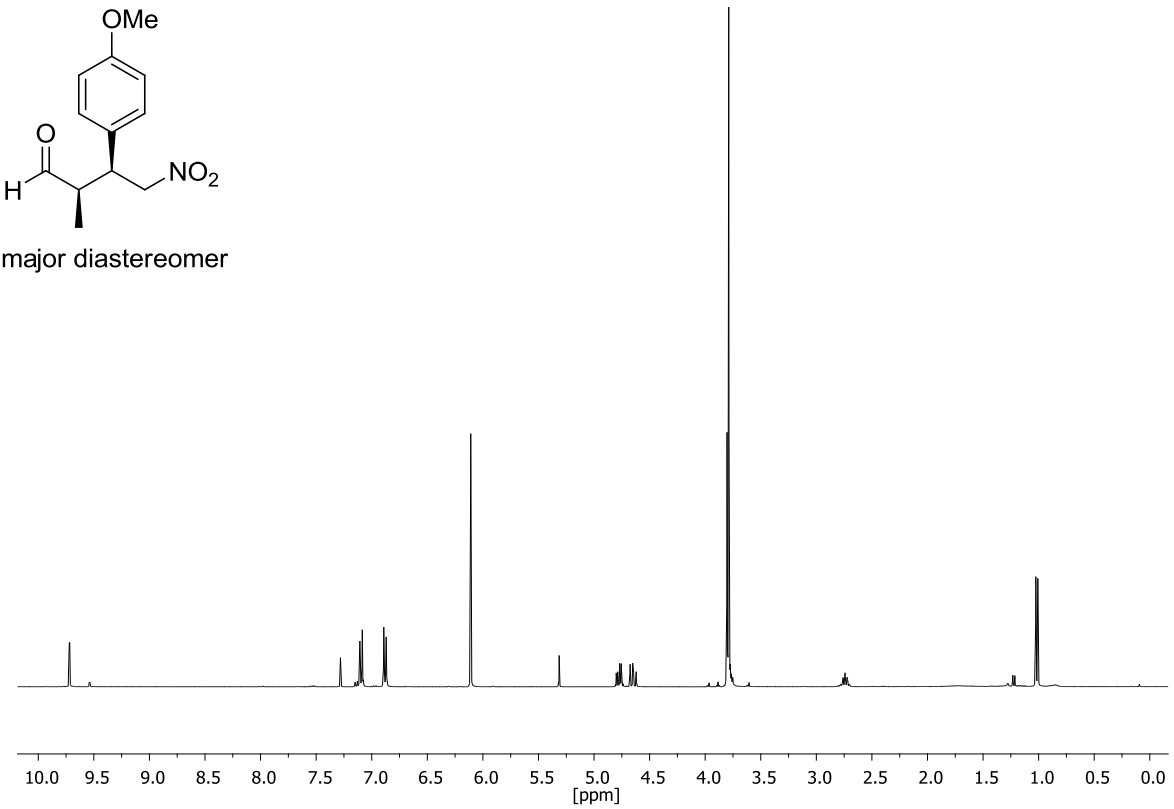

3-Furyl-2-methyl-4-nitrobutyraldehyde (36g) (*syn* and *anti*)

major diastereomer

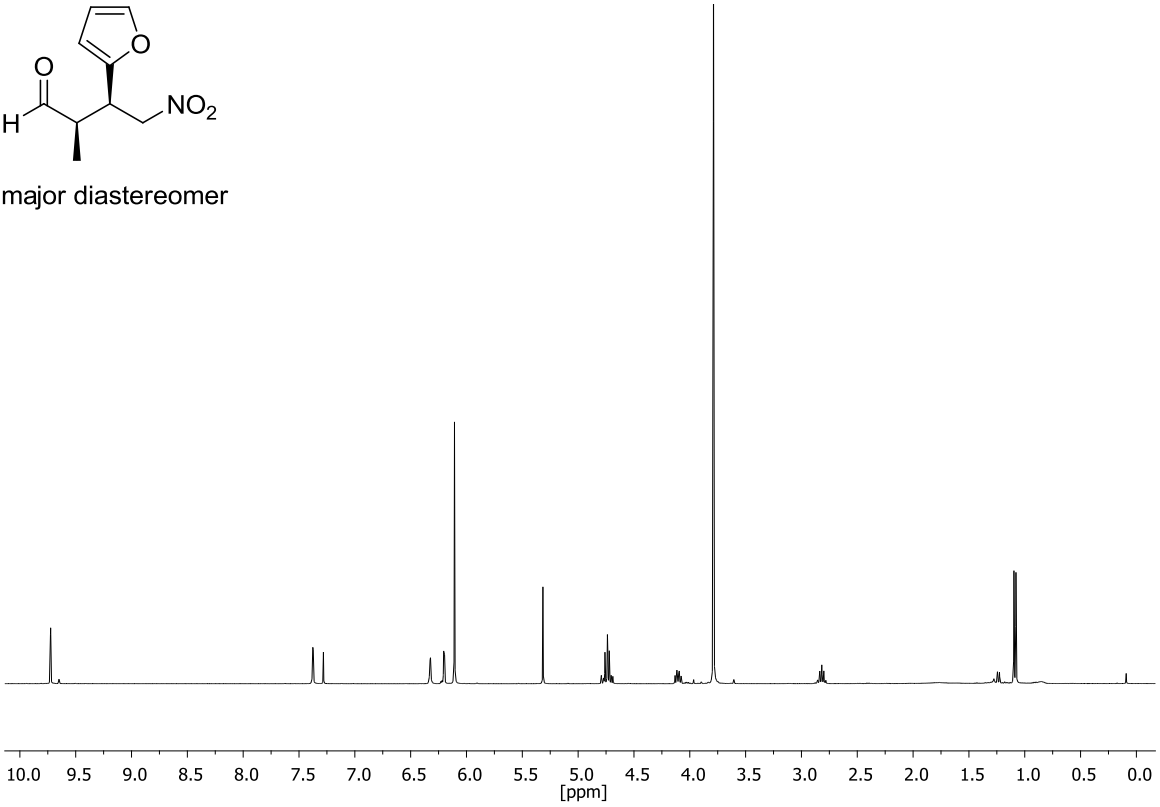

1,3-Diphenylpropan-1-one (12g)

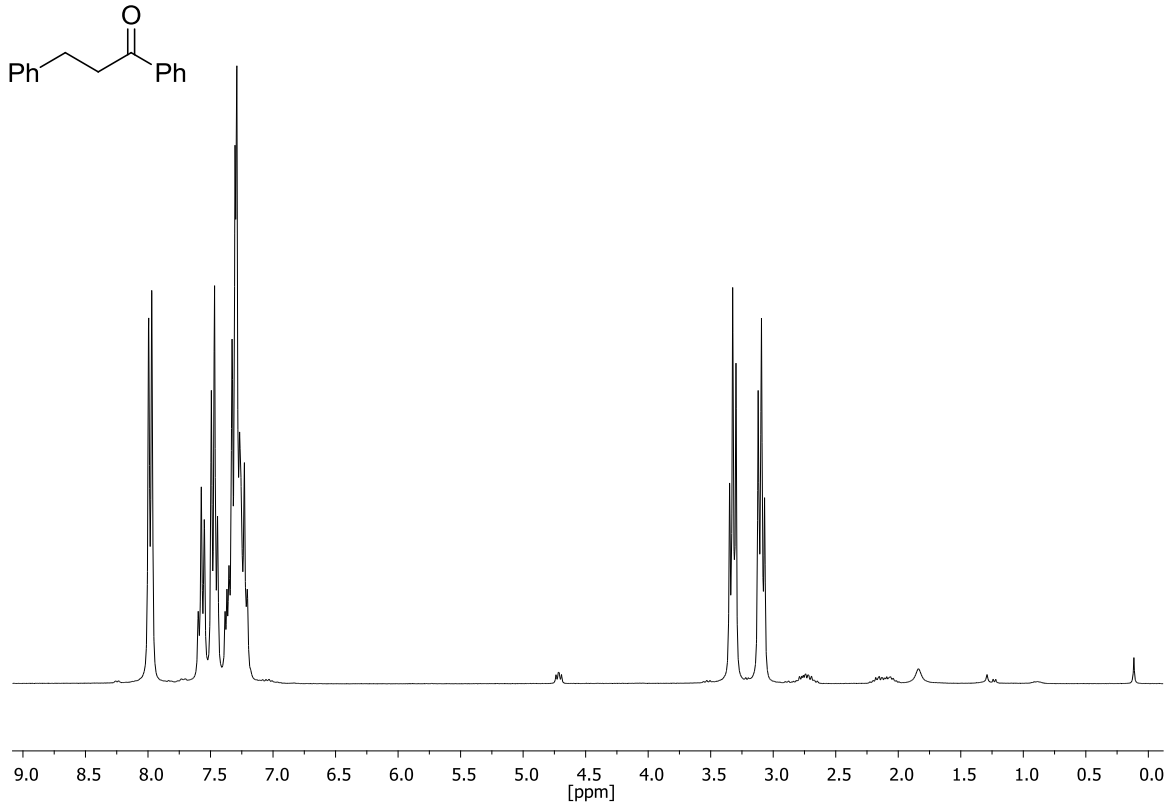

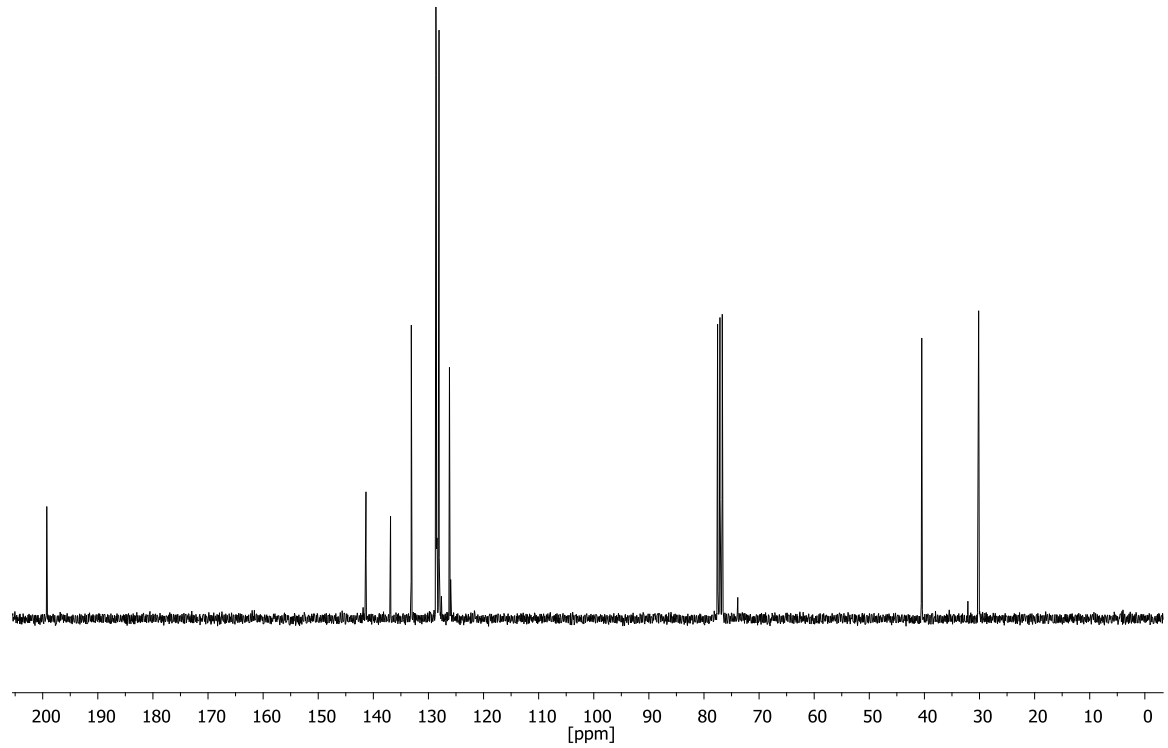

2. HPLC data

(2*R*, 3*S*)-2-Methyl-4-nitro-3-phenylbutanal (36a)

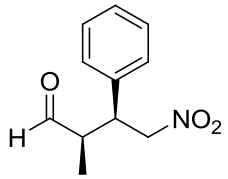

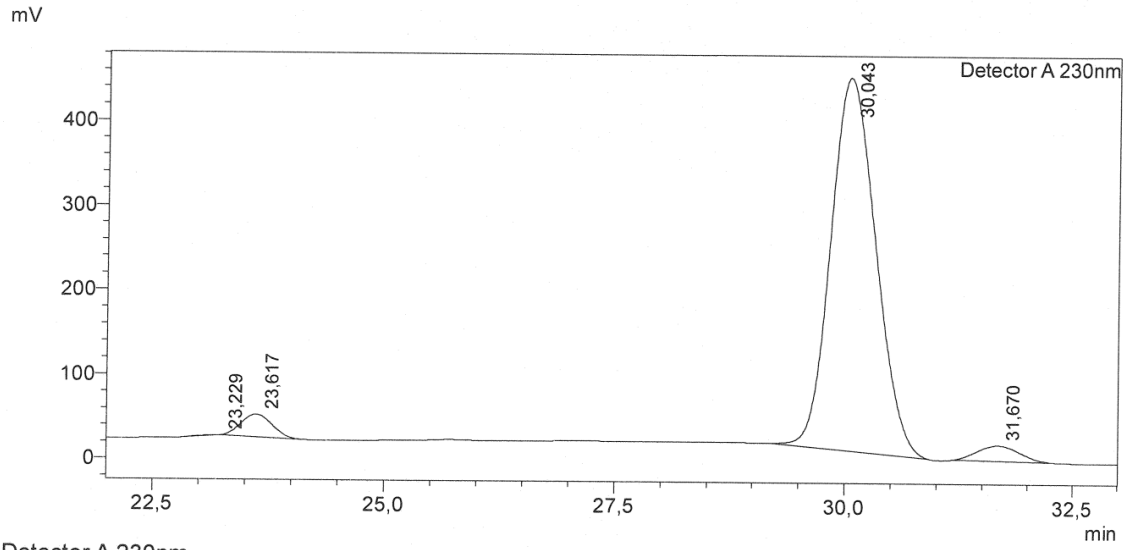

Detector A 230nm

Peak#	Ret. Time	Area	Height	Conc.	Unit	Mark	Name
1	23,229	11238	-63	0,069		M	
2	23,617	612021	26688	3,781		M	
3	30,043	14972717	440928	92,511		M	
4	31,670	588854	18416	3,638		M	
Total		16184829	485969				

(2*R*, 3*S*)-2-Ethyl-4-nitro-3-phenylbutanal (36b)

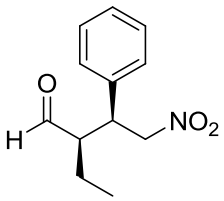

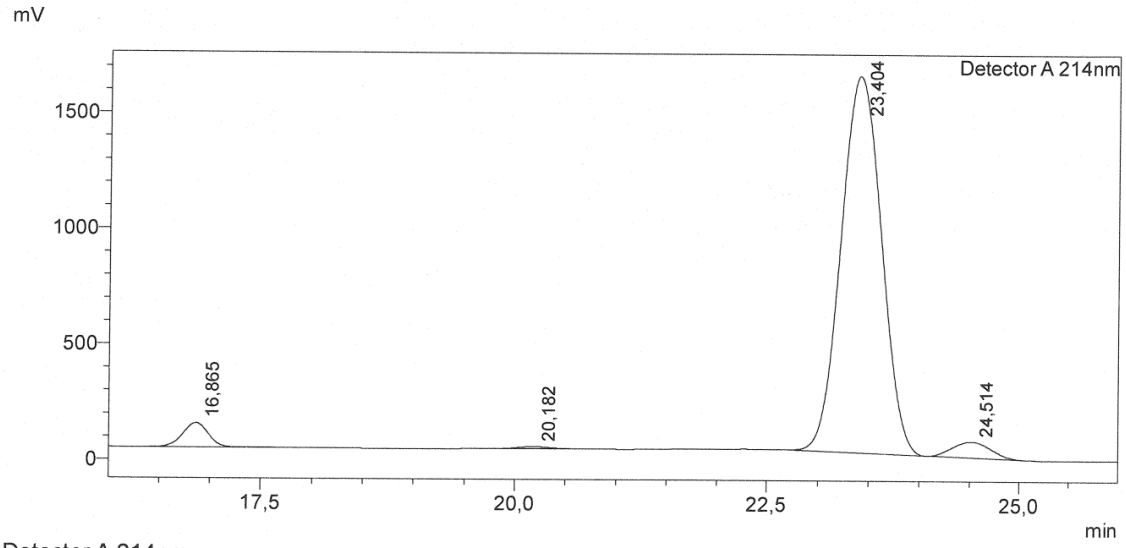

Detector A 214nm

Peak#	Ret. Time	Area	Height	Conc.	Unit	Mark	Name
1	16,865	1859246	105322	3,801		M	
2	20,182	205267	9319	0,420		M	
3	23,404	45080714	1627128	92,154		M	
4	24,514	1773652	68783	3,626		M	
Total		48918879	1810553				

(2*R*)-((*S*)-2-Nitro-1-phenylethyl)-pentanal (36c)

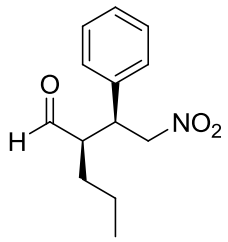

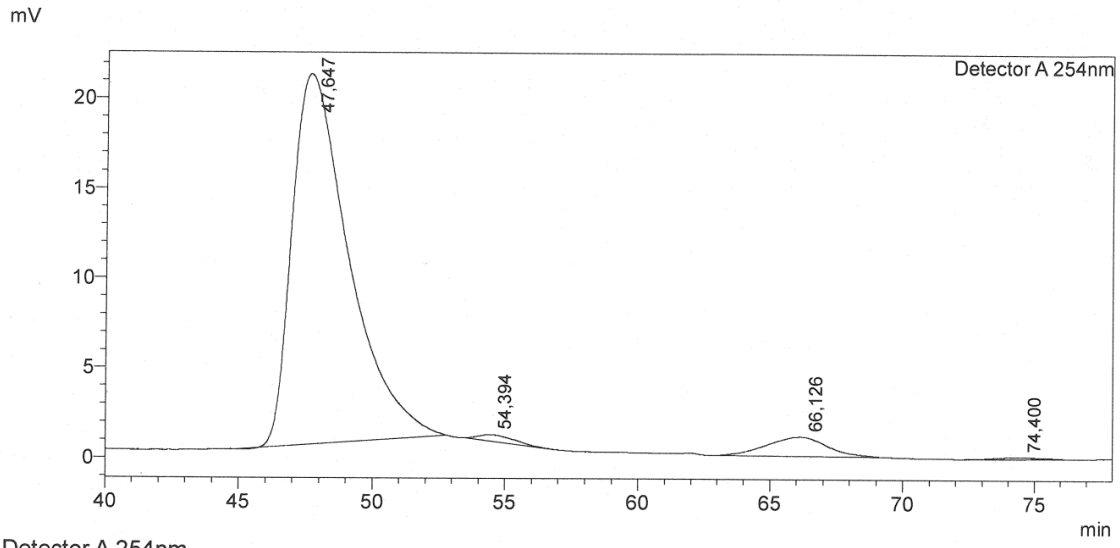

Detector A 254nm

Peak#	Ret. Time	Area	Height	Conc.	Unit	Mark	Name
1	47,647	3043329	20626	93,199		M	
2	54,394	36347	355	1,113		M	
3	66,126	172023	1086	5,268		M	
4	74,400	13711	102	0,420		M	
Total		3265410	22168				

(2*R*)-((*S*)-2-Nitro-1-phenylethyl)-heptanal (36d)

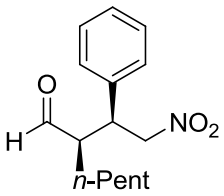

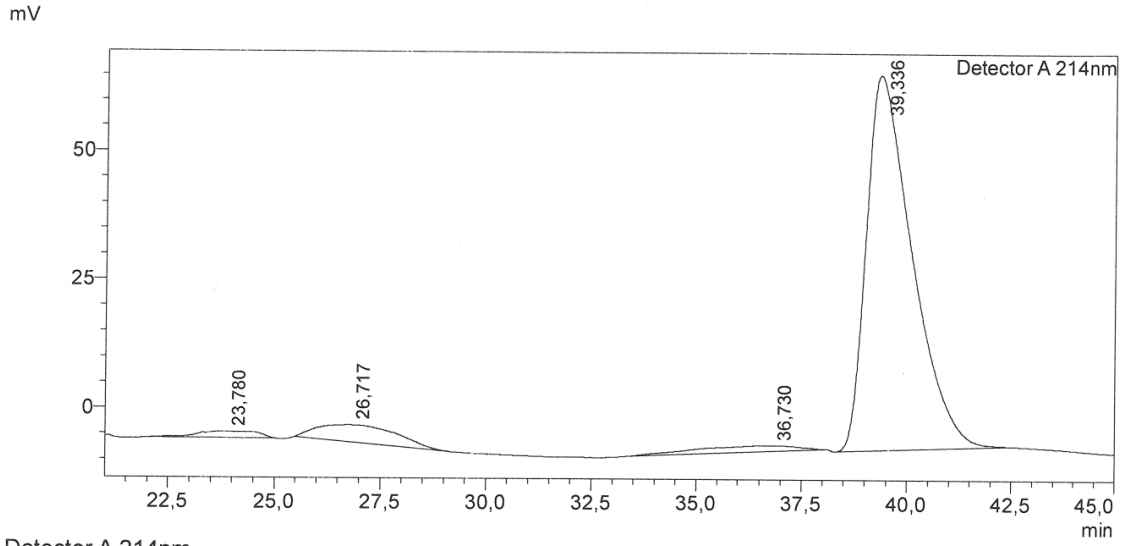

Detector A 214nm

Peak#	Ret. Time	Area	Height	Conc.	Unit	Mark	Name
1	23,780	128374	1293	2,038		M	
2	26,717	443845	3302	7,047		M	
3	36,730	205491	1140	3,263		M	
4	39,336	5520596	73017	87,652		M	
Total		6298306	78753				

(2*R*, 3*S*)-(4-Bromophenyl)-2-methyl-4-nitrobutyraldehyde (36e)

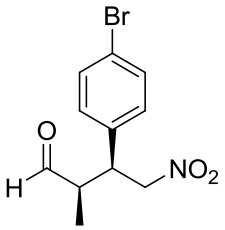

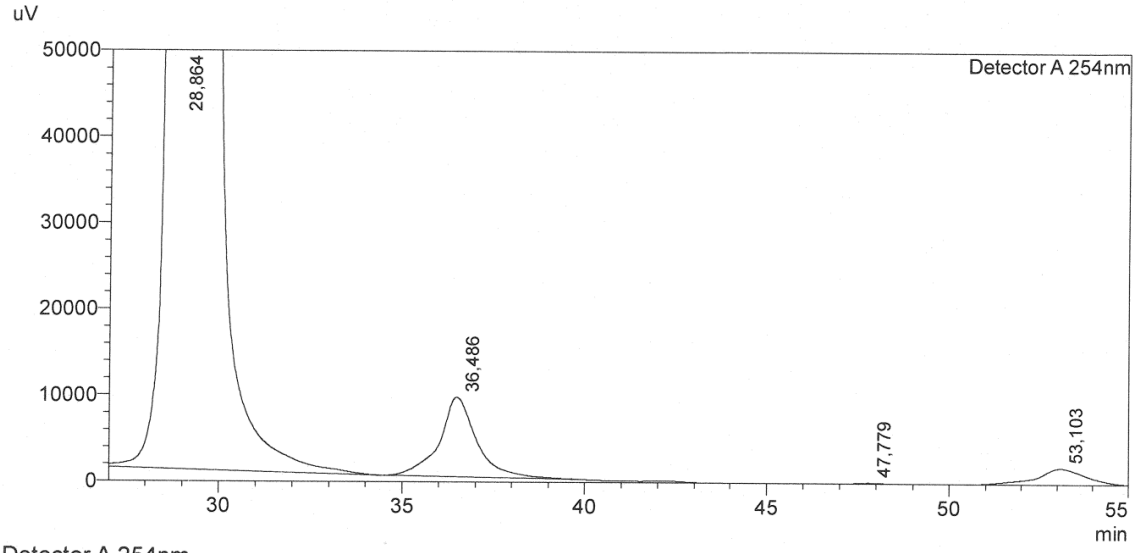

Detector A 254nm

Peak#	Ret. Time	Area	Height	Conc.	Unit	Mark	Name
1	28,864	67654927	1595395	98,701		M	
2	36,486	659265	9230	0,962		M	
3	47,779	4641	135	0,007		M	
4	53,103	226560	2009	0,331		M	
Total		68545392	1606768				

(2*R*, 3*S*)-2-Methyl-4-nitro-3-(4-methoxyphenyl)-butanal (36f)

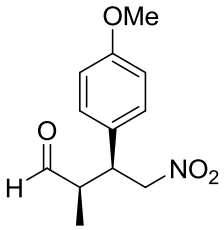

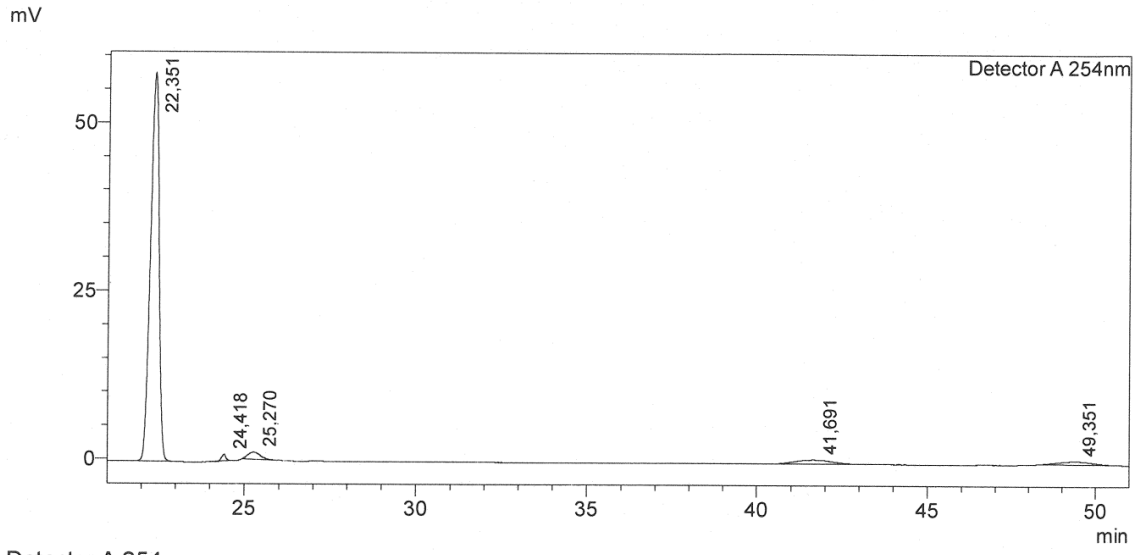

Detector A 254nm

Peak#	Ret. Time	Area	Height	Conc.	Unit	Mark	Name
1	22,351	1007808	57665	90,093		M	
2	24,418	8246	1001	0,737		M	
3	25,270	27280	1067	2,439		M	
4	41,691	43496	569	3,888		M	
5	49,351	31806	442	2,843		M	
Total		1118635	60744				

(2*R*, 3*S*)-3-Furyl-2-methyl-4-nitrobutyraldehyde (36g)

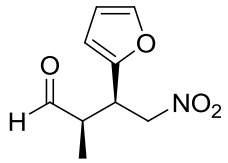

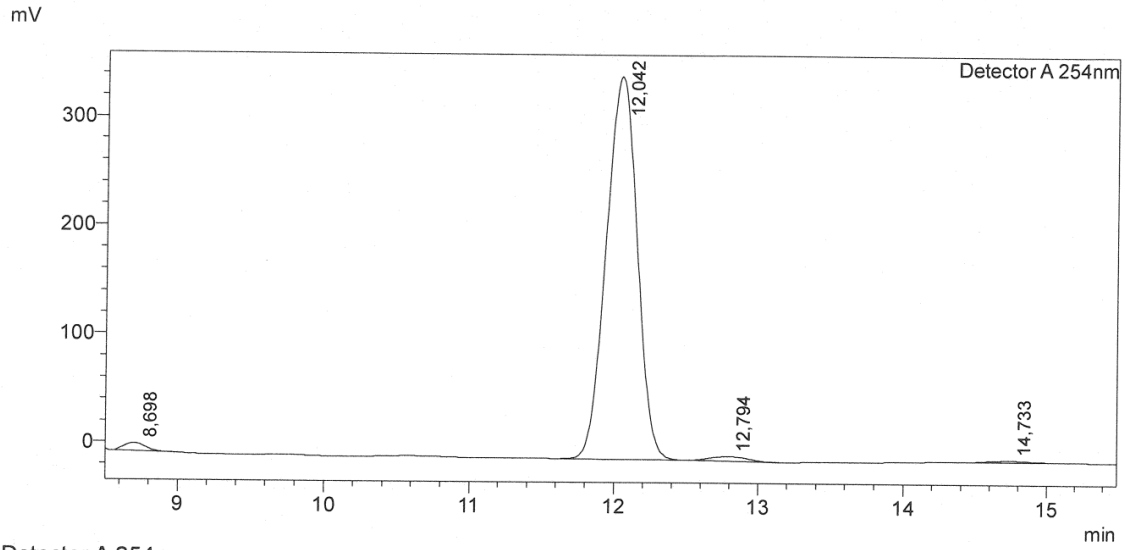

Detector A 254nm

Peak#	Ret. Time	Area	Height	Conc.	Unit	Mark	Name
1	8,698	74751	7307	1,381		M	
2	12,042	5230762	352467	96,630		M	
3	12,794	74785	4302	1,382		M	
4	14,733	32877	1518	0,607		M	
Total		5413175	365594				

3. GC data

1,2-Diphenylethane (12a)

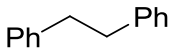

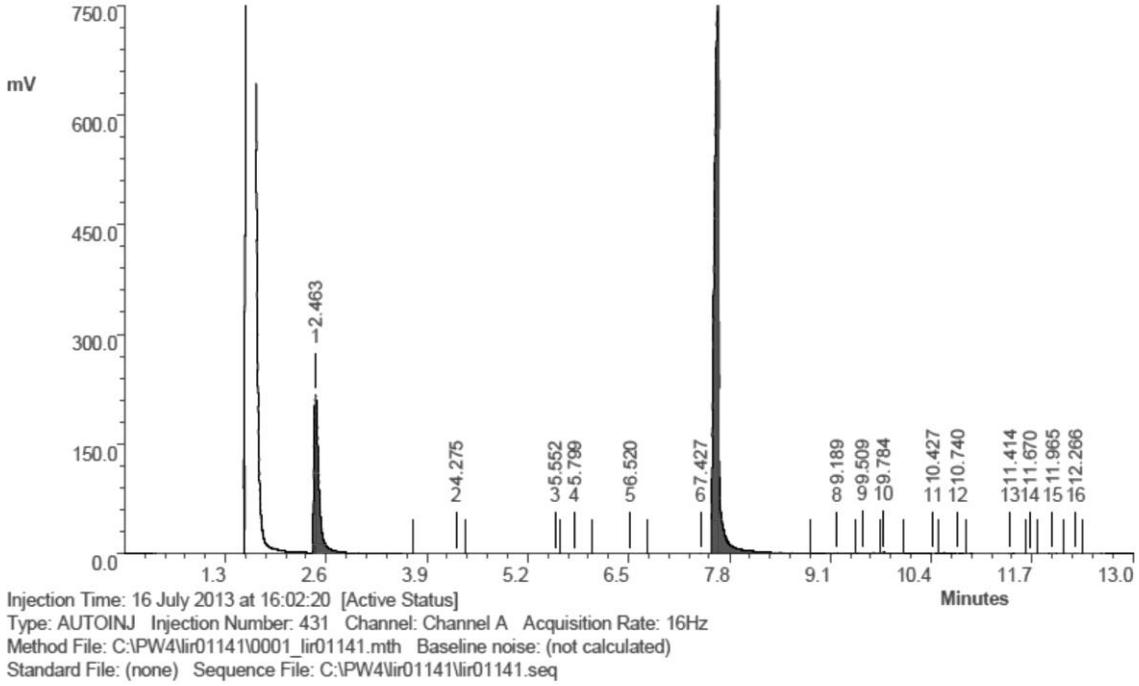

Injection Time: 16 July 2013 at 16:02:20 [Active Status]
Type: AUTOINJ Injection Number: 431 Channel: Channel A Acquisition Rate: 16Hz
Method File: C:\PW4\lir01141\0001_lir01141.mth Baseline noise: (not calculated)
Standard File: (none) Sequence File: C:\PW4\lir01141\lir01141.seq

Peak	RT	Area	%Ar	Conc.(Ar)	Height	M	Units	Name
1	2.463	952.847	21.15	Not Calculated	215.819	0		
2	4.275	2.101	0.05	Not Calculated	0.257	0		
3	5.552	0.501	0.01	Not Calculated	0.138	0		
4	5.799	2.794	0.06	Not Calculated	0.506	0		
5	6.520	1.299	0.03	Not Calculated	0.263	0		
6	7.427	0.775	0.02	Not Calculated	0.510	0		
7	7.657	3518.558	78.10	Not Calculated	915.895	0		
8	9.189	3.053	0.07	Not Calculated	0.645	0		
9	9.509	10.669	0.24	Not Calculated	1.048	0		
10	9.784	7.034	0.16	Not Calculated	1.779	0		
11	10.427	0.652	0.01	Not Calculated	0.476	0		
12	10.740	0.894	0.02	Not Calculated	0.250	0		
13	11.414	0.963	0.02	Not Calculated	0.420	0		
14	11.670	0.375	0.01	Not Calculated	0.105	0		
15	11.965	2.144	0.05	Not Calculated	0.557	0		
16	12.266	0.760	0.02	Not Calculated	0.436	0		

Ethylbenzene (12b)

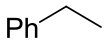

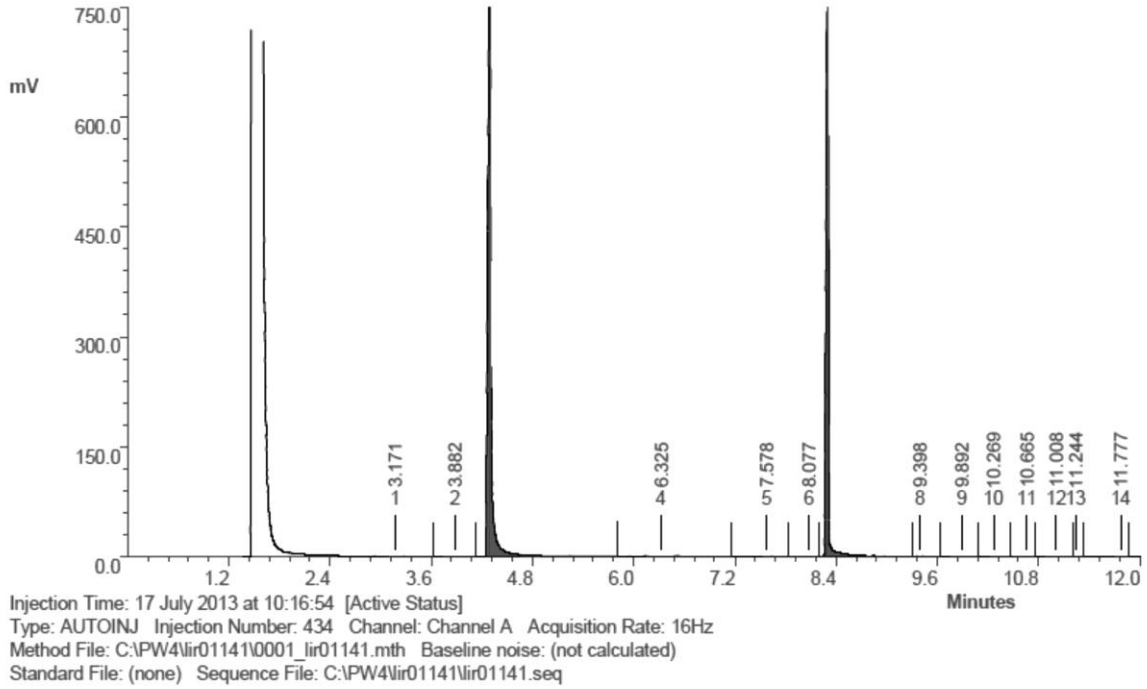

Injection Time: 17 July 2013 at 10:16:54 [Active Status]
Type: AUTOINJ Injection Number: 434 Channel: Channel A Acquisition Rate: 16Hz
Method File: C:\PW4\lir01141\0001_lir01141.mth Baseline noise: (not calculated)
Standard File: (none) Sequence File: C:\PW4\lir01141\lir01141.seq

Peak	RT	Area	%Ar	Conc.(Ar)	Height	M	Units	Name
1	3.171	4.679	0.11	Not Calculated	0.356	0		
2	3.882	1.389	0.03	Not Calculated	0.211	0		
3	4.294	2272.628	55.30	Not Calculated	885.794	0		
4	6.325	6.873	0.17	Not Calculated	0.324	0		
5	7.578	5.416	0.13	Not Calculated	0.710	0		
6	8.077	3.393	0.08	Not Calculated	0.343	0		
7	8.303	1804.629	43.91	Not Calculated	1006.890	0		
8	9.398	4.294	0.10	Not Calculated	0.634	0		
9	9.892	2.022	0.05	Not Calculated	0.410	0		
10	10.269	0.641	0.02	Not Calculated	0.142	0		
11	10.665	1.268	0.03	Not Calculated	0.430	0		
12	11.008	1.431	0.03	Not Calculated	0.361	0		
13	11.244	0.265	0.01	Not Calculated	0.123	0		
14	11.777	0.613	0.01	Not Calculated	0.391	0		

Ethane-1,1-diyldibenzene (12c)

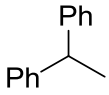

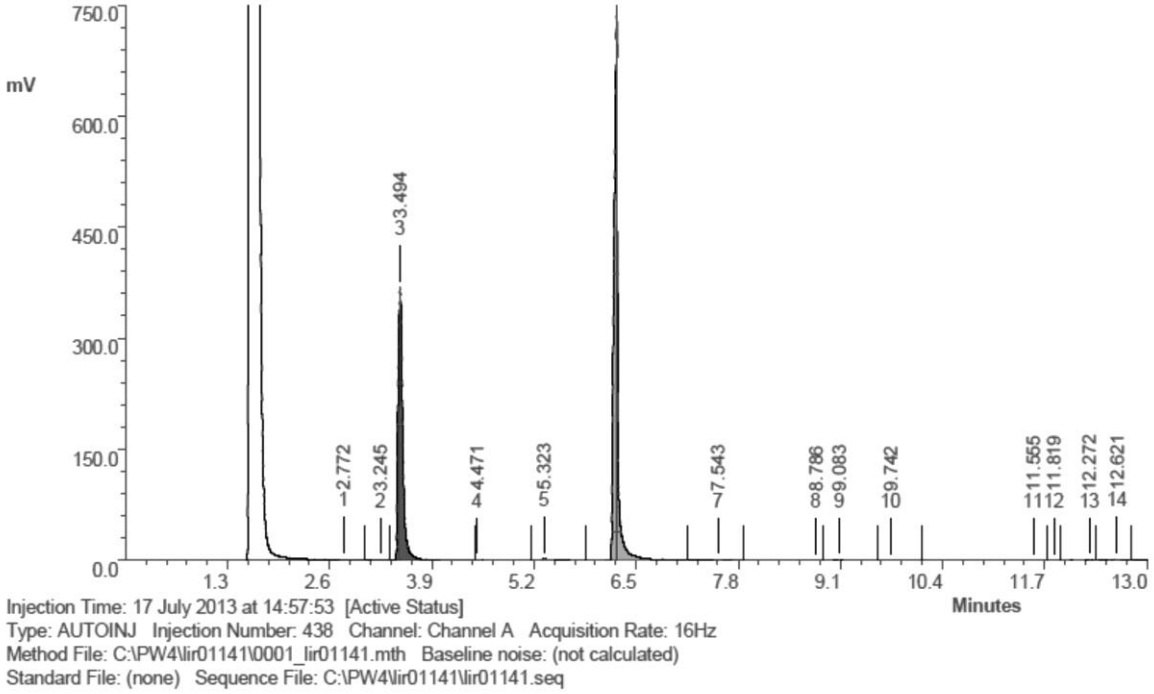

Injection Time: 17 July 2013 at 14:57:53 [Active Status]
Type: AUTOINJ Injection Number: 438 Channel: Channel A Acquisition Rate: 16Hz
Method File: C:\PW4\lir01141\0001_lir01141.mth Baseline noise: (not calculated)
Standard File: (none) Sequence File: C:\PW4\lir01141\lir01141.seq

Peak	RT	Area	%Ar	Conc.(Ar)	Height	M	Units	Name
1	2.772	4.681	0.11	Not Calculated	1.084	0		
2	3.245	0.791	0.02	Not Calculated	0.119	0		
3	3.494	1536.123	37.06	Not Calculated	368.205	0		
4	4.471	5.860	0.14	Not Calculated	1.078	0		
5	5.323	24.560	0.59	Not Calculated	2.299	0		
6	6.255	2548.905	61.49	Not Calculated	772.895	0		
7	7.543	1.556	0.04	Not Calculated	0.237	0		
8	8.786	0.634	0.02	Not Calculated	0.132	0		
9	9.083	8.531	0.21	Not Calculated	0.280	0		
10	9.742	3.767	0.09	Not Calculated	0.243	0		
11	11.555	0.887	0.02	Not Calculated	0.128	0		
12	11.819	0.350	0.01	Not Calculated	0.111	0		
13	12.272	1.253	0.03	Not Calculated	0.237	0		
14	12.621	7.529	0.18	Not Calculated	1.406	0		

Isobutylbenzene (12d)

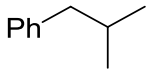

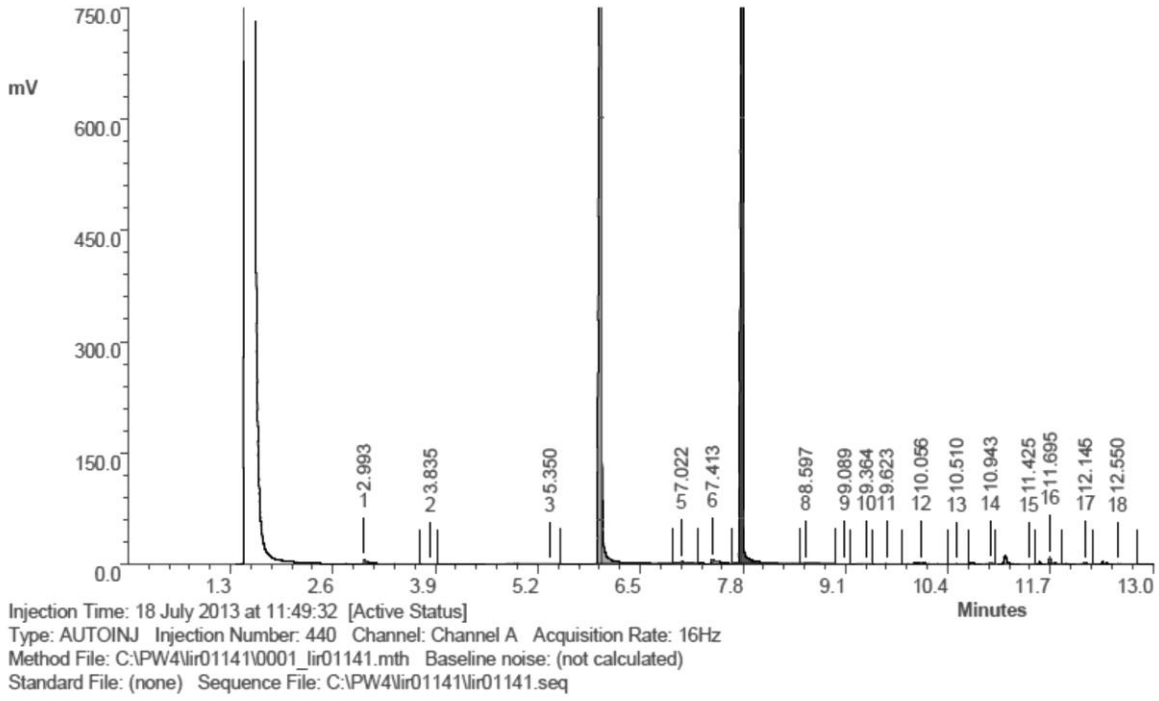

Injection Time: 18 July 2013 at 11:49:32 [Active Status]
Type: AUTOINJ Injection Number: 440 Channel: Channel A Acquisition Rate: 16Hz
Method File: C:\PW4\lir01141\0001_lir01141.mth Baseline noise: (not calculated)
Standard File: (none) Sequence File: C:\PW4\lir01141\lir01141.seq

Peak	RT	Area	%Ar	Conc.(Ar)	Height	M	Units	Name
1	2.993	34.331	0.61	Not Calculated	5.644	0		
2	3.835	0.721	0.01	Not Calculated	0.164	0		
3	5.350	4.139	0.07	Not Calculated	0.207	0		
4	6.009	3225.401	57.59	Not Calculated	1200.762	0		
5	7.022	14.010	0.25	Not Calculated	2.314	0		
6	7.413	31.046	0.55	Not Calculated	4.686	0		
7	7.797	2197.576	39.24	Not Calculated	1200.390	0		
8	8.597	16.807	0.30	Not Calculated	1.181	0		
9	9.089	5.140	0.09	Not Calculated	0.591	0		
10	9.364	1.743	0.03	Not Calculated	0.422	0		
11	9.623	7.350	0.13	Not Calculated	0.613	0		
12	10.056	21.392	0.38	Not Calculated	1.799	0		
13	10.510	2.483	0.04	Not Calculated	0.513	0		
14	10.943	7.147	0.13	Not Calculated	2.496	0		
15	11.425	1.568	0.03	Not Calculated	0.462	0		
16	11.695	17.822	0.32	Not Calculated	9.325	0		
17	12.145	6.750	0.12	Not Calculated	1.820	0		
18	12.550	4.755	0.08	Not Calculated	0.780	0		

1-Chloro-4-ethylbenzene (12e)

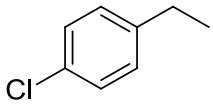

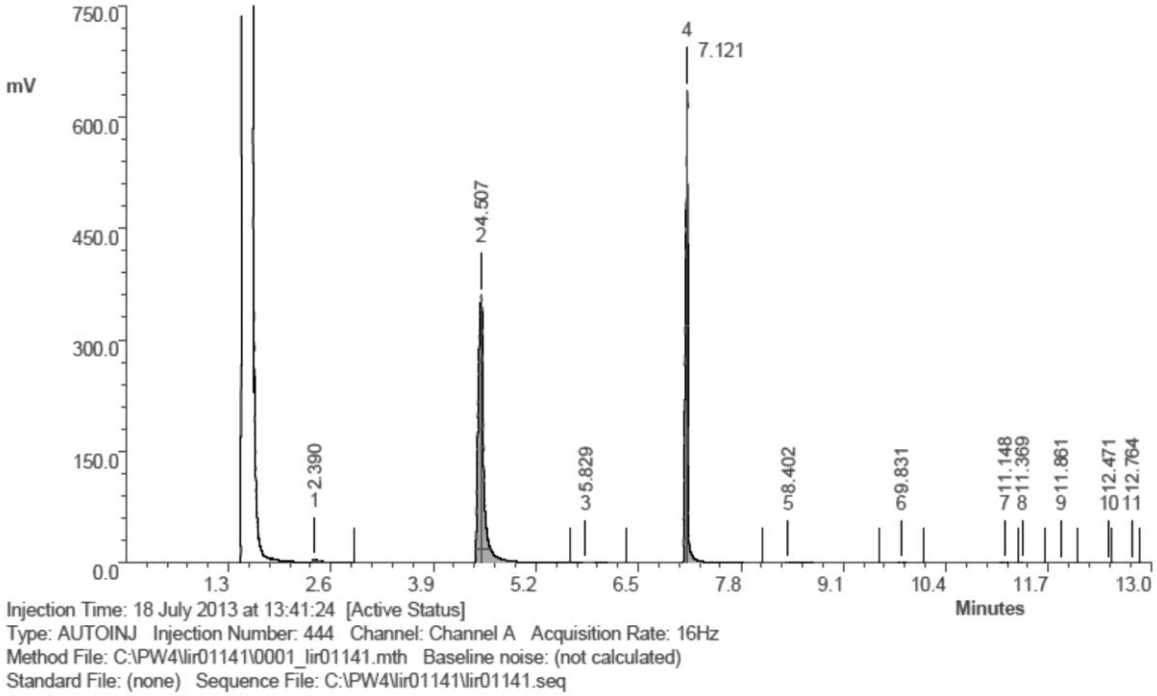

Injection Time: 18 July 2013 at 13:41:24 [Active Status]
Type: AUTOINJ Injection Number: 444 Channel: Channel A Acquisition Rate: 16Hz
Method File: C:\PW4\lir01141\0001_lir01141.mth Baseline noise: (not calculated)
Standard File: (none) Sequence File: C:\PW4\lir01141\lir01141.seq

Peak	RT	Area	%Ar	Conc.(Ar)	Height	M	Units	Name
1	2.390	24.948	0.76	Not Calculated	4.037	0		
2	4.507	1838.661	56.32	Not Calculated	360.568	0		
3	5.829	19.939	0.61	Not Calculated	1.276	0		
4	7.121	1351.653	41.40	Not Calculated	636.341	0		
5	8.402	9.284	0.28	Not Calculated	0.338	0		
6	9.831	7.262	0.22	Not Calculated	0.392	0		
7	11.148	7.606	0.23	Not Calculated	0.615	0		
8	11.369	2.338	0.07	Not Calculated	0.513	0		
9	11.861	1.962	0.06	Not Calculated	0.474	0		
10	12.471	0.335	0.01	Not Calculated	0.246	0		
11	12.764	0.623	0.02	Not Calculated	0.100	0		

1-Ethyl-4-methoxybenzene (12f)

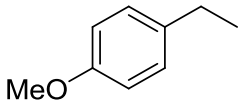

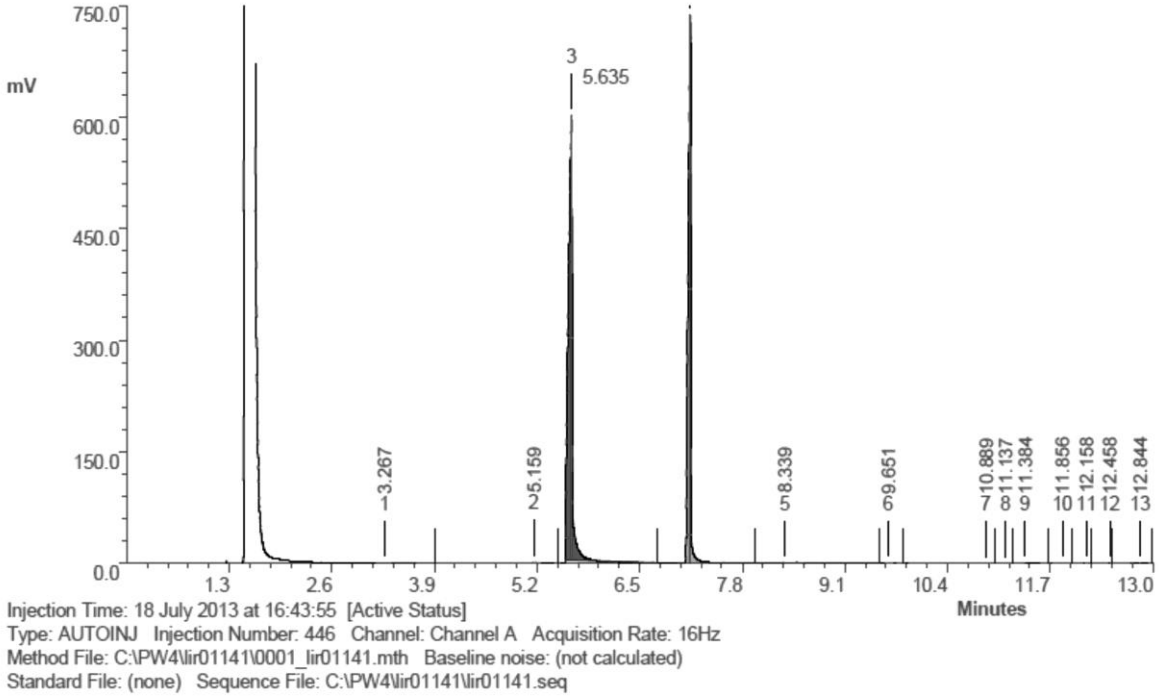

Injection Time: 18 July 2013 at 16:43:55 [Active Status]
Type: AUTOINJ Injection Number: 446 Channel: Channel A Acquisition Rate: 16Hz
Method File: C:\PW4\lir01141\0001_lir01141.mth Baseline noise: (not calculated)
Standard File: (none) Sequence File: C:\PW4\lir01141\lir01141.seq

Peak	RT	Area	%Ar	Conc.(Ar)	Height	M	Units	Name
1	3.267	2.875	0.08	Not Calculated	0.177	0		
2	5.159	10.701	0.28	Not Calculated	1.541	0		
3	5.635	2041.483	54.06	Not Calculated	597.593	0		
4	7.142	1685.834	44.64	Not Calculated	737.156	0		
5	8.339	24.058	0.64	Not Calculated	0.853	0		
6	9.651	1.469	0.04	Not Calculated	0.227	0		
7	10.889	0.536	0.01	Not Calculated	0.104	0		
8	11.137	0.521	0.01	Not Calculated	0.087	0		
9	11.384	3.045	0.08	Not Calculated	0.331	0		
10	11.856	1.189	0.03	Not Calculated	0.403	0		
11	12.158	2.158	0.06	Not Calculated	0.863	0		
12	12.458	0.335	0.01	Not Calculated	0.219	0		
13	12.844	1.936	0.05	Not Calculated	0.157	0		

1,3-Diphenylpropan-1-one (12g)

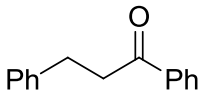

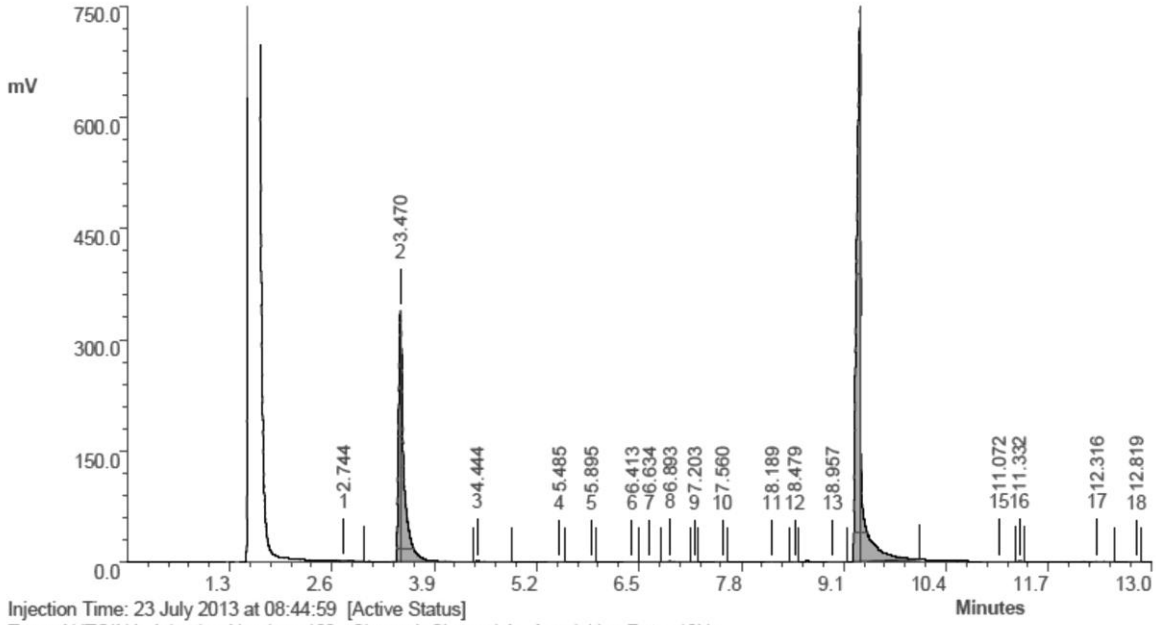

Injection Time: 23 July 2013 at 08:44:59 [Active Status]
Type: AUTOINJ Injection Number: 463 Channel: Channel A Acquisition Rate: 16Hz
Method File: C:\PW4\lir01141\0001_lir01141.mth Baseline noise: (not calculated)
Standard File: (none) Sequence File: C:\PW4\lir01141\lir01141.seq

Peak	RT	Area	%Ar	Conc.(Ar)	Height	M	Units	Name
1	2.744	5.125	0.10	Not Calculated	0.961	0		
2	3.470	1628.673	33.14	Not Calculated	338.076	0		
3	4.444	6.079	0.12	Not Calculated	1.088	0		
4	5.485	1.808	0.04	Not Calculated	0.521	0		
5	5.895	0.496	0.01	Not Calculated	0.138	0		
6	6.413	0.288	0.01	Not Calculated	0.068	0		
7	6.634	0.958	0.02	Not Calculated	0.155	0		
8	6.893	7.471	0.15	Not Calculated	1.537	0		
9	7.203	0.255	0.01	Not Calculated	0.135	0		
10	7.560	0.524	0.01	Not Calculated	0.211	0		
11	8.189	2.274	0.05	Not Calculated	0.213	0		
12	8.479	1.571	0.03	Not Calculated	0.789	0		
13	8.957	1.125	0.02	Not Calculated	0.156	0		
14	9.311	3249.099	66.11	Not Calculated	775.177	0		
15	11.072	4.469	0.09	Not Calculated	0.286	0		
16	11.332	1.399	0.03	Not Calculated	0.763	0		
17	12.316	2.069	0.04	Not Calculated	0.817	0		
18	12.819	1.207	0.02	Not Calculated	0.253	0		

Methyl-3-phenylpropanoate (12h)

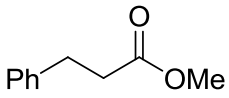

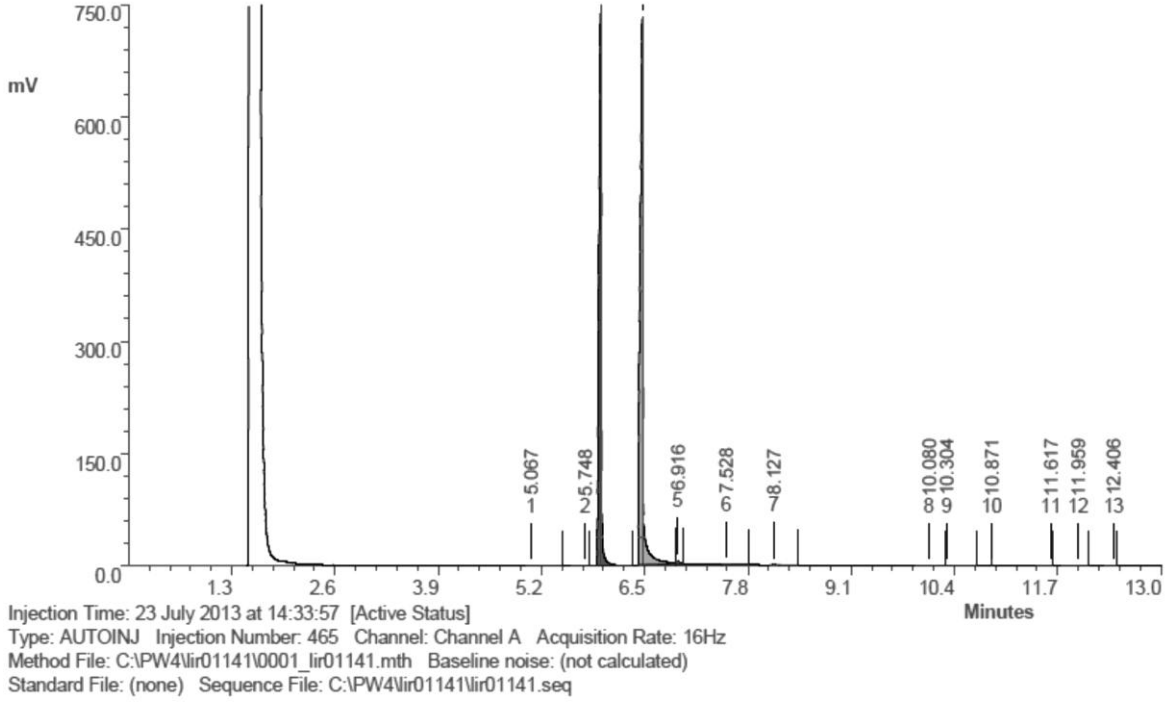

Injection Time: 23 July 2013 at 14:33:57 [Active Status]
Type: AUTOINJ Injection Number: 465 Channel: Channel A Acquisition Rate: 16Hz
Method File: C:\PW4\lir01141\0001_lir01141.mth Baseline noise: (not calculated)
Standard File: (none) Sequence File: C:\PW4\lir01141\lir01141.seq

Peak	RT	Area	%Ar	Conc.(Ar)	Height	M	Units	Name
1	5.067	4.356	0.12	Not Calculated	0.422	0		
2	5.748	0.702	0.02	Not Calculated	0.122	0		
3	5.948	1579.440	44.64	Not Calculated	776.993	0		
4	6.471	1932.483	54.62	Not Calculated	731.455	0		
5	6.916	8.034	0.23	Not Calculated	4.363	0		
6	7.528	4.099	0.12	Not Calculated	0.527	0		
7	8.127	3.192	0.09	Not Calculated	0.490	0		
8	10.080	1.454	0.04	Not Calculated	0.178	0		
9	10.304	1.975	0.06	Not Calculated	0.282	0		
10	10.871	0.029	0.00	Not Calculated	0.169	0		
11	11.617	0.802	0.02	Not Calculated	0.215	0		
12	11.959	0.715	0.02	Not Calculated	0.094	0		
13	12.406	0.531	0.02	Not Calculated	0.277	0		

Bicyclo[2.2.1]heptanes (12i)

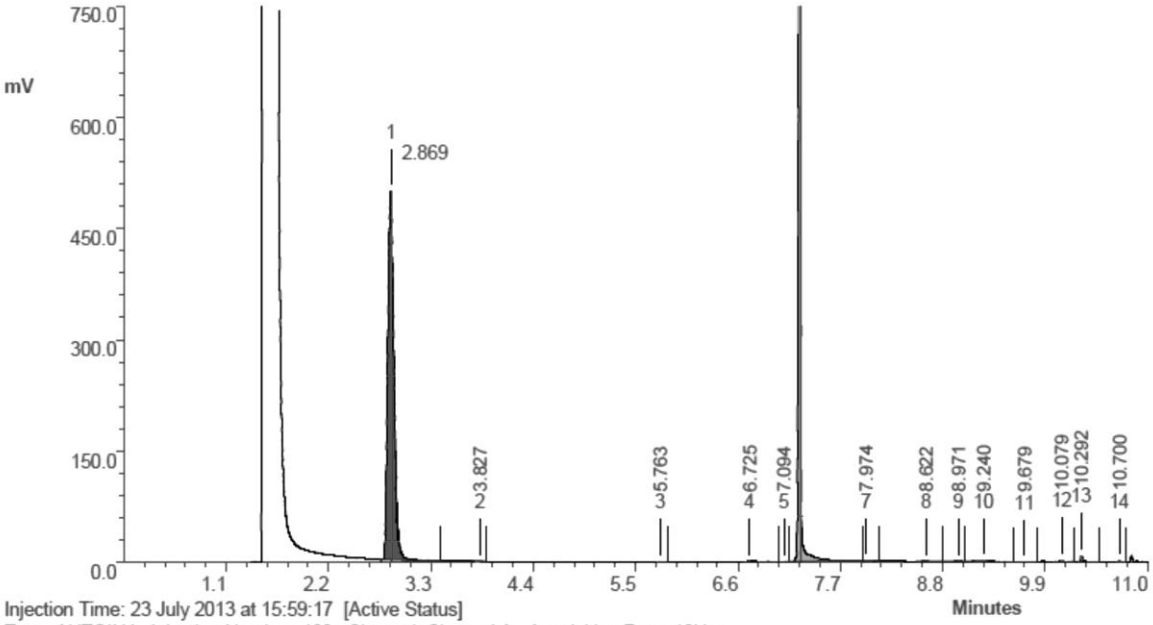

Injection Time: 23 July 2013 at 15:59:17 [Active Status]
Type: AUTOINJ Injection Number: 466 Channel: Channel A Acquisition Rate: 16Hz
Method File: C:\PW4\lir01141\0001_lir01141.mth Baseline noise: (not calculated)
Standard File: (none) Sequence File: C:\PW4\lir01141\lir01141.seq

Peak	RT	Area	%Ar	Conc.(Ar)	Height	M	Units	Name
1	2.869	2286.245	51.50	Not Calculated	496.284	0		
2	3.827	0.556	0.01	Not Calculated	0.183	0		
3	5.763	0.460	0.01	Not Calculated	0.203	0		
4	6.725	6.754	0.15	Not Calculated	0.965	0		
5	7.094	1.010	0.02	Not Calculated	0.326	0		
6	7.269	2065.084	46.52	Not Calculated	1201.415	0		
7	7.974	4.952	0.11	Not Calculated	1.044	0		
8	8.622	8.188	0.18	Not Calculated	0.927	0		
9	8.971	9.791	0.22	Not Calculated	1.291	0		
10	9.240	26.854	0.60	Not Calculated	2.027	0		
11	9.679	1.944	0.04	Not Calculated	0.470	0		
12	10.079	7.507	0.17	Not Calculated	2.782	0		
13	10.292	16.517	0.37	Not Calculated	8.571	0		
14	10.700	3.114	0.07	Not Calculated	2.552	0		

4-Methoxyaniline (12j)

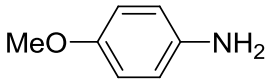

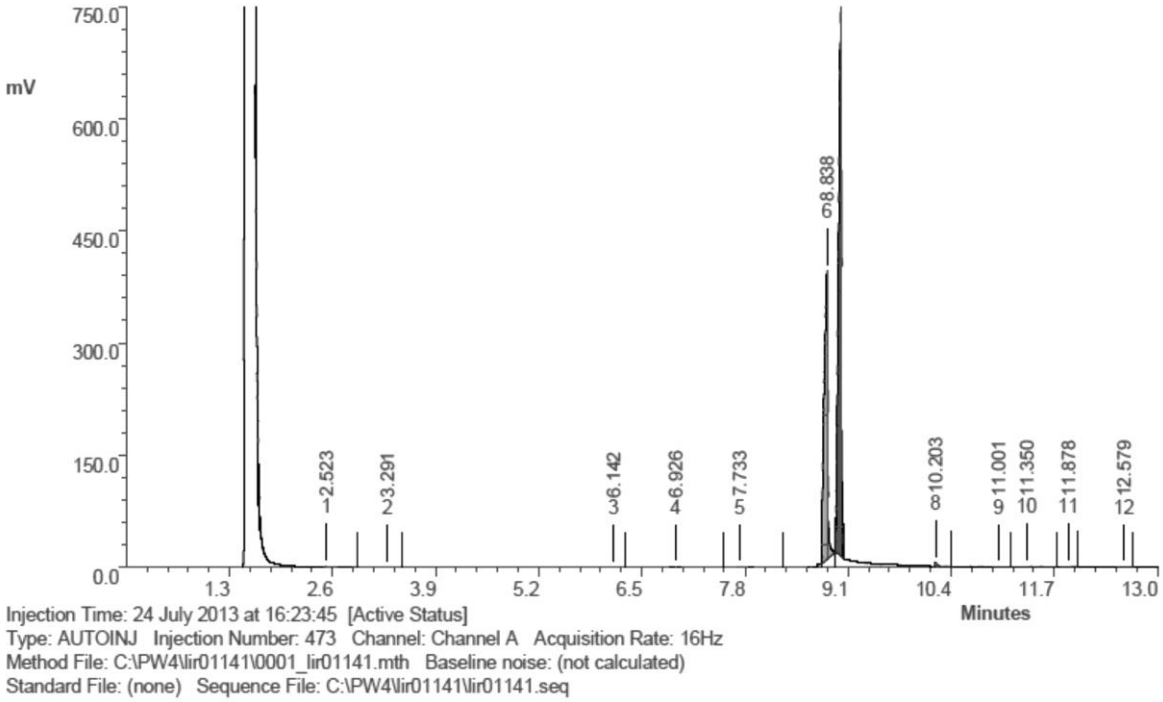

Injection Time: 24 July 2013 at 16:23:45 [Active Status]
Type: AUTOINJ Injection Number: 473 Channel: Channel A Acquisition Rate: 16Hz
Method File: C:\PW4\lir01141\0001_lir01141.mth Baseline noise: (not calculated)
Standard File: (none) Sequence File: C:\PW4\lir01141\lir01141.seq

Peak	RT	Area	%Ar	Conc.(Ar)	Height	M	Units	Name
1	2.523	5.458	0.17	Not Calculated	0.897	0		
2	3.291	0.846	0.03	Not Calculated	0.109	0		
3	6.142	0.481	0.02	Not Calculated	0.094	0		
4	6.926	3.120	0.10	Not Calculated	0.169	0		
5	7.733	7.804	0.25	Not Calculated	0.839	0		
6	8.838	1229.807	39.34	Not Calculated	385.122	0		
7	9.011	1852.730	59.26	Not Calculated	783.859	1		
8	10.203	7.880	0.25	Not Calculated	4.445	0		
9	11.001	1.969	0.06	Not Calculated	0.338	0		
10	11.350	11.494	0.37	Not Calculated	1.022	0		
11	11.878	3.912	0.13	Not Calculated	0.591	0		
12	12.579	0.756	0.02	Not Calculated	0.186	0		

4-Chloraniline (12k)

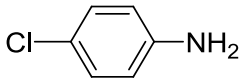

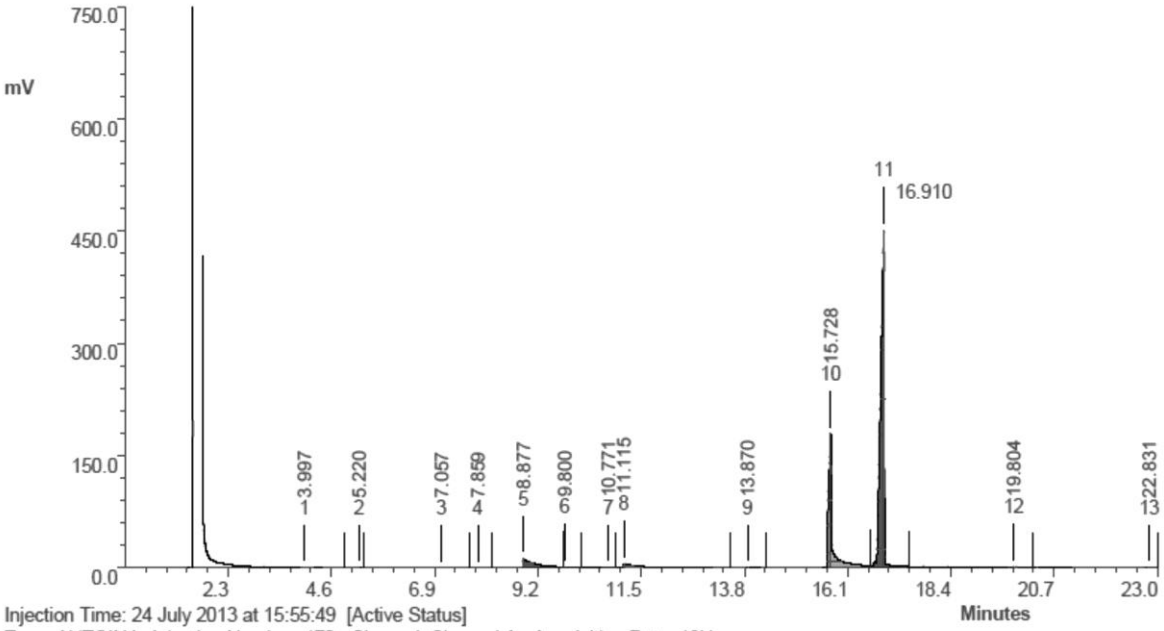

Injection Time: 24 July 2013 at 15:55:49 [Active Status]
Type: AUTOINJ Injection Number: 472 Channel: Channel A Acquisition Rate: 16Hz
Method File: C:\PW4\lir01141\0001_lir01141.mth Baseline noise: (not calculated)
Standard File: (none) Sequence File: C:\PW4\lir01141\lir01141.seq

Peak	RT	Area	%Ar	Conc.(Ar)	Height	M	Units	Name
1	3.997	4.461	0.12	Not Calculated	0.221	0		
2	5.220	1.039	0.03	Not Calculated	0.304	0		
3	7.057	3.753	0.10	Not Calculated	0.171	0		
4	7.859	1.392	0.04	Not Calculated	0.105	0		
5	8.877	217.127	5.63	Not Calculated	12.058	0		
6	9.800	12.419	0.32	Not Calculated	0.922	0		
7	10.771	0.983	0.03	Not Calculated	0.187	0		
8	11.115	115.789	3.00	Not Calculated	4.805	0		
9	13.870	5.734	0.15	Not Calculated	0.522	0		
10	15.728	1042.247	27.00	Not Calculated	178.750	0		
11	16.910	2442.587	63.28	Not Calculated	449.743	0		
12	19.804	8.945	0.23	Not Calculated	1.336	0		
13	22.831	3.469	0.09	Not Calculated	0.326	0		

4. List of publications

[1] Q. M. Kainz, R. Linhardt, P. K. Maity, P. R. Hanson, O. Reiser, *ChemSusChem* **2013**, *6*, 721–729:
Ring-Opening Metathesis Polymerization-based Recyclable Magnetic Acylation Reagents

[2] M. Keller, A. Perrier, R. Linhardt, S. Wittmann, L. Travers, O. Reiser, A.-M. Caminade, J.-P. Majoral, A. Ouali, *Adv. Synth. Catal.* **2013**, *355*, 1748–1754:
Dendrimers or Nanoparticles as Supports for the Design of Efficient and Recoverable Organocatalysts?

[3] Q. M. Kainz, R. Linhardt, R. N. Grass, W. J. Stark, O. Reiser, *Adv. Funct. Mat.* **2013**, DOI: 10.1002/adfm.201303277:
Palladium Nanoparticles Supported on Highly Magnetic Carbon-Coated Cobalt Nanobeads

[4] R. Linhardt, Q. M. Kainz, R. N. Grass, W. J. Stark, O. Reiser, *RSC Adv.* **2014**, *4*, 8541–8549:
Palladium Nanoparticles Supported on Ionic Liquid Modified, Magnetic Nanobeads – Recyclable, High-Capacity Catalysts for Alkene Hydrogenation

5. Congresses and scientific meetings

Oral contributions

[1] GLOBUCAT meeting, Universität Regensburg, Regensburg (Germany), October 11-12, 2010:
Synthesis of Novel Dendritic Scaffolds for Catalyst Immobilization on C/Co-Nanoparticles

[2] GLOBUCAT meeting, Laboratoire de Chimie de Coordination, Toulouse (France), October 23-24, 2011:
Purification and Catalyst Recovery with the Aid of Nanomagnets

Poster contributions

[1] Heidelberg Forum of Molecular Catalysis, Heidelberg (Germany), July 22, 2011:
Baylis-Hillman Reaction Promoted by *N*-Alkylimidazole Immobilized on Nanomagnets

[2] GDCh Wissenschaftsforum, Bremen (Germany), September 04-07, 2011:
Baylis-Hillman Reaction Promoted by *N*-Alkylimidazole Immobilized on Nanomagnets

[3] Mini-symposium „Iron: Earth‘s Favourite Metal for Synthesis, Catalysis & Energy Supply”, Universität Regensburg, Regensburg (Germany), June 04-06, 2012:
Baylis-Hillman Reaction Promoted by Recyclable, Fe/C-Supported *N*-Alkylimidazole

[4] 4th EuCheMS Chemistry Congress, Prague (Czech Republic), August 26-30, 2012:
A Highly Selective Diarylprolinol Silyl Ether Catalyst Immobilized on Phosphorus Dendrimers and Magnetic Nanobeads

[5] ORCHEM, Weimar (Germany), September 24-26, 2012:
A Highly Selective Diarylprolinol Silyl Ether Catalyst Immobilized on Phosphorus Dendrimers and Magnetic Nanobeads

[6] Heidelberg Forum of Molecular Catalysis, Heidelberg (Germany), June 06, 2013:
Carbon-coated Magnetic Nanoparticles as Highly Efficient and Recyclable Catalyst Support

[7] 18th European Symposium on Organic Chemistry, Marseille (France), July 07-12, 2013:
Carbon-coated Magnetic Nanoparticles as Highly Efficient and Recyclable Catalyst Support

[8] GDCh Wissenschaftsforum, Darmstadt (Germany), September 01-04, 2013:
Carbon-coated Magnetic Nanoparticles as Highly Efficient and Recyclable Catalyst Support

6. Curriculum vitae

Roland Linhardt

University of Regensburg
Institute of Organic Chemistry
Universitätsstrasse 31
93053 Regensburg
Phone: +49 177 2385205
E-Mail: Roland.Linhardt@chemie.uni-regensburg.de

Personal Data

Date and place of birth	January 10, 1985, Nuernberg
Nationality	German

Education

since 10/2010	Doctoral studies within the Elite Network of Bavaria (ENB) under chairmanship of Prof. Dr. W. A. Herrmann, TU Muenchen and supervision of Prof. Dr. O. Reiser, University of Regensburg (Part of the international doctorate program NANOCAT – Nanodesign of High Performance Catalysts)
10/2012	Research stay in the group of Prof. Dr. Jean-Pierre Majoral, LCC Toulouse, France
09/2010	Master of Science (M.Sc.) in chemistry
05/2010-07/2010	Research stay in the group of Prof. Dr. Jean-Pierre Majoral, LCC Toulouse, France
01/2010-09/2010	Master thesis in the research group of Prof. Dr. Oliver Reiser: “Synthesis of novel dendritic scaffolds for catalyst immobilization on C/Co-nanoparticles”
09/2008	Bachelor of Science (B.Sc.) in chemistry

03/2008-06/2008	Bachelor thesis in the research group of Prof. Dr. Oliver Reiser: “Studies towards cyclopropanation of triazoles”
04/2006-09/2010	Studies in chemistry at the University of Regensburg, Germany
10/2004-03/2006	Studies in chemical- and bio-engineering at the FAU Erlangen-Nuernberg, Germany
06/2004	Abitur (University entrance diploma), Willibald-Gluck-Gymnasium Neumarkt i. d. Opf., Germany

Professional Experience

since 10/2010	Research assistant, Institute of Organic Chemistry, University of Regensburg, Germany
08/2009-09/2009	Industrial placement: “Studies towards selective edging of metals on novel materials for OLED electrodes” and “Optimization of process parameters for laser structuring”, OSRAM Opto Semiconductors, Regensburg, Germany

Languages

German	native
English	fluently
French	advanced

Professional References

Prof. Dr. Oliver Reiser
Institut für Organische Chemie
Universität Regensburg, Universitätsstr. 31
93053 Regensburg, Germany
Phone: +49 941 943 4631
Email: Oliver.Reiser@chemie.uni-regensburg.de

Prof. Dr. Jean-Pierre Majoral
Laboratoire de Chimie de Coordination du CNRS
205, Route de Narbonne
31077 Toulouse Cedex 4, France
Phone: +33 561 333123
Email: majoral@lcc-toulouse.fr

Prof. Dr. Wendelin J. Stark
Institut für Chemie- und Bioingenieurwissenschaften
Department Chemie und Angewandte Biowissenschaften
ETH Zürich, Wolfgang-Pauli-Strasse 10
8093 Zürich, Switzerland
Phone: +41 44 6320980
Email: wstark@ethz.ch

G. Acknowledgement

Universität Regensburg

Bei **Prof. Dr. Oliver Reiser** möchte ich mich für die Überlassung des interessanten Themas, die Ermöglichung meiner Auslandsaufenthalte sowie die vielen Ratschläge während Masterarbeit und Promotion bedanken.

Bei **Priv. Doz. Dr. Sabine Amslinger**, **Prof. Dr. Arno Pfitzner** und **Prof. Dr. Antje J. Baeumner** bedanke ich mich herzlich für die schnelle und problemlose Begutachtung der Arbeit sowie der Bereitschaft im Prüfungskomitee mitzuwirken.

Des Weiteren möchte ich **Dr. Peter Kreitmeier**, **Georg Adolin**, **Klaus Döring** und **Helena Konkel** sehr herzlich für deren technische Hilfe sowie das Erledigen etlicher kleinerer und größerer Arbeiten danken. Spezieller Dank gilt dabei **Roxane Harteis** für die synthetische Unterstützung eines Projektes.

Der zentralen Analytik der Universität Regensburg bin ich sehr dankbar für die Durchführung aller MS-, NMR- und vor allem EA-Messungen.

Für zahlreiche ICP-OES Messungen und die Aufopferung unendlicher Arbeitszeit möchte ich **Joachim Rewitzer** ganz herzlich danken. Des Weiteren danke ich **Philipp Peter** für die Durchführung der XRD-Messungen und **Dr. Wendy Patterson** für zahlreiche Raman-Messungen.

Für das Korrekturlesen der vorliegenden Arbeit danke ich **Paul Kohls** und meiner Freundin **Julia Sporer** ganz herzlich.

Allen aktuellen und ehemaligen Mitarbeitern des Arbeitskreises danke ich für die super Arbeitsatmosphäre sowie diverse Grillabende und Freizeitaktivitäten. Spezieller Dank geht dabei an die Ehemaligen **Dr. Alexander Schätz**, **Dr. Florian Sahr**, **Dr. Klaus Harrar**, **Dr. Markus Hager**, **Dr. Michael Schwarz**, **Dr. Julian Bodensteiner**, **Dr. Tobias Olbrich**, **Dr. Sebastian Wittmann**, **Dr. Kathrin Ulbrich**, die aktuellen Kollegen **Paul Kohls**, **Ludwig Pilsl**, **Andreas Bergmann**, **Andreas Kreuzer**, **Viktor Kais**, **Andreas Okun**, **Daniel Rackl**, **Matthias Knorn**, **Christian Faderl**, **Daniel Dobler** sowie die aktuelle Nanopartikel-Crew **Corina Eichenseer**, **Francesca Besostri** und **Soraia Fernandes**.

Meinem langjährigen Laborkollegen **Dr. Quirin Kainz** möchte ich speziell für die stets gute Atmosphäre im Labor und viele nützliche Diskussionen zu unserer Projekten danken.

Meinen Bachelor-Studenten und Forschungspraktikanten **Benjamin Kastl**, **Matthias Gnahn**, **Romy Freund**, **Sabrina Fürst**, **Vera Hirschbeck** und meiner Freundin **Julia Sporer** möchte ich ganz herzlich für die engagierte und sorgfältige Arbeit danken.

Meinen Freunden **Dennis Kühbeck**, **Florian Pielnhofer**, **Steffen Pockes**, **Mumu Meier**, **Tobias Lang**, **Wolfram Klosterhuber** und **Stefan Balk** danke ich für die zahlreichen, enorm wichtigen Mittags- und Kaffeepausen sowie ereignisreiche chemische und nicht-chemische Diskussionen. Spezieller Dank geht dabei noch nach Karlsruhe an **Christian Wellner**, der mir mit Unterstützung des KIT etliches an Literatur verschaffen konnte.

Laboratoire de Chimie de Coordination, Toulouse

Ein herzliches Dankeschön nach Toulouse an **Prof. Dr. Jean-Pierre Majoral**, **Prof. Dr. Anne-Marie Caminade** und **Dr. Armelle Ouali**, die mir meine Auslandsaufenthalte mit ermöglicht haben. Spezieller Dank geht dabei an **Dr. Michel Keller**, der mir sowohl in organisatorischer als auch fachlicher Weise sehr behilflich war. Des Weiteren möchte ich aus der Equipe M speziell **Laurie Travers**, **Dr. Aurélien Hameau**, **Mykhailo Ianchuk**, **Dr. Nabil El Brahmi**, **Dr. Arnaud Perrier**, **Dr. Cédric-Olivier Turrin**, **Dr. Régis Laurent** sowie allen anderen Freunden aus den Nachbar-Arbeitskreisen ganz herzlich für Hilfe, Unterstützung sowie zahlreiche Feierabendbiere und natürlich –weine danken.

TU München

An der TU München möchte ich ganz herzlich **Prof. Dr. W. A. Hermann** und **Prof. Dr. F. E. Kühn** und dem Koordinator **Dr. Markus Drees** danken, die mir es ermöglich haben im internationalen Doktorandenprogramm NANOCAT zu arbeiten und dadurch finanziert zu werden.

ETH Zürich

An der ETH Zürich möchte ich mich bei **Prof. Dr. Wendelin J. Stark**, **Dr. Robert N. Grass** für die gelungene Zusammenarbeit, bei **Dr. Martin Zeltner** für die Messung von Elementaranalysen und bei **Daniela Paunescu** für die Durchführung der Transmissionselektronen-Mikroskopie bedanken. Spezieller Dank gilt dabei **Dr. Alexander Schätz** für die intensive Unterstützung zu Beginn der Promotion.

Ganz besonderen und sicherlich den größten Dank schulde ich jedoch meiner Familie, besonders meinen Eltern sowie meiner Freundin Julia. Ohne eure anhaltende Unterstützung wären weder mein Studium noch diese Arbeit möglich gewesen.

Declaration

Herewith I declare that this present thesis is a presentation of my original work prepared single-handed. Wherever contributions from others are involved, all of them are marked clearly, with reference to the literature, licence, and acknowledgement of collaborative research.

Regensburg, 10 March 2014

Roland Linhardt